*Report No. UT-03.14*

# *FACTORS AFFECTING SAMPLE DISTURBANCE IN BONNEVILLE CLAYS*

**By: James Bay**
**Loren Anderson**
**Jon Hagen**
**Aaron Budge**

**Department of Civil & Environmental Engineering**
**Utah State University**

**Utah Department of Transportation**
**Research Division**

**May 2003**

# UDOT RESEARCH & DEVELOPMENT REPORT ABSTRACT

| | | | |
|---|---|---|---|
| **1. Report No.** UT-03.14 | | **2. Government Accession No.** | **3. Recipient's Catalog No.** |
| **4. Title and Subtitle**<br>FACTORS AFFECTING SAMPLE DISTURBANCE IN BONNEVILLE CLAYS | | **5. Report Date** 13 May 2003<br>**6. Performing Organization Code** | |
| **7. Author(s)**<br>Bay, James A.<br>Anderson, Loren R.<br>Hagen, Jon C.<br>Budge, Aaron S. | | **8. Performing Organization Report No.** | |
| **9. Performing Organization Name and Address**<br>Department of Civil and Environmental Engineering<br>Utah State University<br>Logan, UT 84322-4110 | | **10. Work Unit No.**<br>**11. Contract No.**<br>019118 | |
| **12. Sponsoring Agency Name and Address**<br>Utah Department of Transportation<br>Research Division<br>4501 South 2700 West<br>Salt Lake City, Utah | | **13. Type of Report and Period Covered**<br>Research 1999 - 2002<br>**14. Sponsoring Agency Code** | |
| **15. Supplementary Notes**<br>Clifton Farnsworth, UDOT Research Project Manager | | | |
| **16. Abstract**<br>This report contains a study of the effects of drilling and sampling method on sample disturbance on samples of Bonneville clay taken near 3600 South and I-15 during and after the I-15 reconstruction project. Comparisons of disturbance in soil samples obtained using Shelby tube samplers and two types of piston samplers were made based upon radiograph images of the samples, consolidation tests and triaxial tests. It was found that samples obtained using the piston samplers were much less disturbed than those obtained using Shelby tube samplers. The effects of two drilling methods on sample disturbance were also studied. Rotary wash drilling was found to cause slightly less disturbance in soil samples than hollow stem auger drilling. Specific recommendations are made as to methods that should be employed to minimize disturbance in soft Bonneville clay samples. | | | |
| **17. Key Words**<br>Soil sample disturbance, piston sampler, Shelby tube sampler, hollow stem auger, rotary wash method, soil sample x-ray | | **18. Distribution Statement** | |
| **19. Security Classification (of this report)**<br>N/A | **20. Security Classification (of this page)**<br>N/A | **21. No. of Pages**<br>249 | **22. Price**<br>N/A |

# EXECUTIVE SUMMARY

The purpose of this project was to evaluate the effects of sampling method on sample disturbance in soft Bonneville clays. To obtain samples for this work, two drilling methods, rotary wash and hollow stem auger, were used. Samples were obtained using a shelby tube sampler and two different piston samplers. Sample disturbance was evaluated using radiograph images of the specimens, and laboratory consolidation and triaxial tests.

Comparisons of piston and shelby tube samples indicate that piston samples are less disturbed than shelby tube samples. X-rays show significantly fewer fractures in piston samples than shelby tube samples. The average radius of the consolidation curves at the points of maximum past pressure was less (indicating a sharper break between reconsolidation and virgin consolidation) for the piston samples than the shelby tube samples, resulting in less uncertainty in maximum past pressure predictions. Interestingly, there was no significant difference in maximum past pressure or $C_{c\varepsilon}$ between the piston and the shelby tube samples. This may be because the radiograph images were used to select portions of the sample to use in consolidation tests. Thus, the most disturbed portions of the samples were not tested. The piston samples also exhibited higher initial moduli ($E_{50}$) values than the shelby tube samples in the unconfined compression test. This is also indicative of less sample disturbance. The shape of the consolidation curves for piston samples are generally better than those of shelby tube samples with the same drilling method.

The differences in sample disturbance were not as recognizable or significant between the two drilling methods. The quantities of fractures and cracks identified in radiograph images were practically identical for the two drilling methods. The CRS tests show slightly less disturbance in the rotary wash samples than the hollow stem auger samples. The average radius of the consolidation curves at the points of maximum past pressure was somewhat lower for the rotary wash samples than the hollow stem auger samples, resulting in less uncertainty in maximum past pressure for the rotary wash samples. Again, there was no significant difference in the average maximum past pressure or $C_{c\varepsilon}$ between rotary wash and hollow stem auger samples.

Based upon this research, several recommendations can be made as to methods that should be employed in drilling and sampling to minimize the effects of sample disturbance in soft Bonneville clays. These are:

- Piston samplers along with thin-walled sampling tubes should be used rather than shelby tube samplers for obtaining specimens for consolidation, triaxial, and other critical geotechnical tests.
- Both fixed piston, and free piston samplers obtain samples of similar high quality.
- Radiograph (x-ray) images of the soil specimens provide a powerful tool for assessing sample disturbance, selecting the least disturbed portions of the sample for critical tests, and identifying locations of sand lenses in Bonneville clay samples.
- Rotary wash drilling methods result in slightly less sample disturbance than hollow stem auger drilling.

- When hollow stem auger drilling is used, the auger should be advanced slowly using slow rotation (as was done in this work) to minimize disturbance to the surrounding soil.

- Sample recovery can be increased by waiting a period of several minutes after pushing a sample tube before attempting to extract the sample from the ground.

TABLE OF CONTENTS

Page

Page

# LIST OF TABLES

# LIST OF FIGURES

Page

Page

Page

Page

Page

Page

Page

Page

Page

Page

Page

Page

Page

Page

Page

Page

Page

# CHAPTER 1

# INTRODUCTION

## 1.1 Sample Disturbance

The basis of a good design in geotechnical engineering is the correct determination of the soil's characteristics and engineering properties. Undisturbed or slightly disturbed soil samples are needed to accurately determine these properties. For many years processes have been developed and improved upon to successfully retrieve undisturbed soil samples.

Many factors can play a role in the quality of a sample taken. The type of sampling device used can greatly affect the sample. The geometry of a tube and also the method used to keep the sample in the tube during extraction of the tube can lead to sample disturbance. One factor that is often overlooked is the experience of the driller and the care he takes in the job. Many times a driller is chosen based on availability or price and experience is overlooked. The method of transportation and storage of soil samples can cause disturbance. The in situ state of the soil needs to be replicated as closely as possible during transportation and storage. This report will also cover other factors that can cause sample disturbance along with suggestions and the methods employed to deal with them.

There have been many concerns having to do with the sample disturbance and the need to develop a method of determining the extent of disturbance and methods to overcome it, particularly with the Lake Bonneville deposits in the Salt Lake Valley. Research has been conducted to determine stress history and normalized soil engineering properties (SHANSEP) parameters of deposits of this material. In October 1999, soil

samples were taken from the site of an MSE wall during its construction in the I-15 corridor near 3600 South in Salt Lake City. Samples were taken using a 3-inch diameter (76.2 mm), 30-inch long (762 mm) thin-walled tube and a shelby tube sampler from two boreholes. Fourteen samples were recovered. Constant-rate-of-strain (CRS) consolidation testing began in June of 2000 to determine the maximum past pressure for the SHANSEP parameters. Ten tests were performed. Results were inconclusive due to the disturbance of the samples. It was determined that extensive research into the effects of sample disturbance was needed.

New samples were then taken from the same location. Four boreholes were drilled, two with the rotary wash method and two with a hollow-stem auger. Samples from one of each type of borehole were sampled with a shelby tube sampler while the other samples were taken using either a fixed piston sampler or a free piston sampler. Eleven samples were recovered with a shelby tube sampler from one hollow-stem auger borehole, and 11 were recovered from a rotary wash borehole. Six samples were recovered with the fixed piston, three from each type of borehole. Seven samples were recovered with the free piston sampler from one hollow-stem auger borehole and eight from one rotary wash borehole.

The 43 tubes that were recovered were x-rayed. Three exposures for each tube were used to characterize the contents. In total, 129 x-rays were used. Fractures in each x-ray were counted and histograms were made to compare the amount of fracturing that took place with each sampling method. It was concluded that the samples taken with shelby tube samplers had the most fractures and were therefore the most disturbed after sampling. Samples taken with piston samplers had minimal fracturing.

Specimens were then trimmed and used for CRS consolidation testing. Nineteen tests were performed. The shape of the strain versus the log of effective stress curves was then examined and curves were compared for each boring and sampling method. Also compared were the error bands for the maximum past pressure and the slope of the virgin compression curves.

Additional laboratory testing was performed on most samples to determine their soil properties. This testing included the determination of Atterberg Limits, unit weight, moisture content, and grain size distribution. The results of these tests are presented in Appendix A.

# CHAPTER 2

# REVIEW OF LITERATURE

## 2.1 Introduction

This chapter discusses some of the previous studies done on causes of sample disturbance and how it might affect consolidation test results. Olson (1986) stated, "Testing truly undisturbed samples is more a goal than a reality (p. 54)." Even Hvorslev (1949) admitted that the criteria for undisturbed samples are impossible to meet. A discussion on methods of sampling and sampling devices used in this research is also included along with possible methods of limiting sample disturbance. Some basic theory on the subject of radiography is given.

## 2.2 Sample Disturbance

Sample disturbance can occur anywhere from drilling to testing. A look at causes of disturbance will help to identify ways in which more care can be taken and methods can be improved to prevent disturbance. Some common causes of soil disturbance are shown in Table 2.1.

Different methods of drilling affect the sample. When a boring is drilled, the removal of soil causes a removal of stress. Heaving of the sample at the bottom of the hole can occur, as well as piping and caving of the hole. During sampling there may be a failure to recover a sample, and after sampling, vibration during transportation will cause disturbance. Hvorslev (1949) defined several ways in which samples may be disturbed

Table 2.1. Causes of soil disturbance (adapted from ASCE, 2000).

| **Before Sampling** | **During Sampling** | **After Sampling** |
|---|---|---|
| Base heave | Failure to recover | Chemical changes |
| Piping | Mixing or segregation | Migration of moisture |
| Caving | Remolding | Changes of water content |
| Swelling | Stress relief | Stress relief |
| Stress relief | Displacement | Freezing |
| Displacement | Stones along cutting edge | Overheating |
| | | Vibration |
| | | Disturbance caused during extrusion |
| | | Disturbance caused during transportation and handling |
| | | Disturbance caused due to storage |
| | | Disturbance caused during sample preparation |

during the sampling process. One factor is the area ratio or kerf ratio of the sampling tube:

$$c_a = \frac{D_w^2 - D_e^2}{D_e^2}, \tag{2.1}$$

where $D_w$ is the external diameter and $D_e$ is the internal diameter.

Hvorslev (1949) suggested that area ratio values should be kept to a minimum, less than 10 to 15 percent. Sample tubes that have area ratios that are too small, however, are more susceptible to bending and buckling.

The length and diameter of the sample are important factors. Hvorslev (1949) suggested having length-to-diameter ratios between 5 and 10 for cohesionless soils and between 10 and 20 for cohesive soils. Variables such as sampling depth, the type of sampler, the rate and uniformity of penetration, and the inside clearance ratio will make it necessary to change the length-to-diameter ratio. The inside clearance ratio, $C_i$, is

defined as the inside diameter of the tube minus the internal diameter of the cutting shoe divided by the internal diameter of the cutting shoe.

The method of advancing the sampling tube affects sample disturbance. Hammering the tube with driving blows causes the most disturbance. Hvorslev (1949) suggested that the most suitable method of tube advancement be with a steady force and a continuous uniform motion. Twisting should be prevented because it may cause a shear failure in the sample by torsion. A single heavy blow may be effective in producing an even longer and less disturbed sample than fast pushing. However, the high velocity and impact may have adverse effects.

Some causes of disturbance occur in sample recovery. In design guides adapted from the Army Corps of Engineers, (ASCE, 2000), several factors were suggested that may result in poor sample recovery. Increased pressure in the top due to poor venting may force the sample from the tube as it is extracted. Suction below the sample during extraction may pull the sample out of the tube. In order to pull the sample from the hole, the soil's tensile strength must be overcome. To do this, rotating the tube one or two revolutions to shear the sample at the bottom is suggested. However, this contradicts what Hvorslev suggested above. Another suggestion is to leave the sample in the hole for several minutes after pushing the tube in order to allow the soil to swell and increase adhesion with the wall of the tube.

Olson (1986) noted several ways in which disturbance may occur in the top and bottom of samples. He suggested that the top portion (30% to 40% typically) is disturbed "due to stress relief at the bottom of the borehole, due to shearing strains beneath the fixed-piston (when one is used), due to a greater distance of movement in the tube, and

perhaps due to a moisture inhibition" (p. 56). The bottom diameter or so of the sample may be disturbed due to suction when the sampler is withdrawn. He states that the best consolidation specimens, other than those from block samples, are trimmed from the middle or lower part of the tube with some edge trimming.

Olson (1986) noted that storing samples in the sampling tube results in a "time-dependent increase in the degree of saturation" (p. 58). Arman and McManis (1976) found that in one soil the maximum past pressure decreased from 4.05 tons per square foot just after sampling to 2.8 tsf after one year of storage and the void ratio versus log of effective stress became more rounded. Olson explained that one reason for the time-dependent disturbances of the middle of the sample is the slow inward migration of moisture from the disturbed outer area. Olson suggested extruding the samples in the field, trimming away the outer ¼ inch, wrapping the rest in foil or plastic film, and storing them in a suitable airtight container.

Hvorslev (1949) explained, "A disturbance of the soil structure may consist of a weakening of the bond between particles or a rearrangement of the structural pattern formed by the soil grains" (p. 190). The bond may be reestablished after disturbance has ceased. When the structural pattern of soil particles is rearranged there tends to be a change in void ratio and pore water pressures at the surface of the sample. The amount of change depends on whether the soil is normally or overconsolidated. A loose cohesionless soil or a normally consolidated to slightly overconsolidated cohesive soil will show a decrease in void ratio and increase in pore pressure with disturbance. A dense cohesionless or highly overconsolidated soil will show the opposite effect.

## 2.3 Influence of Sample Disturbance on Consolidation Tests

A disturbed soil sample is one which has its properties altered. It reacts to stress changes differently than it would if it was left in situ. This section looks at the expected shape of consolidation curves of disturbed and undisturbed soil samples.

When a disturbed soil specimen is used in a consolidation test, results can be difficult to interpret. The process of drilling and sampling a soil causes changes in the stress state of the soil. Holtz and Kovacs (1981) described the effects of sample disturbance on a soil's void ratio during consolidation testing and maximum past pressure (preconsolidation stress) determined from consolidation testing. Figure 2.1 presents a curve of void ratio versus the log of effective consolidation stress that illustrates deposition, sampling, and reconsolidation in a consolidation apparatus. In Figure 2.1, if an element of soil at stress and void ratio O experiences deposition of additional material above it, it will consolidate to point A. The path from point O to point A is the field compression curve. The clay is in a normally consolidated condition. Upon making a boring and sampling the soil, the overburden is taken away and the sample swells and follows the line AB. When the sample is taken and consolidated in a ring, it follows line BC, the reloading curve. Continuing consolidation will cause the soil structure to break down and the laboratory consolidation test curve CD is obtained. The field curve, OAD, and the laboratory curve, BCD, will eventually converge beyond D. When sampling is poor and the soil structure is disturbed, the curve will follow BC'D. Increasing sample disturbance will cause the curve to move down and to the left with an increasingly rounded curve between the reload and virgin loading portions of the consolidation curve.

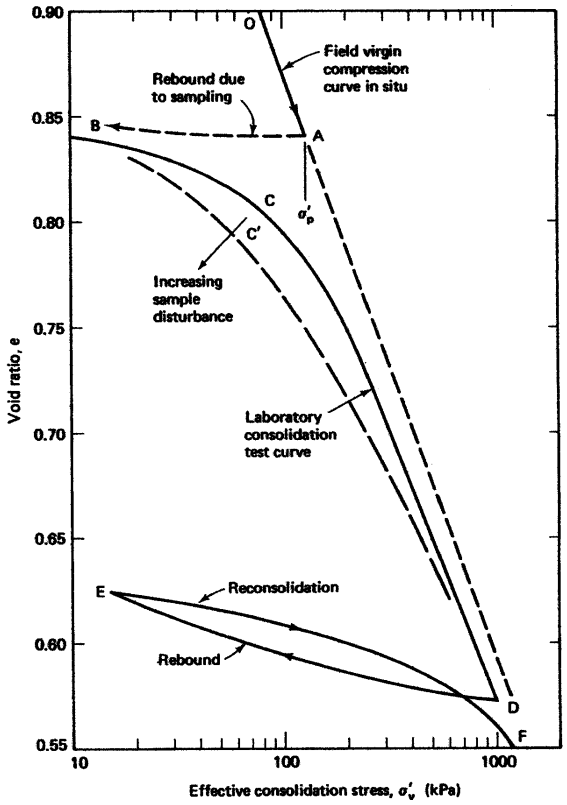


Figure 2.1 Plot showing effects of deposition, sampling, and reconsolidation (after Holtz and Kovacs, 1981).

Casagrande (1936) used a similar consolidation curve to develop his procedure for determining the maximum past pressure. Figure 2.2 shows the Casagrande construction. The Casagrande procedure is outlined as follows after Holtz and Kovacs (1981):

1. Choose by eye the point of minimum radius (or maximum curvature) on the consolidation curve (point A in Figure 2.2).
2. Draw a horizontal line from point A.
3. Draw a line tangent to the curve at point A.
4. Bisect the angle made by steps 2 and 3.

5. Extend the straight-line portion of the virgin compression curve up to where it meets the bisector line obtained in step 4. The point of intersection of these two lines is the preconsolidation stress (point B of Figure 2.2).

Also, a minimum and maximum possible maximum past pressure can be determined by extending a straight line from the virgin portion of the curve. Maximum possible is at point C in Figure 2.2, where the virgin curve first deviates from a straight line, and the

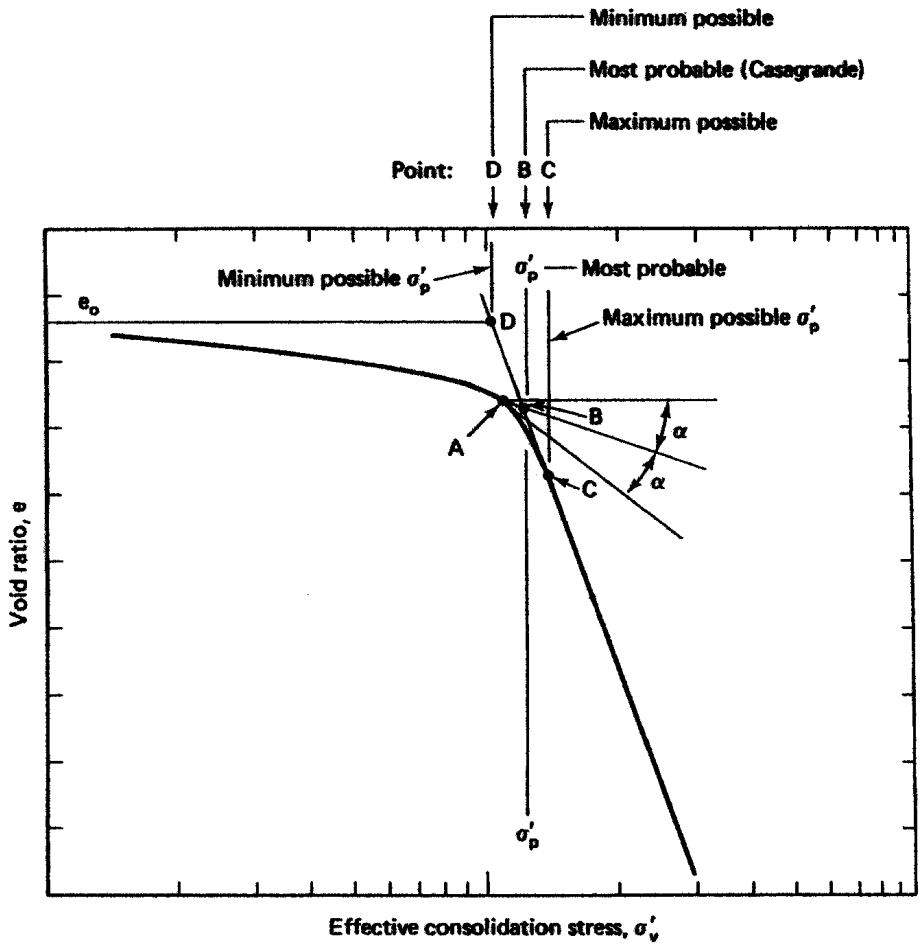


Figure 2.2 Casagrande construction for determining the maximum past pressure (after Holtz and Kovacs, 1981).

minimum possible, point D, is the intersection of this straight line with a line drawn horizontal from $e_o$ or initial strain. As the soil becomes more disturbed, it is increasingly difficult to locate a point of minimum radius, and it becomes impossible to determine the maximum past pressure. Also, the range of maximum past pressure becomes increasingly larger with increasing disturbance.

The maximum past pressure can also be determined using a modulus curve. Figure 2.3 is a generalized plot of the tangent modulus versus effective stress. The maximum past pressure is at the point where modulus abruptly decreases. A modulus curve from a highly disturbed sample will not exhibit high modulus while overconsolidated, and there will not be an abrupt decrease in modulus as the soil transitions from overconsolidated to normally consolidated.

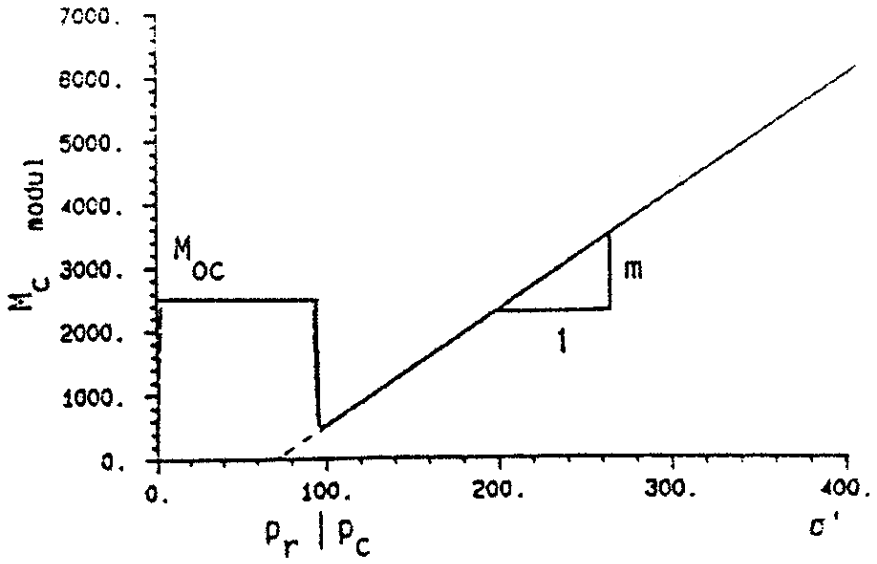


Figure 2.3 Determination of maximum past pressure from a plot of modulus vs. effective stress (from Emdal, 1999).

## 2.4 Radiography

Radiography is the use of radiation, such as x-rays or gamma rays, to penetrate a material and produce an image on film. This technology has been used since 1895 when x-rays were discovered by Wilhelm Roentgen, but not to a great extent in soil mechanics until the last half of the 20$^{th}$ century. X-ray images of soil specimens show fractures, fissures, deformations of bedding planes, and soil type.

Krinitzsky (1970) explained that x-rays are generated when high velocity electrons are slowed upon striking a target. Absorption of x-rays is dependent upon several things, the wavelength of the radiation, the material's density, and its atomic number. Wavelength is a function of the voltage applied to the x-ray tube. Voltage is usually measured in kilovolts, kV. A higher voltage results in a shorter wavelength and a higher penetrating power. Longer wavelengths (soft radiation) require more exposure time and produce more scatter, but are superior for thin specimens. Shorter wavelengths (hard radiation) are better for thick specimens. Scatter of x-rays causes the film to blur and obscure details. Besides using a shorter wavelength, scatter may also be avoided by limiting the area of exposure with masks and shields of lead. Another problem that may arise while x-raying sample tubes is the burning of the film by the x-rays passing through narrow chords. Krinitzsky (1970) recommended using plaster-of-paris or lead molds to give a rectangular shape to the soil specimen.

The amount of radiation that the material is exposed to can be summarized using distance, d, and intensity, I, relationships as given in Krinitzsky (1970). The focal distance is the distance between the tube (source) and the film. The inverse-square law relates intensity and distance of two exposures, 1 and 2, as follows:

$$\frac{I_1}{I_2} = \frac{{d_2}^2}{{d_1}^2}. \tag{2.2}$$

Radiation intensity is measured as a combination of amperage (generally mA) and time of exposure. Amperage, M, may be varied in an inverse proportion to time, t:

$$\frac{M_1}{M_2} = \frac{t_2}{t_1}. \tag{2.3}$$

The relation of amperage to focal distance is:

$$\frac{M_1}{M_2} = \frac{{d_1}^2}{{d_2}^2}. \tag{2.4}$$

The relation of time to focal distance is:

$$\frac{t_1}{t_2} = \frac{{d_1}^2}{{d_2}^2}. \tag{2.5}$$

An exposure factor, $E_f$, can be obtained by combining the equations:

$$E_f = \frac{Mt}{d^2}. \tag{2.6}$$

For the x-raying of sample tubes, it is often necessary to use trial and error to find the correct exposure and time. Radiographs of equal quality can be obtained by keeping $E_f$ constant. Radiographic exposure charts such as the one in Figure 2.4 are important tools in for adjusting amperage, time, and focal distance to obtain a desired film density. The horizontal axis in an exposure chart shows the thickness of the specimen and the

vertical axis gives the exposure (mA-min). Each exposure chart for a certain material has several curves of different voltages.

Film density is the darkness of the film on a scale of 0 to 5 (0 = totally clear, 5 = totally opaque). Film densities of 0.75 to 1.5 are easiest to scan and can be seen in almost any light source, but they do not provide much detail. Densities of between 1.8 and 2.5 are more useful if an image on paper is desired and they provide greater detail. Care must be taken in using results from other workers because of differences in the measured energy output of different machines. Since trial and error may be wasteful and tedious, the use of exposure charts can provide a helpful starting point.

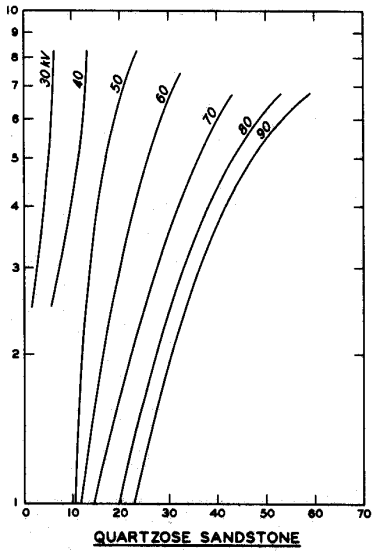


Figure 2.4 Exposure chart for quartzite sandstone, Kodak type AA film, 40-inch focal distance (after Fraser and James, 1969).

In an x-ray, layering is identified by the different shades of gray that appear. Since the absorption of x-rays depends on a material's density, then the density of the

exposure will indicate a certain material. Dense gravels absorb more x-rays and allow fewer to pass to the film, thus making a light exposure. Sands tend to absorb fewer x-rays and give dark exposures. Clay is just darker than gravel and silt is between clay and sand.

Olson (1986) explained, "If the compressibility of the clay greatly exceeds that of the sand, as would be expected, then only the clay layers are relevant. Laboratory tests should be performed on the clay layers alone…." (p. 52). For consolidation testing, it is more desirable to trim a sample that excludes the thin sand lenses found in many of the Bonneville clays. In addition to sand lenses, small gravel also presents a problem in consolidation testing due to the effects it has on compressibility. When testing small samples, it is ideal to exclude gravel because it is not representative of the soil on a large scale. Arman and McManis (1976) reported on variations in sample properties along the length of a 36-inch-long tube sample that was considered to be locally uniform. Values of unconfined strength from the sample varied from 1100 psf and 2700 psf. Selecting an arbitrary sample may result in either underdesign or overdesign. Radiographs of these specimens showed "slickensides not visible to the naked eye, very thin sand and silt layers, calcareous nodules, and marine shells" (p. 85). Figure 2.5 is a radiograph of stiff clay and shows edge turning caused by sampling. The arrow shows the direction of movement of the soil relative to the tube. The use of radiographs in selecting portions of a sample to be tested provides a way to determine where the most representative sample may be obtained.

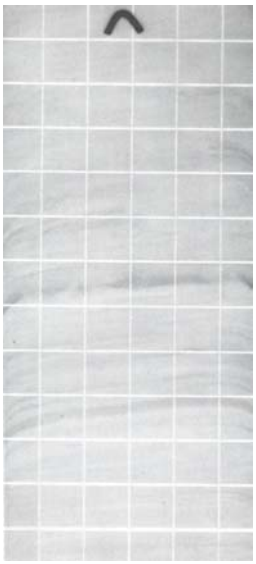

Figure 2.5 Radiograph showing edge turning in stiff clay (from Arman and McManis, 1976).

## 2.5 Drilling

In this section the different drilling methods used in this research are discussed. Some advantages and disadvantages of each method that are given in the literature are explained.

Boreholes may be advanced using methods such as augering and rotary drilling. ASCE (2000) advised that augering is best for holes that are to remain open, typically above the water table. Augers are best in loose, moderately cohesive, moist soils but may also be used in hard clays, silt, and/or sands that contain enough fines to keep them from caving. Applying a downward pressure and rotating the auger advances the borehole. A rotational velocity of 50 to 150 revolutions per minute is suggested but may be adjusted for different soil conditions. A lower rate will result in smaller cuttings. A higher rate will cause excessive vibrations and soil disturbance. To decrease disturbance at the

sampling depth, the rate should be decreased at about four or five hole diameters above sampling depth.

Short flight augers are best for shallow depths of up to 20 feet. They are advanced until the auger is full. It is then brought to the surface. Cuttings are removed by increasing the rotational speed, thus causing the soil to be thrown from the auger. Continuous flight augers work in all soils except for loose sands and gravels. The flights of augers move the soil cuttings up to the surface. Hollow stem augers are continuous flight and may be used as a casing to prevent caving of soils. The sampler is advanced down the center of the auger.

Rotary wash drilling is a method that employs a drilling fluid to carry the cuttings to the surface. The hole is advanced by gravity or pressure from the drill rig. The drilling fluid is pumped through the drill rods to the rotating bit to cool the bit and carry cuttings to the surface. A casing in the first 5 feet can be used to prevent caving of near surface soils. A drilling fluid consisting of a ratio of 50 pounds of bentonite per 100 gallons of water is usually sufficient in most conditions. If the mixture is too thin, the fluid will be like water and will not carry cuttings to the surface. A very thick mixture will not allow the cuttings to settle out in the main mud pit at the surface before it is pumped into the rods again. The drilling mud is also a means of lowering the stress relief in the bottom of the hole.

## 2.6 Sampling

One of the main objectives of this report is to show the effect of the sampler type on soil disturbance. This section reviews some of the literature and analysis of the types

of samplers used in the research.

Tubes are usually cold-drawn-seamless or welded and drawn-over-a-mandrel steel tubing. They may be coated with galvanization to prevent rusting in the tube. The lengths of the tubes vary but are generally 30 or 36 inches and normally have an outside diameter of three or five inches. The tube with the thinnest wall thickness will generally provide the least disturbed samples. Typical wall thicknesses are 14 gauge (0.083 in.) for the 3-inch tube and 11 gauge (0.120 in.) for the 5-inch tube. The area ratio for a 3-inch tube is 10.8 percent. The area ratio for a 5-inch tube is 9.4 percent. The tube is sharpened at the cutting edge (ASCE, 2000).

There are two basic types of push-tube samplers: open samplers (shelby) and piston samplers. Each type was employed in this research. Shelby samplers are open tubes attached to a vented head. Figure 2.6 shows a cross-sectional view of a shelby-tube sampler. The tubes may be either thick-walled or thin-walled. Thick-walled tubes have an area ratio of 10 to 20 percent, so the quality of sample is usually suspect. The head is attached to the tube with four screws as suggested by ASTM D 1587-94 (ASTM, 1994) and may have a ball check valve. The check valve provides venting in the tube as it is advanced and suction on the top of the sample during extraction to aid in sample retention. Shelby samplers are best for obtaining samples of soft to medium stiff cohesive soils. They are not recommended for obtaining undisturbed samples from boreholes. During sampling the pressure on the top of the sample may be increased because of pressure from drilling fluids in the rod. During extraction of the tube, sample may be lost because vibration may cause the ball check valve to open.

Piston samplers have a piston located in the sample tube. Before sampling the piston is at the bottom of the tube to prevent entrance of cuttings or fluid before the sample is taken. The piston also helps hold the sample in the tube during withdrawal by applying a partial vacuum. Hvorslev (1949) stated that the piston sampler "has more advantages and comes closer to fulfilling the requirements for an all-purpose sampler than any other type" (p. 255). However, the piston sampler is more complex and expensive.

There are three general types of piston sampler: free- or semi-fixed-piston samplers, fixed-piston samplers, and retractable-piston samplers. Free- or semi fixed-piston samplers are clamped when the tube is withdrawn but free to move up and down with respect to the ground and the sample tube during actual sampling. The fixed-piston sampler is the same as the free- or semi fixed-piston sampler except that it remains fixed relative to the ground during sampling. The retractable-piston sampler prevents cuttings and fluid from entering the tube when it is placed in the hole. Prior to sampling it is retracted to the top of the tube. Since this operation may draw soil into the tube when the piston is retracted, it is not recommended for undisturbed sampling. Fixed-piston samples are used for sampling very soft to stiff clays above and below the water table. When a sample tube has little or no inside clearance ratio, or swage, a fixed-piston sampler is used.

Although open tube and piston tube samplers are not the only types of samplers available, they are the only ones covered here because they were used in this research. Much can also be said about block samples for obtaining undisturbed samples. Olson

(1986) stated, “Fixed-piston samplers appear to be better than open tube samplers. Hand carved block samples [appear] to be of best quality” (p. 56).

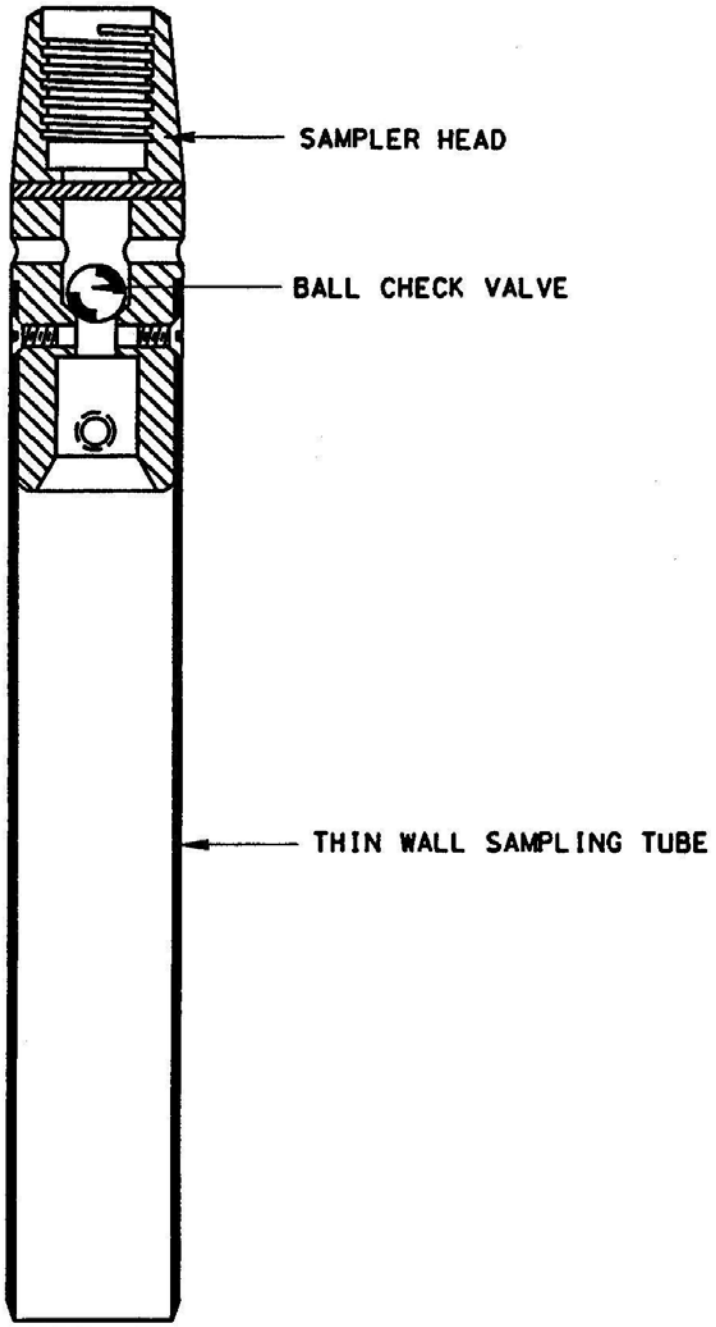


Figure 2.6 Cross-sectional view of a typical shelby tube sampler (adapted from ASCE, 2000).

# CHAPTER 3

# SAMPLING EQUIPMENT AND PROCEDURES

## 3.1 Introduction

The first phase of the research was to retrieve new soil samples for x-raying and testing. This can be considered as the most critical part of the research. This is where it is determined if there will even be undisturbed samples to test. In this chapter sampling equipment is described in detail. There were three samplers and two different drilling methods used. Samples were collected from four borings using a combination of samplers and drilling methods. Details of the exploration are given as well as care that went into the sampling and transporting of the soil.

## 3.2 Samplers

Three types of samplers were used in the project in order to compare the influence each one has on sample disturbance. One sampler was a fixed-piston sampler designed and built for this project. The other two samplers were provided by the driller, Ron Sigafus. One was a typical shelby-tube sampler (AW type). The other sampler was a free-piston sampler, but with some modifications.

### 3.2.1 Fixed-piston sampler

Before drilling began, a new fixed-piston sampler was designed and built. The design was a concept of James Bay and Jon Hagen designed it. Ken Jewkes machined the new piston. A cross-sectional view of this sampler is shown in Figure 3.1.

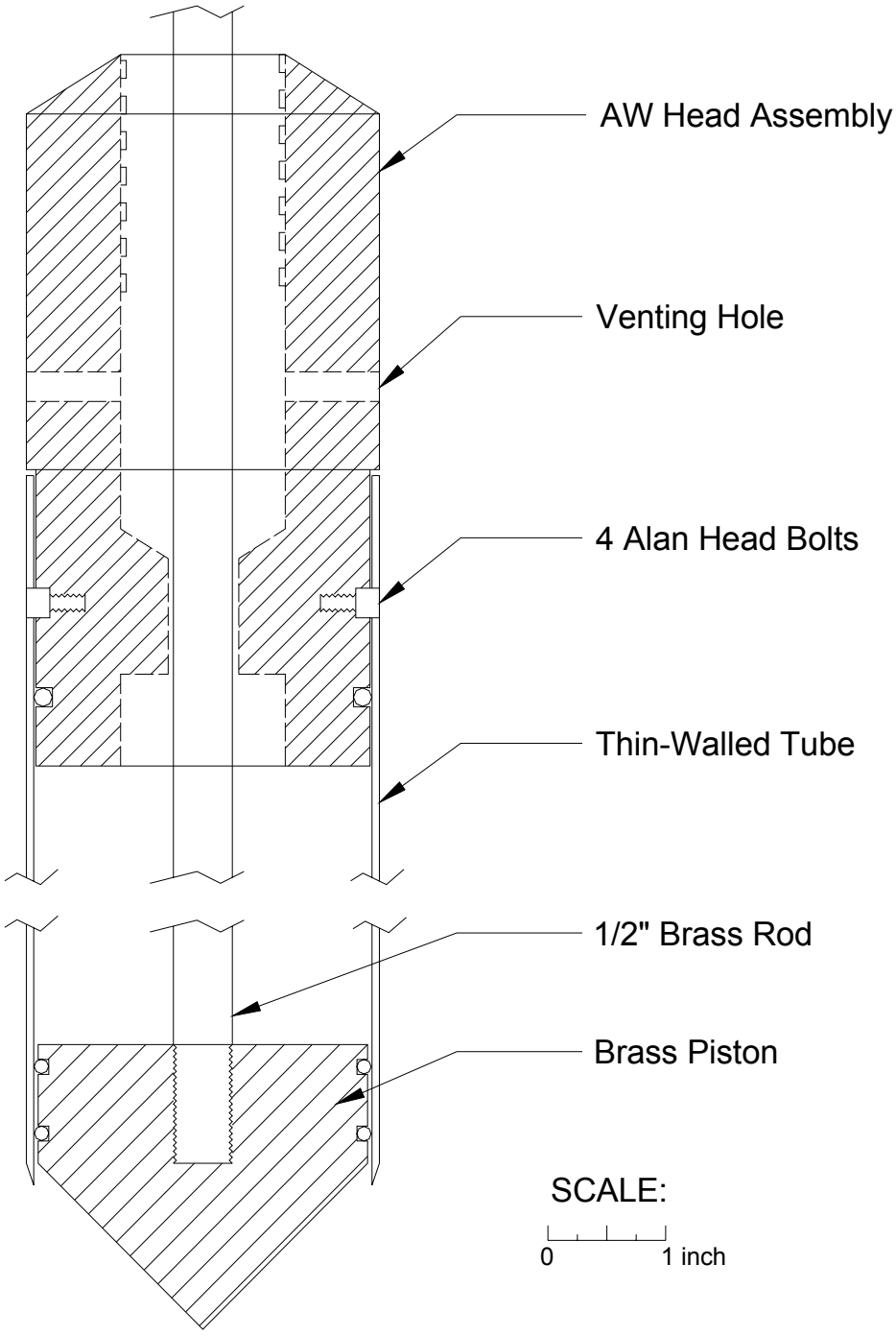


Figure 3.1 Cross-sectional view of the fixed-piston sampler.

The piston has a cone shape to push through slough at the bottom of the hole to minimize the amount of disturbed material that enters the tube. Rods attached to the piston lead through the AW head and up the center of the drill rods where it can be fixed in place with vice grips.

It was decided to make the piston and rods out of brass. The alternative choices were steel, aluminum, or plastic. Steel was not used because of corrosion problems. Aluminum would be too soft and susceptible to excessive wear. Plastic would be very light and easy to machine, but is not very durable and has a tendency to crack.

Piston rods were constructed from ½-inch solid brass rod in six-foot and four-foot lengths. One 4-foot length was machined with threads on the end to screw onto the piston. All of the other rods had holes drilled and tapped in the ends. A length of threaded steel rod was screwed in one end of each rod and secured with locktite. One inch of thread extended out to screw into the female end of an adjoining rod. An eyebolt was attached to the end of the last rod for holding the piston in place as the tube is pushed during sampling. Figures 3.2 and 3.3 show photographs of the piston and rods.

Two pistons were machined out of one 6-inch piece of 3-inch diameter solid

Figure 3.2 Fixed-piston sampler.

brass. Each piston is 2.8 inches in diameter in order to fit into the 2-7/8-inch inside diameter tube and leave a small clearance. One inch of the piston was left square and two grooves were machined into this space to hold rubber o-rings for a tight fit in the tube. It was discovered in the field that two rings made the piston too tight in the tube. The top ring was then taken off, and sufficient suction and seal were still maintained. The piston was machined below the 1-inch section at a 45-degree angle to form a cone. In the top of the piston a 1-inch hole was drilled and tapped so it could be connected to the piston rod.

Figure 3.3 Fixed-piston sampler with piston rods.

This fixed piston was used with a modified AW head assembly from Durham Geo Enterprises, Inc. (Figure 3.2). This type of head assembly is an open sampler with a ball held in the sampler with a pin. For operation of the fixed-piston sampler, the pin and ball were taken out. The brass rods were then free to move through this space. The head was attached to the sample tube with four Allen-type screws.

The fixed-piston sampler is operated as follows. When placing the tube in the borehole, the piston is at the end of the tube with the cone extended past the end of the tube. The rod and piston are locked into that position with vice-grips that clamp the brass rod to the drill rod. When the piston is at the elevation where a sample is to be recovered, the vice grips are taken off. The piston rod and piston are then locked in place with a taut line from the drill rig that is connected to the eyebolt. The drill rod is then pushed while the piston remains in a fixed position relative to the ground. After the sample tube is pushed to the bottom of the sample interval, the piston rod and piston are fixed to the drill rod with vice grips to prevent the weight of the rods and piston from pushing the sample out of the tube.

### 3.2.2 Other samplers

The driller provided the other two samplers used in the project. One sampler was of the shelby tube sampler type as described in the literature review. This head was an AW assembly similar to that used for the fixed-piston sampler. It was attached to the tube using four screws and attached directly to the drill rods.

The driller's piston sampler was a free-piston sampler. The piston did not have rod extensions. Instead, there is a cone clamp that allows the piston to move upwards but

prevents downward movement. The sampler is operated by first placing the piston flush with the end of the tube and then attaching the drill rods. The sampler is then lowered to the bottom of the borehole. The piston is free to move up with respect to the tube if pressure from cuttings or slough in the bottom of the borehole provides enough force against the piston to overcome friction between the piston and the tube. The piston has a leather seal around the edges to provide a tight fit in the tube. When the sample tube is pushed, the piston remains at the same elevation. When the tube is extracted, the piston is fixed with the cone clamp so that it does not move down with respect to the tube. This aids in sample recovery.

## 3.3 Drilling and Sampling

The boring site was located next to Interstate-15 near 3600 South in Salt Lake City, Utah. The location is the site of a mechanically stabilized earth (MSE) wall that was built as part of the highway expansion. Samples were taken from the same location in October 1999 (Goodsell 2000, Bay et al. 2003). The new borings were drilled in a square pattern near the older borings. The goal was to sample soil from the same area so that results from both explorations could be compared closely. Figure 3.4 is a site map showing boring locations.

### 3.3.1 1999 Exploration

In October 1999 six boreholes were made. Two of these boreholes were logged and are labeled S2 and I2. The details of this exploration are found in a thesis by Mark Goodsell (2000) and in the instrumentation report submitted to UDOT (Bay et al. 2003). Boring logs for the 1999 exploration are shown in Figures 3.5, 3.6, 3.7, and 3.8. Figures

3.5 and 3.6 are logs for boring I2 while Figures 3.7 and 3.8 are logs of boring S2. The borings were drilled with a truck mounted drill rig using wet rotary techniques. Samples were taken from borings I2 and S2. These borings were located 8 feet from the face of the wall (Figure 3.4). Soil from S2 was sampled with a shelby tube sampler and split spoon sampler. Samples were taken starting at 5-foot intervals beginning at a depth of 10 feet to a depth of 85 feet. Soil from boring I2 was sampled every five feet with a piston sampler starting at ten feet and ending at 65 feet. Three-inch diameter thin-walled tubes were pushed hydraulically to obtain the samples. The tubes were sealed with wax and capped and then transported back to Utah State University for testing. A vertical inclinometer and a sondex extensometer were installed in the two borings and the annular space was filled with a cement-bentonite grout.

### 3.3.2 2001 Exploration

New borings were drilled from February 5-7, 2001. The driller was Ron Sigafus. He was recommended by geotechnical engineers from the Utah Department of Transportation because he has a reputation as a knowledgeable and careful driller with more than twenty years of experience. Also important was the fact that he is willing to take the time required to provide high quality samples. The driller operated an ATV mounted drill rig shown in Figure 3.9. Details of the exploration are given in this section.

The exploration consisted of four boreholes. Two of the holes were drilled using rotary wash techniques while the other two were drilled with a continuous-flight hollow-stem auger. Samples were obtained by pushing 30-inch thin-walled Shelby tubes 24

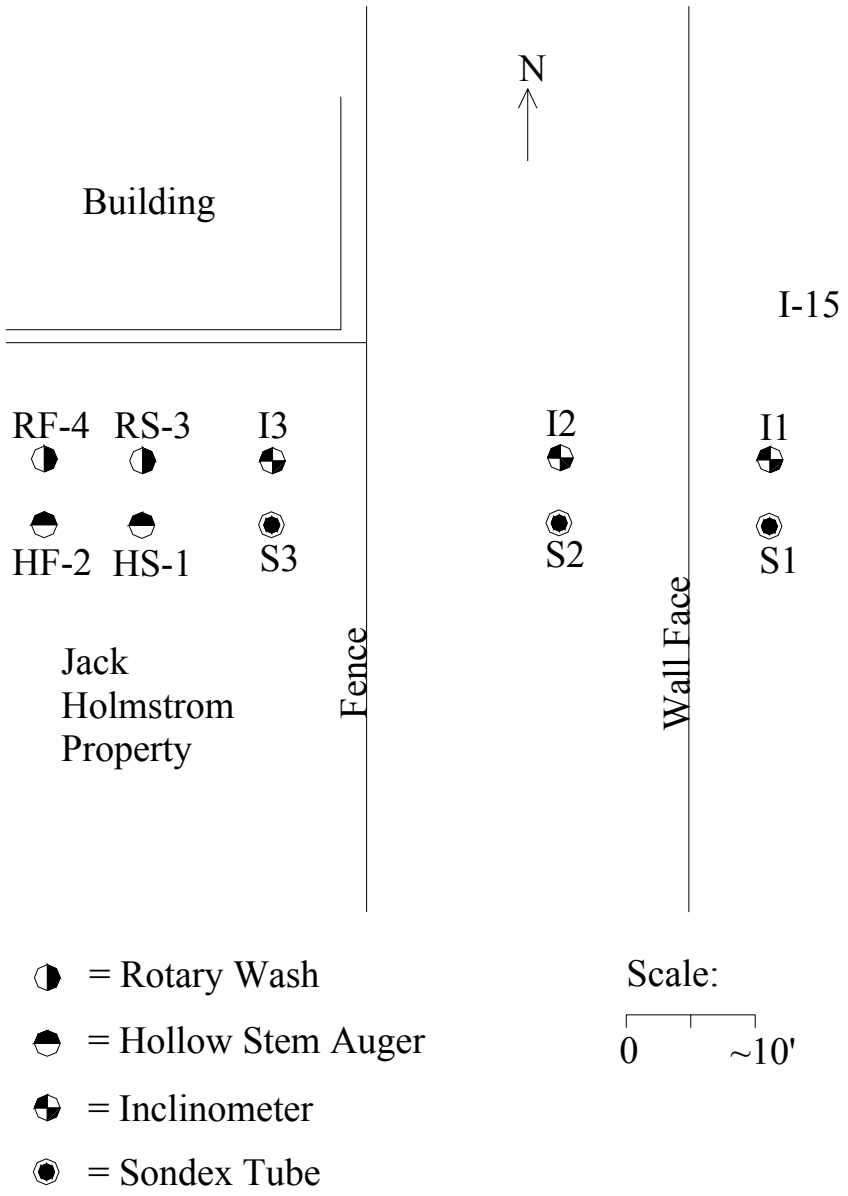


Figure 3.4 Site map showing boring locations.

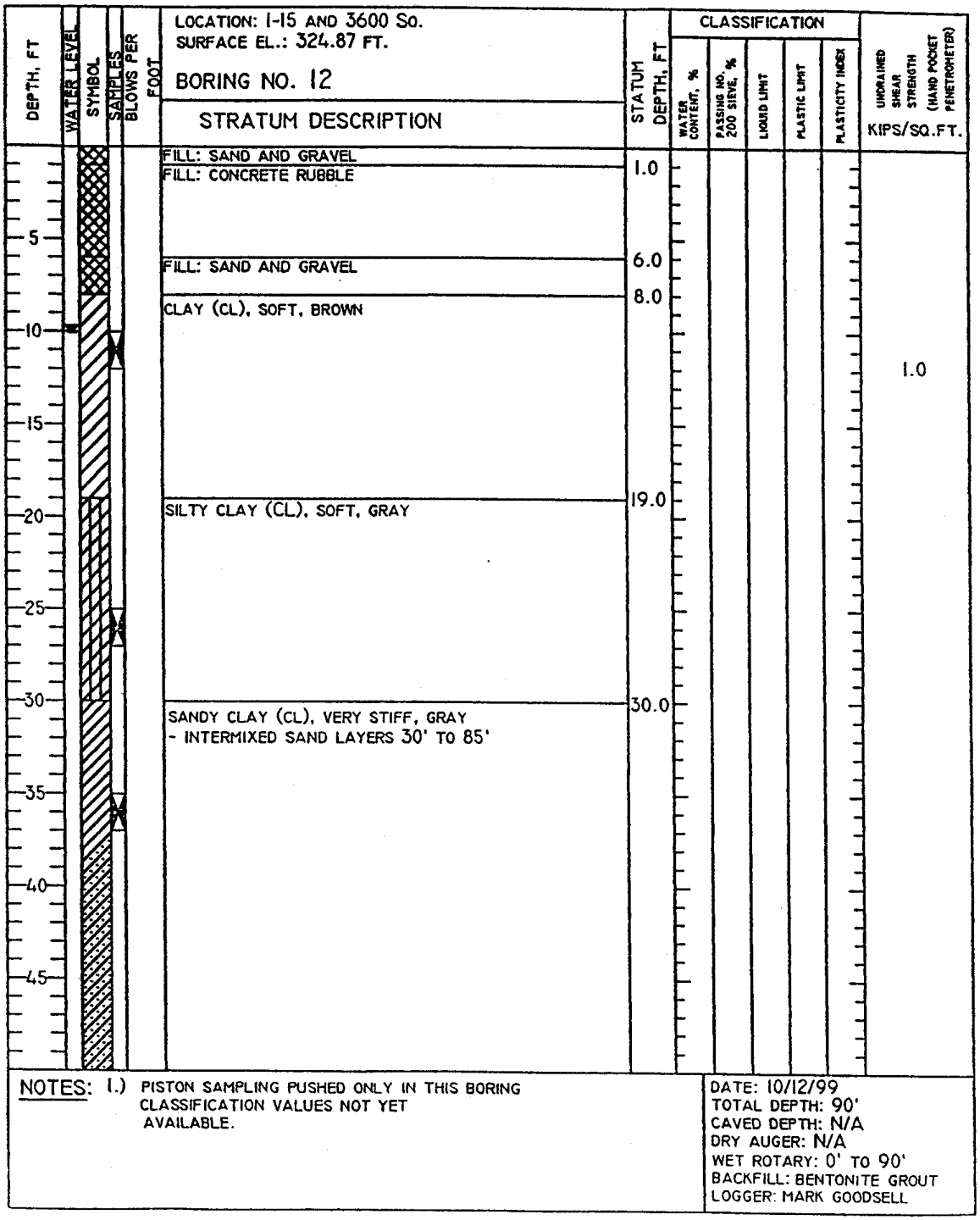


Figure 3.5 Log of boring I2 (sheet 1).

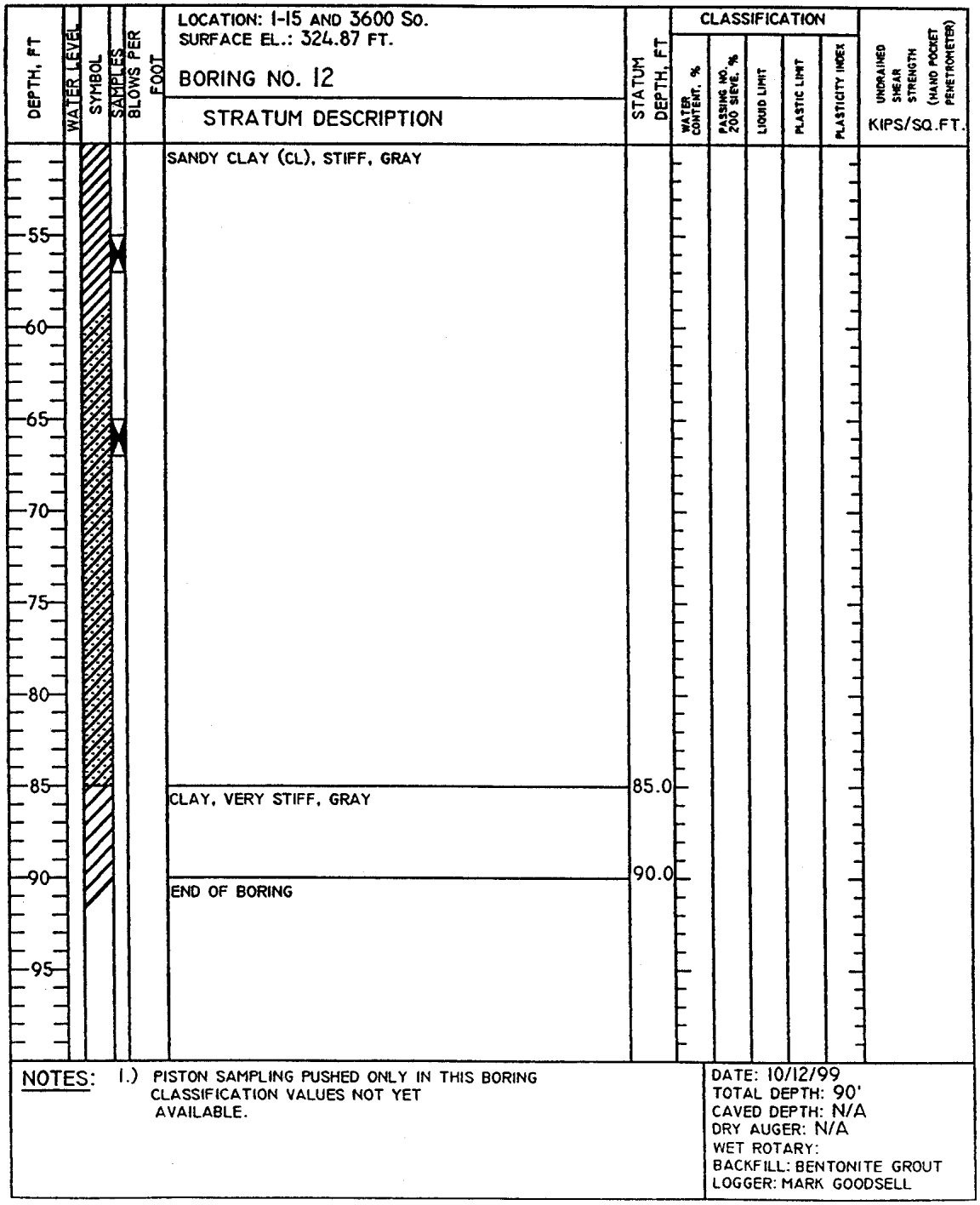


Figure 3.6 Log of boring I2 (sheet 2).

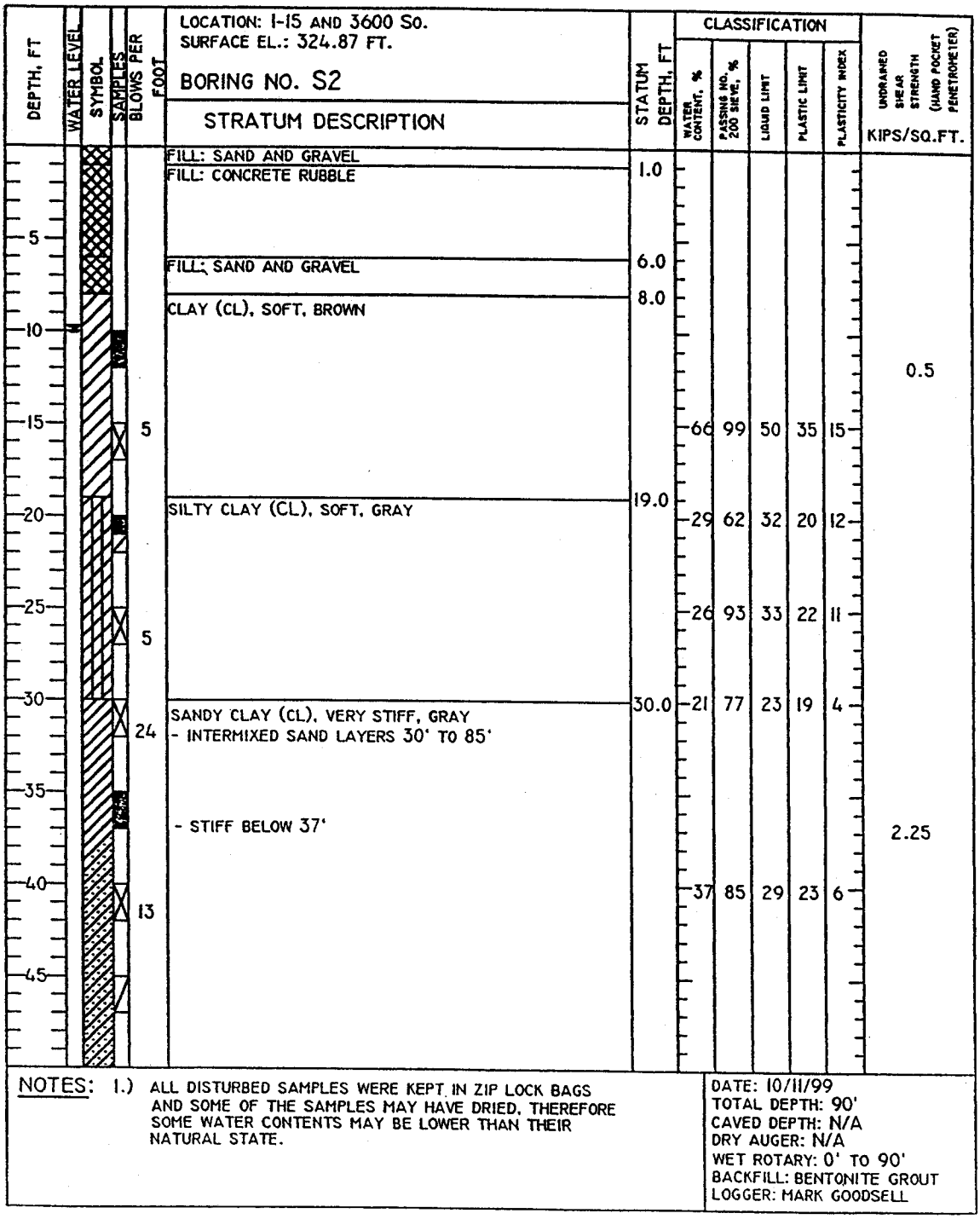


Figure 3.7 Log of boring S2 (sheet 1).

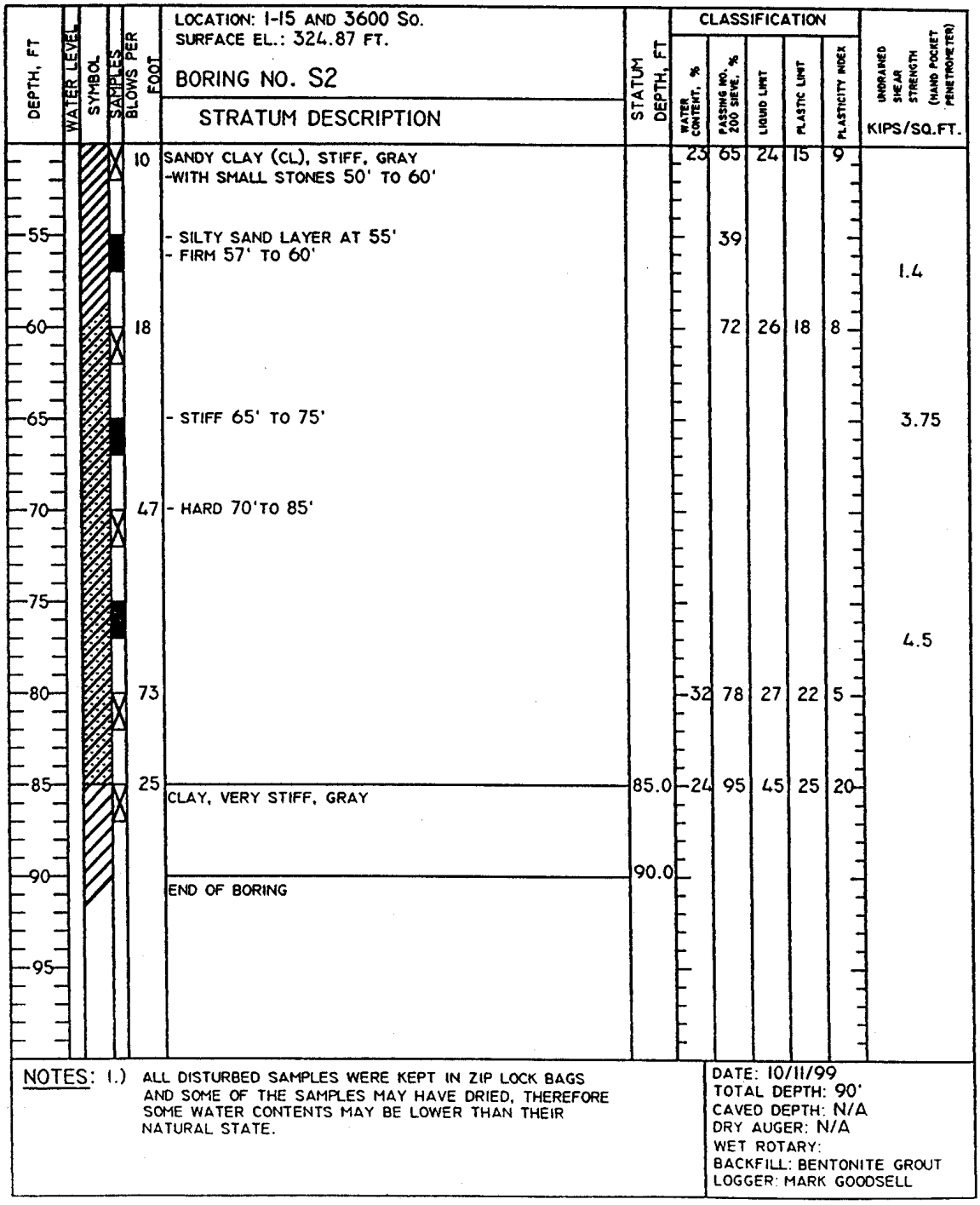


Figure 3.8 Log of boring S2 (sheet 2).

Figure 3.9 ATV drill rig.

inches. Table 3.1 shows which samplers were used in the various borings, the sample labels, and the number of samples obtained with each sampler.

Boring logs and locations are shown in Figures 3.10 (HS-1), 3.11 (HF-2), 3.12 (RS-3), and 3.13 (RF-4). The first two borings were drilled using a continuous-flight hollow-stem auger. Sampling started at 9-½ feet. The top 3 or 4 feet consisted of fill and desiccated material. Samples were taken at 30-inch intervals, and the same pattern was followed for each borehole. Sampling depths were as follows: 9-½ to 11-½, 12 to 14, 14-½ to 16-½, 17 to 19, 19-½ to 21-½, 22 to 24, 24-½ to 26-½, 27 to 29, 29-½ to 31-

½, 32 to 34, and 34-½ to 36-½ feet or refusal. The driller pushed the tubes hydraulically at a steady rate of approximately one foot every 10 seconds. To allow room for possible slough and the sampler head in the tube, the driller only pushed the tubes for 24 inches. All samples were allowed to sit for at least five minutes in the hole before extraction to aid in recovery.

The first hole was drilled on February 5, 2001. The weather was sunny with temperatures in the 50s. The samples from the first hole were taken with a shelby tube sampler. After the boring was advanced to 11-½ feet, the boring was kept full of water to prevent a blow-out in the bottom of the hole. On the 19-½ to 21-½ sample, the tube extracted after 5 minutes with no recovery. The driller noticed that it was primarily sand or silt at this depth. He suggested trying to recover the sample with his piston sampler. That was attempted and the entire sample was recovered. This sample was labeled disturbed. The setup and use of the shelby tube sampler was very fast and easy. At the 34-½ to 36-½ interval the soil got stiff refusal occurring at 36 feet. Eighteen inches of sample was recovered in this sample including slough. The end of the tube was severely

Table 3.1 List of borings.

| Sample Label | Drilling Method | Sampler | Boring Number | Number of Samples |
|---|---|---|---|---|
| HS-1 | Hollow stem auger | Shelby | 1 | 11 |
| HF-2 | Hollow stem auger | Fixed-piston | 2 | 3 |
| HF-2P | Hollow stem auger | Free-piston | 2 | 7 |
| RS-3 | Rotary wash | Shelby | 3 | 11 |
| RF-4 | Rotary wash | Fixed-piston | 4 | 3 |
| RF-4P | Rotary wash | Free-piston | 4 | 8 |

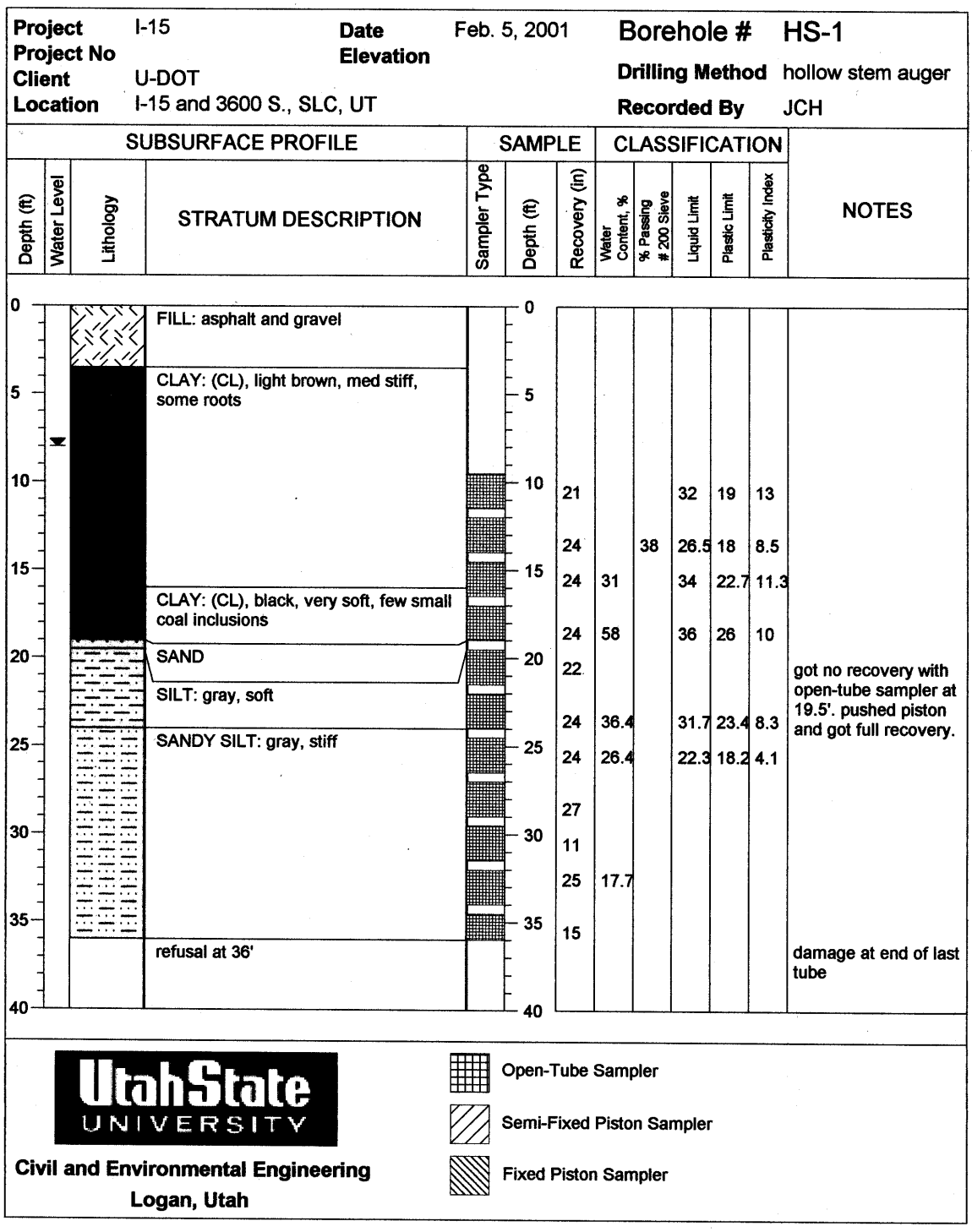


Figure 3.10 Log of boring HS-1.

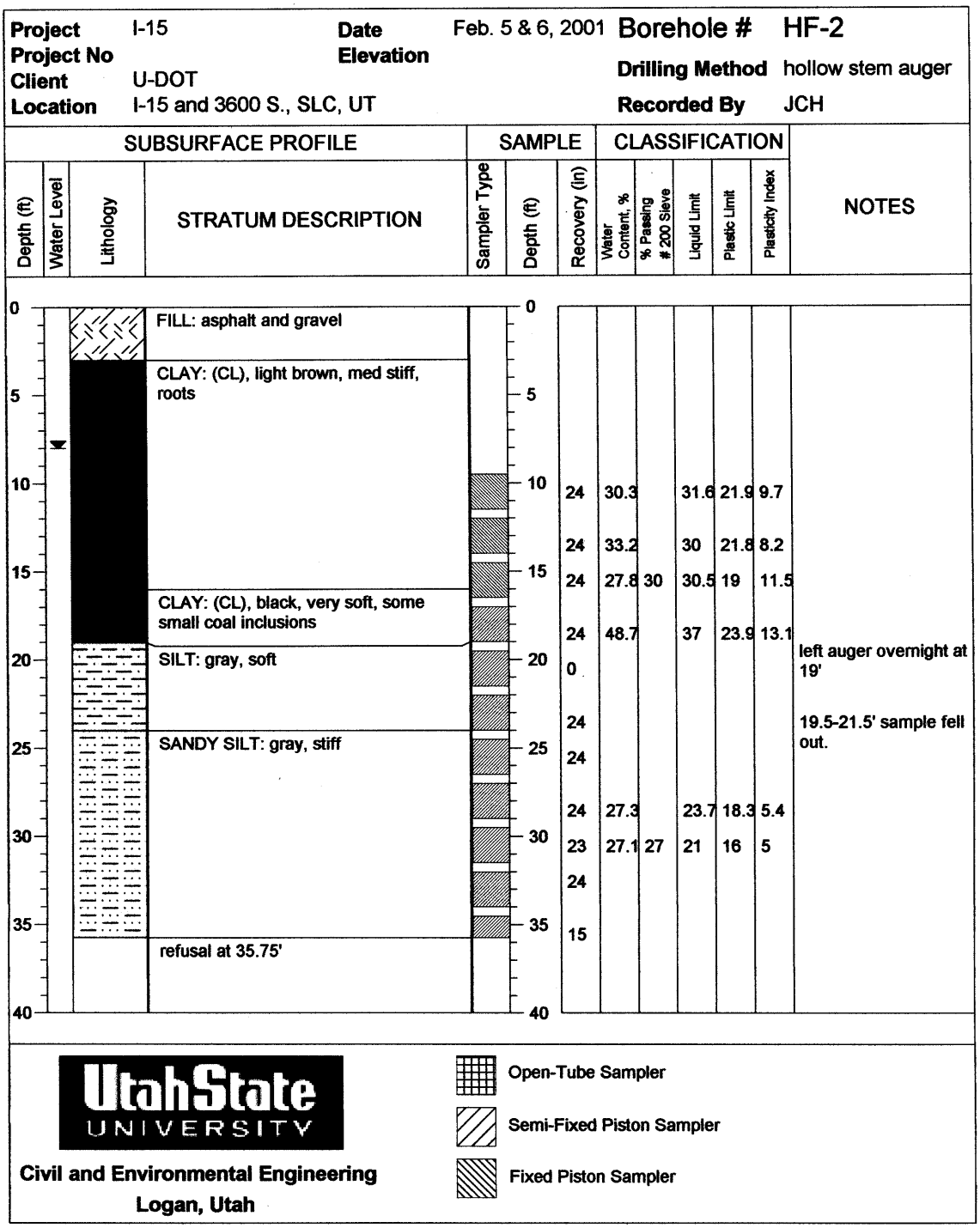


Figure 3.11 Log of boring HF-2.

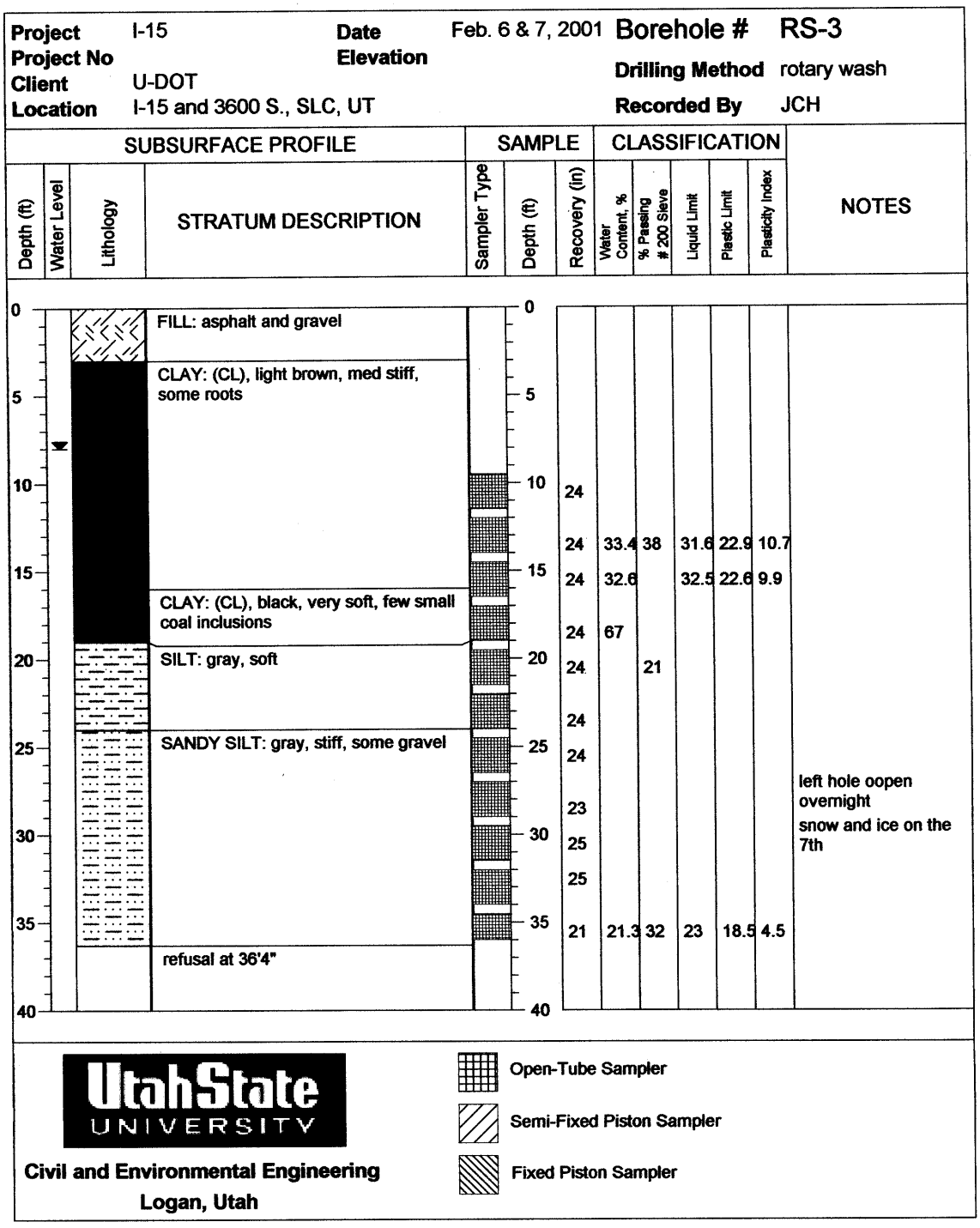


Figure 3.12 Log of boring RS-3.

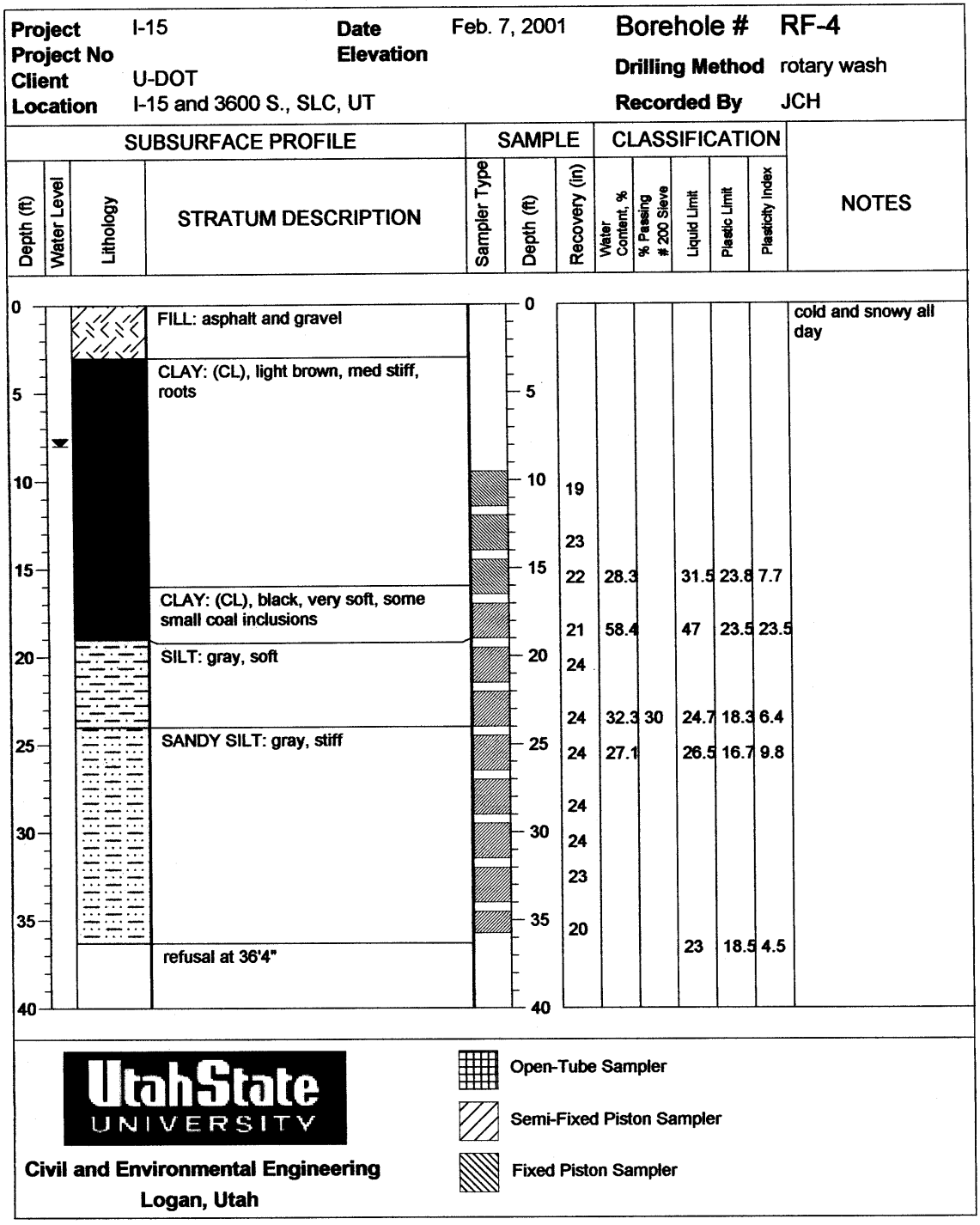


Figure 3.13 Log of boring RF-4.

damaged and imprints of large gravel were seen in the clay at the bottom of the tube. It was determined that this was the stiff layer encountered in the 1999 exploration. The hole was backfilled with compacted cuttings and mud.

The second borehole was placed seven feet from the first. Drilling of this borehole began on February 5, and concluded the next day. The first three samples in this hole were taken with the fixed-piston sampler. Assembling and using this sampler was a complicated process. Full recovery was obtained in all three samples. At a depth of 17 feet, the fixed-piston sampler became too cumbersome, so all deeper samples were taken with the free-piston sampler. After recovering a sample at 17-19 feet it became too dark to continue. The auger was left in the hole at 19 feet so that there would still be some overburden pressure applied to the soil at 19-½ feet, which was to be sampled the next day. There was probably still some pressure relief.

On the next day, February 6, the second borehole was continued. The weather was colder with frost on the ground in the morning, but it warmed up to the 50s later in the early afternoon. Refusal occurred while pushing a sample at a depth of 35-feet 9-inches. The end of this tube was bent from gravel. The tube also fell over while wax was drying in it. It was labeled disturbed. This borehole was also backfilled in the same manner as the first.

Drilling on the third borehole commenced upon completion of the second. The rotary wash technique was used in this borehole. The driller used one flight of the hollow stem auger as a casing for the first five feet. A “medium” mixture of bentonite and water was used for the drilling fluid. A pump on the ATV pumped the fluid down through the drilling rods. At the bit the mud came out and carried cuttings to the surface. A pipe

attached to the top of the auger carried the mud and cuttings to a strainer in a settling bucket in a large tub shown in Figure 3.14. Mud was recirculated from the tub into the hole. The driller could tell if mud was being lost through seepage by the change in depth of the mud in the tub. The driller frequently cleaned out the strainer and checked the cuttings to see what kind of soil was being encountered in the borehole. The driller said that some drillers use the cuttings to determine the depth a certain soil is encountered, but this can be erroneous because considerable time can elapse between when the soil is cut and when it arrives at the strainer. The driller advanced the bit slowly in order to avoid applying too much pressure to the soil. One problem with the rotary wash method is that the hole is no bigger than the sample tube. When lowering the tube in the hole, it can shave the sides letting unrepresentative cuttings enter the tube. This is especially true if a shelby tube sampler is used and the tube and drill rods are not pushed perfectly straight.

Samples from the third borehole were taken with a shelby tube sampler. Sampling stopped for the day after the 24-½ to 26-½ foot sample was taken. Weather was overcast and in the low 30s at that time. It began to snow when the last sample was pushed. The next morning, February 7, there was two inches of snow on the ground and most equipment was frozen. It snowed throughout the day. A makeshift tent was set up for the waxing operation. The third borehole was finished with refusal occurring at a depth of 36-feet 4-inches. No sampling problems were encountered. It was backfilled with mud and cuttings as before.

The fourth borehole was also drilled using the rotary wash method on the same day as the third borehole. Sampling in this hole was done in the same manner as for the second borehole, with the fixed-piston sampler used for the first three samples. The free-

Figure 3.14 The casing and tub with strainer for the rotary wash method.

piston sampler was used for the remainder of the samples. Refusal occurred in the fourth borehole at a depth of 36-feet 4-inches. The borehole was backfilled with drilling fluid and cuttings.

## 3.4 Sample Waxing

After each tube was extracted from the hole, the outside of the tube and the exposed inside surfaces of the tube were cleaned with a rag. A wax mixture of 50 percent bee's wax and 50 percent paraffin wax was melted in a pot over a gas flame at the site.

At least ½ inch of hot wax was poured into the top of the tube as shown in Figure 3.15. When it had cooled and hardened, the tube was turned over. A glazing tool was used to clean out ½ inch of soil from the bottom of the sample, and hot wax was poured in its place.

Problems occurred with the wax shrinking in the tube when it cooled. Different ratios of bee's wax to paraffin wax were tried, but the shrinking still occurred. It was determined that the cold weather was aggravating the shrinking problem. To get a better seal, the wax was worked into the spaces with a finger until a suitable bond with the tube was achieved.

When the wax was hard, caps were placed on the ends of the tube. The caps were taped with electrical tape, which provides a more airtight seal than duct tape. The caps were marked with a permanent marker "bottom" or "top" and included the boring label and sample depth.

## 3.5 Sample Transport and Storage

After the sample tubes were sealed, they were placed in special padded boxes shown in Figure 3.16 for transportation back to Utah State University. The boxes were tied to the bed of a pickup truck. Driving the 80-mile trip was done cautiously and slowly in order to avoid unnecessary shocks and jolts.

Sample tubes were stored at the end of each day upright in the laboratory at the university. There is a humid closet in the lab for curing concrete samples, and it was considered to store the soil in the closet. However, the humidity in the closet was so high that it was thought that it might have adverse effects on the soil. Tubes stored in the lab

Figure 3.15 Waxing operation.

were placed in a secure corner where they would not be bumped or knocked over until sample tube racks could be built to store the samples.

Figure 3.16 Tube transport boxes.

# CHAPTER 4

# X-RAYING SOIL SAMPLES

## 4.1 Introduction

After the soil samples were brought back to Utah State University from the field they were x-rayed. Each tube was x-rayed in three 10-inch segments covering the entire tube. X-rays were taken with the objective of characterizing the soil and locating any visible disturbance. It was found that the x-rays were very useful in identifying fractures caused by sampling disturbance. The x-rays were taken and analyzed before any laboratory tests were performed. The x-rays were used to locate the soil in the tube that would provide the best specimen for testing. X-rays worked very well for this. This chapter will describe in detail the x-ray procedure and explain how the x-rays were used to identify disturbance and the type of soil in the sample tubes.

## 4.2 Safety

In accordance with university regulations, prior to using x-ray equipment, James Bay, Ken Jewkes, and Jon Hagen attended a radiation safety training session that outlined the basics of radiation safety and required safety procedures. Each person using the equipment was required to wear two radiation dosimeters. One was worn on the belt and the other was a ring worn on a finger. These dosimeters measure the amount of radiation a person is exposed to. Ken Jewkes was the person operating the x-ray machine because, according to university regulations, students are not allowed to operate the machine. Jon Hagen developed the x-rays while Ken ran the machine.

The x-ray machine shown in Figure 4.1 is located in the Technology building at Utah State University. Students and professors use the machine to x-ray welds. Reed Nielsen, associate professor in the Industrial Technology and Education (ITE) Department, explained the operation of the x-ray machine and offered advice on the process. He also went over some guidelines that he uses to ensure that x-raying was safe and efficient.


Figure 4.1 X-ray machine in the Welding Engineering Lab at Utah State University.

## 4.3 X-Ray Procedure

Sample tubes were taken to the Technology building in the padded transport boxes with a dolly. To hold the tubes in place during x-raying, a wooden frame, shown in Figure 4.2, was made that would fit the tube and make it easier to make exposures from the same plane in every shot. The tube that would be x-rayed was placed horizontally on the frame. In order to ensure that the x-rays were all taken from the same direction, the tube was rotated so that the seam of the tube was flush with the tops of the front brackets in the frame. All x-rays were taken from this angle.

The x-ray film used was Kodak AA film. The dimensions of the film are 4x10 inches. The film is loaded in a darkroom. The sleeves that hold the film are made in such a way that the film cannot be exposed to light. In the sleeve there is a 0.01-inch thick sheet of lead placed on top of the film and a 0.005-inch thick sheet below the film. The sleeve is taped shut with a piece of masking tape. The tape is then marked "AA" to tell that the sleeve is loaded with AA film. After the film is exposed, "EXP" is written on

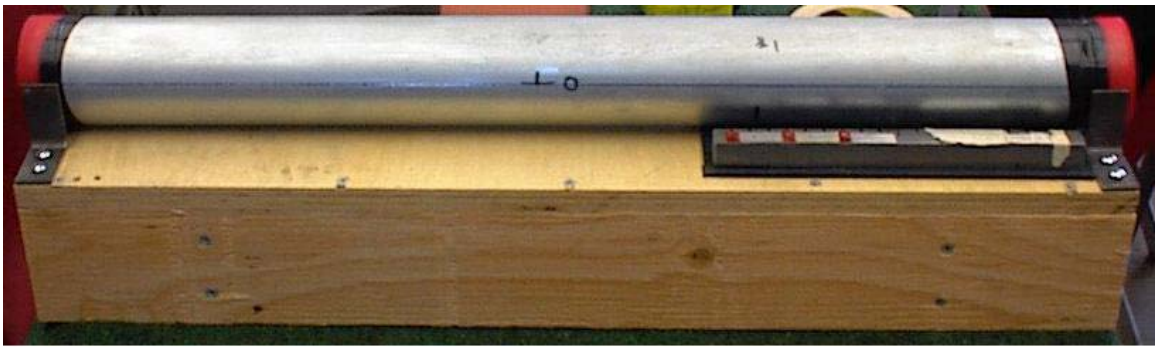

Figure 4.2 Frame with sample tube, film, ruler, and lead letters.

the tape to tell that the film is exposed and ready to be developed. These procedures help prevent exposing of the film by opening the sleeve in the light.

The tubes are of such a length that three x-rays are needed for each tube. Each x-ray overlaps by about one inch. The film is placed between the tube and the frame, and marks are made on the frame so that the film would be placed in the same location every time. A ten-inch long piece of 5/8-inch square steel was used as a ruler in the x-ray. Slits were cut in the steel every ½ inch. These slits would allow x-rays to pass through and expose the film while the rest of the bar would prevent passage. This bar is placed on top of the film next to the tube. The 5-inch mark is aligned with the centerline of the film and a corresponding mark is made on the tube so that features on the x-ray image could be located exactly on the tube.

Lead letters were used to identify each exposure. Each exposure has the letters "USU GEOT" to identify the project that the x-rays belong to. Also included are letters to identify the sample and the exposure used. For example, the set of letters on one tube is, "USU GEOT HS1 5TA." "HS1" identifies what boring the sample is from. "5" identifies the sample depth, which in this case is 19-1/2 to 21-1/2 feet. There are 11 sample tubes from each borehole. A "1" signifies that the sample is from 9-1/2 to 11-1/2 feet and so on to "11", which signifies a sample from 34-1/2 to 36-1/2 feet. The "T" in the identification tells that the x-ray is from the top third of the tube. An "M" would signify the middle third, and a "B" would signify the bottom third of the tube. The last letter, "A", tells that it is the first exposure of that part of the tube. Subsequent exposures of the same place would be labeled "B, C, D," etc. Also placed over the steel bar were penetrometers (pennies). Holes in the penetrometer that show up in the x-ray image

indicate that a detail of that size would show up in the image. If a hole from a "10" penny shows up, it means that a detail that is 0.010-inches will show up. This is a method of determining image quality. However, after a few exposures it was decided to not use the penetrometers. The holes were not showing up and provided no useful information.

When the sample is set up and ready for exposure, it is placed in the x-ray machine. The frame is placed directly under the x-ray tube at the desired focal distance. A plumb bob is used to line up the center of the x-ray tube with the centerline of the film and sample tube. The door is then closed. The machine is turned on with a key and the exposure time is set on the control panel shown in Figure 4.3.


Figure 4.3 X-ray machine control panel.

The amperage is set at 5 mA and a button is pushed to start the machine. When the x-raying starts, the voltage is set to the desired level. The machine will automatically turn off if the time is up or the voltage is set higher than 150 kV. If the door is opened, the machine will also turn off. The only way that a person can get exposed to radiation is to get under the machine, which is nearly impossible. A red light flashes at the top of the machine when x-rays are being emitted.

Each exposure was logged in a logbook, which has been reproduced in Appendix B. After the exposure time lapses, the machine automatically turns off. The tube can then be taken from the machine. "EXP" was written on the film sleeve and the next exposure was prepared.

## 4.4 Developing Procedure

A similar process for developing photographs is used for developing radiographs (x-rays). The exposed film is taken into a darkroom illuminated with only red light. Figure 4.4 shows the tanks in the darkroom used for developing the x-rays. These tanks are maintained at a constant temperature of 68 degrees Fahrenheit. The film is taken out of the sleeve and clipped onto a film holder. The film is then placed for five minutes in a container filled with developer. The film is shaken lightly for the first 30 seconds while most of the reaction takes place. This prevents bubbles from collecting on the film. Bubbles would prevent developer from getting to the film and would cause light spots. After 5 minutes in the developer, the film is transferred to water for rinsing for 1 minute. The film is then transferred to a container filled with a fixer chemical and allowed to soak for 5 minutes. When the film is in the fixer, it is all right to open the door of the

darkroom. After the fixer, the film is again placed in water to rinse. This is done for approximately 15 minutes. The longer it rinses, the longer the x-ray will last. Fifteen minutes was thought to be sufficient for the time that the x-rays would be needed. After rinsing in water, the film is rinsed for a minute in a chemical that prevents spots from forming when the x-ray is drying. The film is then taken out and hung to dry.

When the developing chemicals wear out, they lose their ability to develop the film, and images become lighter. After 2 weeks of x-raying, the chemicals wore out and exposures were transparent. After changing the chemicals, x-rays with the same exposures as before were too dark. This was because the chemicals were not working at full strength to begin with. The exposure time and voltage were then lowered until a suitable exposure was found.


Figure 4.4 Developing tank in darkroom.

## 4.5 Exposure

Since Reed Nielsen had not had experience with x-raying soil in tubes before, he could only give advice on the exposure to use. A trial and error process was required to obtain the optimum exposure. In this section, the process of determining the optimum exposure is explained as well as several problems encountered in the process.

The trial and error process for finding the correct exposure parameters started with a focal distance of 18-1/2 inches for 7 minutes, an amperage of 5 mA, and a voltage of 150 kV. The first negative came out too dark, with a film density of nearly 4. For the second trial, it was decided to increase the focal distance to 36 inches and keep the time at 7 minutes. The negative came out lighter, with a film density of about 2, but was still slightly too dark. A film density of about 1.8 or 1.9 would give the best detail. The next trial was at 36 inches for 6 minutes, and this gave the desired detail. When this was determined to be the correct combination of parameters, the frame was made so that the film would always be at the same focal distance. Subsequent shots were then made and resulted in equal quality.

All of the sample tubes from boring HS-1 were successfully x-rayed at the same exposure. After a few days, tubes from boring RF-4 were then taken to be x-rayed. At the same exposure the negatives turned out transparent. This is when the developing chemicals wore out. After the chemicals were changed, the same exposures resulted in negatives that were totally opaque. Exposure times were then brought down to 4, 3, 2, and 1 minute. The x-rays were still too dark and details were grainy. At 1 minute, the features on the x-ray could be seen, but the x-ray was very grainy and of poor quality. Exposure times of 45 and 30 seconds showed no improvements. It was determined that

the film had been exposed. This was proven when film was developed without being exposed in the x-ray machine. The negative came out completely opaque. Film from this package was no longer used. Using new film, new exposure levels were obtained. It was determined that with good film and good developing chemicals, an exposure of 5 mA and 135 kV for 2 minutes at 36 inches gives a good quality image. All of the remaining sample tubes were exposed in this manner.

## 4.6 Results

Satisfactory x-rays were the result of a trial-and-error process to find the correct exposure. A sacrificial sample tube was used along with its x-rays to see what features in the x-ray actually were. By doing this, the soil in all of the sample tubes was classified. Typical x-rays in this section show some of the important features found in the x-rays.

Upon inspecting x-ray images of soil, sands, gravel, and clay can be distinguished. In radiography, the more closely packed the specimen, the lighter it will appear in the negative. Therefore, sand shows up darker than clay. Clay is then darker than gravel. The top of the tube where there is no sample will be completely black, whereas a wax seal may appear very slightly lighter.

The x-ray negatives can be examined using a light table. The x-rays in Figures 4.5a and 4.6a were scanned from 35-mm negatives of the x-ray negatives. In the images the steel ruler with the outlines every half-inch is easily seen. In both images the lead letters that tell from what sample the images were taken are not seen in the figures but are seen in the actual x-rays. The details in the x-rays are not seen as well in the figures as

they would be by directly viewing the x-ray with a light table. All of the x-ray images were scanned with a transparency setting and are presented in Appendix C.

Figure 4.5 shows an x-ray and photograph from the bottom of a hollow stem auger, shelby tube sample at 19.5-21.5 feet. This is designated "HS1 5BA." Figure 4.5a is a typical x-ray of the bottom section of a sample tube. Figure 4.5b is a photographic image of the same specimen split down the middle after it was extruded. The image in Figure 4.5a is mostly a medium dark gray, indicating that most of the tube is clayey silt. At the bottom of Figure 4.5a is a thin layer of clay that can be seen in the bottom of the photograph in Figure 4.5b.

The images in Figure 4.6 come from the middle of the same sample tube and are designated "HS1 5MA." One prominent horizontal streak in Figure 4.6a indicates a fracture. The dark, horizontal line near the middle of Figure 4.6b is the same fracture. Gravel was found throughout the sample. These are seen as the light spots near the middle of Figure 4.6a.

Figure 4.7 is an x-ray from the middle of the hollow stem auger, fixed-piston sample tube at 12-14 feet designated HF2 2MA. Running vertically down the x-ray are dark lines that indicate roots or holes where roots once were. The photograph in Figure 4.8 shows the roots in the soil sample when it is split down the middle. Roots were important to identify because samples with roots cannot be back-pressure saturated in a CRS test. These samples need to be avoided. This is discussed further in Chapter 5.

One problem encountered had to do with vertical or nearly vertical layers of material. Some samples from the deeper depths had ¼-inch layers of sand and clay at an angle of nearly 45 degrees. By chance, the x-rays were shot perpendicular to the plane of

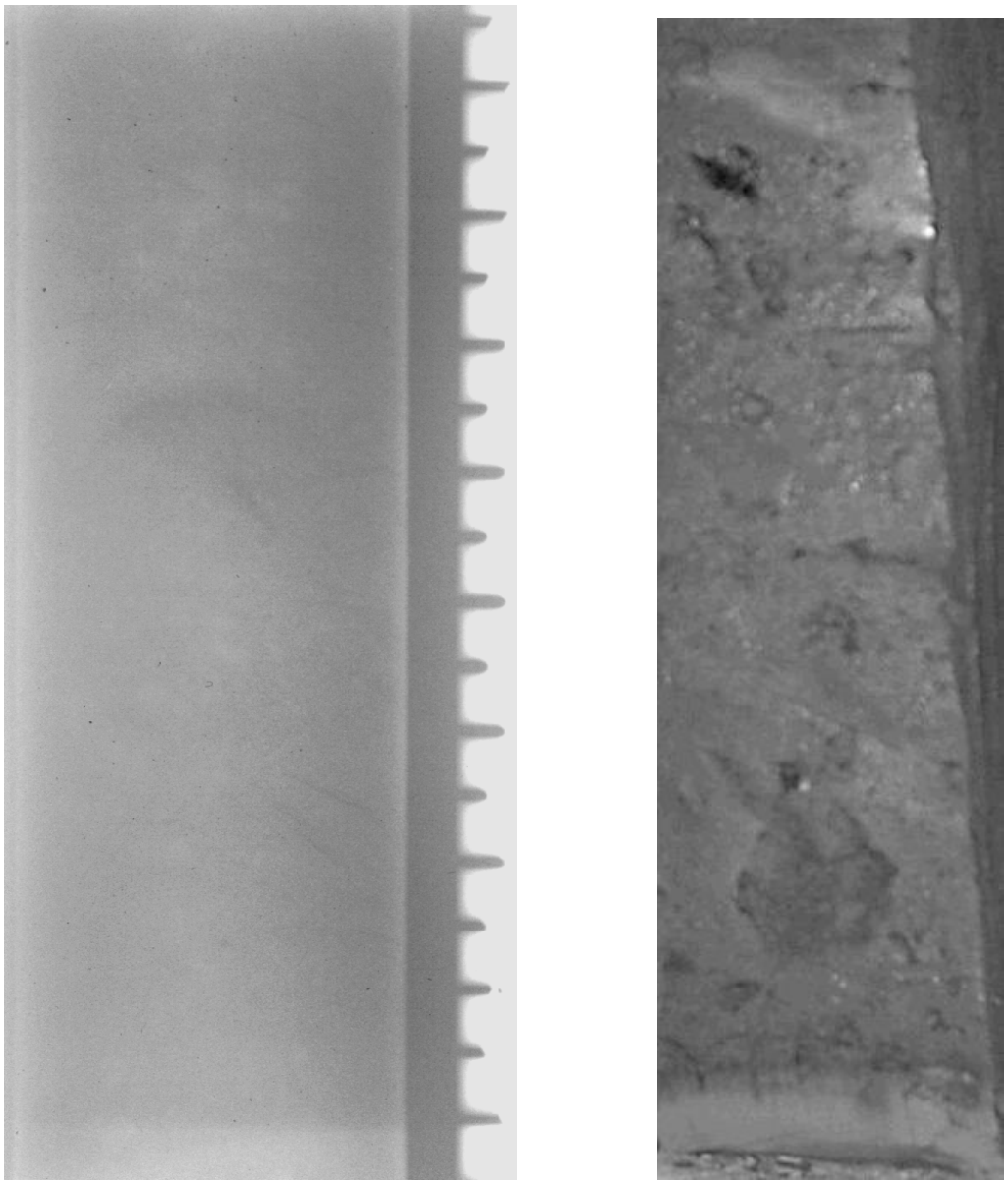

a) X-Ray image b) Photographic image

Figure 4.5 Images of the bottom of the hollow stem auger, shelby tube sample at 19.5-21.5 feet designated as HS1 5BA.

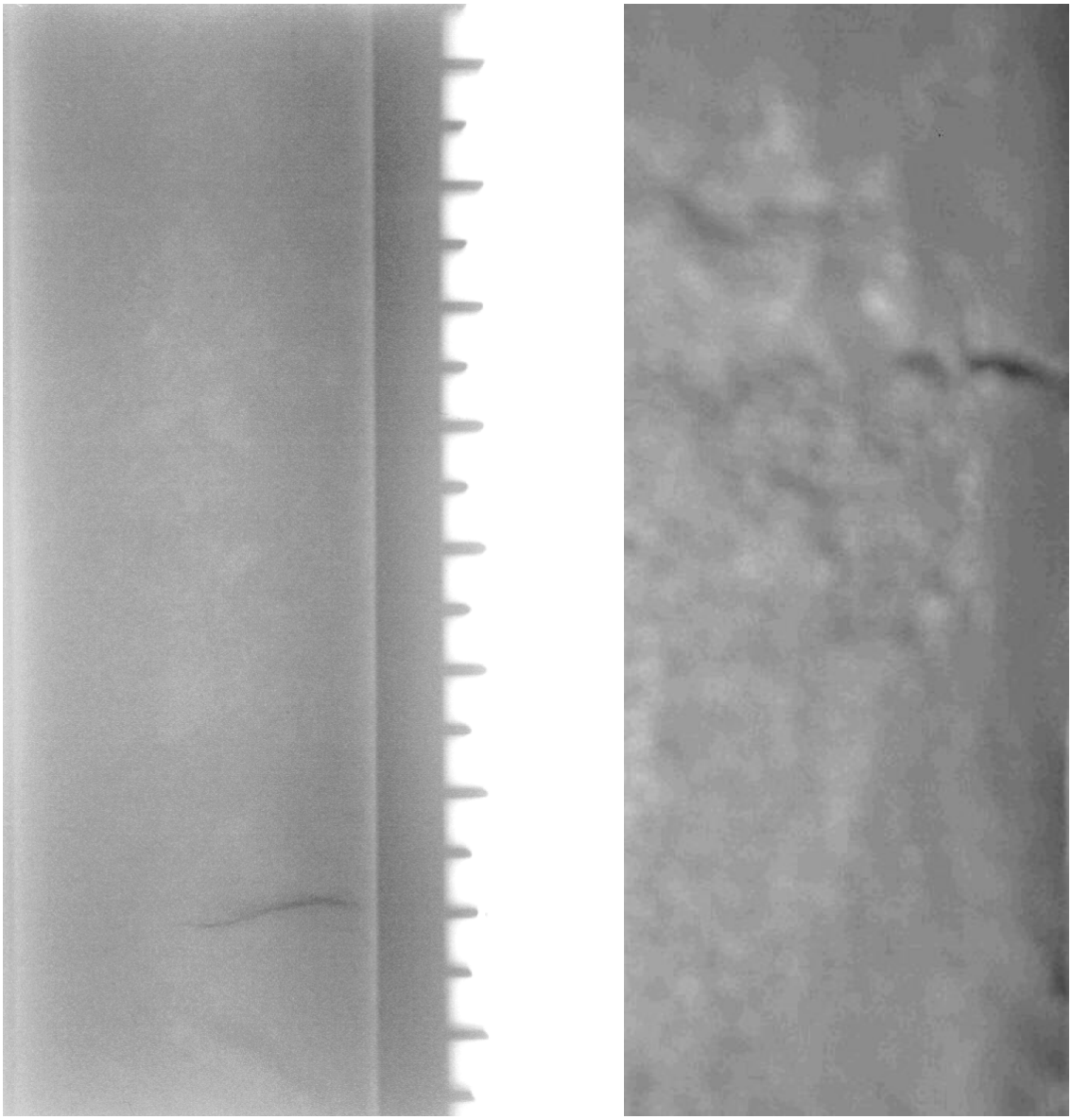

a) X-Ray image b) Photographic image

Figure 4.6 Images of the middle of the hollow stem auger, shelby tube sample at 19.5-21.5 feet designated as HS1 5MA.

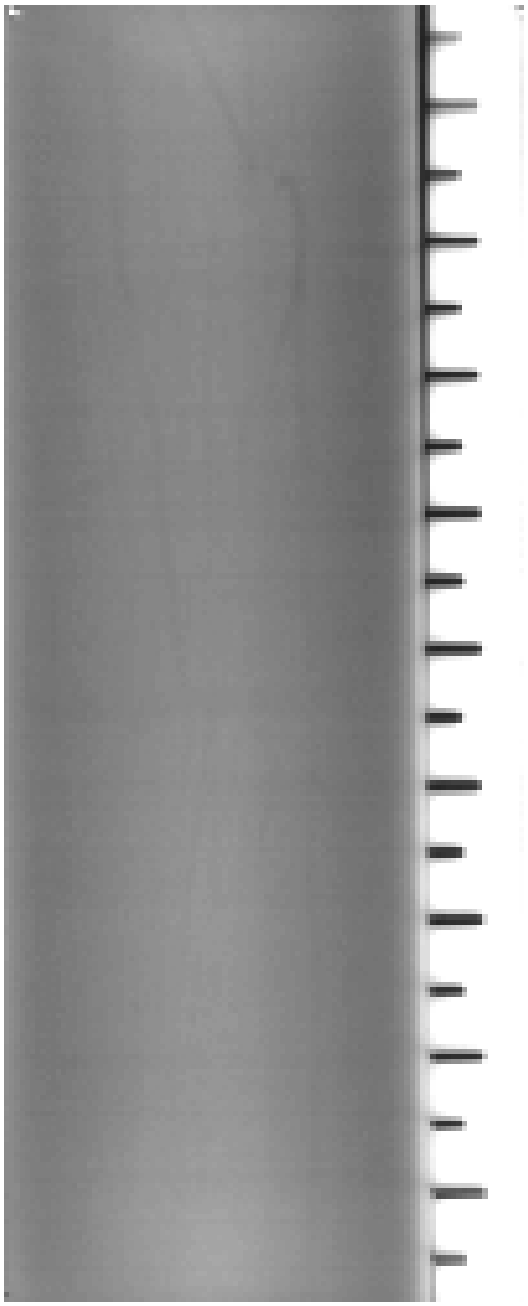

Figure 4.7 Images of the middle of the hollow stem auger, fixed-piston sample at 12-14 feet designated as HF2 2MA.

Figure 4.8 Soil with roots from the hollow stem auger, fixed-piston sample at 12-14 feet.

the layers. The images, therefore, showed up as one homogeneous material. Had the tube been oriented in the x-ray machine so that the x-rays were shot parallel to the planes then the image would have shown the alternating layers at 45 degrees. A solution to this problem would be to take one x-ray and then rotate the tube 90 degrees and take a second x-ray of the same location.

The results from x-raying were very useful in the research. Using the x-rays, it became easier to locate and trim samples without extrusion. A rough classification of the strata could be made and fewer samples were wasted because of the elimination of the trial and error process of locating a specimen. Disturbances resulting in fractures were also located and used to analyze sampling methods. Details of this analysis are given in Chapter 6.

# CHAPTER 5

# CRS TESTING

## 5.1 Introduction

After the x-rays were developed and analyzed, soil testing began. The laboratory tests were as important as the sampling process and x-rays for determining the effect of sampling method on the soil. Ten samples from the 1999 exploration and 19 samples from the 2001 exploration were tested. This chapter explains how the samples were trimmed and the parameters used for the tests. The most important results from these tests are the strain versus the log of effective stress, strain versus effective stress, and modulus versus effective stress curves for which examples and explanations are given in this chapter.

## 5.2 Trimming Techniques and CRS Setup

Significant disturbance can occur during trimming and setting up the test. Prior to testing the samples from this research, the procedures and techniques were practiced and improved upon using other samples until trimming and setup could be done with minimal disturbance. The procedures outlined in this section were determined to be the best way to trim and set up the samples for testing.

To set up the CRS consolidation tests, homogeneous samples are located using x-rays. Sections of 2.5 to 3 inches are marked off on the tube and cut with a manually turned pipe cutter. This sample tube cutter is shown in Figure 5.1. The tube is then slowly cut lengthwise with a band saw. When the tube is cut, it spreads apart slightly allowing room for the sample to be taken out. The specimen is then carefully taken out

Figure 5.1 Sample tube cutter at Utah State University.

and trimmed into a stainless steel consolidation ring with a wire-trimming tool. The diameter of the ring is 2.5 inches and the height is 1 inch. The stainless steel consolidation ring has a sharp edge on one end and is advanced into the soil specimen about 2 millimeters at a time by slightly applying pressure to it. This trimming procedure and the consolidation ring are shown in Figure 5.2. After each small advance, the excess soil is trimmed. A small amount of grease applied to the inside of the ring reduces friction with the soil as the ring is advanced. The ring is advanced to the middle of the specimen and excess soil at the ends is then trimmed and used for water content and Atterberg limit measurements.

CRS testing was done on a Sigma-1 load frame built by Trautwein Soil Testing Equipment shown in Figure 5.3. The ring with soil is placed between porous stones with filter paper and set in a ring for loading. It is then placed in an acrylic cell with a frictionless piston on the top. The piston comes in contact with a 2.5-inch diameter

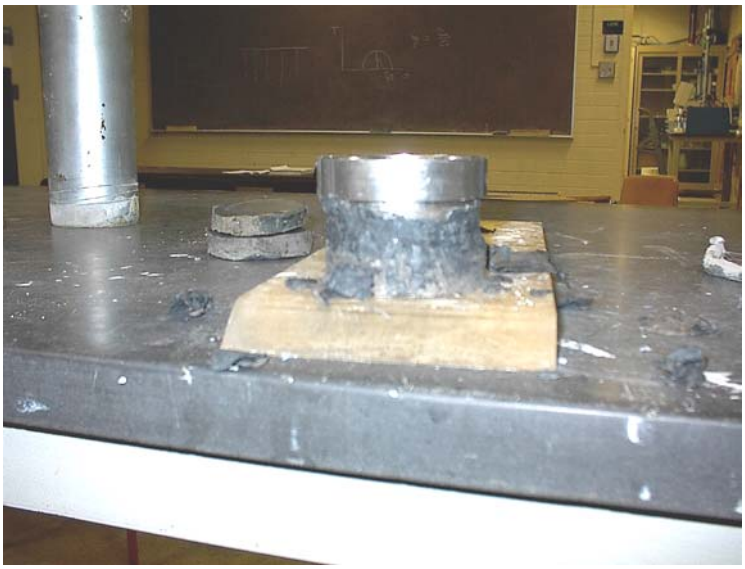

Figure 5.2 CRS combined trimming and consolidation ring.

acrylic cylinder that is placed over the porous stone. Initial contact between the piston and load frame is made. After initial contact the piston is seated on the sample until 0.2 percent strain was attained.

The cell is next filled with de-aired water and backpressure saturation is performed to ensure a saturated sample. The strain is held constant while backpressure saturation takes place. Backpressure saturation is accomplished by increasing the pressure in the cell while measuring the pore pressure. Pressures are measured with pressure transducers attached to the cell and the bottom of the specimen. Pressure is added to the cell by means of a panel board with pipettes connected to an air compressor. The pressure in the pipette is read on the panel board and then the valve for the line leading to the cell is opened. In this way, an instantaneous pressure increase is applied.


Figure 5.3 CRS test cell and loading frame.

Pressure is raised is 10-psi increments. The increase in pore pressure is then read. A separate line from the panel board to the bottom of the specimen is used to equalize the pore and cell pressure between increments. Pressure is raised to at least 60 psi. The goal of backpressure saturation is to achieve a B value of close to one. The B value is the increase in pore pressure divided by the increase in cell pressure.

## 5.3 Test Parameters

The different strain rates and testing procedures used can have effects on sample disturbance. In order to come up with the best testing parameters, trial tests were run on

similar soils. Results from these preliminary tests were examined and adjustments were made until satisfactory parameters were found. These are outlined in this section.

Loading was done at a rate of strain of 4.5 percent/hour for samples from borings HS-1, HF-2, RS-3, and RF-4. A strain rate of 2.5 percent/hour was used for samples from borings I2 and S2. To achieve these strain rates, the load frame moves at a rate of 0.045 inches/hour and 0.025 inches/hour, respectively, for a 1-inch specimen. ASTM (D 4186, 1998) recommends that the pore pressure ratio be kept between 3 and 30 percent. This is the ratio of the pore pressure divided by the total vertical stress. Trial tests were run to make sure that a 4.5 percent/hour strain rate would not cause a pore pressure ratio in excess of 30 percent. The load on the specimen is taken with a 2000-pound external load cell. A linear voltage displacement transducer (LVDT) attached to the load frame measures displacements. Values of maximum allowable strain and load are input into the computer program. If the strain or load exceeds the maximum values, the load frame will stop moving. The load frame is also capable of performing an unload and reload cycle. The unload cycle in these tests was set to last for one log cycle for most tests. Fifteen minutes of creep was allowed before unloading and reloading.

Readings of load, displacement, and pressures are taken by the computer every minute. Output for the program is given in spreadsheet format in terms of voltages. A spreadsheet template was made that each output file could be pasted into. The voltages are converted in the spreadsheet to actual values by using calibration factors. Values of strain are found by dividing the displacement by the original height. Effective stress is calculated as well as the tangent modulus. Results of each test are plotted and shown in Appendix E.

## 5.4 Results

The three main curves that were sought after for this research were the strain vs. the log of effective stress, strain vs. effective stress (linear), and effective stress vs. modulus curves.

CRS tests were performed on ten samples from the 1999 exploration (borings I2 and S2). These tests were done at a strain rate of 2.5 percent/hour. Testing went on during July and August of 2000, 10 months after the samples were taken. It was difficult to obtain specimens that were easy to be trimmed because of sand and silt seams as well as gravel inclusions. X-rays were not available to view these samples before they were cut and trimmed.

Nineteen CRS tests were performed on samples from the 2000 exploration (borings HS-1, HF-2, RS-3, and RF-4). The strain rate of 4.5 percent/hour was used for these tests. Trimming and testing of these samples was done promptly after x-raying was completed. It was significantly easier to trim and test these samples.

Typical curves from the same test are given in Figures 5.4, 5.5, and 5.6. Figure 5.4 is a curve of strain versus the log of effective vertical stress. Figure 5.5 shows a linear plot of strain versus effective vertical stress. Figure 5.6 is a curve of effective vertical stress versus modulus. Values of maximum past pressure can be determined from these curves as explained in the literature review. Results of all of the tests are given in Appendix B.

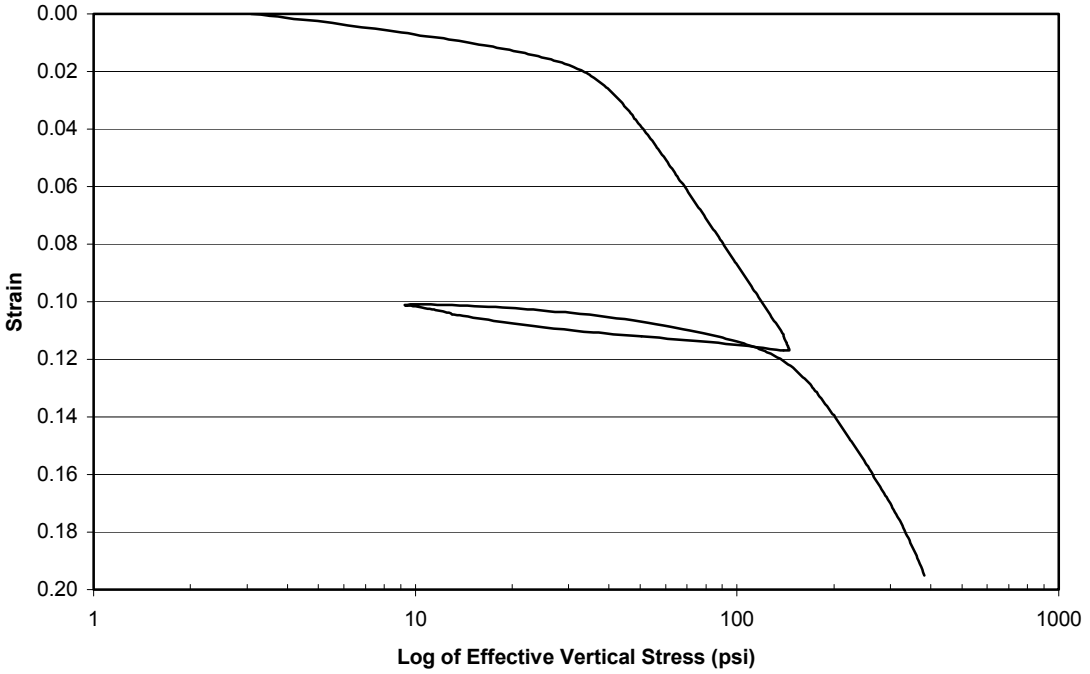


Figure 5.4 Curve of strain vs. the log of effective vertical stress for a shelby tube, rotary wash sample at 14.5-16.5 feet.

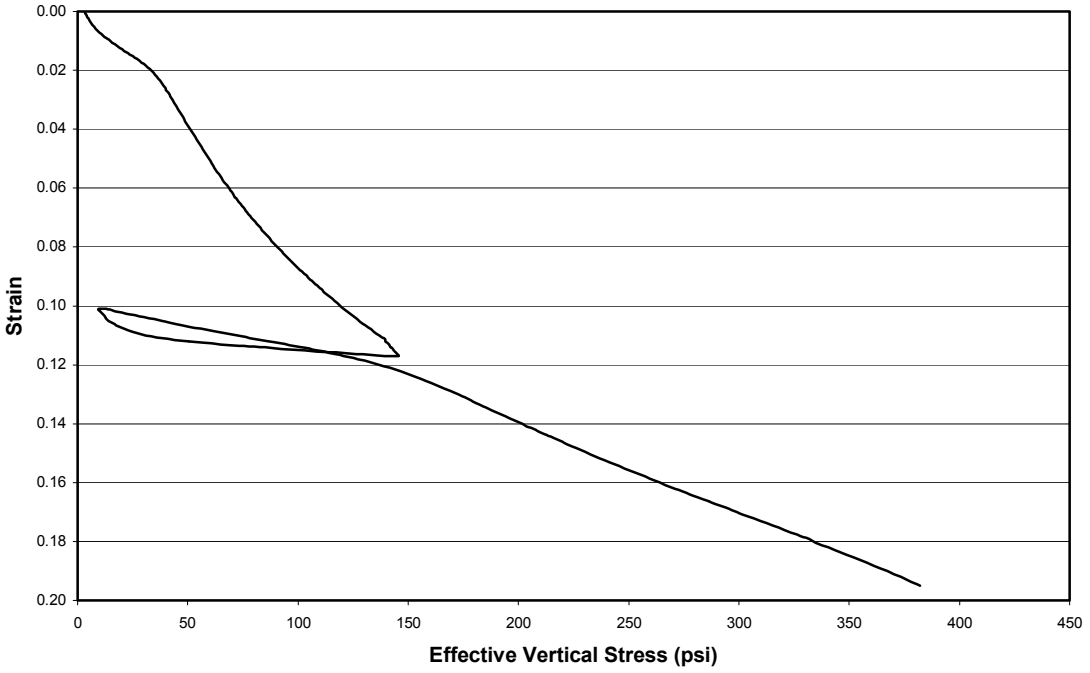


Figure 5.5 Linear curve of strain vs. effective vertical stress for a shelby tube, rotary wash sample at 14.5-16.5 feet.

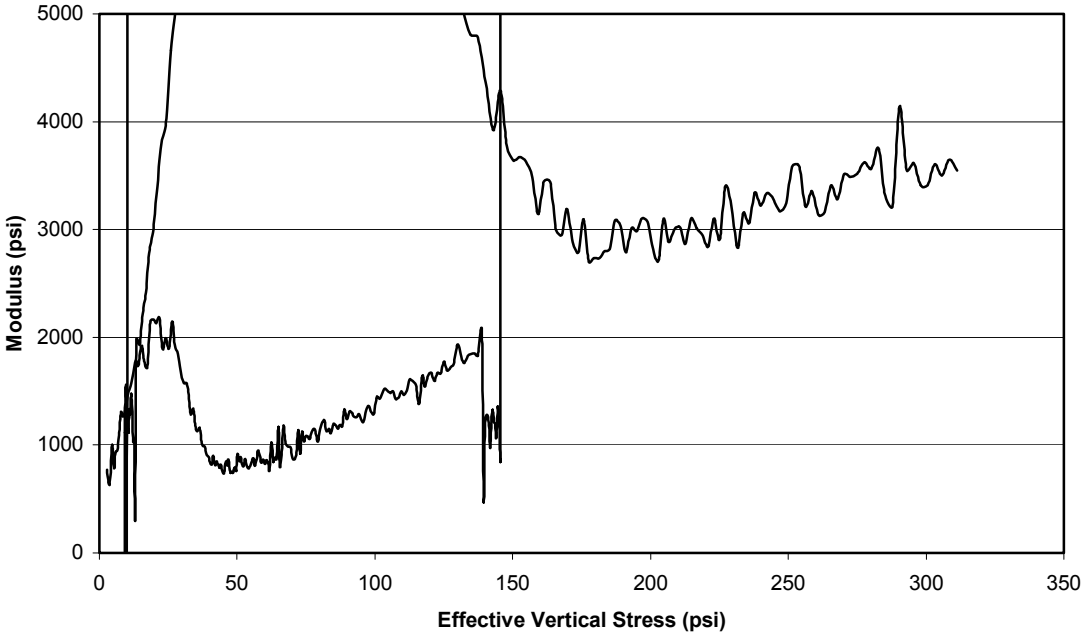


Figure 5.6 Curve of modulus vs. effective vertical stress for a shelby tube, rotary wash sample at 14.5-16.5 feet.

# CHAPTER 6

# SAMPLE DISTURBANCE COMPARISONS

## 6.1 Introduction

In this chapter the relative degree of sample disturbance in specimens obtained using different samplers and different drilling methods is compared. These comparisons are based upon the number of fractures identified in the sample x-rays, the shape of the consolidation curves, and the results of unconfined compression tests. Several different parameters are used to compare the shape of the consolidation curves. These parameters are: the minimum radius of curvature on the consolidation curve, the range of possible maximum past pressures, the estimated magnitude of maximum past pressure, and the slope of the virgin consolidation curve.

These comparisons show that the longer the samples are stored before testing, the more rounded the consolidation curve will be. It becomes more difficult to determine the maximum past pressure. Comparisons in consolidation curves also show that samples taken with the shelby tube sampler are more disturbed. Comparisons of hollow stem auger and rotary wash samples suggest that rotary wash samples are slightly better. Fractures seen in x-rays give substantial conclusions that shelby tube samples were more disturbed. Histograms and bar graphs in this chapter illustrate the results of these comparisons.

## 6.2 Disturbance Shown in X-Rays

The x-rays were used to compare the amount of sample disturbance caused by different sampling techniques. One type of disturbance that was easily seen in x-rays was

fracturing. Fracturing can be caused by stress relief in the sample, and tension developed while extracting the sample. Fractures are seen in the x-rays as thin dark lines or streaks. One type of disturbance that is seen very little was rounding of the edges caused by the friction of the tube with the soil. This is noticeable with layered material that curves at the edges of the tube in the direction that the tube is pushed during sampling.

Each x-ray was examined to identify fractures. Fractures were categorized by length. Large fractures were those that were greater than 1.5 inches. Medium fractures were from 0.5 to 1.5 inches long. Small fractures were those that were less than 0.5 inches long. The number of each fracture size as well as the total number of fractures in each tube was counted and tabulated. Appendix D contains tables that show the number of fractures in each tube along with their location. Notes from each tube indicate if edge turning was visible.

To compare fracturing, the average recurrence interval of fractures in each sample tube was determined. This was done by dividing the length of the recovered sample by the number of fractures in the sample. Histograms are used to compare the degree of fracturing. To prepare these histograms, six ranges of fracture recurrence intervals were selected and the percentage of samples that fell in each range was calculated. Tubes with no fractures in a recovery of 25 inches or less were plotted in the >25 inches/fracture range.

Histograms comparing shelby tube and piston samplers are shown in Figure 6.1. Conclusive results were found with the histograms. Figure 6.1 shows that over 60 percent of the shelby tube samples had fractures every 0 to 5 inches, but less than ten percent of piston samples fall in this range. The average distance between fractures is

19.3 inches for piston samples and 2.5 inches for shelby tube samples. Over 60 percent of the piston samples had no fractures.

However, there is not a significant difference between the hollow stem auger and rotary wash samples. This comparison is shown with the histogram in Figure 6.2. Figure 6.2 shows that there is approximately the same percentage of tubes from each drilling method in various ranges. The average distance between fractures is 7.3 inches for hollow stem auger samples and 3.0 inches for rotary wash samples. It appears that hollow stem auger samples are slightly better, but the difference is not substantial enough to make that conclusion. Results of fracture data from x-rays are shown in Table 6.1 and 6.2 (shown later).

Table 6.1 Sample disturbance comparisons using fractures from x-rays

| **Sampler or drilling method** | **Avg. distance between fractures (in.)** | **% of tubes with no fractures** |
|---|---|---|
| Shelby tube | 2.5 | 32 |
| Piston | 19.3 | 62 |
| Rotary wash | 3.0 | 52 |
| Hollow stem auger | 7.3 | 41 |

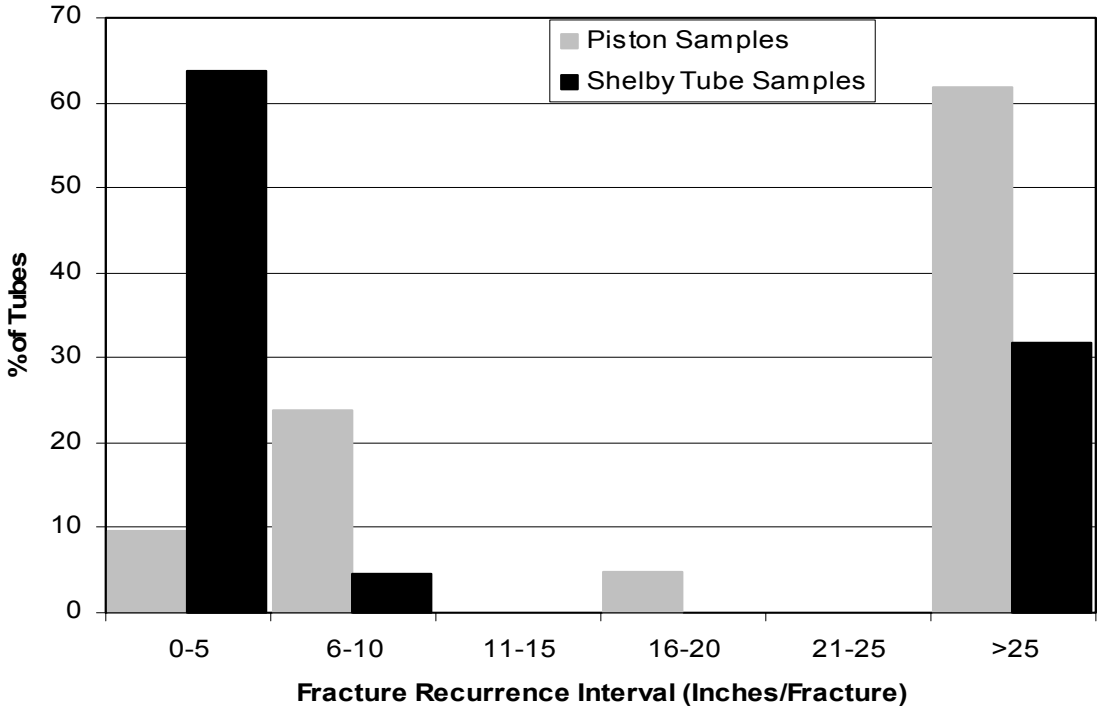


Figure 6.1 Histogram of fracture data comparing piston and shelby tube samples.

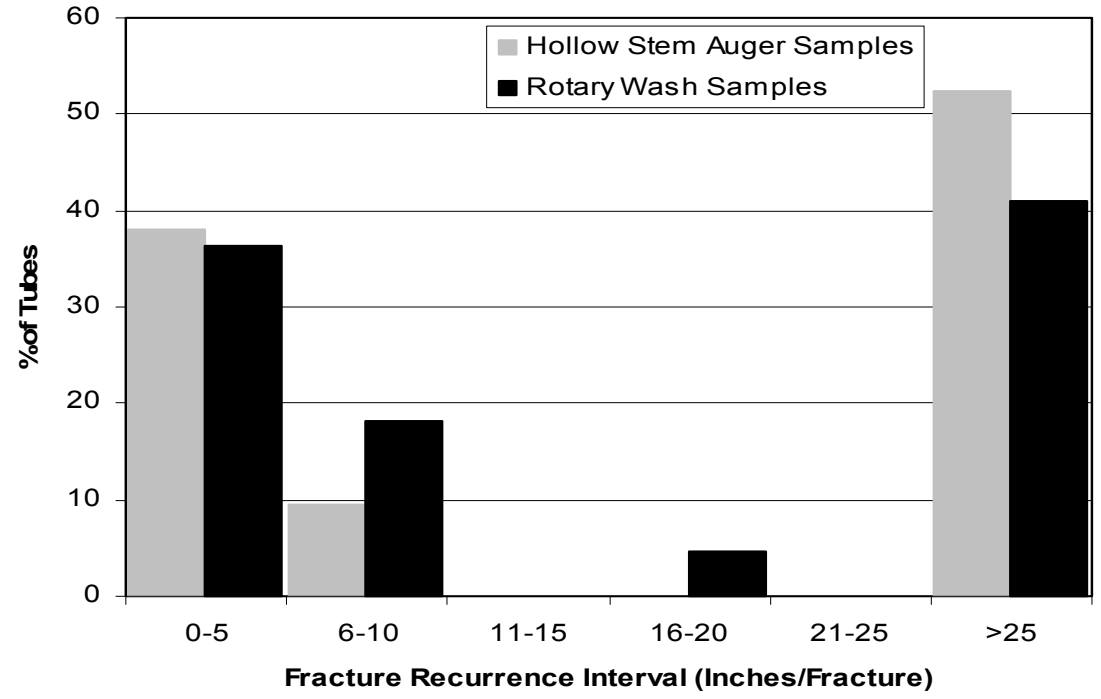


Figure 6.2 Histogram of fracture data comparing hollow stem auger and rotary wash samples.

## 6.3 Disturbance Shown in CRS Consolidation Testing

CRS test data are compared to show the effects of storage time, drilling method, and sampler type. Tests from the 1999 exploration are compared with those from the 2001 exploration to show the effects of storage time. The test results from the 2001 samples are used to compare the effects of drilling method and sampler type. Specifically, this is done by comparing the shape of the consolidation curve, error bands, maximum past pressures, and the slope of the virgin curve, $C_{c\varepsilon}$.

### 6.3.1 Effects of sample storage time

By examining the results of the 10 tests from the 1999 exploration, it was obvious that the samples were disturbed. This could be seen from any of the curves. The curve in Figure 6.3 is a typical curve of strain versus the log of effective vertical stress for a disturbed sample. The rounding of the curve makes it impossible to determine the location of the maximum past pressure. Casagrande's construction cannot be used because it is difficult to locate the point of maximum curvature as explained in the literature review. Furthermore, there is no straight-line portion of the curve as is expected when the soil exceeds the maximum past pressure. These curves have very large maximum past pressure error bands. Maximum past pressure and error band values for samples from borings I2 and S2 are not given in Appendix B because of difficulty in determining them.

Figure 6.4 shows the results of the same test on the specimen from I2 25-27 feet with stress plotted in the linear scale. With an undisturbed soil, there would typically be

a small bump in the curve at the point of maximum past pressure (somewhere under 50 psi). This curve shows no indication of a maximum past pressure.

Sample disturbance can also be identified in a plot of modulus versus effective vertical stress as shown in Figure 6.5. This curve shows the modulus increase with increasing stress. During initial loading the modulus increases greatly and then decreases as it passes the maximum past pressure. As the sample becomes normally consolidated and the stress is increased, the modulus continues to increase steadily with about the same slope that it had during initial consolidation in the overconsolidated range. During unloading and reloading, the modulus curve goes very low and then very high. A modulus curve for a typical undisturbed soil would generally have a small peak at the beginning and then hit a low point at about the point of maximum past pressure. The

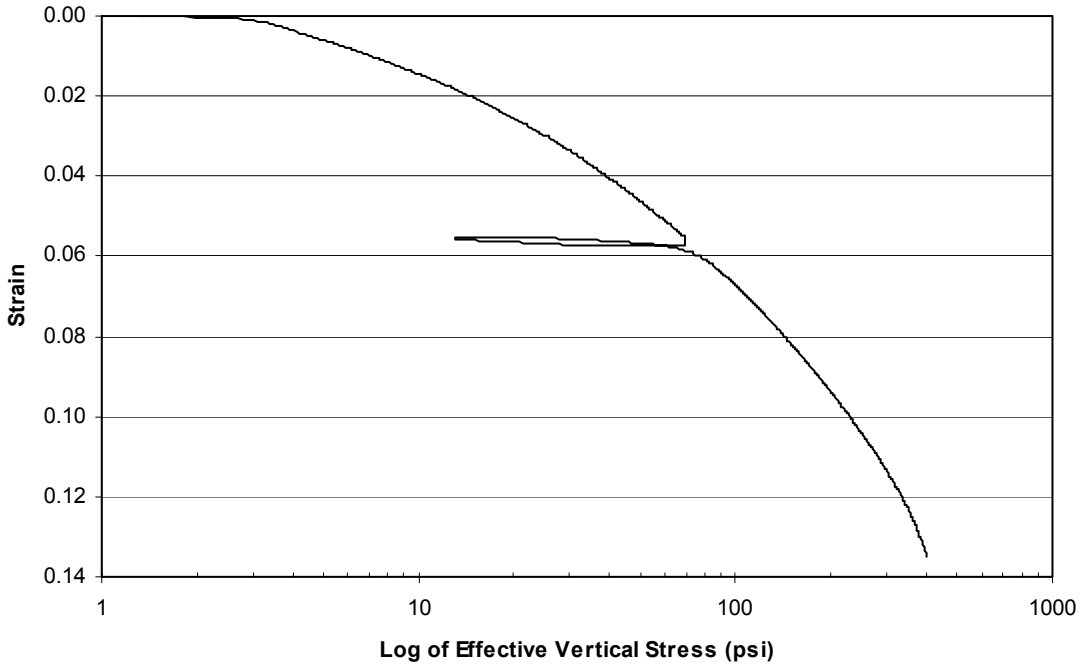


Figure 6.3 Curve of strain vs. the log of effective vertical stress for I2 25-27 feet.

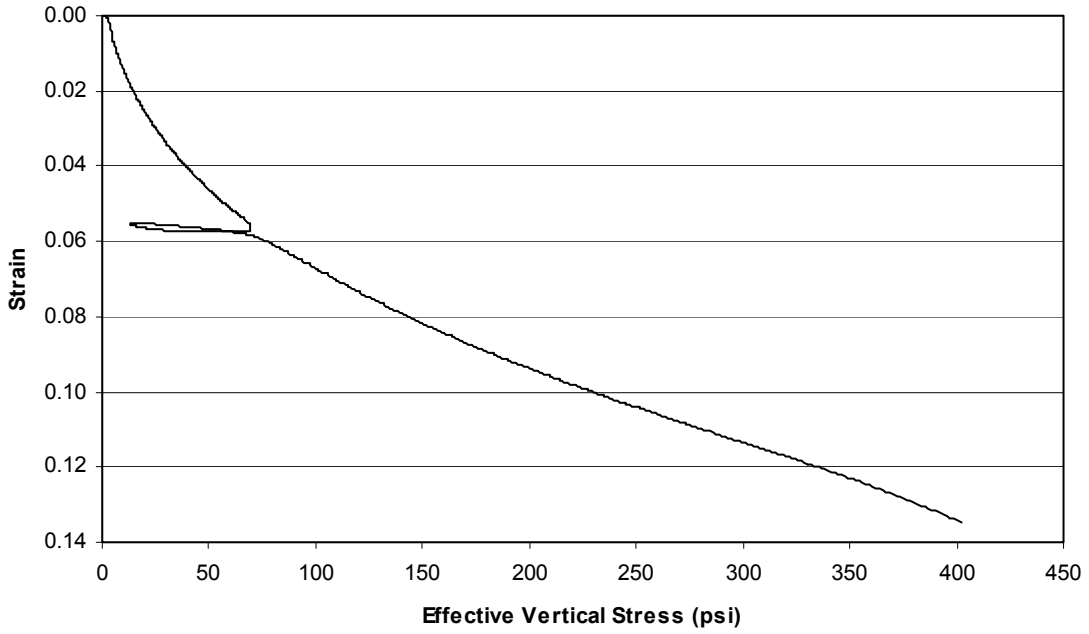


Figure 6.4 Curve of strain vs. effective vertical stress for I2 25-27 feet.

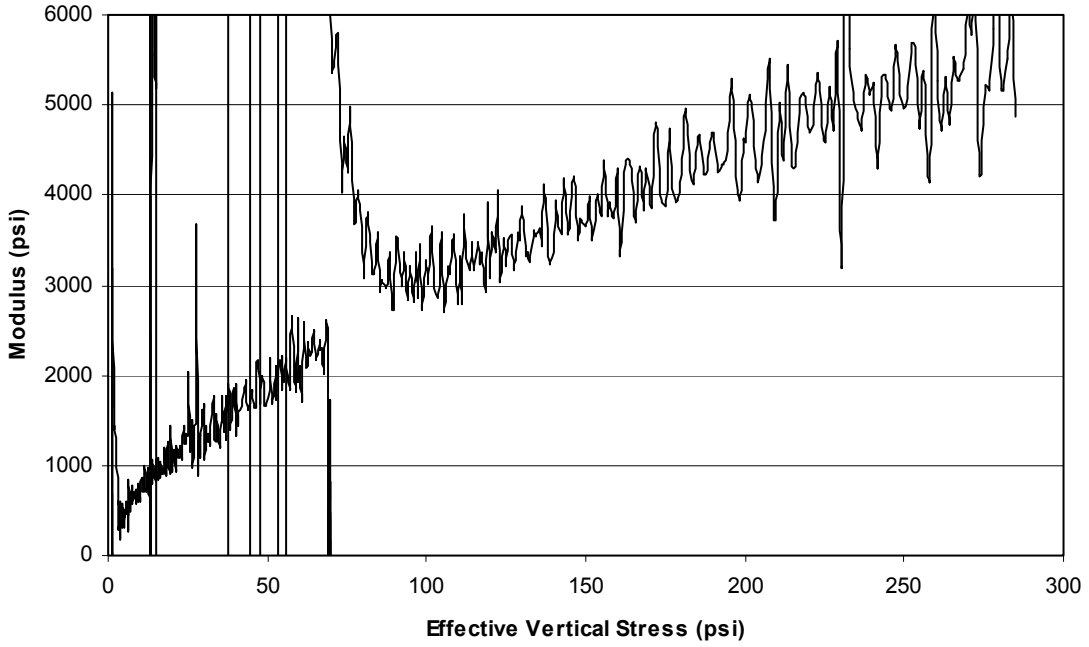


Figure 6.5 Curve of modulus vs. effective vertical stress for I2 25-27 feet.

disturbed curve shown in Figure 6.5 has no initial peak and no identifiable maximum past pressure. Nearly all of the tests on samples from borings I2 and S2 gave curves that had the same basic shape as those in Figures 6.3, 6.4, and 6.5.

The results from tests on 1999 samples are compared with those of 2001 samples to show the effects of storage time. The tests on samples from the 2001 exploration were run from two to three months after they were taken. Results from these tests are also shown in Appendix E, as are the results from borings I2 and S2. There was a large improvement in the results from the 2001 samples compared to the 1999 samples. Figures 6.6, 6.7, and 6.8 show the results of the test on a sample from boring RS-3 at 14.5-16.5 feet.

Figure 6.6 shows the strain versus the log of effective vertical stress curve. In this curve there is definitely a break, or change in slope, at the point of maximum past pressure. Using the straight-line portion of the curve and the point of maximum curvature, the Casagrande construction can be used on this curve to determine the maximum past pressure. Error bands for this curve are much smaller than those of the I2 and S2 samples. The maximum past pressure for this sample was determined to be 43 psi with a 30 to 55 psi error band. This is not a very significant error band.

Figure 6.7 shows the curve of strain vs. effective stress in the linear scale. Seen in this curve is the slight bump in the curve in the area of maximum past pressure. Extending the curve above the bump to the right and extending the curve below the bump upward can determine the maximum past pressure. The intersection of these two extensions is the maximum past pressure. A value of 40 psi was obtained from Figure 6.7.

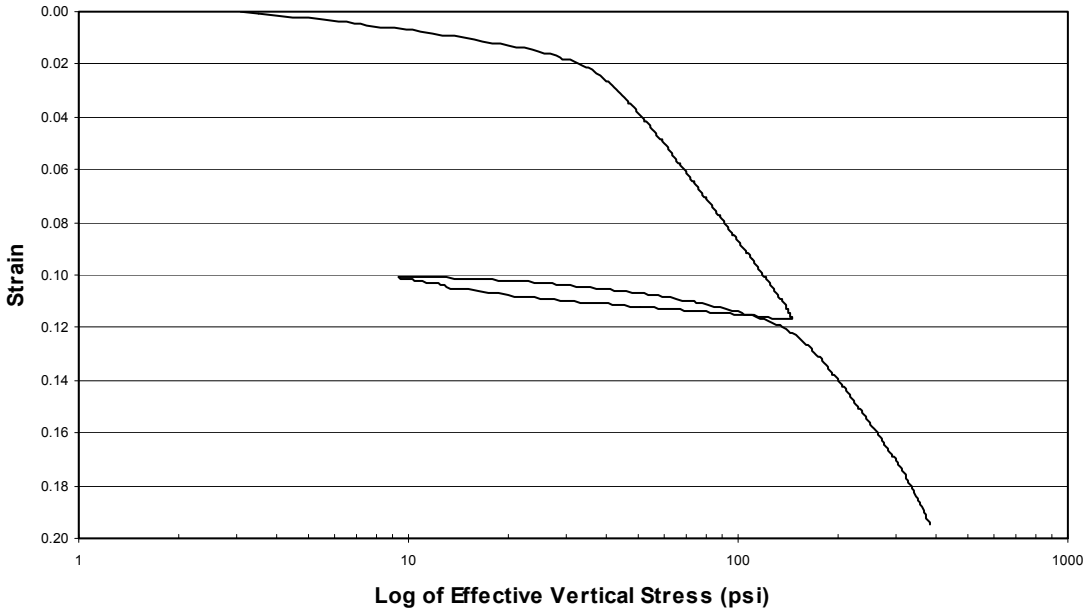


Figure 6.6 Curve of strain vs. the log of effective vertical stress for RS-3 14.5-16.5 feet.

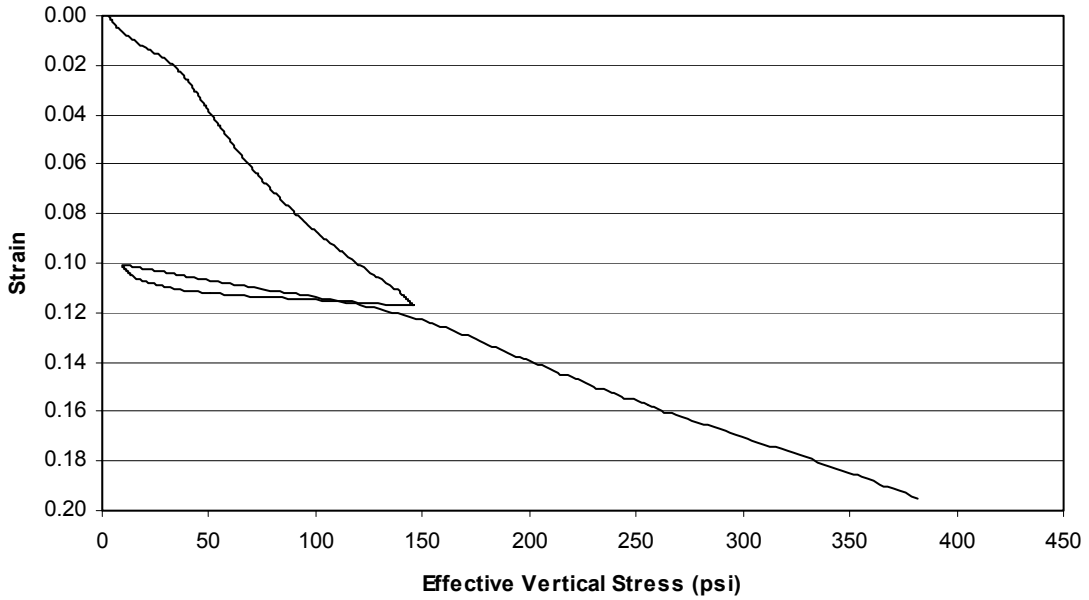


Figure 6.7 Curve of strain vs. effective vertical stress for RS-3 14.5-16.5 feet.

The modulus curve in Figure 6.8 shows a maximum past pressure of approximately 43 psi. There is noise in the curve. This is because the program records data every minute and the modulus is calculated with consecutive values of stress and strain. If larger increments of data are used for calculating modulus, the noise would be reduced. However, even with the noise, the general shape of the curve is easily recognized. Figures 6.6 through 6.8 show typical results for nearly undisturbed soil. A reasonably accurate value for the maximum past pressure can be obtained from the results.

The effects of storage time on consolidation curves can be easily compared by plotting two curves together. Figure 6.9 shows two consolidation curves together to compare the effects of storage time. The soil from HF-2 was tested less than 2 months

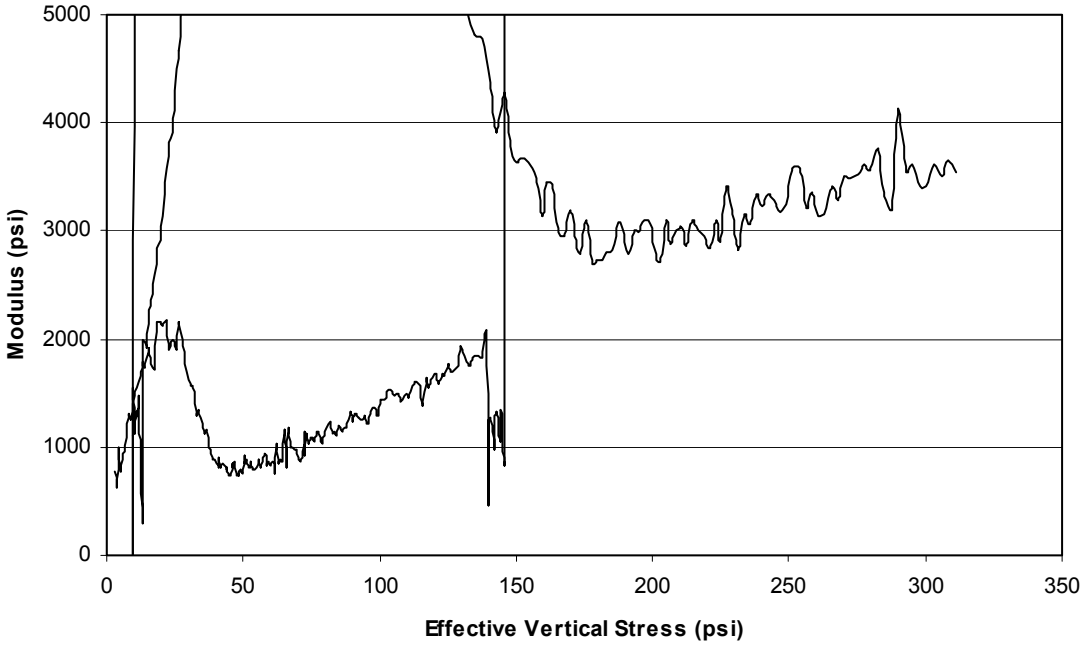


Figure 6.8 Curve of modulus vs. effective vertical stress for RS-3 14.5-16.5 feet.

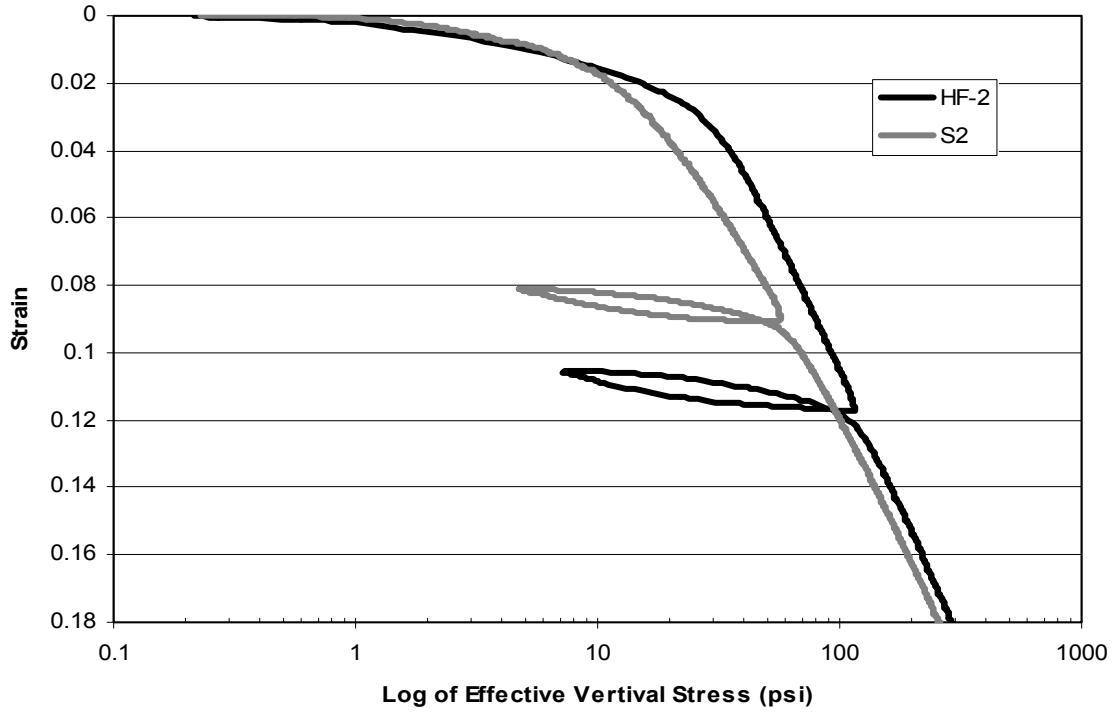


Figure 6.9 The effect of storage time on the consolidation curve.

after sampling while the soil from S2 was tested 10 months after sampling. The effects of storage time are seen as the S2 curve is more rounded and shifted to the left.

### 6.3.2 Comparisons using the shape of the consolidation curve

Comparing the shape of the consolidation curve, error bands, maximum past pressures, and $C_{c\varepsilon}$ shows the effects of drilling method and sampler type. These comparisons were made on samples from the 2001 exploration. The older samples were not used because the roundness of the curves made it impossible to determine these values. Histograms and bar graphs represent the data and are useful in comparisons.

This section compares the effect of different drilling method and sampler type using the shape of the consolidation curve. The strain versus log of effective vertical

stress curves of different samples from the same depth are shown in Figures 6.10 through 6.15. As explained in the literature review, a curve that is shifted to the left and has a flatter slope is considered to be more disturbed.

Figure 6.10 compares two hollow stem auger samples from 9.5 to 11.5 feet. The piston sample in this figure definitely has a better curve than the shelby tube sample because it has a more distinct slope change. The shelby tube sample is more rounded.

In Figures 6.11 and 6.12 samples from each boring are compared. In both figures, the samples from the hollow stem auger borings are both shifted slightly to the left. The piston/rotary wash samples are furthest to the right. However, the shelby tube/rotary wash samples have a more distinct break. Both of these figures tend to show that the rotary wash samples have less disturbed-shaped curves than the hollow stem auger samples. The curves in Figure 6.13 show the same thing as those from Figures 6.11 and 6.12 except that the shelby tube/hollow stem auger sample looks like the best curve. This sample was actually tested at 2.5 percent/hour unlike the others; therefore, it is probably not entirely accurate to compare this curve to the others.

Figures 6.14 and 6.15 compare piston/rotary wash samples with shelby tube/hollow stem auger samples. In both figures the piston/rotary wash samples have better curves. It cannot be concluded that this is a result of the sampler or the drilling technique, but it follows the same pattern that is seen in the other figures.

The comparisons of consolidation curve shapes showed in one example that the curve from a piston sample was less disturbed than that of a shelby tube sample. This comparison was a good one because both samples were from the boreholes drilled with the same method. In the other comparisons samples from every different combination of

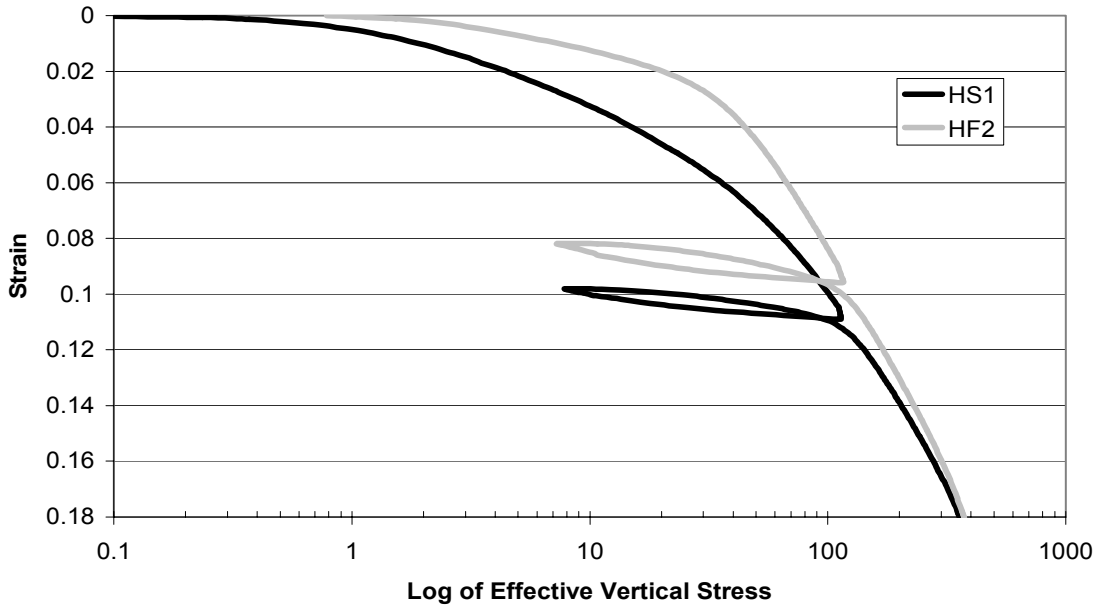


Figure 6.10 Strain vs. the log of effective vertical stress curves for samples at 9.5-11.5 feet.

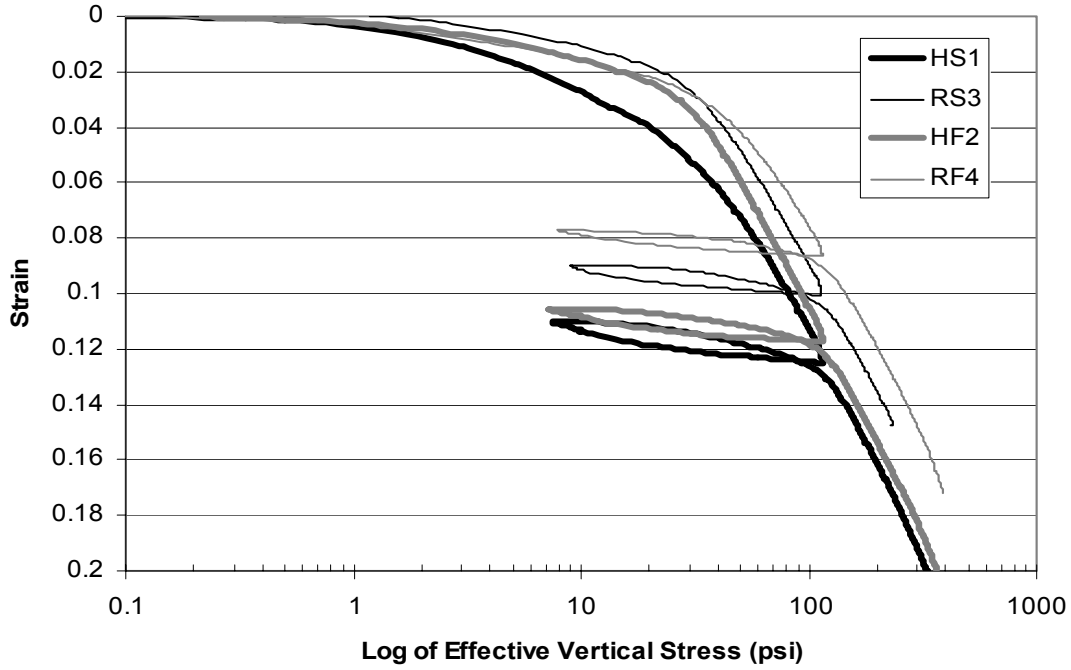


Figure 6.11 Strain vs. the log of effective vertical stress curves for samples at 12-14 feet.

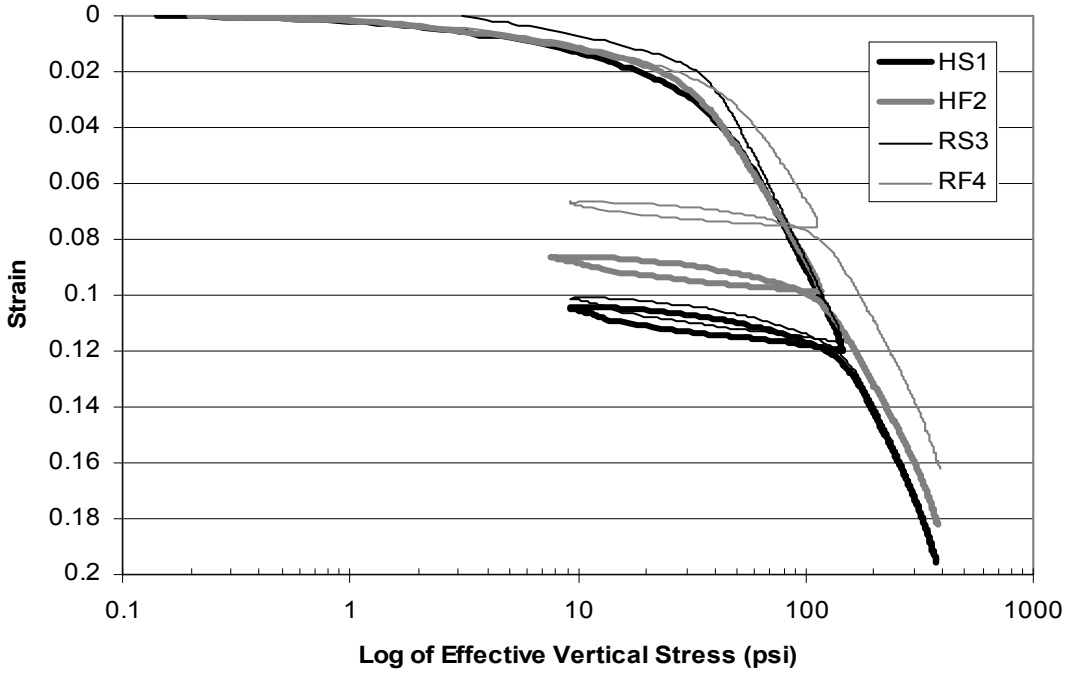


Figure 6.12 Strain vs. the log of effective vertical stress curves for samples at 14.5-16.5 feet.

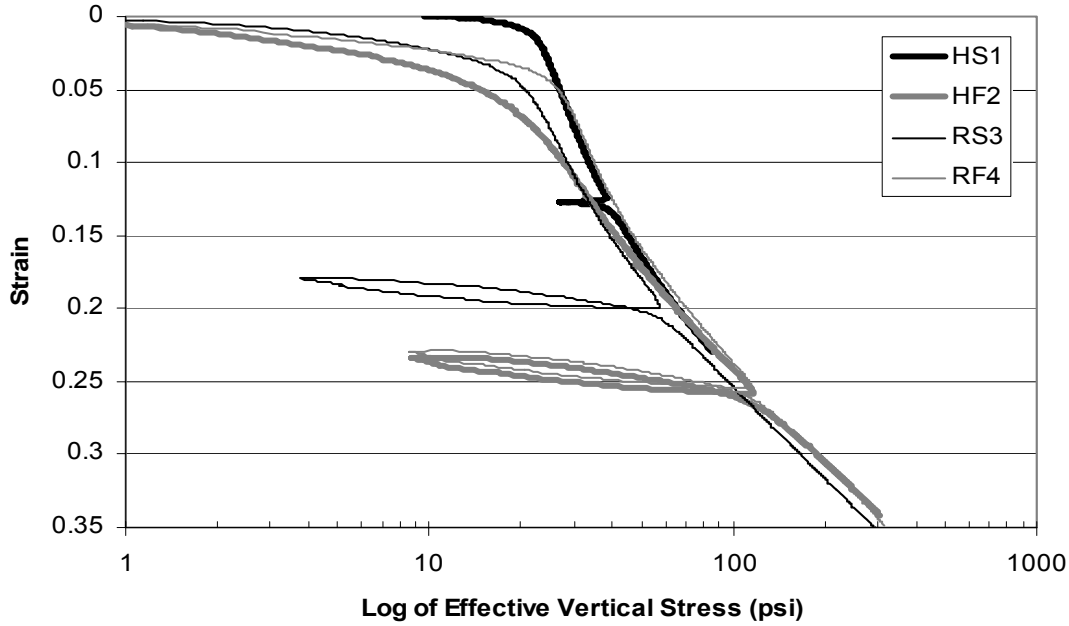


Figure 6.13 Strain vs. the log of effective vertical stress curves for samples at 17-19 feet.

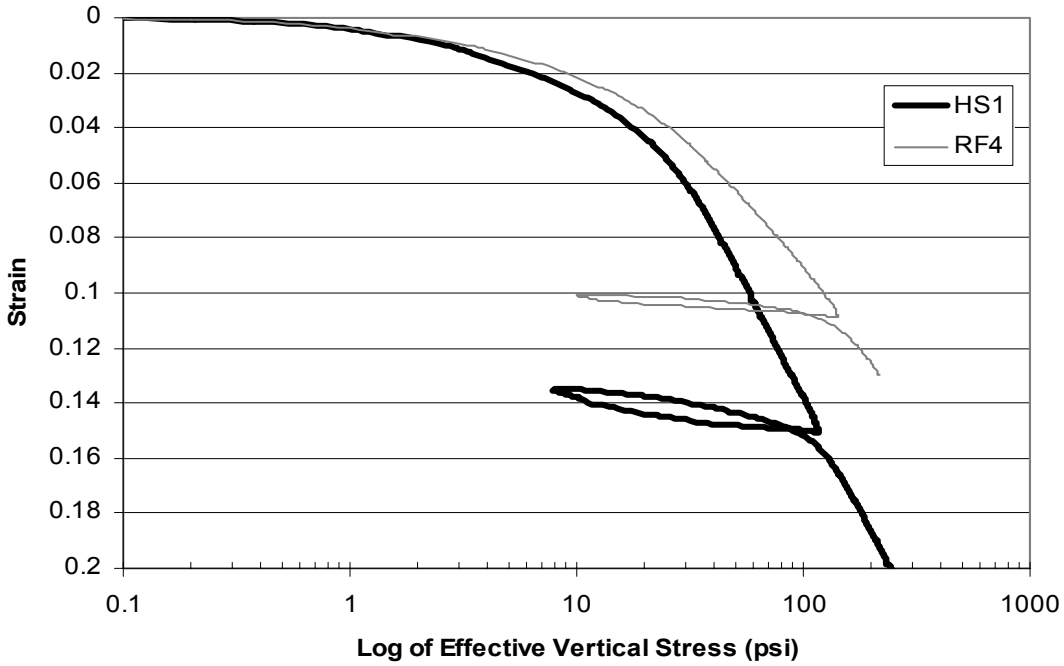


Figure 6.14 Strain vs. the log of effective vertical stress for samples at 22-24 feet.

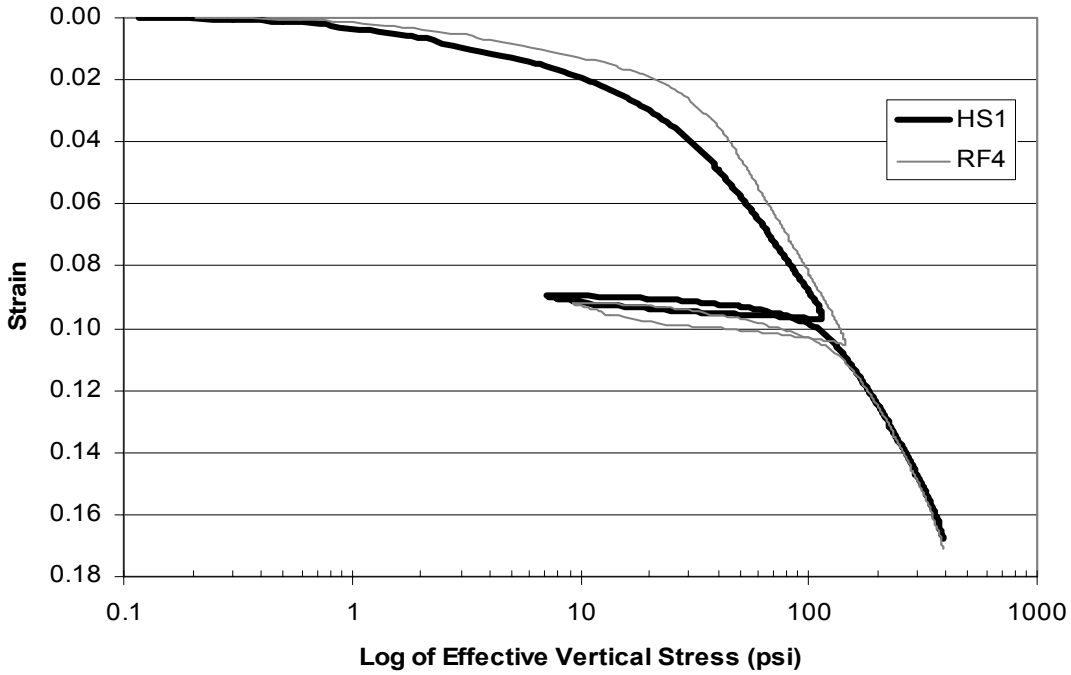


Figure 6.15 Strain vs. the log of effective vertical stress for samples at 24.5-26.5 feet.

factors were shown together. These comparisons showed that rotary wash samples tended to be less disturbed, but the difference was not very significant and some samples showed the opposite.

The shape of the consolidation curves was then compared by finding the radius of the curves at the point of transition to the virgin compression curve. This is a way to quantitatively compare the strain versus log of effective stress curves. This was done by plotting all curves on the same scale. A spiral curve, as shown in Figure 6.16, was plotted on a transparency and placed over the consolidation curve at the point in question and adjusted until the spiral matched up with the consolidation curve. The radius was found to be the distance on the spiral to the middle of the spiral. A curve with a small radius is less disturbed because it comes closer to looking like the undisturbed curve (BAD) in Figure 2.1.

The radius for each sample was found and data was plotted in histograms to compare drilling methods and sampler types. Figure 6.17 compares the radius of curves from piston and shelby tube samples. A greater percentage of the shelby tube samples plot at the right with higher radii. The average shelby tube sample radius is 1.76 inches while the average for piston samples is 1.59 inches. The mean value for both sampler types is 1.70 inches. The difference is not very large, but still shows that piston samples are typically less disturbed than shelby tube samples. This comparison is probably more meaningful than comparing the shapes of two curves side-to-side, as in Figure 6.10, because the histograms average all samples instead of comparing just two.

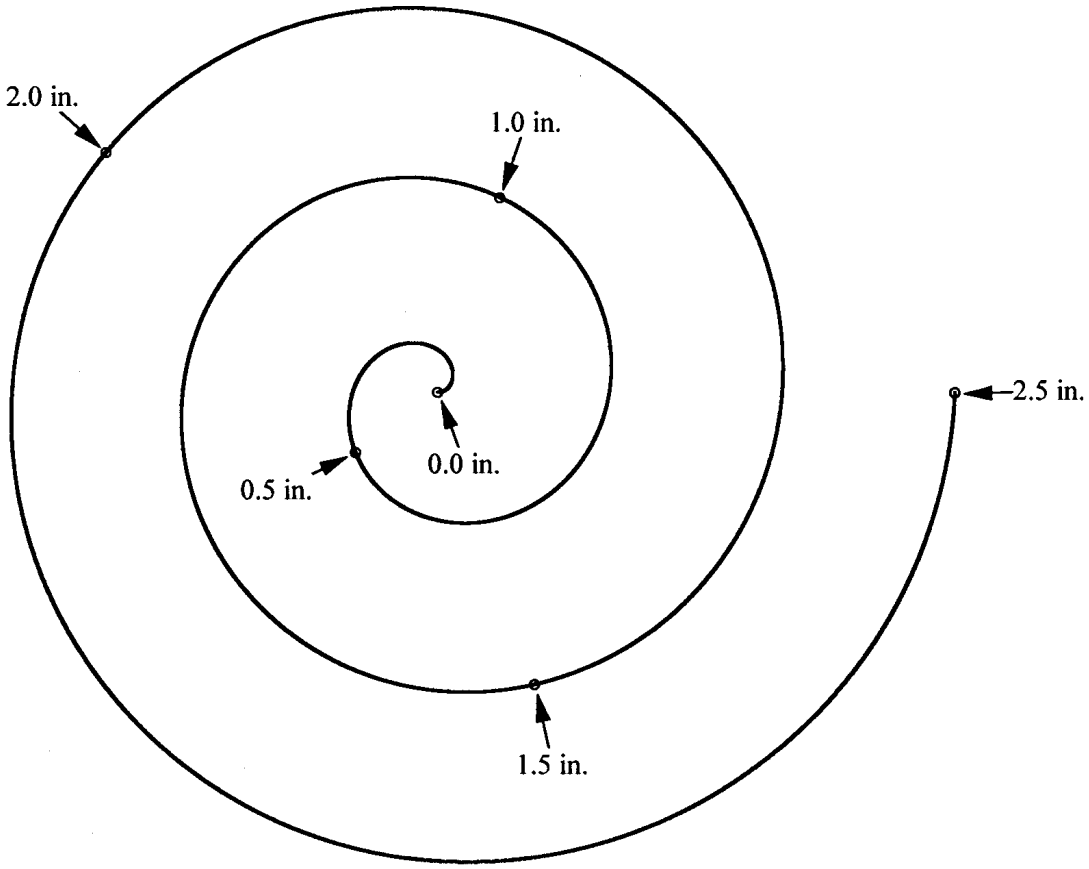


Figure 6.16 Spiral used to determine the radius of consolidation curves (not to scale).

Figure 6.18 compares hollow stem auger samples with rotary wash samples. Again, a greater percentage of hollow stem auger samples plot to the right on the histogram. The average hollow stem auger radius is 1.85 inches with a mean value of 1.70 inches. The average rotary wash sample radius is 1.45 inches with a mean value of 1.45 inches, suggesting that the rotary wash samples are less disturbed.

Results from the radius histograms tend to support the results from the strain vs. log of effective stress curves. That is, the rotary wash samples are generally better than hollow stem auger samples, and piston samples are better than shelby tube samples.

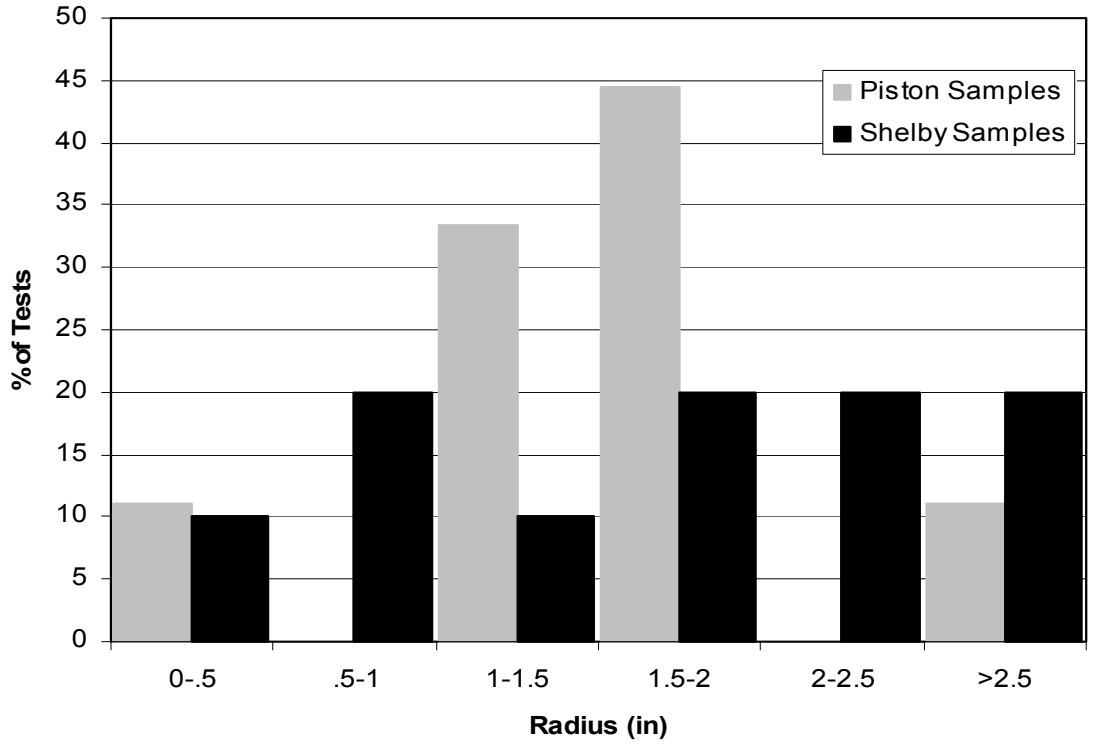


Figure 6.17 Histogram of radii comparing sampler type.

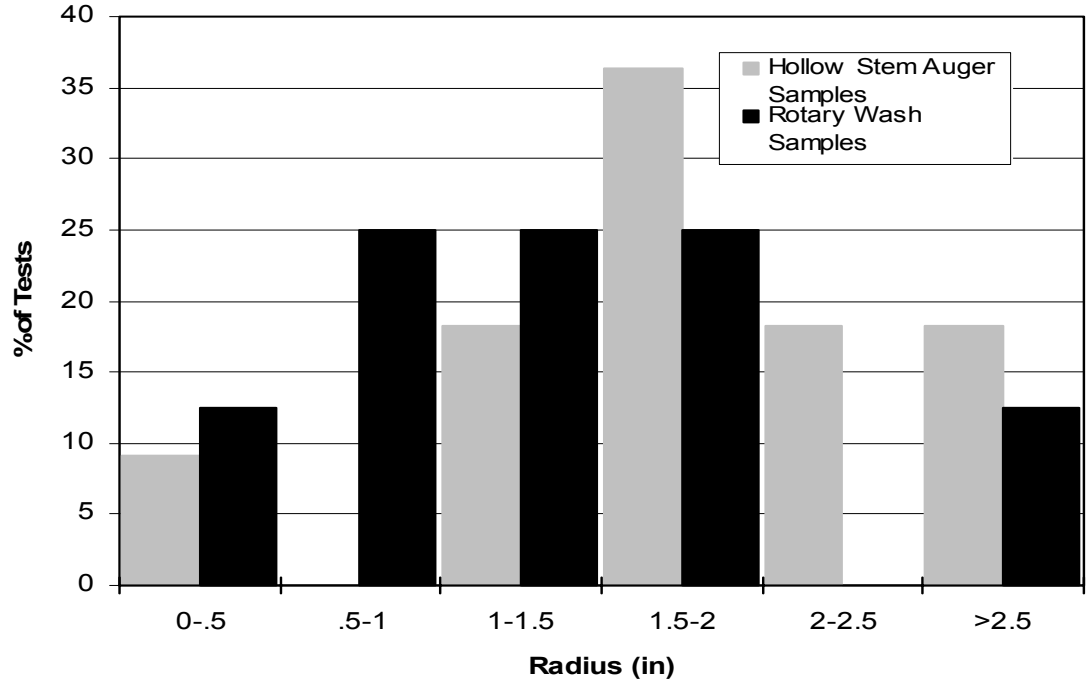


Figure 6.18 Histogram of radii comparing drilling methods.

Table 6.2 Results of fractures, radii, and error band data

| | Average Distance Between Fractures (inches) | Radius (inches) | | % Error | |
|---|---|---|---|---|---|
| | | Average | Mean | Average | Mean |
| Piston Samples | 19.3 | 1.59 | 1.6 | 79.6 | 70.1 |
| Shelby Tube Samples | 2.5 | 1.76 | 1.6 | 84.4 | 87.4 |
| Hollow Stem Auger Samples | 7.3 | 1.85 | 1.7 | 90.1 | 85.7 |
| Rotary Wash Samples | 3.0 | 1.44 | 1.45 | 71.3 | 69.8 |

6.3.3 Comparisons using maximum past pressure error bands

Sample disturbance was compared further using error bands. The minimum possible to maximum possible maximum past pressure error bands were determined as shown in Figure 2.2 and explained in the literature review. A consolidation curve that has a small error band is less disturbed. The error bands from each test were determined. The error bands were normalized by dividing the difference in maximum and minimum by the calculated (most probable) maximum past pressure. For easier comparison, the percent error was plotted in histograms that are explained in this section.

Figure 6.19 is a histogram that compares the error bands of the different sampler types. The shelby tube samples have a greater percentage of samples plotting at the right of the histogram, meaning that they have a greater percent error on average. The roundness of the curves for shelby tube samples caused larger error bands. The average error for piston samples is 79.6 percent with a mean value of 70.1 percent. The average

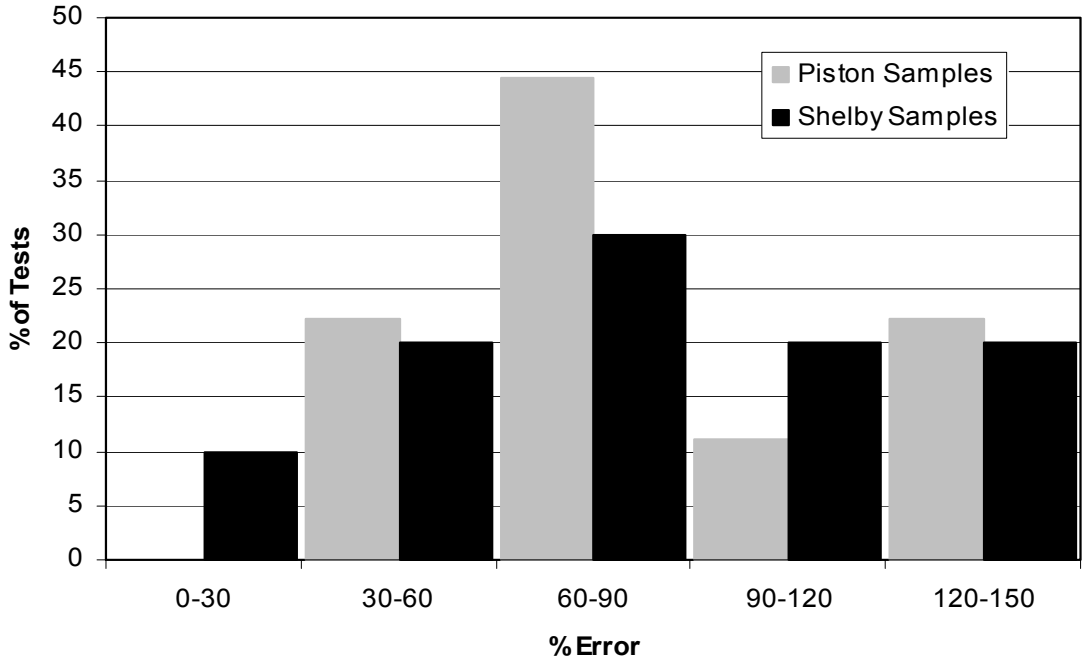


Figure 6.19 Histogram comparing sampler types by means of percent error.

for shelby tube samples is 84.4 percent with a mean value of 87.4 percent. Although not a large difference, the piston samples on average have smaller error bands.

Figure 6.20 is a histogram showing the comparison of drilling methods with error bands. The comparison of error bands shows a more noticeable difference between the drilling methods. The average hollow stem auger sample has an error of 90.1 percent with a mean value of 85.7 percent. The average rotary wash sample has an error of 71.3 percent with a mean value of 69.8 percent. The results of this comparison show that rotary wash samples are again less disturbed.

Conclusions from error band comparisons tend to agree with those arrived at by looking at other comparisons. Error band comparisons show that rotary wash samples have smaller error bands than hollow stem auger samples. On average, piston samples

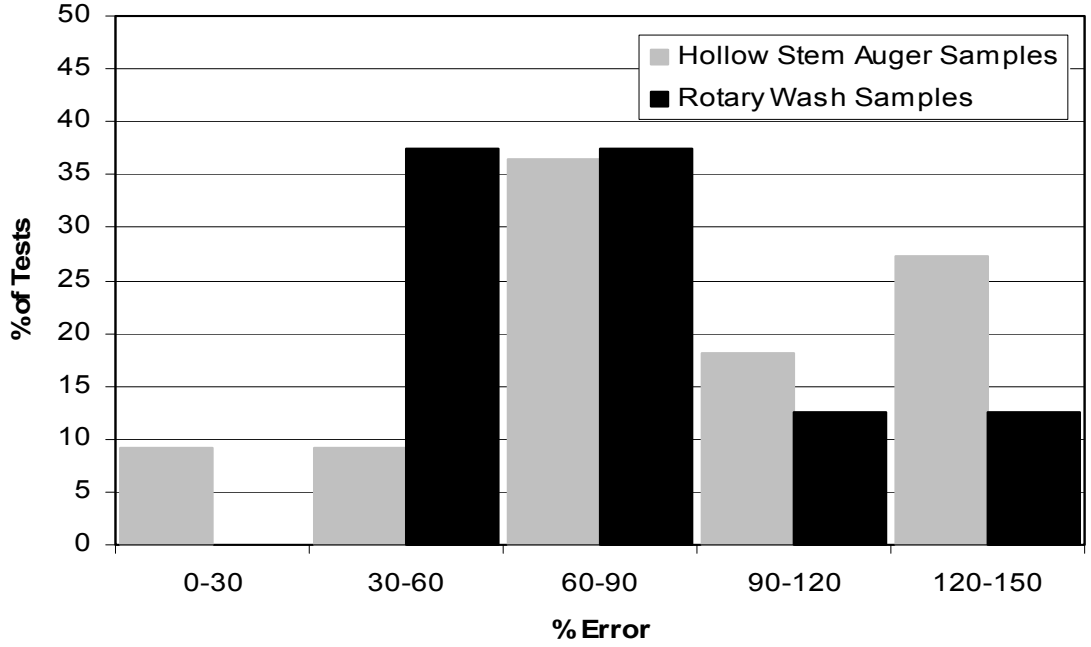


Figure 6.20 Histogram comparing drilling method by means of percent error.

have slightly smaller error bands. The average and mean percent errors are tabulated in Table 6.2.

6.3.4 Comparisons using maximum past pressures

The values of maximum past pressure were then compared to find an indication of sample disturbance. Lower values of maximum past pressure are expected for a disturbed sample. The average values for all piston and shelby tube samples at each depth were taken. The same was done for all hollow stem auger and rotary wash samples. Bar graphs comparing the sampler types and drilling methods are shown in Figures 6.21 and 6.22, respectively.

From Figures 6.21 and 6.22 there is no substantial evidence of one sampler type or drilling method being better than the other. The piston and shelby tube samples have

nearly the same average maximum past pressures at every depth as shown in Figure 6.21. Figure 6.22 shows that the rotary wash samples generally have higher average maximum past pressures, but the difference is not significant enough to make any conclusion.

### 6.3.5 Comparisons using the slope of the virgin compression curve

The slopes of the virgin compression curves, $C_{c\varepsilon}$, were then calculated and compared. Average values at every depth were calculated for each sampler type and drilling method. The results are plotted in bar graphs. Figure 6.23 is the bar graph comparing sampler types. Figure 6.24 is the bar graph comparing drilling methods.

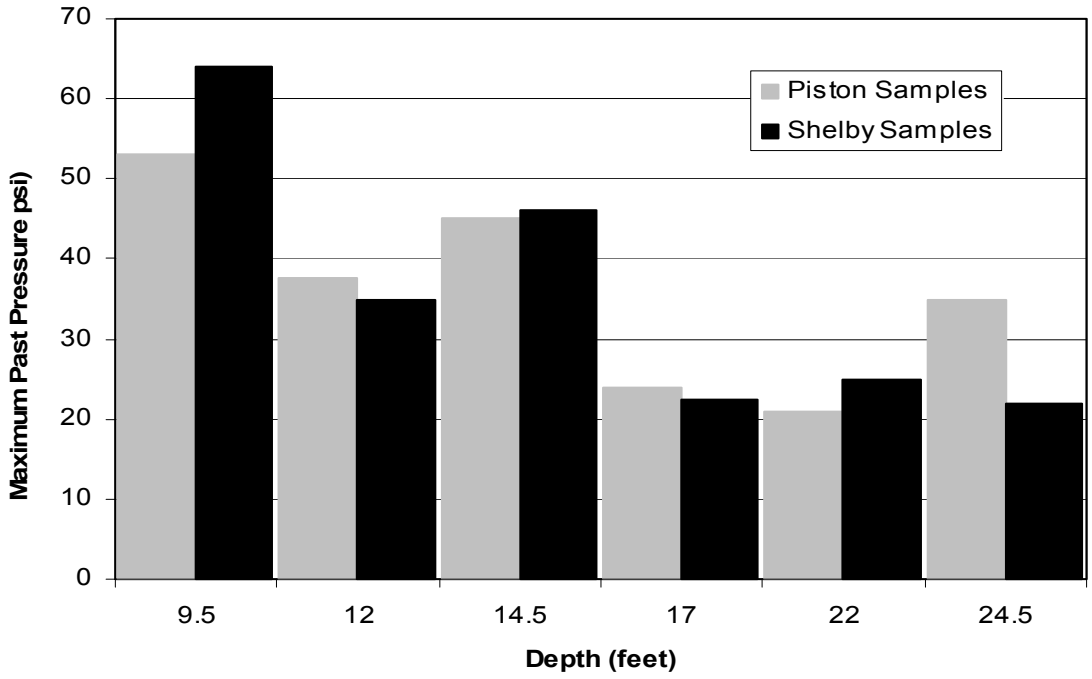


Figure 6.21 Bar graph of maximum past pressures comparing sampler types.

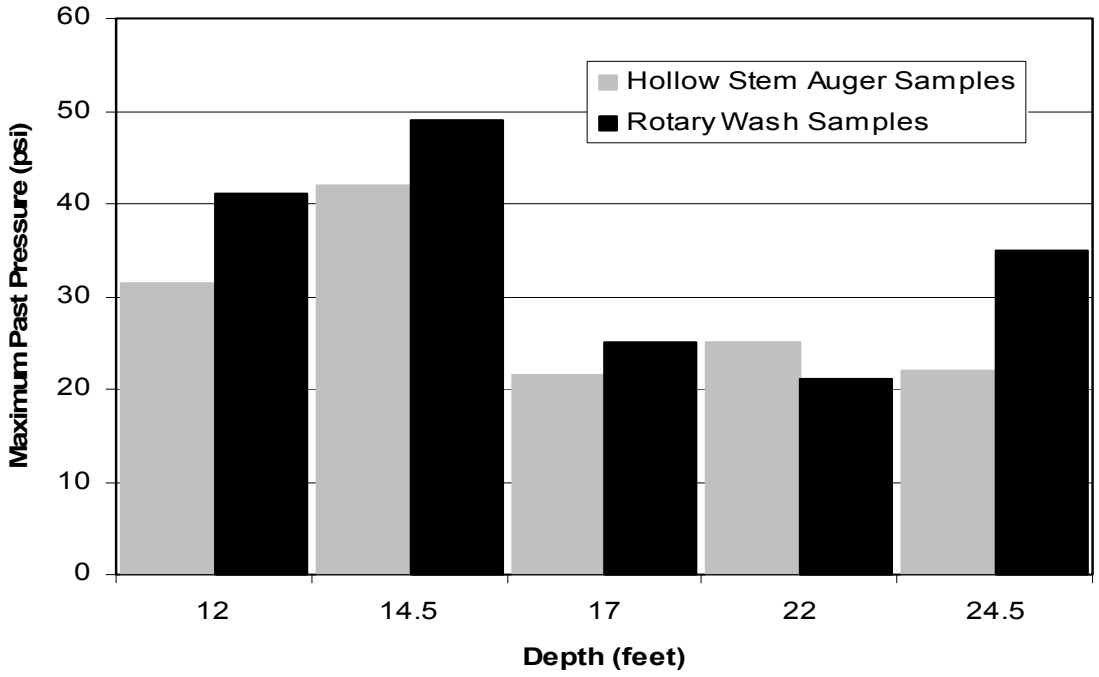


Figure 6.22 Bar graph of maximum past pressures comparing drilling methods.

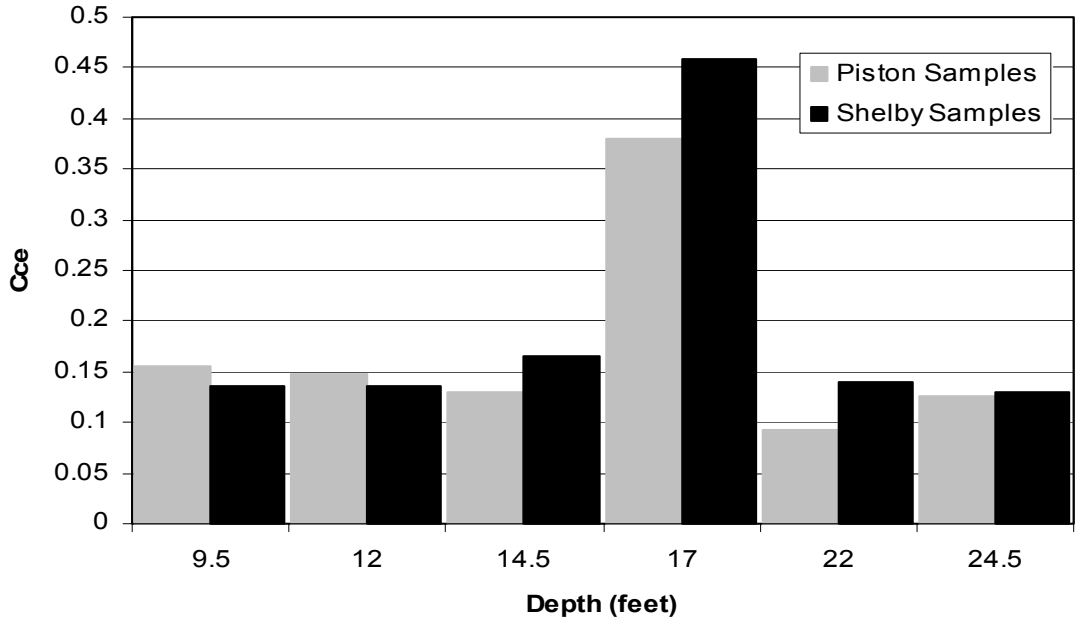


Figure 6.23 Bar graph of $C_{c\varepsilon}$ values vs. depth comparing sampler types.

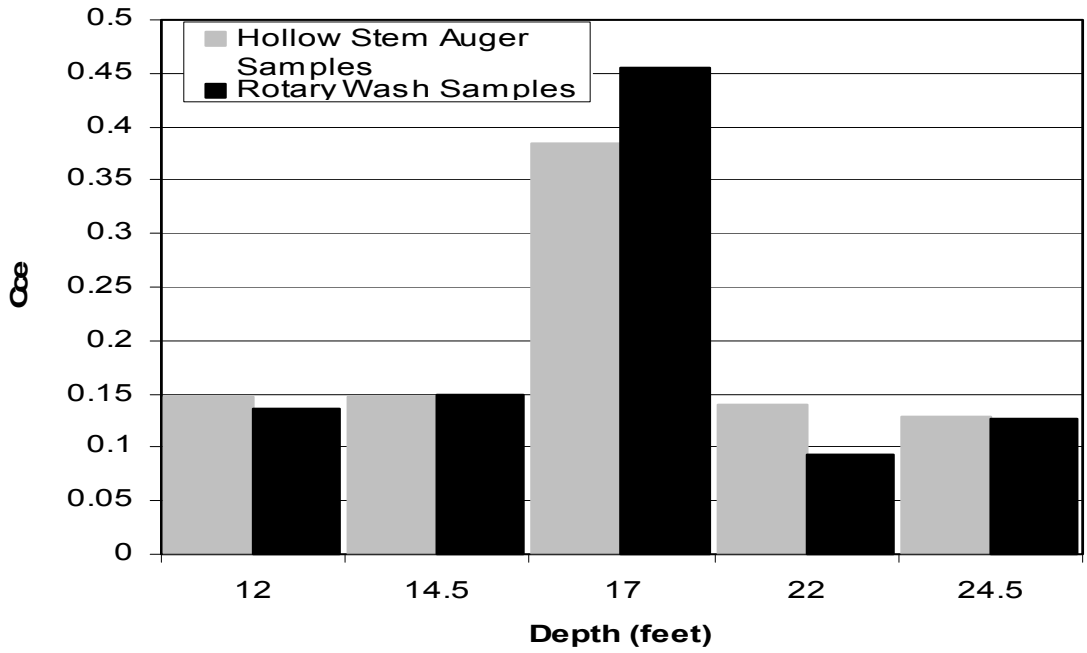


Figure 6.24 Bar graph of $C_{c\varepsilon}$ values vs. depth comparing drilling methods.

From the two figures there is no conclusion that can be made. At every depth in both graphs the values of $C_{c\varepsilon}$ are nearly the same. Any differences are not significant enough to make any conclusions.

## 6.4 Unconfined Compression Tests

Four unconfined compression tests were performed on samples from 9.5 to 11.5 feet. The strain rate was held constant for all tests. Examining the initial slope of the stress-strain curve can show sample disturbance. A more disturbed sample will have a lower value of E50. E50 is the secant modulus at 50 percent of the maximum stress and is taken by dividing the half of the maximum stress by the strain at that stress. Values of E50 for the tests were as follows: 11.8 psi for HS-1, 13.4 psi for HF-2, 8.3 psi for RS-3, and 21.3 psi for RF-4. A plot of these curves is shown in Figure 6.25. From these

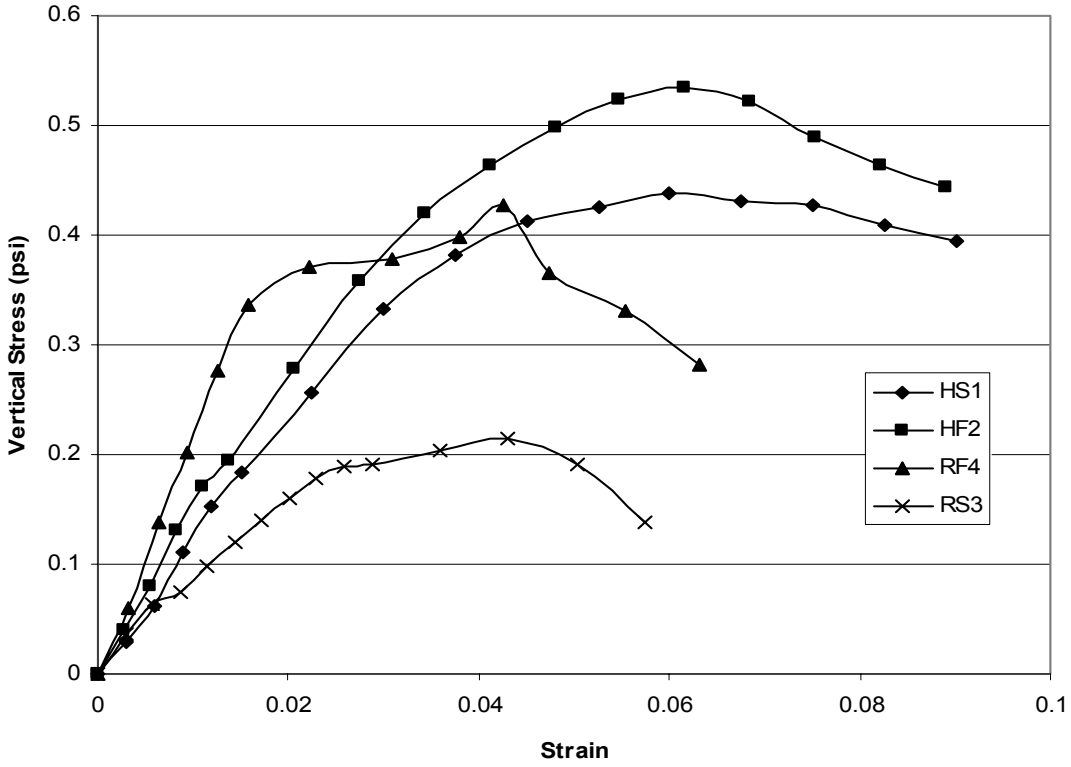


Figure 6.25 Unconfined compression test results for 9.5-11.5 feet.

values, the sample from RS-3 is the most disturbed. The piston samples have the highest modulus and are considered the least disturbed.

## 6.5 Conclusions

This section summarizes the outcomes of the comparisons used in this chapter. Some comparisons were more effective than others in showing the effects of sampling method or drilling technique. Final conclusions and recommendations are given in Chapter 7.

Several comparisons were made in this chapter. As noted earlier, it was generally more desirable to average the results of all the tests of one type of sample and compare them to other types. This was done to avoid the mistake of comparing the results from

tests that may have been outliers and did not represent the average results. It was more reasonable to compare averages.

Comparing the shape of consolidation curves was an effective way of showing sample disturbance caused by storage time. Comparisons that were successful in showing disturbance effects of sampling methods and drilling techniques were fracture data, radius, error bands, and unconfined compression test results. Average maximum past pressures and the average slope of virgin compression curves were not very effective means of comparison. The conclusions from these comparisons are given in the following chapter.

# CHAPTER 7

# CONCLUSIONS AND RECOMMENDATIONS

## 7.1 Conclusions

The purpose of this project was to evaluate the effects of sampling method on sample disturbance in soft Bonneville clays. To obtain samples for this work two drilling methods, rotary wash and hollow stem auger, where used. Samples where obtained using a shelby tube sampler and two different piston samplers. Sample disturbance was evaluated using radiograph images of the specimens, and laboratory consolidation and triaxial tests.

Comparisons of piston and shelby tube samples indicate that piston samples are less disturbed than shelby tube samples. X-rays show significantly fewer fractures in piston samples than shelby tube samples. The average radius of the consolidation curves at the points of maximum past pressure was less (indicating a sharper break between reconsolidation and virgin consolidation) for the piston samples than the shelby tube samples, resulting in less uncertainty in maximum past pressure predictions. Interestingly, there was no significant difference in maximum past pressure or $C_{c\varepsilon}$ between the piston and the shelby tube samples. This may be because the radiograph images were used to select portions of the sample to use in consolidation tests. Thus, the most disturbed portions of the samples were not tested. The piston samples also exhibited higher initial moduli ($E_{50}$) values than the shelby tube samples in the unconfined compression test. This is also indicative of less sample disturbance. The shape of the

consolidation curves for piston samples are generally better than those of shelby tube samples with the same drilling method.

The differences in sample disturbance were not as recognizable or significant between the two drilling methods. The quantities of fractures and cracks identified in radiograph images were practically identical for the two drilling methods. The CRS tests show slightly less disturbance in the rotary wash samples than the hollow stem auger samples. The average radius of the consolidation curves at the points of maximum past pressure was somewhat lower for the rotary wash samples than the hollow stem auger samples, resulting in less uncertainty in maximum past pressure for the rotary wash samples. Again, there was no significant difference in the average maximum past pressure or $C_{c\varepsilon}$ between rotary wash and hollow stem auger samples.

## 7.2 Recommendations

Based upon this research, several recommendations can be made as to methods that should be employed in drilling and sampling to minimize the effects of sample disturbance in soft Bonneville clays. These are:

- Piston samplers along with thin-walled sampling tubes should be used rather than shelby tube samplers for obtaining specimens for consolidation, triaxial, and other critical geotechnical tests.
- Both fixed piston, and free piston samplers obtain samples of similar high quality.
- Radiograph (x-ray) images of the soil specimens provide a powerful tool for assessing sample disturbance, selecting the least disturbed portions of the sample for critical tests, identifying locations of sand lenses in Bonneville clay samples.

- Rotary wash drilling methods result in slightly less sample disturbance than hollow stem auger drilling.

- When hollow stem auger drilling is used, the auger should be advanced slowly using slow rotation (as was done in this work) to minimize disturbance to the surrounding soil.

- Sample recovery can be increased by waiting a period of several minutes after pushing a sample tube before attempting to extract the sample from the ground.

# LITERATURE CITED

ASCE (American Society of Civil Engineers). 2000. Soil sampling. Technical engineering and design guides as adapted from the US Army Corps of Engineers, No. 30. ASCE Press, Reston, Virginia. 214 p.

ASTM (American Society for Testing and Materials). 1994. 1994 Annual book of ASTM standards. Volume 04.08, Soil and rock; dimension stone; geosynthetics. American Society for Testing and Materials, Philadelphia, Pennsylvania. 144 p.

Arman, Ara, and K.L. McManis. 1976. Effects of storage and extrusion on sample properties. Soil specimen preparation for laboratory testing. ASTM STP 599, American Society for Testing and Materials, Philadelphia, Pennsylvania. 340 p.

Bay, J. A., L. R. Anderson, A. S. Budge, and M. W. Goodsell. 2003. Instrumentation and installation scheme of a mechanically stabilized earth wall on I-15 with results of wall and foundation behavior. Report No. UT-03.11, Utah Department of Transportation, Salt Lake City, Utah. 353 p.

Casagrande, A. 1936. The determination of the pre-consolidation load and its practical significance. Discussion D-34, Proceedings of the First International Conference on Soil Mechanics and Foundation Engineering, June 22-26, 1936, Cambridge, Massachusetts. Vol. III, p. 60-64.

Colocino, T. 2001. Characterization of the Bonneville clays underlying the I-15 project in Salt Lake City, using stress history and normalized soil engineering properties. Unpublished MS thesis. Utah State University, Logan, Utah. 160 p.

Emdal, A. 1999. Janbu's solutions for modulus representation and consolidation of soils. Lecture Notes. Utah State University, Logan, Utah. 29 p.

Fraser, G.S., and A.T. James. 1969. Radiographic exposure guides for mud, sandstone, limestone and shale. Circular 443. Illinois State Geologic Survey, Urbana, Illinois. 19 p.

Goodsell, M.W. 2000. Instrumentation and installation scheme on a mechanically stabilized earth wall on I-15. Unpublished MS thesis. Utah State University, Logan, Utah. 133 p.

Holtz, R.D., and W.D. Kovacs. 1981. An introduction to geotechnical engineering. Prentice Hall, Englewood Cliffs, New Jersey. 733 p.

Hvorslev, M.J. 1949. Subsurface exploration and sampling of soils for civil engineering purposes. Waterways Experiment Station, Vicksburg, Mississippi. 521 p.

Krinitzsky, E.L. 1970. Radiography in the earth sciences and soil mechanics. Plenum Press, New York. 164 p.

Olson, R.E. 1986. State of the art: Consolidation testing, p. 52-58. In R.N. Yong and F.C. Townsend (Eds.). Consolidation of soils: Testing and evaluation. ASTM STP 892. American Society of Testing and Materials, Philadelphia, Pennsylvania. p. 52-58.

# APPENDICES

# Appendix A

## Laboratory Results

Table A.1 Laboratory results from boring HS-1

| Depth (ft) | $\sigma'_v$ (psi) | $\sigma'_p$ (Casagrande) (psi) | $\sigma'_p$ (Modulus) (psi) | $\sigma'_p$ error band (psi) | m | $w_n$ (%) | PL (%) | LL (%) | $C_{CE}$ | $\gamma_t$ (pcf) | $\gamma_d$ (pcf) | Grain Size %>75mm | Grain Size %2-75mm | Grain Size %<2mm |
|---|---|---|---|---|---|---|---|---|---|---|---|---|---|---|
| 9.5-11.5 | 7.5 | 64.0 | | 19-107 | | | 19 | 32 | .135 | 120.9 | | | | 31.0 |
| 12-14 | 10.0 | 33.0 | 23.0 | 15-53 | 12.2 | | 18 | 26.5 | .134 | | | | | 38 |
| 14.5-16.5 | 10.8 | 49.0 | 39.0 | 28-70 | 13.7 | 31 | 22.7 | 34 | .162 | 119 | 90.5 | .4 | 64.6 | 35.0 |
| 17-19 | 11.8 | 23.0 | 24.0 | 22-24 | 9.10 | 58 | 36 | 26 | 0.50 | 101.6 | 62.7 | 3.3 | 61.7 | 35.0 |
| 19.5-21.5 | 12.4 | | | | | | | | | | | | | |
| 22-24 | 13.6 | 25.0 | 30.0 | 12-38 | 14.6 | 36.4 | 23.4 | 31.7 | .139 | 115.6 | 84.1 | | | 33.0 |
| 24.5-26.5 | 14.4 | 22.0 | 31.0 | 16-46 | 17.3 | 26.4 | 18.2 | 22.3 | .129 | 124.4 | 97 | 17.9 | 62.1 | 20.0 |
| 27-29 | 15.7 | 36.0 | 33.0 | 18-46 | 19.6 | | | | .112 | 124.8 | 98.6 | 13.2 | 67.8 | 19.0 |
| 29.5-31.5 | | | | | | | | | | | | | | |
| 32-34 | | | | | | 17.7 | | | | | | | | |
| 34.5-36.5 | 19.1 | | | | | | 20.0 | 26.4 | | | | 26.0 | 51.0 | 23.0 |

Table A.2 Laboratory results from boring HF-2

| Depth (ft) | $\sigma'_v$ (psi) | $\sigma'_p$ (Casagrande) (psi) | $\sigma'_p$ (Modulus) (psi) | $\sigma'_p$ error band (psi) | m | $w_n$ (%) | PL (%) | LL (%) | $C_{CE}$ | $\gamma_t$ (pcf) | $\gamma_d$ (pcf) | Grain Size %>75mm | Grain Size %2-75mm | Grain Size %<2mm |
|---|---|---|---|---|---|---|---|---|---|---|---|---|---|---|
| 9.5-11.5 | | 53.0 | 45.0 | 30-98 | 11.5 | 30.3 | 21.9 | 31.6 | 0.156 | 118.8 | 90.4 | 0.1 | 59.9 | 40.0 |
| 12-14 | | 30.0 | 32.0 | 20-41 | 13.4 | 33.2 | 21.8 | 30.0 | 0.159 | 117.8 | 88.2 | 1.1 | 78.9 | 20.0 |
| 14.5-16.5 | | 35.0 | 34.0 | 22-42 | 14.4 | 27.8 | 19.0 | 30.5 | 0.132 | 119.1 | 90.9 | 0.6 | 69.4 | 30.0 |
| 17-19 | | 20.0 | 34.0 | 12-26 | 12.0 | 48.7 | 23.9 | 37.0 | 0.269 | 101.2 | 62.5 | 1.1 | 60.9 | 38.0 |
| 19.5-21.5 | | | | | | | | | | | | | | |
| 22-24 | | | | | | | | | | | | | | |
| 24.5-26.5 | | | | | | | | | | | | | | |
| 27-29 | | | | | | 27.3 | 18.3 | 23.7 | | | | | | |
| 29.5-31.5 | | | | | | 27.1 | 16.0 | 21.0 | | | | 25.0 | 48.0 | 27.0 |
| 32-34 | | | | | | | | | | | | | | |
| 34.5-36.5 | | | | | | 23.2 | | | | | | 8.8 | 56.2 | 35.0 |

Table A.3 Laboratory results from boring RS-3

| Depth (ft) | $\sigma'_v$ (psi) | $\sigma'_p$ (Casagrande) (psi) | $\sigma'_p$ (Modulus) (psi) | $\sigma'_p$ error band (psi) | m | $w_n$ (%) | PL (%) | LL (%) | $C_{CE}$ | $\gamma_t$ (pcf) | $\gamma_d$ (pcf) | Grain Size %>75mm | Grain Size %2-75mm | Grain Size %<2mm |
|---|---|---|---|---|---|---|---|---|---|---|---|---|---|---|
| 9.5-11.5 | 7.5 | | | | | | | | | | | | | |
| 12-14 | 10.0 | 37.0 | 35.0 | 22-55 | 13.7 | 33.4 | 22.9 | 31.6 | 0.138 | 118.5 | 89.8 | 0.7 | 61.7 | 38.0 |
| 14.5-16.5 | 10.8 | 43.0 | 44.0 | 30-55 | 13.7 | 32.6 | 22.6 | 32.5 | 0.170 | 119.5 | 90.7 | 0.6 | 69.4 | 30.0 |
| 17-19 | 11.8 | 22.0 | 21.0 | 17-24 | 12.0 | 67.0 | | | 0.419 | 101.1 | 81.0 | 5.2 | 60.8 | 34.0 |
| 19.5-21.5 | 12.4 | | | | | | | | | | | 51.0 | 28.0 | 21.0 |
| 22-24 | 13.6 | | | | | | | | | | | | | |
| 24.5-26.5 | 14.4 | | | | | | | | | | | | | |
| 27-29 | 15.7 | | | | | | | | | | | | | |
| 29.5-31.5 | | | | | | | | | | | | | | |
| 32-34 | | | | | | | | | | | | | | |
| 34.5-36.5 | 19.1 | | | | | 21.3 | 18.5 | 23.0 | | | | 10.2 | 57.2 | 32.0 |

Table A.4 Laboratory results from boring RF-4

| Depth (ft) | $\sigma'_v$ (psi) | $\sigma'_p$ (Casagrande) (psi) | $\sigma'_p$ (Modulus) (psi) | $\sigma'_p$ error band (psi) | m | $w_n$ (%) | PL (%) | LL (%) | $C_{CE}$ | $\gamma_t$ (pcf) | $\gamma_d$ (pcf) | Grain Size %>75mm | Grain Size %2-75mm | Grain Size %<2mm |
|---|---|---|---|---|---|---|---|---|---|---|---|---|---|---|
| 9.5-11.5 | 7.5 | | | | | | | | | | | | | 29.0 |
| 12-14 | 10.0 | 45.0 | 47.0 | 27-70 | 12.6 | | | | 0.136 | | | | | |
| 14.5-16.5 | 10.8 | 55.0 | 57.0 | 31-70 | 10.6 | 28.3 | 23.8 | 31.5 | 0.129 | 119.7 | 94.3 | 0.9 | 59.6 | 39.5 |
| 17-19 | 11.8 | 28.0 | 31.0 | 22-31 | 13.0 | 58.4 | 23.5 | 47.0 | 0.490 | 102.4 | 63.2 | 0.9 | 62.1 | 37.0 |
| 19.5-21.5 | 12.4 | | | | | | | | | | | | | |
| 22-24 | 13.6 | 21.0 | 25.0 | 11.3-37 | 19.4 | 32.3 | 18.3 | 24.7 | 0.093 | 123.5 | 105.4 | 77.2 | 47.2 | 30.0 |
| 24.5-26.5 | 14.4 | 35.0 | 43.0 | 22-46 | 15.6 | 27.1 | 16.7 | 26.5 | 0.126 | 122.5 | 95.4 | 5.3 | 55.7 | 39.0 |
| 27-29 | 15.7 | | | | | | | | | | | | | |
| 29.5-31.5 | | | | | | | | | | | | | | |
| 32-34 | | | | | | | | | | | | | | |
| 34.5-36.5 | 19.1 | | | | | | 18.5 | 23.0 | | | | | | |

# Appendix B

## X-Ray Logs

Table B.1 X-Ray log (sheet 1)

| DATE | FILM NO. | PROJECT | KV | mA | TIME (min) | DIST (in) |
|---|---|---|---|---|---|---|
| 2/14 | HS1 5TA | I-15 | 150 | 5 | 7 | 18.5 |
| 2/14 | HS1 5TB | I-15 | 150 | 5 | 7 | 36 |
| 2/14 | HS1 5TC | I-15 | 150 | 5 | 6 | 36 |
| 2/14 | HS1 5MA | I-15 | 150 | 5 | 6 | 36 |
| 2/14 | HS1 5BA | I-15 | 150 | 5 | 6 | 36 |
| 2/22 | HS1 1TA | I-15 | 150 | 5 | 6 | 36 |
| 2/22 | HS1 1MA | I-15 | 150 | 5 | 6 | 36 |
| 2/22 | HS1 1BA | I-15 | 150 | 5 | 6 | 36 |
| 2/22 | HS1 2TA | I-15 | 150 | 5 | 6 | 36 |
| 2/22 | HS1 2MA | I-15 | 150 | 5 | 6 | 36 |
| 2/22 | HS1 2BA | I-15 | 150 | 5 | 6 | 36 |
| 2/22 | HS1 3TA | I-15 | 150 | 5 | 6 | 36 |
| 2/22 | HS1 3MA | I-15 | 150 | 5 | 6 | 36 |
| 2/22 | HS1 3BA | I-15 | 150 | 5 | 6 | 36 |
| 2/22 | HS1 6TA | I-15 | 150 | 5 | 6 | 36 |
| 2/22 | HS1 6MA | I-15 | 150 | 5 | 6 | 36 |
| 2/22 | HS1 6BA | I-15 | 150 | 5 | 6 | 36 |
| 2/23 | HS1 4TA | I-15 | 150 | 5 | 6 | 36 |
| 2/23 | HS1 4MA | I-15 | 150 | 5 | 6 | 36 |
| 2/23 | HS1 4BA | I-15 | 150 | 5 | 6 | 36 |
| 2/23 | HS1 7TA | I-15 | 150 | 5 | 6 | 36 |
| 2/23 | HS1 7MA | I-15 | 150 | 5 | 6 | 36 |
| 2/23 | HS1 7BA | I-15 | 150 | 5 | 6 | 36 |
| 2/23 | HS1 8TA | I-15 | 150 | 5 | 6 | 36 |
| 2/23 | HS1 8MA | I-15 | 150 | 5 | 6 | 36 |
| 2/23 | HS1 8BA | I-15 | 150 | 5 | 6 | 36 |
| 2/23 | HS1 9TA | I-15 | 150 | 5 | 6 | 36 |
| 2/23 | HS1 9MA | I-15 | 150 | 5 | 6 | 36 |
| 2/23 | HS1 9BA | I-15 | 150 | 5 | 6 | 36 |
| 2/23 | HS1 10TA | I-15 | 150 | 5 | 6 | 36 |
| 2/23 | HS1 10MA | I-15 | 150 | 5 | 6 | 36 |
| 2/23 | HS1 10BA | I-15 | 150 | 5 | 6 | 36 |
| 2/23 | HS1 11TA | I-15 | 150 | 5 | 6 | 36 |
| 2/23 | HS1 11MA | I-15 | 150 | 5 | 6 | 36 |
| 2/23 | HS1 11BA | I-15 | 150 | 5 | 6 | 36 |
| 2/28 | RF4 1TA | I-15 | 150 | 5 | 6 | 36 |
| 2/28 | RF4 1TB | I-15 | 150 | 5 | 4 | 36 |
| 2/28 | RF4 1MA | I-15 | 150 | 5 | 6 | 36 |
| 2/28 | RF4 1BA | I-15 | 150 | 5 | 6 | 36 |
| 2/28 | RF4 2TA | I-15 | 150 | 5 | 6 | 36 |

Table B.2 X-Ray log (sheet 2)

| DATE | FILM NO. | PROJECT | KV | mA | TIME (min) | DIST (in) |
|---|---|---|---|---|---|---|
| 2/28 | RF4 2MA | I-15 | 150 | 5 | 6 | 36 |
| 2/28 | RF4 2MB | I-15 | 150 | 5 | 4 | 18.5 |
| 2/28 | RF4 2BA | I-15 | 150 | 5 | 6 | 36 |
| 2/28 | RF4 3TA | I-15 | 150 | 5 | 6 | 36 |
| 2/28 | RF4 3MA | I-15 | 150 | 5 | 6 | 36 |
| 2/28 | RF4 3BA | I-15 | 150 | 5 | 6 | 36 |
| 2/28 | RF4 3BB | I-15 | 150 | 5 | 6 | 36 |
| 2/28 | RF4 4TA | I-15 | 150 | 5 | 6 | 36 |
| 2/28 | RF4 4MA | I-15 | 150 | 5 | 6 | 36 |
| 2/28 | RF4 4BA | I-15 | 150 | 5 | 6 | 36 |
| 3/1 | RF4 1TC | I-15 | 150 | 5 | 6 | 36 |
| 3/1 | RF4 1TD | I-15 | 150 | 5 | 4 | 36 |
| 3/1 | RF4 1MB | I-15 | 150 | 5 | 3 | 36 |
| 3/1 | RF4 1MC | I-15 | 150 | 5 | 2 | 36 |
| 3/1 | RF4 1MD | I-15 | 150 | 5 | 1 | 36 |
| 3/1 | RF4 1ME | I-15 | 150 | 5 | .75 | 36 |
| 3/1 | RF4 1TE | I-15 | 150 | 5 | 1 | 36 |
| 3/1 | RF4 1BB | I-15 | 150 | 5 | 1 | 36 |
| 3/1 | RF4 1TB | I-15 | 150 | 5 | 1 | 36 |
| 3/1 | RF4 2MC | I-15 | 150 | 5 | 1 | 36 |
| 3/1 | RF4 2BB | I-15 | 150 | 5 | 1 | 36 |
| 3/1 | RF4 3TB | I-15 | 150 | 5 | 1 | 36 |
| 3/1 | RF4 3MB | I-15 | 150 | 5 | 1 | 36 |
| 3/1 | RF4 3BC | I-15 | 150 | 5 | 1 | 36 |
| 3/1 | RF4 3BD | I-15 | 150 | 5 | .75 | 36 |
| 3/1 | RF4 3BE | I-15 | 150 | 5 | .5 | 36 |
| 3/19 | RF4 2TC | I-15 | 100 | 12 | 4 | 36 |
| 3/19 | RF4 2TD | I-15 | 150 | 12 | 3 | 36 |
| 3/19 | RF4 2TE | I-15 | 90 | 11 | 2.5 | 36 |
| 3/19 | RF4 2TF | I-15 | 75 | 13 | 3 | 36 |
| 3/19 | RF4 2TG | I-15 | 90 | 5 | 3 | 36 |
| 3/20 | RF4 2TH | I-15 | 75 | 5 | 2 | 36 |
| 3/20 | RF4 2TI | I-15 | 75 | 5 | 2 | 36 |
| 3/20 | RF4 2TJ | I-15 | 150 | 5 | 6 | 36 |
| 3/20 | RF4 2TK | I-15 | 150 | 5 | 3 | 36 |
| 3/20 | RF4 2MD | I-15 | 100 | 5 | 3 | 36 |
| 3/20 | RF4 2ME | I-15 | 150 | 5 | 2.5 | 36 |
| 3/20 | RF4 2MF | I-15 | 150 | 5 | 2 | 36 |
| 3/20 | RF4 2MG | I-15 | 140 | 5 | 2 | 36 |
| 3/20 | RF4 2MH | I-15 | 130 | 5 | 2 | 36 |

Table B.3 X-Ray log (sheet 3)

| DATE | FILM NO. | PROJECT | KV | mA | TIME (min) | DIST (in) |
|---|---|---|---|---|---|---|
| 3/21 | RF4 1MF | I-15 | 135 | 5 | 2 | 36 |
| 3/21 | RF4 1BB | I-15 | 135 | 5 | 2 | 36 |
| 3/21 | RF4 2TL | I-15 | 135 | 5 | 2 | 18.5 |
| 3/21 | RF4 2MI | I-15 | 135 | 5 | 2 | 36 |
| 3/21 | RF4 2BC | I-15 | 135 | 5 | 2 | 36 |
| 3/21 | RF4 3TC | I-15 | 135 | 5 | 2 | 36 |
| 3/21 | RF4 3MC | I-15 | 135 | 5 | 2 | 36 |
| 3/21 | RF4 3BF | I-15 | 135 | 5 | 2 | 36 |
| 3/21 | RF4 4TB | I-15 | 135 | 5 | 2 | 36 |
| 3/21 | RF4 4MB | I-15 | 135 | 5 | 2 | 36 |
| 3/21 | RF4 4BB | I-15 | 135 | 5 | 2 | 36 |
| 3/21 | RF4 5TA | I-15 | 135 | 5 | 2 | 36 |
| 3/21 | RF4 5MA | I-15 | 135 | 5 | 2 | 36 |
| 3/21 | RF4 5BA | I-15 | 135 | 5 | 2 | 36 |
| 3/21 | RF4 6TA | I-15 | 135 | 5 | 2 | 36 |
| 3/21 | RF4 6MA | I-15 | 135 | 5 | 2 | 36 |
| 3/21 | RF4 6BA | I-15 | 135 | 5 | 2 | 36 |
| 3/21 | RF4 7TA | I-15 | 135 | 5 | 2 | 36 |
| 3/21 | RF4 7MA | I-15 | 135 | 5 | 2 | 36 |
| 3/21 | RF4 7BA | I-15 | 135 | 5 | 2 | 36 |
| 3/21 | RF4 8TA | I-15 | 135 | 5 | 2 | 36 |
| 3/21 | RF4 8MA | I-15 | 135 | 5 | 2 | 36 |
| 3/21 | RF4 8BA | I-15 | 135 | 5 | 2 | 36 |
| 3/21 | RF4 9TA | I-15 | 135 | 5 | 2 | 36 |
| 3/21 | RF4 9MA | I-15 | 135 | 5 | 2 | 36 |
| 3/21 | RF4 9BA | I-15 | 135 | 5 | 2 | 36 |
| 3/22 | RF4 10TA | I-15 | 135 | 5 | 2 | 36 |
| 3/22 | RF4 10MA | I-15 | 135 | 5 | 2 | 36 |
| 3/22 | RF4 10BA | I-15 | 135 | 5 | 2 | 36 |
| 3/22 | RF4 11TA | I-15 | 135 | 5 | 2 | 36 |
| 3/22 | RF4 11MA | I-15 | 135 | 5 | 2 | 36 |
| 3/22 | RF4 11BA | I-15 | 135 | 5 | 2 | 36 |
| 3/22 | HF2 1TA | I-15 | 135 | 5 | 2 | 36 |
| 3/22 | HF2 1MA | I-15 | 135 | 5 | 2 | 36 |
| 3/22 | HF2 1BA | I-15 | 135 | 5 | 2 | 36 |
| 3/22 | HF2 2TA | I-15 | 135 | 5 | 2 | 36 |
| 3/22 | HF2 2MA | I-15 | 135 | 5 | 2 | 36 |
| 3/22 | HF2 2BA | I-15 | 135 | 5 | 2 | 36 |
| 3/22 | HF2 3TA | I-15 | 135 | 5 | 2 | 36 |
| 3/22 | HF2 3MA | I-15 | 135 | 5 | 2 | 36 |

Table B.4 X-Ray log (sheet 4)

| DATE | FILM NO. | PROJECT | KV | mA | TIME (min) | DIST (in) |
|---|---|---|---|---|---|---|
| 3/22 | HF2 3BA | I-15 | 135 | 5 | 2 | 36 |
| 3/22 | HF2 4TA | I-15 | 135 | 5 | 2 | 36 |
| 3/22 | HF2 4MA | I-15 | 135 | 5 | 2 | 36 |
| 3/22 | HF2 4BA | I-15 | 135 | 5 | 2 | 18.5 |
| 3/22 | HF2 6TA | I-15 | 135 | 5 | 2 | 36 |
| 3/22 | HF2 6MA | I-15 | 135 | 5 | 2 | 36 |
| 3/22 | HF2 6BA | I-15 | 135 | 5 | 2 | 36 |
| 3/22 | HF2 7TA | I-15 | 135 | 5 | 2 | 36 |
| 3/22 | HF2 7MA | I-15 | 135 | 5 | 2 | 36 |
| 3/22 | HF2 7BA | I-15 | 135 | 5 | 2 | 36 |
| 3/23 | HF2 8TA | I-15 | 135 | 5 | 2 | 36 |
| 3/23 | HF2 8MA | I-15 | 135 | 5 | 2 | 36 |
| 3/23 | HF2 8BA | I-15 | 135 | 5 | 2 | 36 |
| 3/23 | HF2 9TA | I-15 | 135 | 5 | 2 | 36 |
| 3/23 | HF2 9MA | I-15 | 135 | 5 | 2 | 36 |
| 3/23 | HF2 9BA | I-15 | 135 | 5 | 2 | 36 |
| 3/23 | HF2 10TA | I-15 | 135 | 5 | 2 | 36 |
| 3/23 | HF2 10BA | I-15 | 135 | 5 | 2 | 36 |
| 3/23 | HF2 10MA | I-15 | 135 | 5 | 2 | 36 |
| 3/23 | HF2 11TA | I-15 | 135 | 5 | 2 | 36 |
| 3/23 | HF2 11MA | I-15 | 135 | 5 | 2 | 36 |
| 3/23 | HF2 11BA | I-15 | 135 | 5 | 2 | 36 |
| 3/23 | RS3 1TA | I-15 | 135 | 5 | 2 | 36 |
| 3/23 | RS3 1MA | I-15 | 135 | 5 | 2 | 36 |
| 3/23 | RS3 1BA | I-15 | 135 | 5 | 2 | 36 |
| 3/23 | RS3 2TA | I-15 | 135 | 5 | 2 | 36 |
| 3/23 | RS3 2MA | I-15 | 135 | 5 | 2 | 36 |
| 3/23 | RS3 2BA | I-15 | 135 | 5 | 2 | 36 |
| 3/23 | RS3 3TA | I-15 | 135 | 5 | 2 | 36 |
| 3/23 | RS3 3MA | I-15 | 135 | 5 | 2 | 36 |
| 3/23 | RS3 3BA | I-15 | 135 | 5 | 2 | 36 |
| 3/23 | RS3 4TA | I-15 | 135 | 5 | 2 | 36 |
| 3/23 | RS3 4MA | I-15 | 135 | 5 | 2 | 36 |
| 3/23 | RS3 4BA | I-15 | 135 | 5 | 2 | 36 |
| 3/26 | RS3 8TA | I-15 | 135 | 5 | 2 | 36 |
| 3/26 | RS3 8MA | I-15 | 135 | 5 | 2 | 36 |
| 3/26 | RS3 8BA | I-15 | 135 | 5 | 2 | 36 |
| 3/26 | RS3 9TA | I-15 | 135 | 5 | 2 | 36 |
| 3/26 | RS3 9MA | I-15 | 135 | 5 | 2 | 36 |
| 3/26 | RS3 9BA | I-15 | 135 | 5 | 2 | 36 |

Table B.5 X-Ray log (sheet 5)

| DATE | FILM NO. | PROJECT | KV | mA | TIME (min) | DIST (in) |
|---|---|---|---|---|---|---|
| 3/26 | RS3 10TA | I-15 | 135 | 5 | 2 | 36 |
| 3/26 | RS3 10MA | I-15 | 135 | 5 | 2 | 36 |
| 3/26 | RS3 10BA | I-15 | 135 | 5 | 2 | 36 |
| 3/26 | RS3 11MA | I-15 | 135 | 5 | 2 | 18.5 |
| 3/26 | RS3 11BA | I-15 | 135 | 5 | 2 | 36 |
| 3/26 | RS3 5TA | I-15 | 135 | 5 | 2 | 36 |
| 3/26 | RS3 5MA | I-15 | 135 | 5 | 2 | 36 |
| 3/26 | RS3 5BA | I-15 | 135 | 5 | 2 | 36 |
| 3/26 | RS3 6TA | I-15 | 135 | 5 | 2 | 36 |
| 3/26 | RS3 6MA | I-15 | 135 | 5 | 2 | 36 |
| 3/26 | RS3 6BA | I-15 | 135 | 5 | 2 | 36 |

# Appendix C

## X-Rays

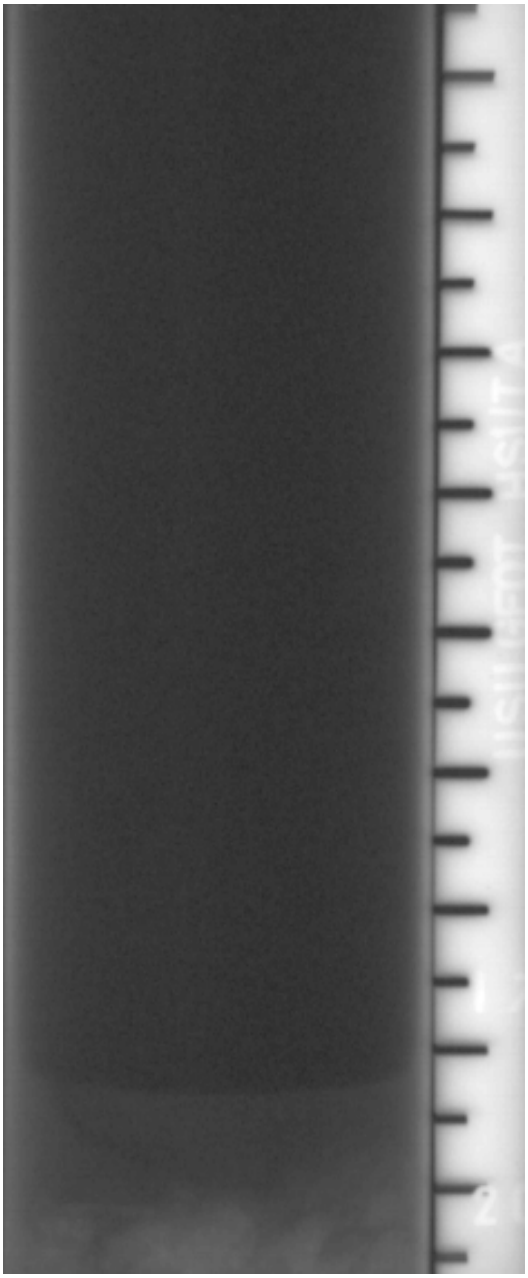

Figure C.1 Top x-ray from the shelby tube, hollow stem auger sample at 9.5-11.5 feet designated HS1 1TA.

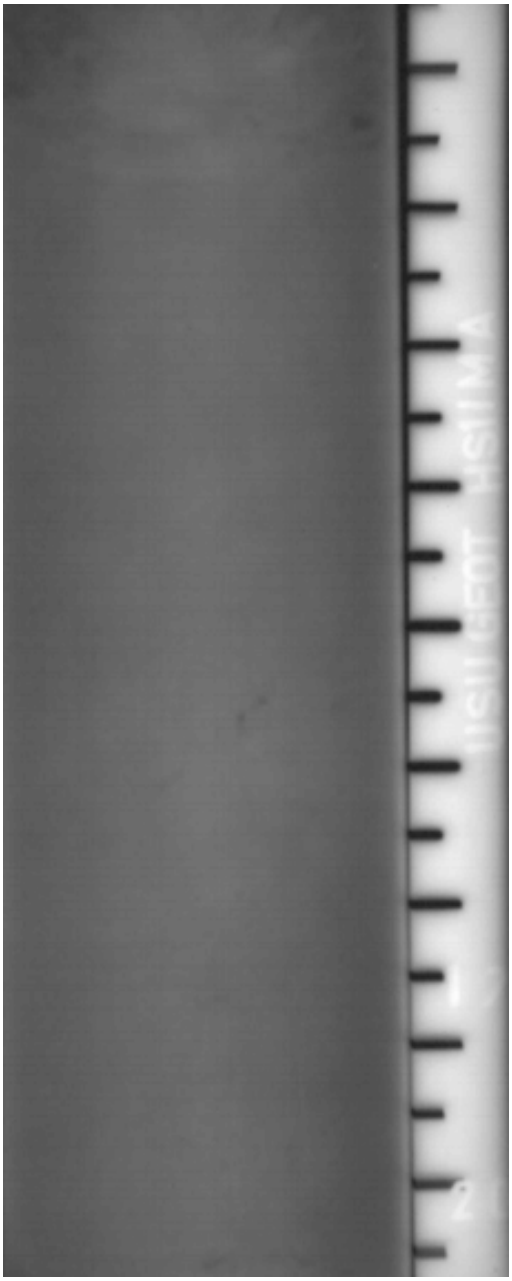

Figure C.2 Middle x-ray from the shelby tube, hollow stem auger sample at 9.5-11.5 feet designated HS1 1MA.

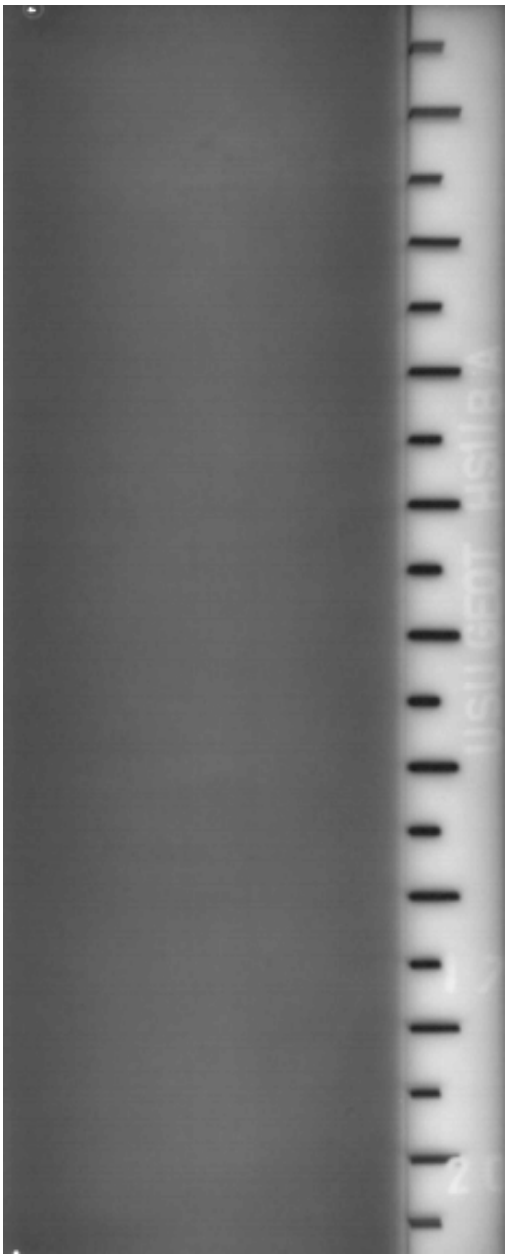

Figure C.3 Bottom x-ray from the shelby tube, hollow stem auger sample at 9.5-11.5 feet designated HS1 1BA.

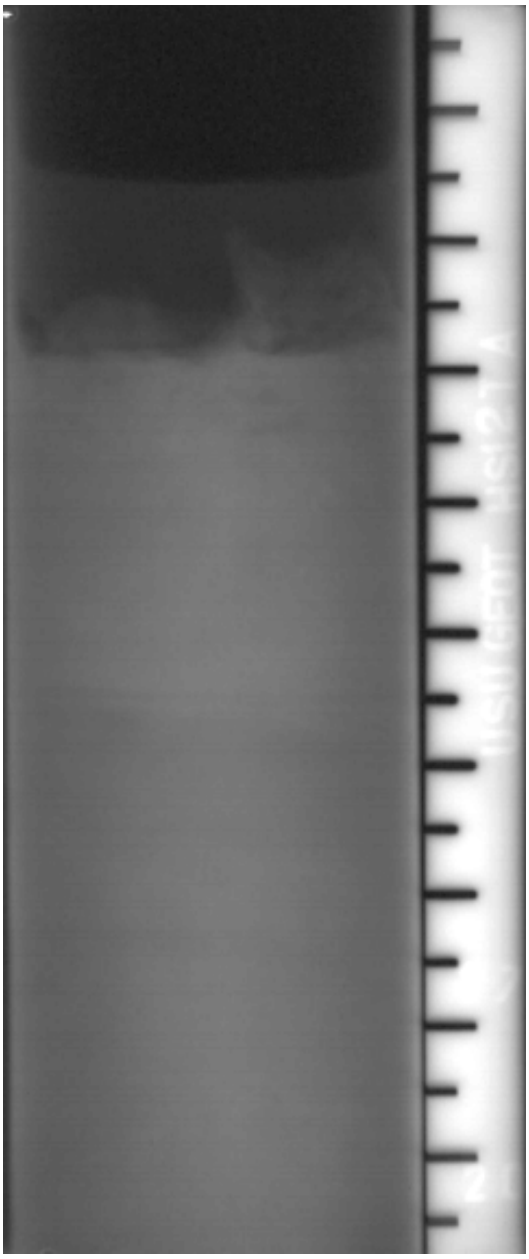

Figure C.4 Top x-ray from the shelby tube, hollow stem auger sample at 12-14 feet designated HS1 2TA.

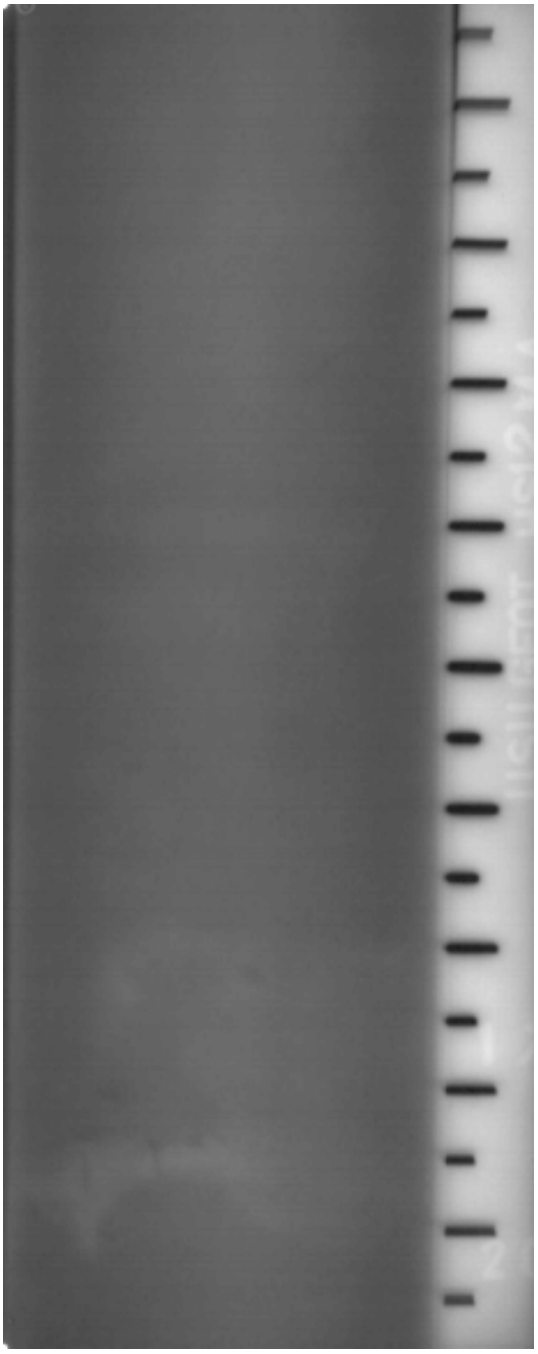

Figure C.5 Middle x-ray from the shelby tube, hollow stem auger sample at 12-14 feet designated HS1 2MA.

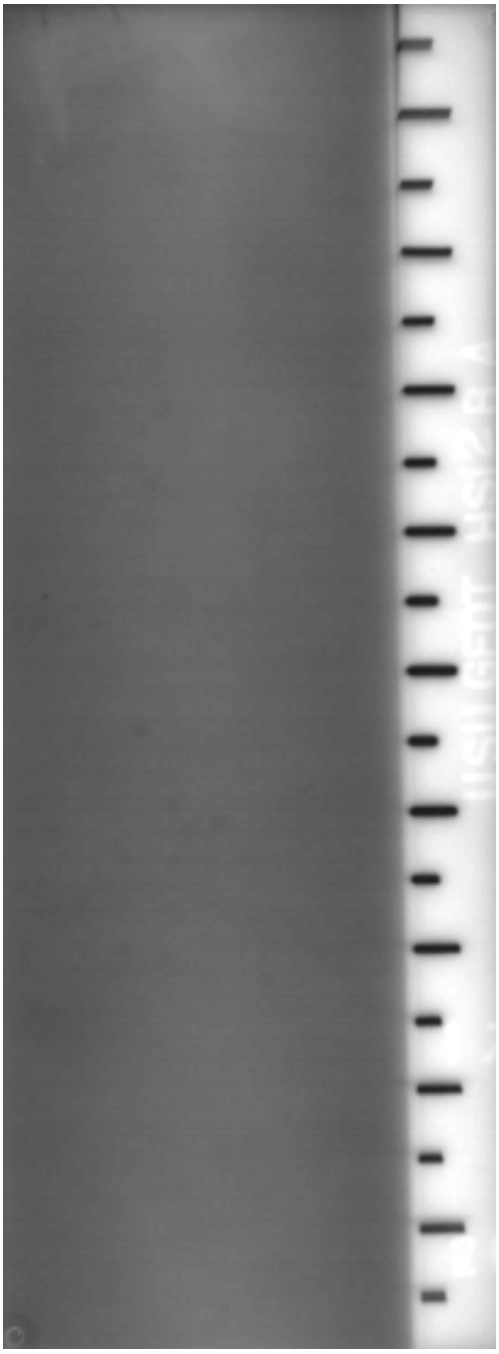

Figure C.6 Bottom x-ray from the shelby tube, hollow stem auger sample at 12-14 feet designated HS1 2BA.

Figure C.7 Top x-ray from the shelby tube, hollow stem auger sample at 14.5-16.5 feet designated HS1 3TA.

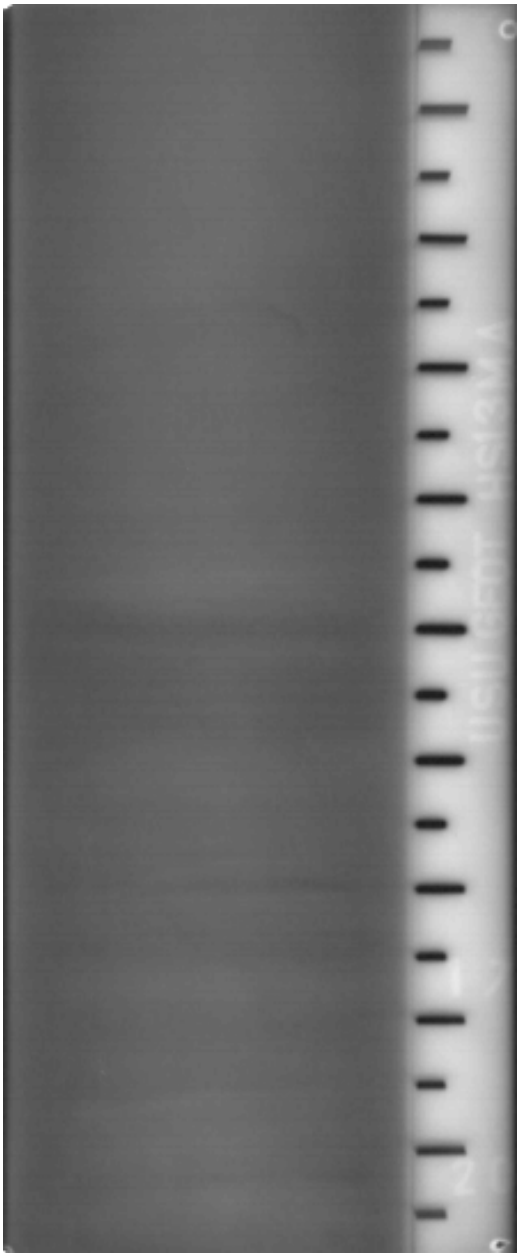

Figure C.8 Middle x-ray from the shelby tube, hollow stem auger sample at 14.5-16.5 feet designated HS1 3MA.

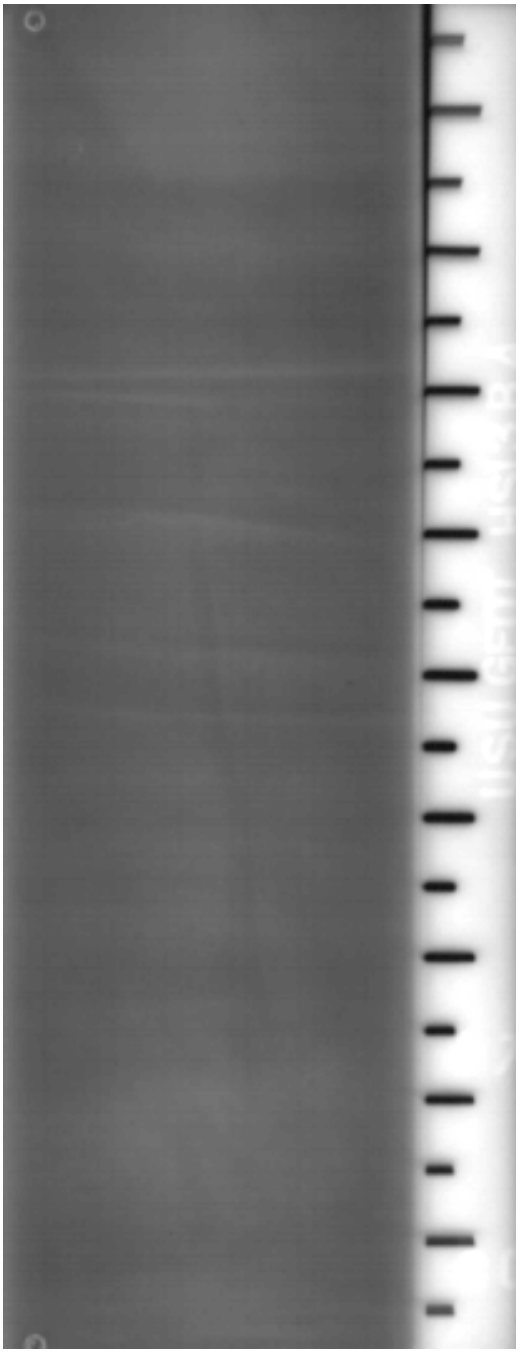

Figure C.9 Bottom x-ray from the shelby tube, hollow stem auger sample at 14.5-16.5 feet designated HS1 3BA.

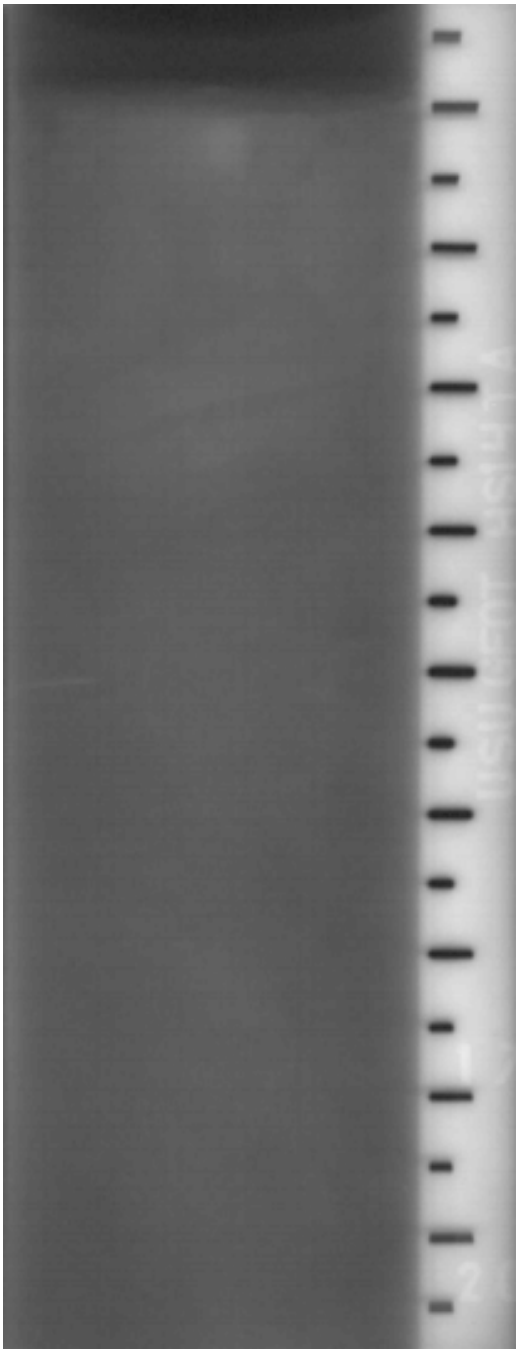

Figure C.10 Top x-ray from the shelby tube, hollow stem auger sample at 17-19 feet designated HS1 4TA.

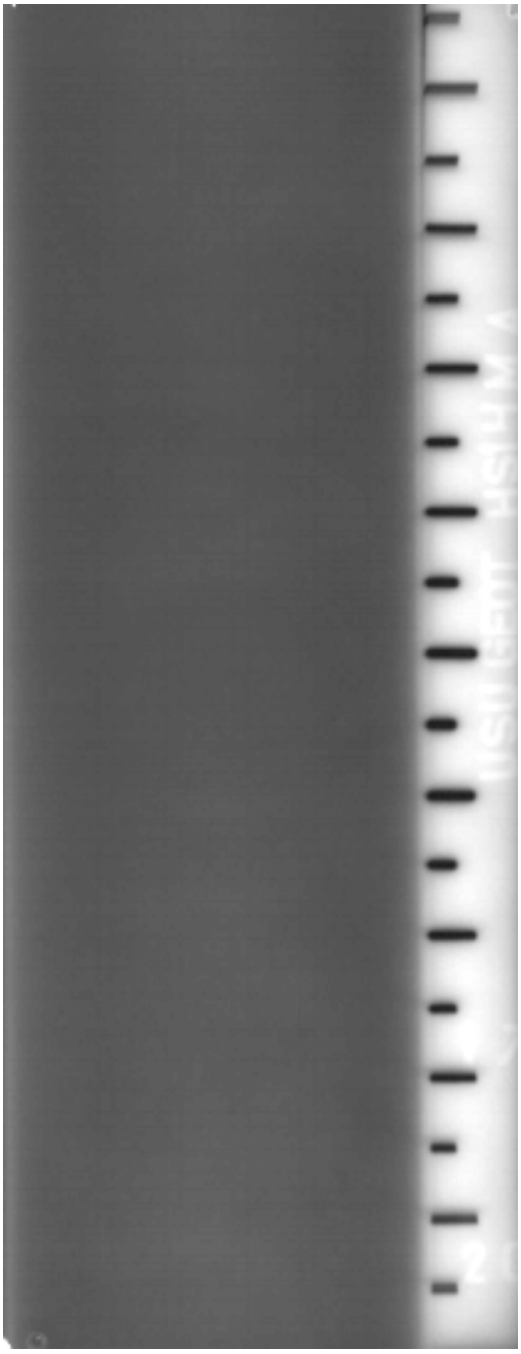

Figure C.11 Middle x-ray from the shelby tube, hollow stem auger sample at 17-19 feet designated HS1 4MA.

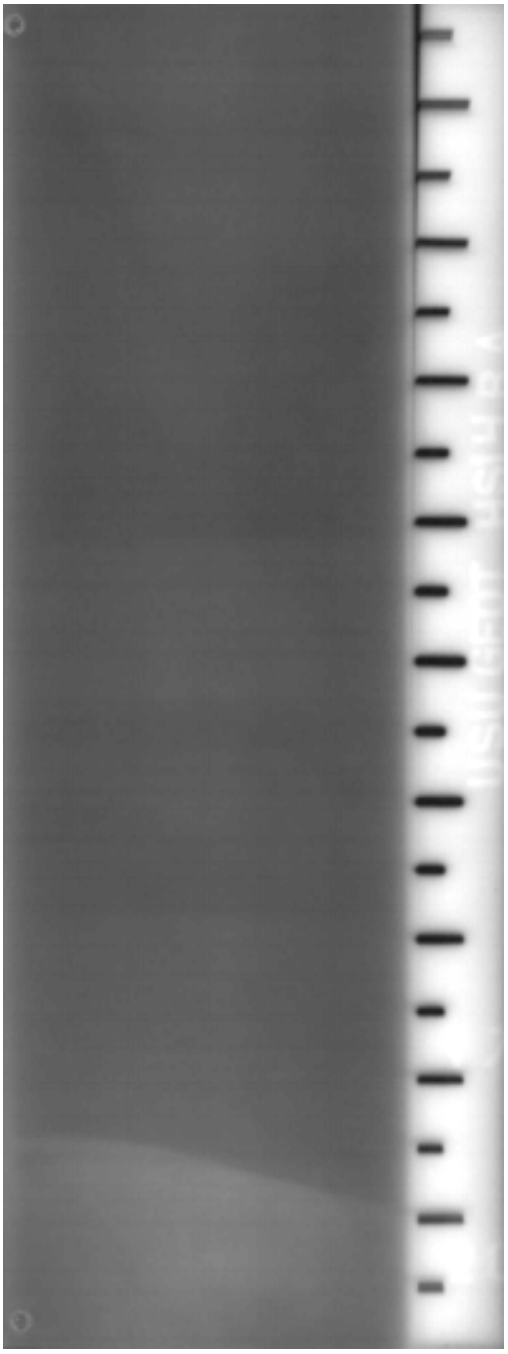

Figure C.12 Bottom x-ray from the shelby tube, hollow stem auger sample at 17-19 feet designated HS1 4BA.

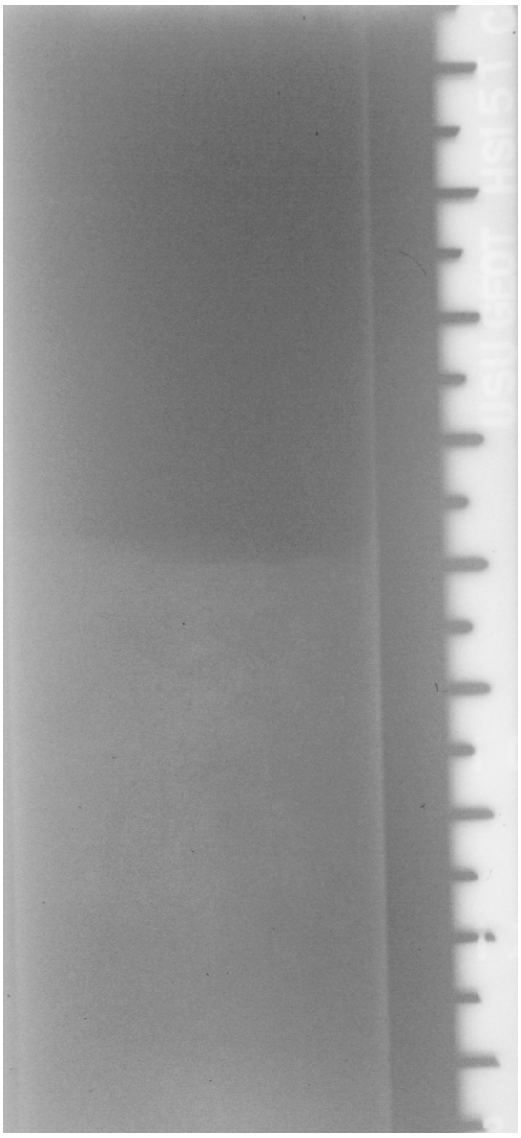

Figure C.13 Top x-ray from the shelby tube, hollow stem auger sample at 19.5-21.5 feet designated HS1 5TA.

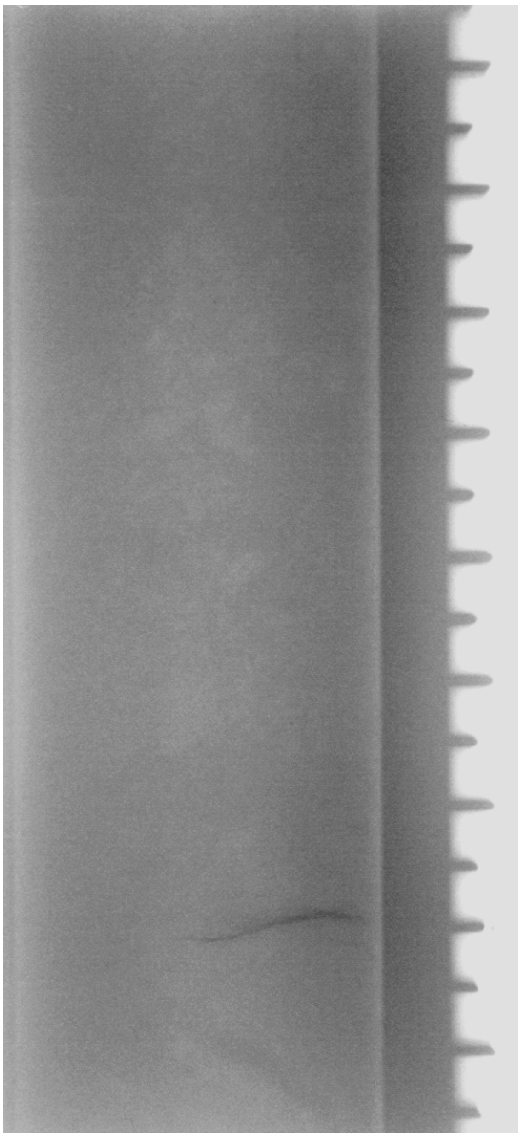

Figure C.14 Middle x-ray from the shelby tube, hollow stem auger sample at 19.5-21.5 feet designated HS1 5MA.

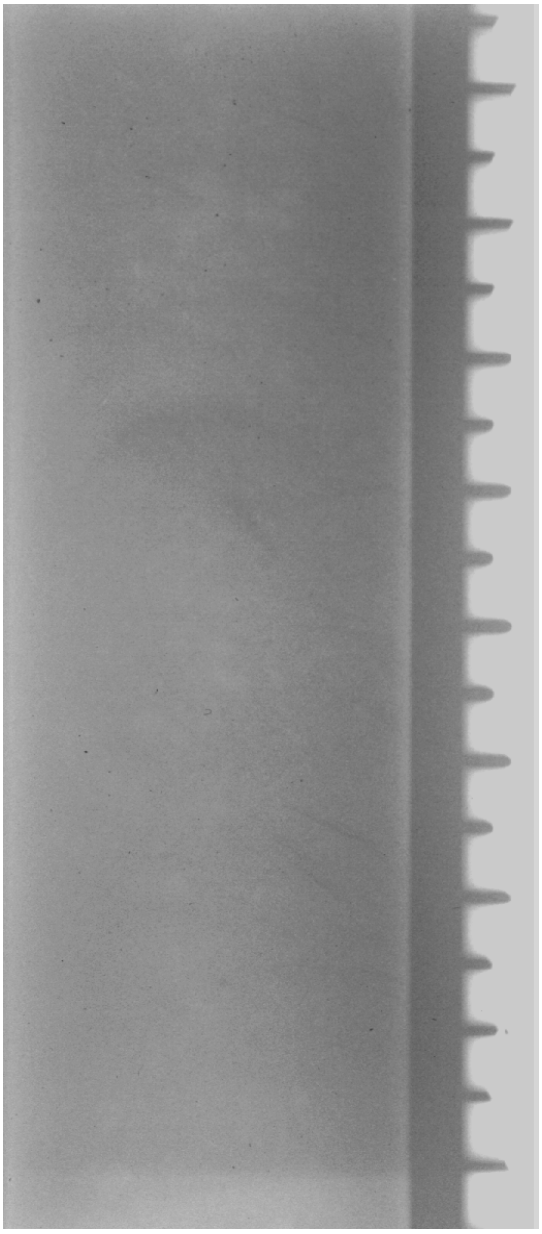

Figure C.15 Bottom x-ray from the shelby tube, hollow stem auger sample at 19.5-21.5 feet designated HS1 5BA.

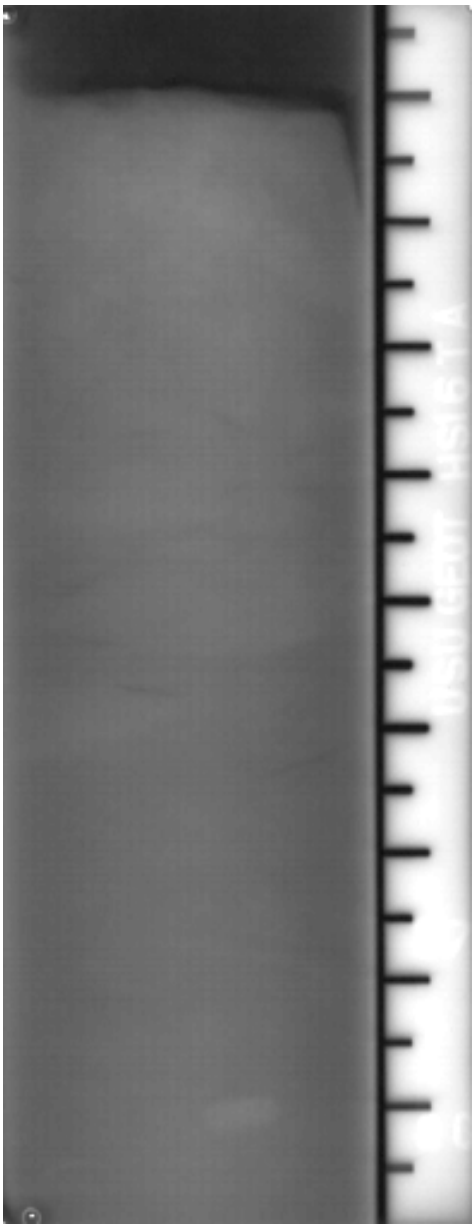

Figure C.16 Top x-ray from the shelby tube, hollow stem auger sample at 22-24 feet designated HS1 6TA.

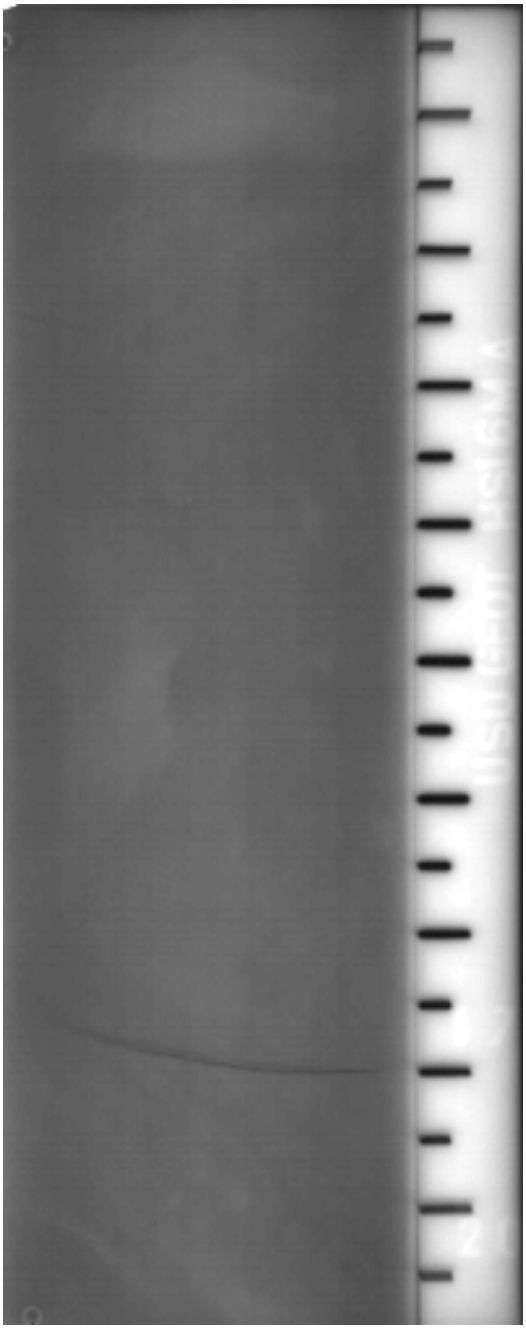

Figure C.17 Middle x-ray from the shelby tube, hollow stem auger sample at 22-24 feet designated HS1 6MA.

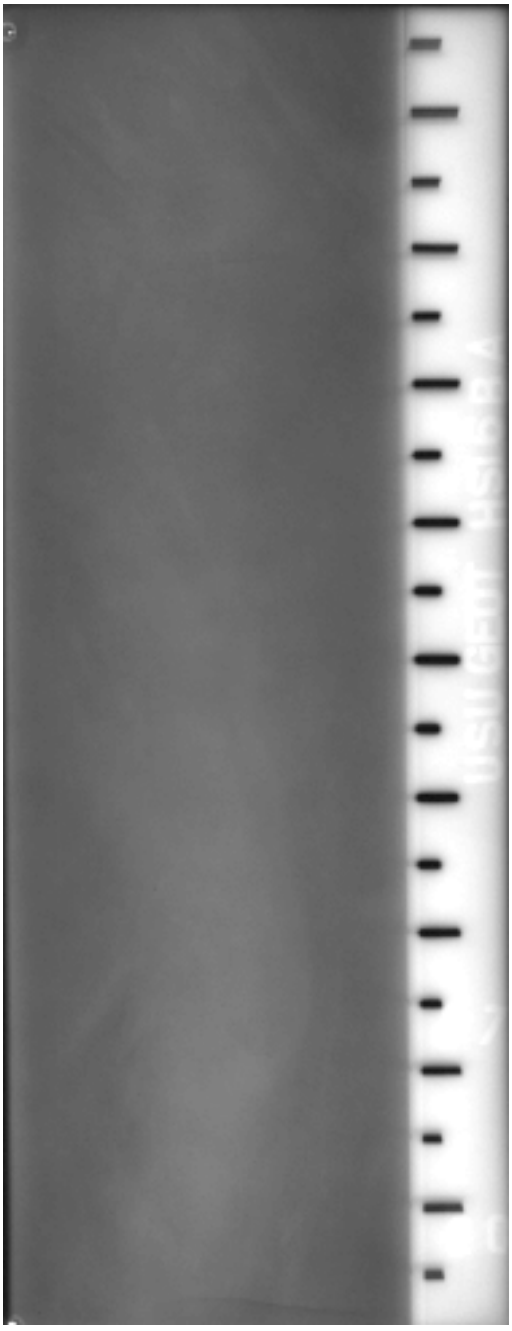

Figure C.18 Bottom x-ray from the shelby tube, hollow stem auger sample at 22-24 feet designated HS1 6BA.

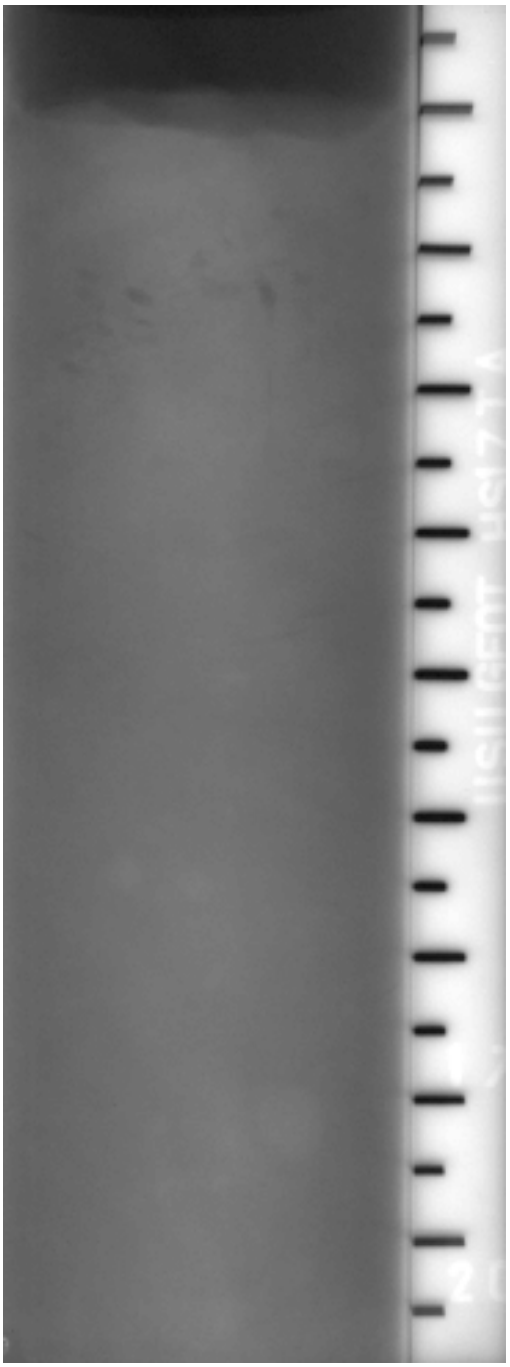

Figure C.19 Top x-ray from the shelby tube, hollow stem auger sample at 24.5-26.5 feet designated HS1 7TA.

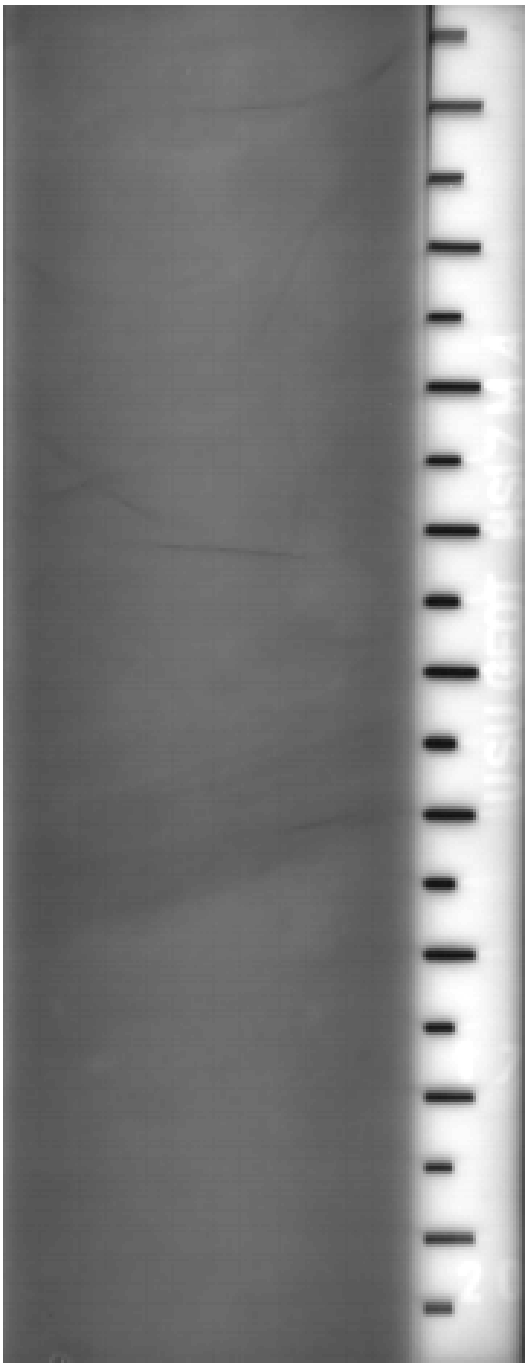

Figure C.20 Middle x-ray from the shelby tube, hollow stem auger sample at 24.5-26.5 feet designated HS1 7MA.

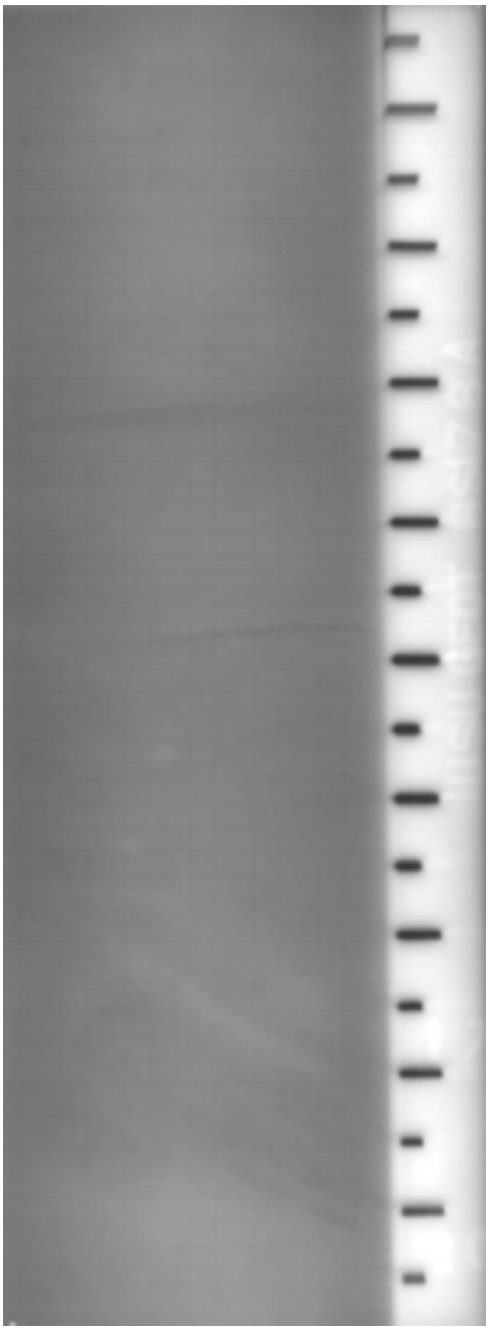

Figure C.21 Bottom x-ray from the shelby tube, hollow stem auger sample at 24.5-26.5 feet designated HS1 7BA.

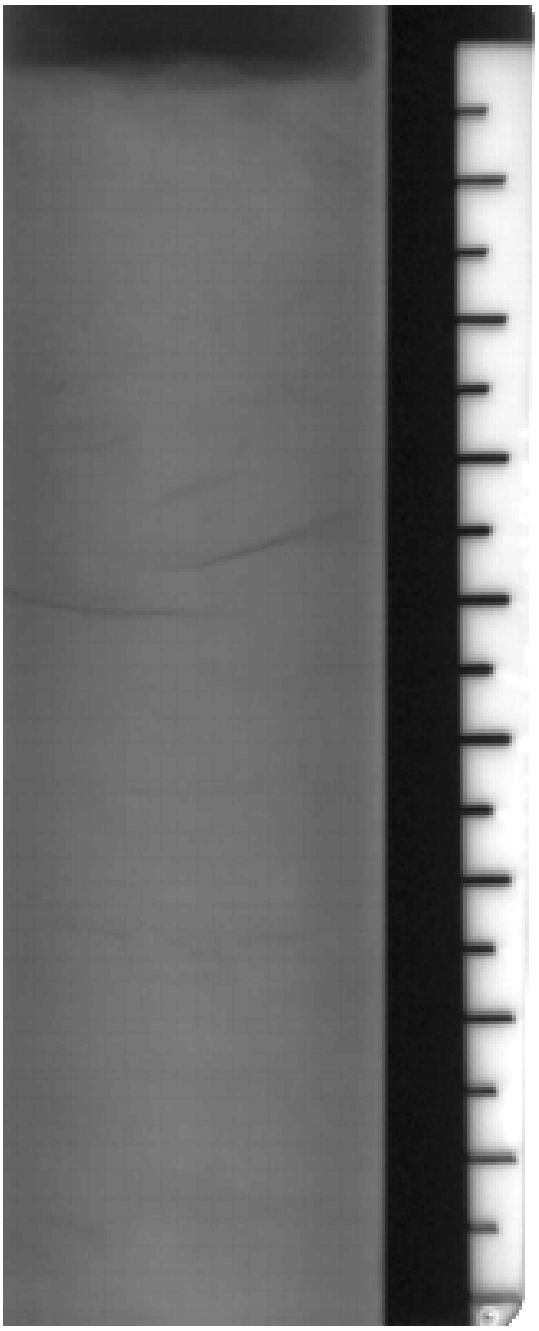

Figure C.22 Top x-ray from the shelby tube, hollow stem auger sample at 27-29 feet designated HS1 8TA.

Figure C.23 Middle x-ray from the shelby tube, hollow stem auger sample at 27-29 feet designated HS1 8MA.

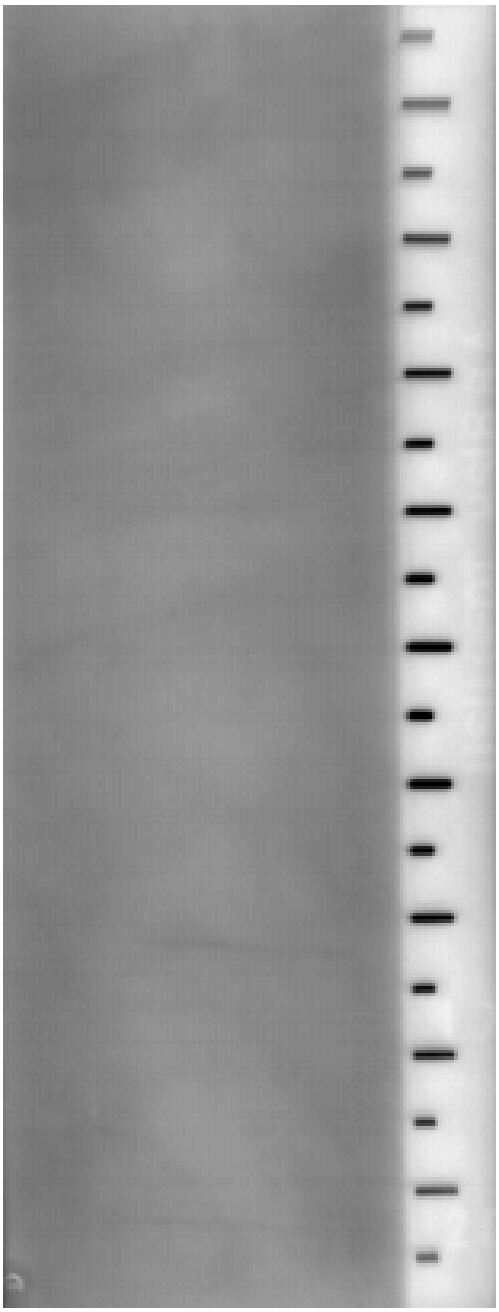

Figure C.24 Bottom x-ray from the shelby tube, hollow stem auger sample at 27-29 feet designated HS1 8BA.

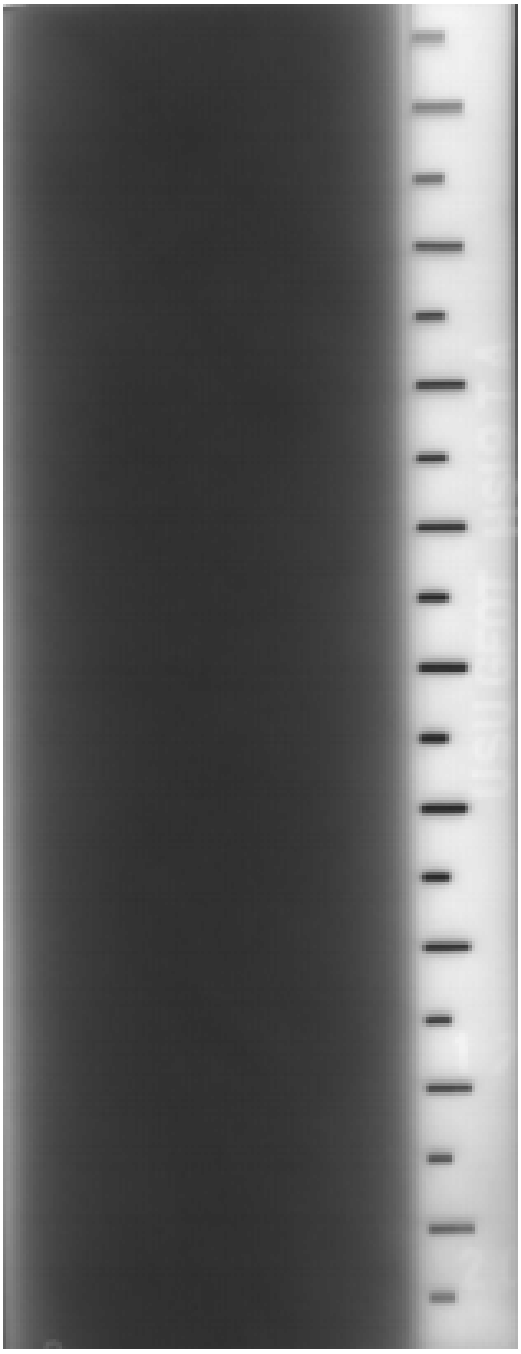

Figure C.25 Top x-ray from the shelby tube, hollow stem auger sample at 29.5-31.5 feet designated HS1 9TA.

Figure C.26 Middle x-ray from the shelby tube, hollow stem auger sample at 29.5-31.5 feet designated HS1 9MA.

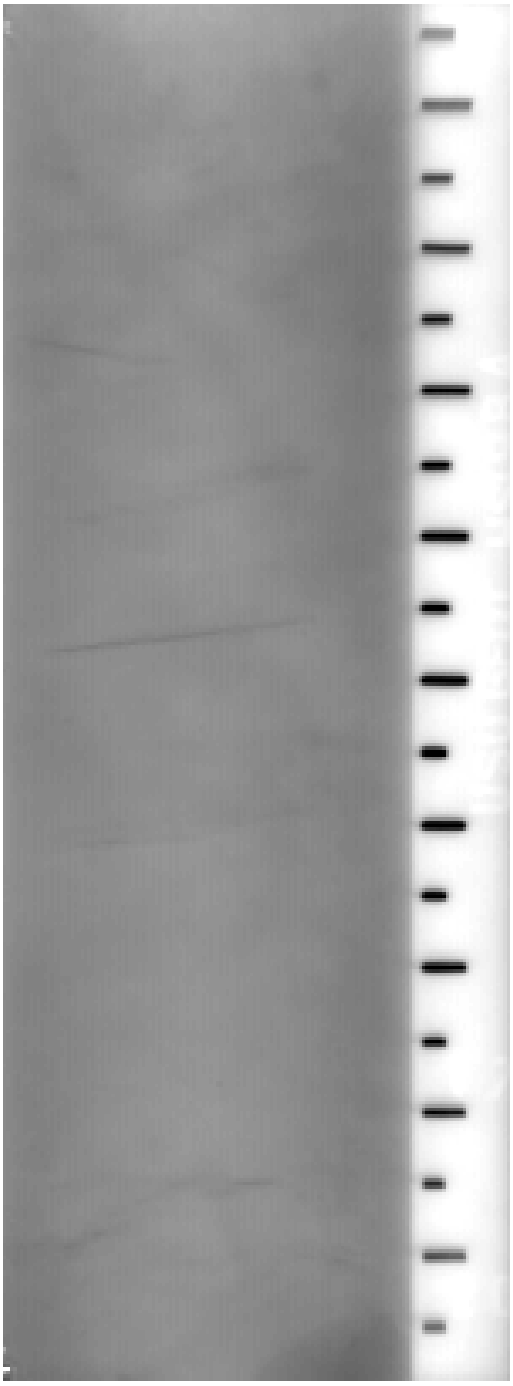

Figure C.27 Bottom x-ray from the shelby tube, hollow stem auger sample at 29.5-31.5 feet designated HS1 9BA.

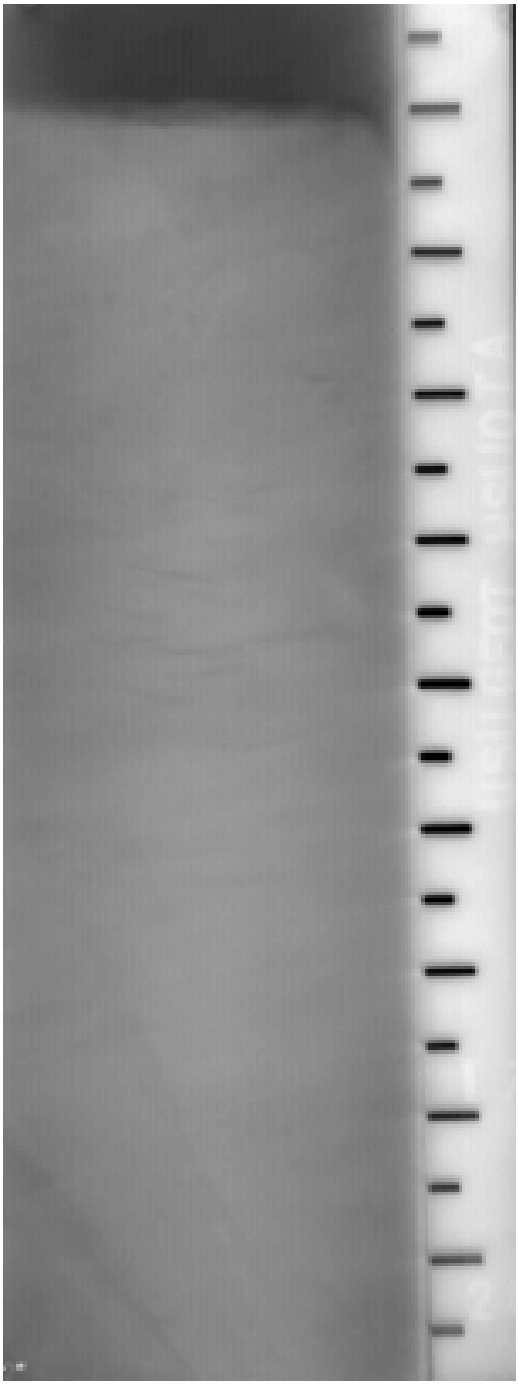

Figure C.28 Top x-ray from the shelby tube, hollow stem auger sample at 32-34 feet designated HS1 10TA.

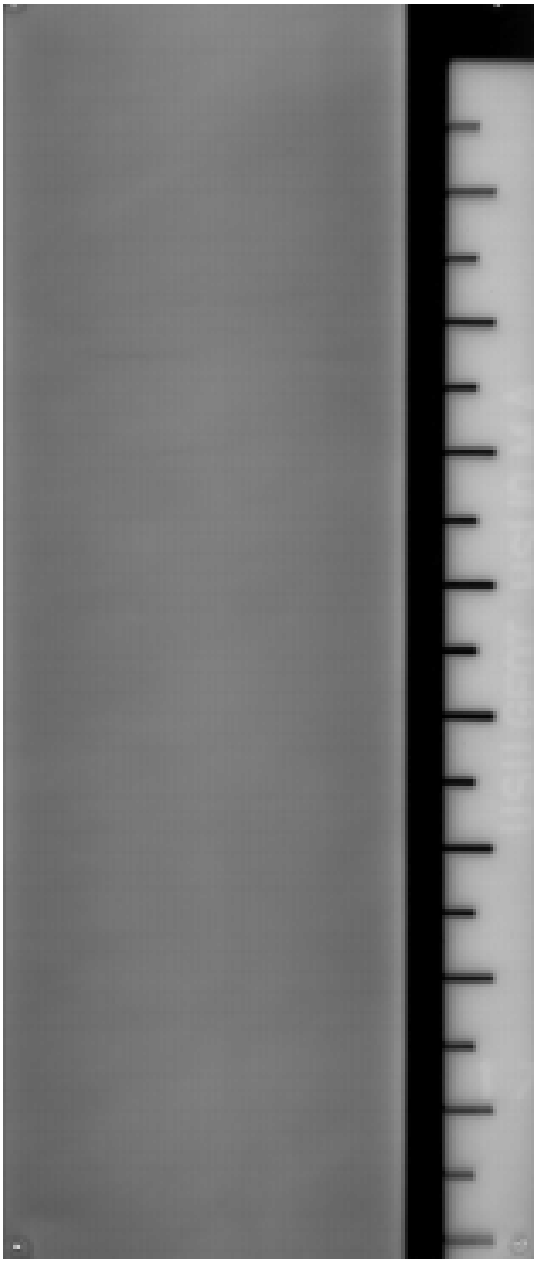

Figure C.29 Middle x-ray from the shelby tube, hollow stem auger sample at 32-34 feet designated HS1 10MA.

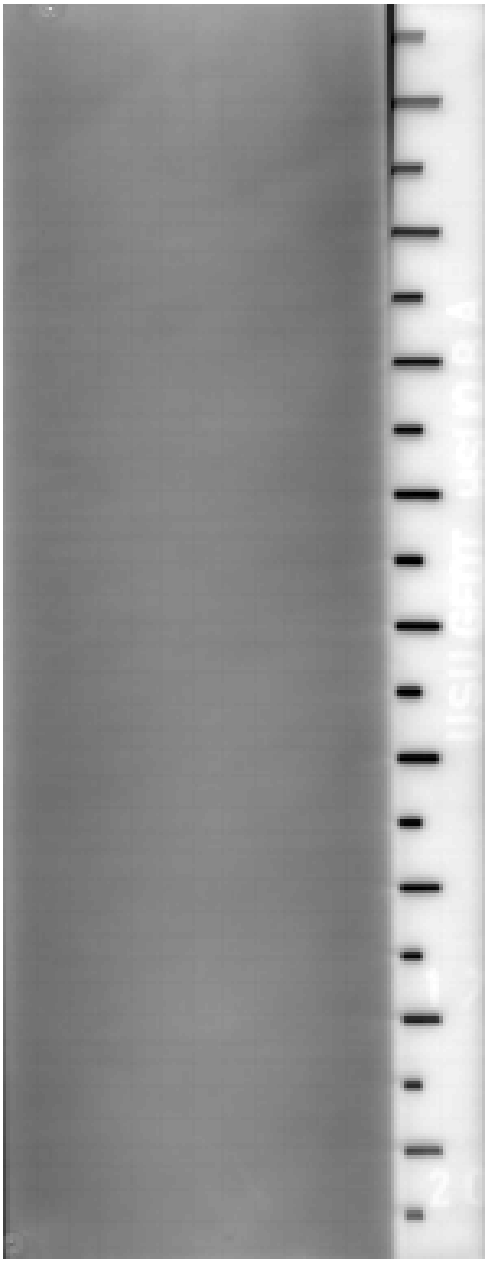

Figure C.30 Bottom x-ray from the shelby tube, hollow stem auger sample at 32-34 feet designated HS1 10BA.

Figure C.31 Top x-ray from the shelby tube, hollow stem auger sample at 34.5-36.5 feet designated HS1 11TA.

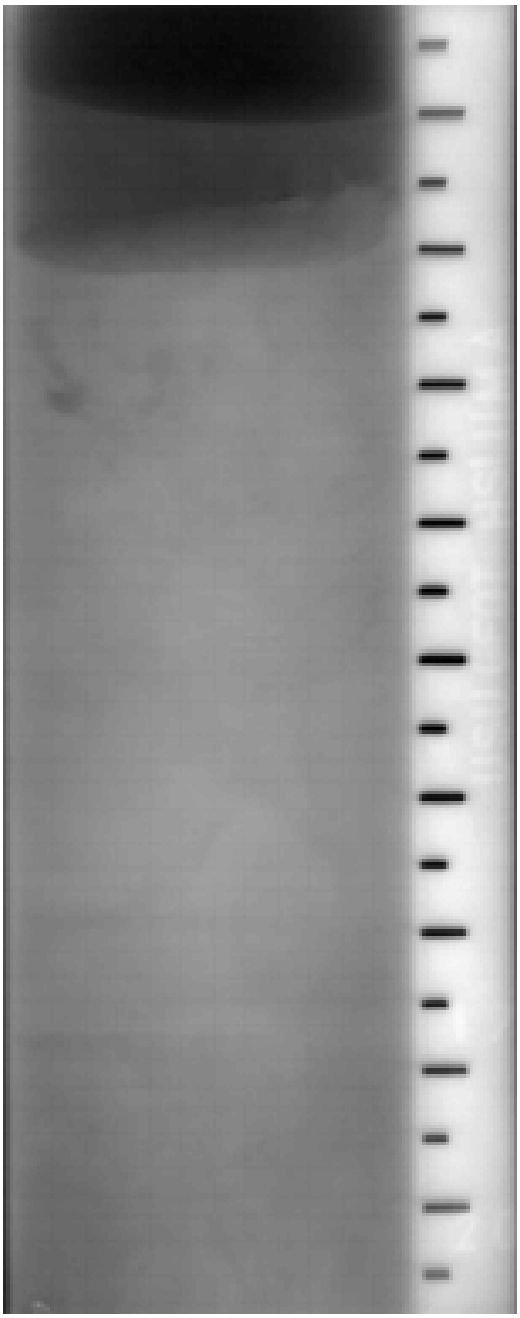

Figure C.32 Middle x-ray from the shelby tube, hollow stem auger sample at 34.5-36.5 feet designated HS1 11MA.

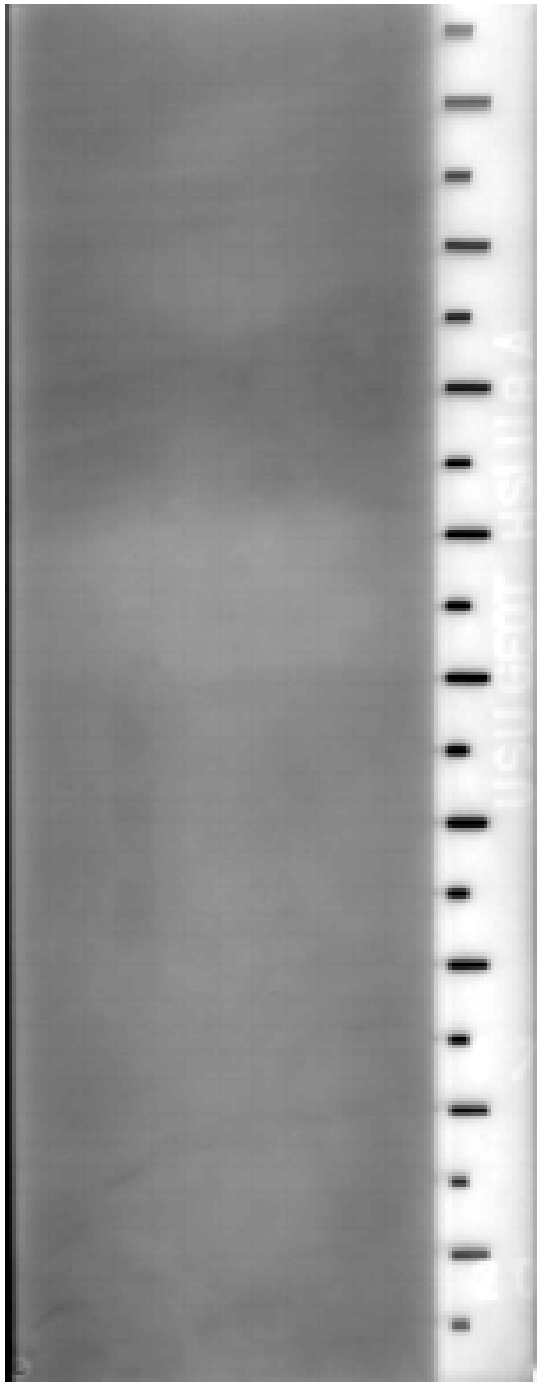

Figure C.33 Bottom x-ray from the shelby tube, hollow stem auger sample at 34.5-36.5 feet designated HS1 11BA.

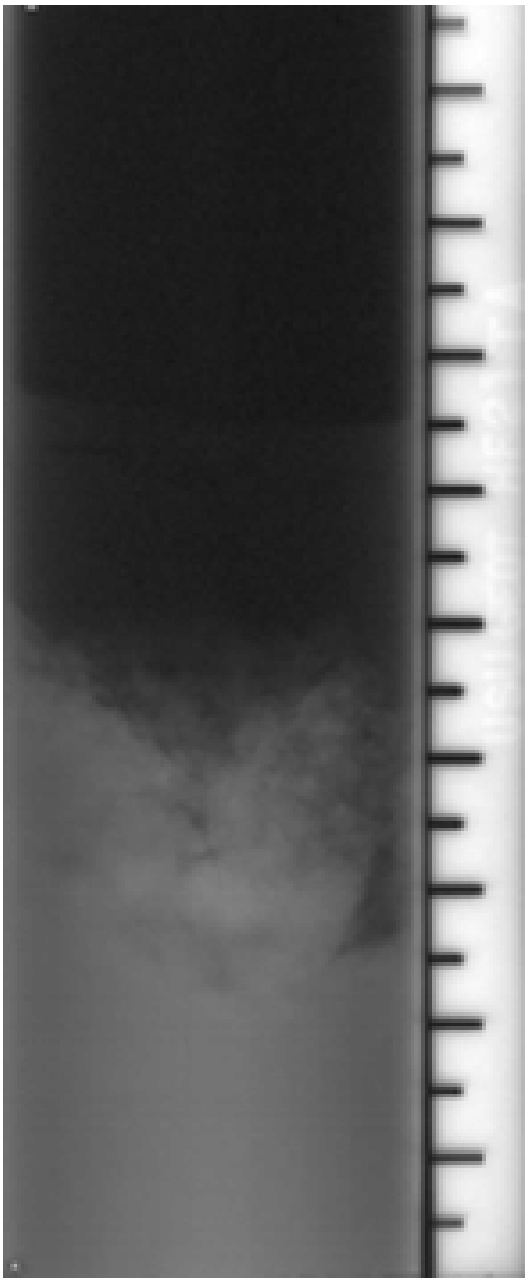

Figure C.34 Top x-ray from the fixed-piston, hollow stem auger sample at 9.5-11.5 feet designated HF2 1TA.

Figure C.35 Middle x-ray from the fixed-piston, hollow stem auger sample at 9.5-11.5 feet designated HF2 1MA.

Figure C.36 Bottom x-ray from the fixed-piston, hollow stem auger sample at 9.5-11.5 feet designated HF2 1BA.

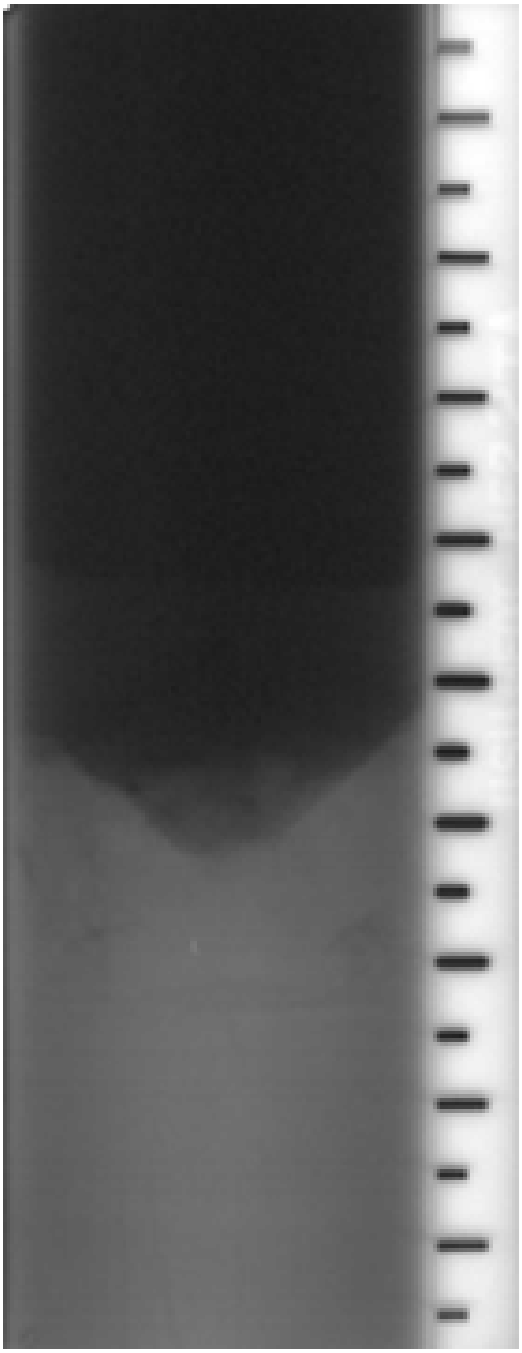

Figure C.37 Top x-ray from the fixed-piston, hollow stem auger sample at 12-14 feet designated HF2 2TA.

Figure C.38 Middle x-ray from the fixed-piston, hollow stem auger sample at 12-14 feet designated HF2 2MA.

Figure C.39 Bottom x-ray from the fixed-piston, hollow stem auger sample at 12-14 feet designated HF2 2BA.

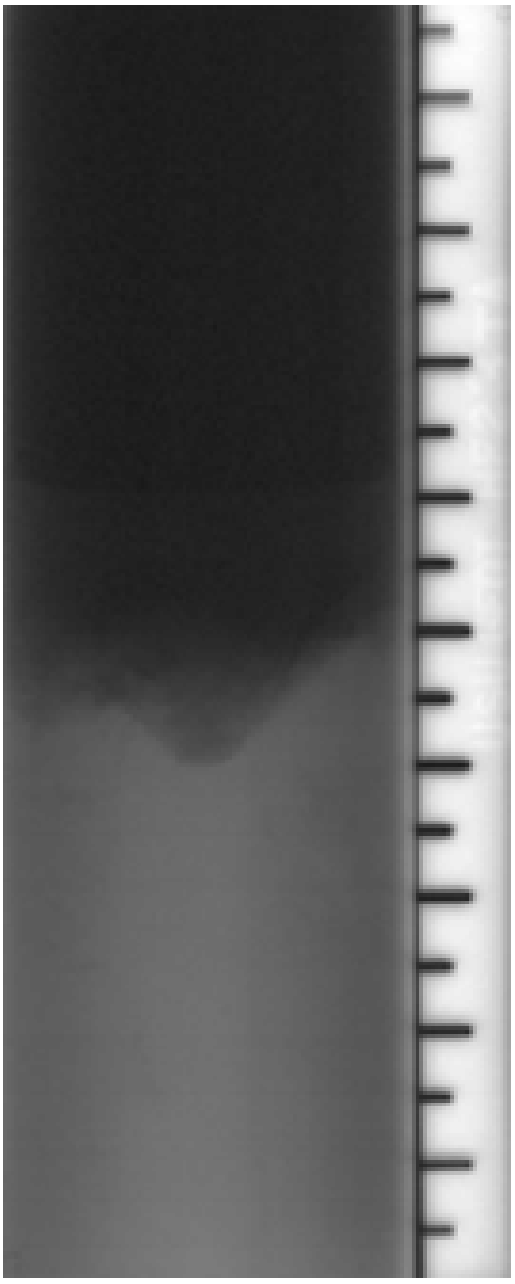

Figure C.40 Top x-ray from the fixed-piston, hollow stem auger sample at 14.5-16.5 feet designated HF2 3TA.

Figure C.41 Middle x-ray from the fixed-piston, hollow stem auger sample at 14.5-16.5 feet designated HF2 3MA.

Figure C.42 Bottom x-ray from the fixed-piston, hollow stem auger sample at 14.5-16.5 feet designated HF2 3BA.

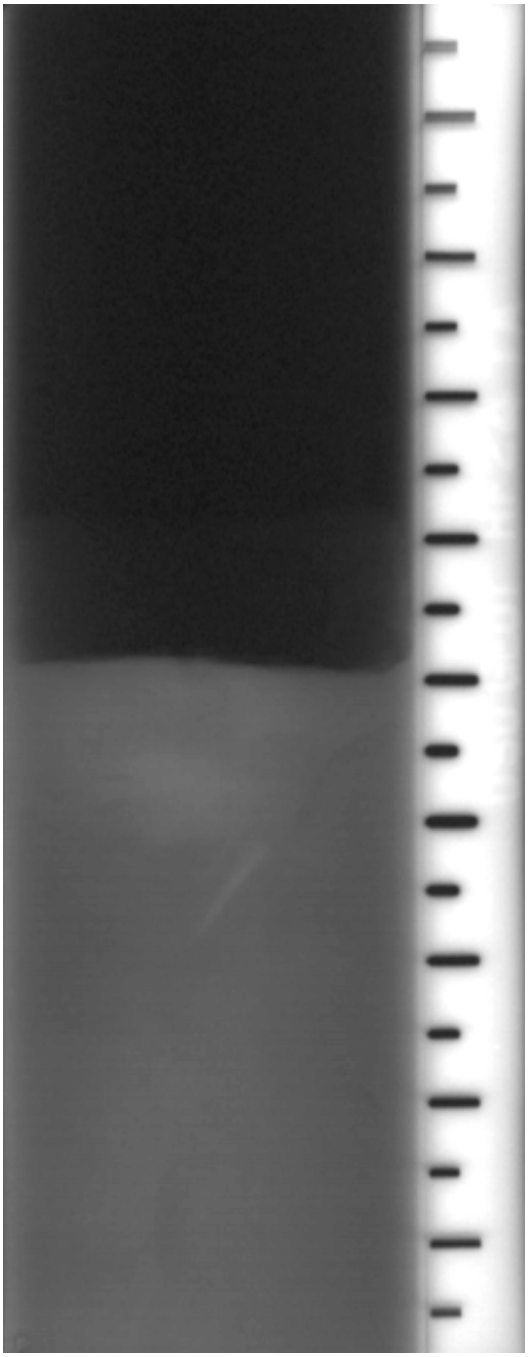

Figure C.43 Top x-ray from the free-piston, hollow stem auger sample at 17-19 feet designated HF2 4TA.

Figure C.44 Middle x-ray from the free-piston, hollow stem auger sample at 17-19 feet designated HF2 4MA.

Figure C.45 Bottom x-ray from the free-piston, hollow stem auger sample at 17-19 feet designated HF2 4BA.

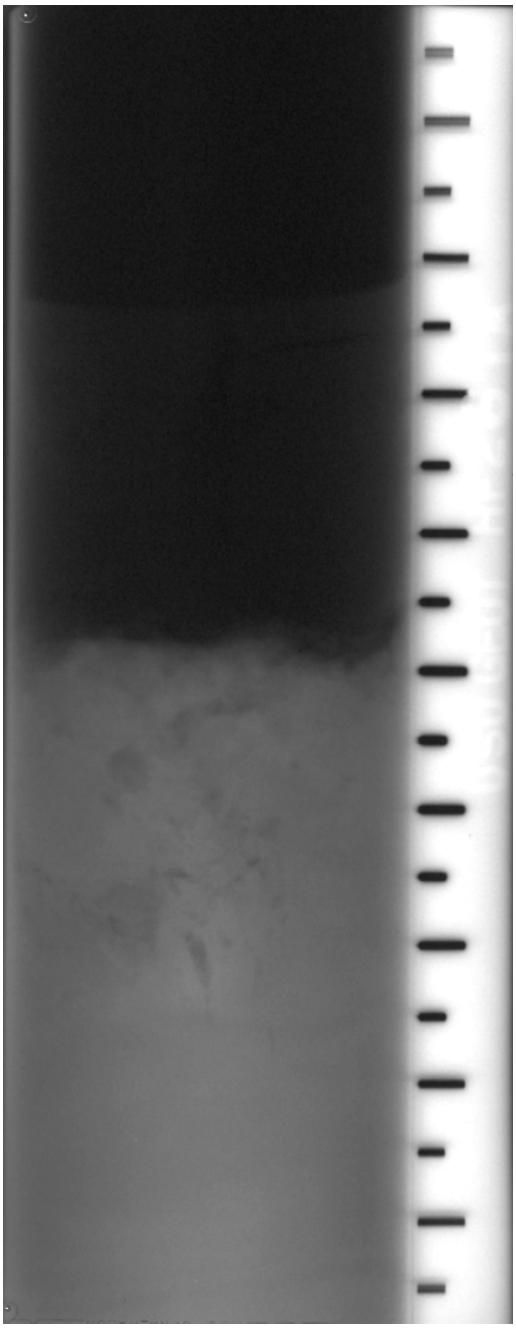

Figure C.46 Top x-ray from the free-piston, hollow stem auger sample at 22-24 feet designated HF2 6TA.

Figure C.47 Middle x-ray from the free-piston, hollow stem auger sample at 22-24 feet designated HF2 6MA.

Figure C.48 Bottom x-ray from the free-piston, hollow stem auger sample at 22-24 feet designated HF2 6BA.

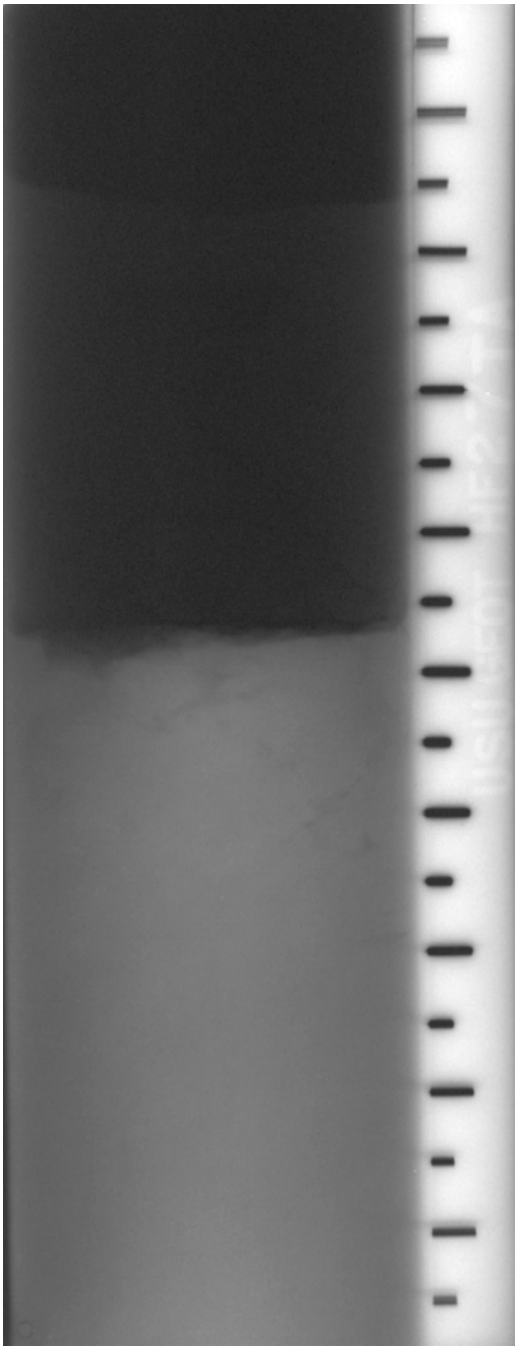

Figure C.49 Top x-ray from the free-piston, hollow stem auger sample at 24.5-26.5 feet designated HF2 7TA.

Figure C.50 Middle x-ray from the free-piston, hollow stem auger sample at 24.5-26.5 feet designated HF2 7MA.

Figure C.51 Bottom x-ray from the free-piston, hollow stem auger sample at 24.5-26.5 feet designated HF2 7BA.

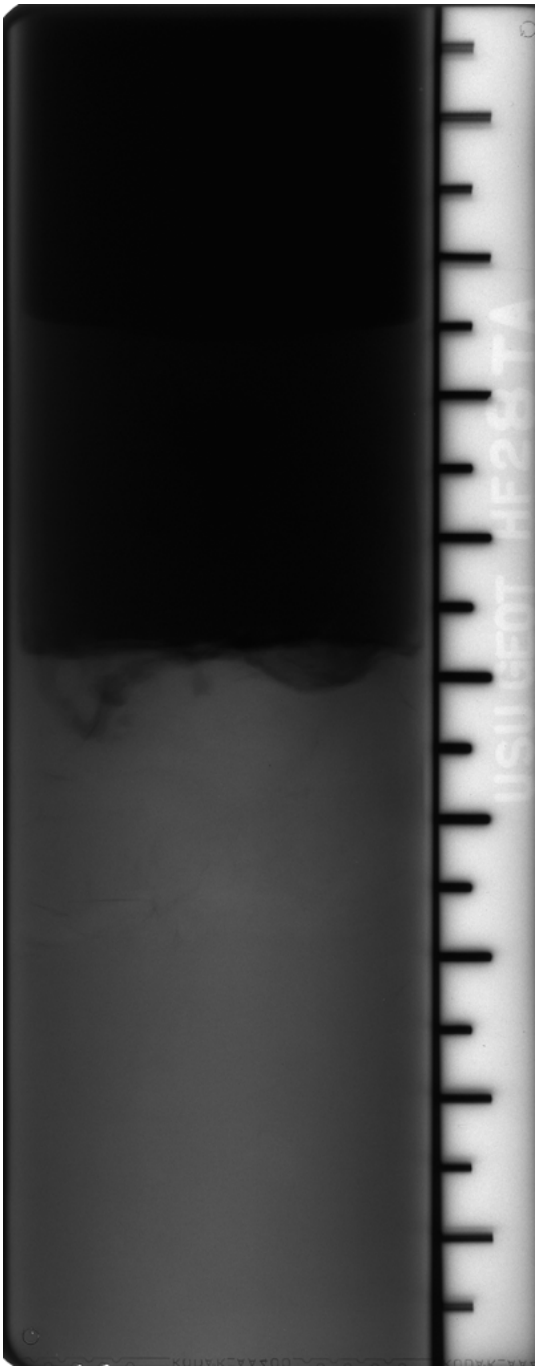

Figure C.52 Top x-ray from the free-piston, hollow stem auger sample at 27-29 feet designated HF2 8TA.

Figure C.53 Middle x-ray from the free-piston, hollow stem auger sample at 27-29 feet designated HF2 8MA.

Figure C.54 Bottom x-ray from the free-piston, hollow stem auger sample at 27-29 feet designated HF2 8BA.

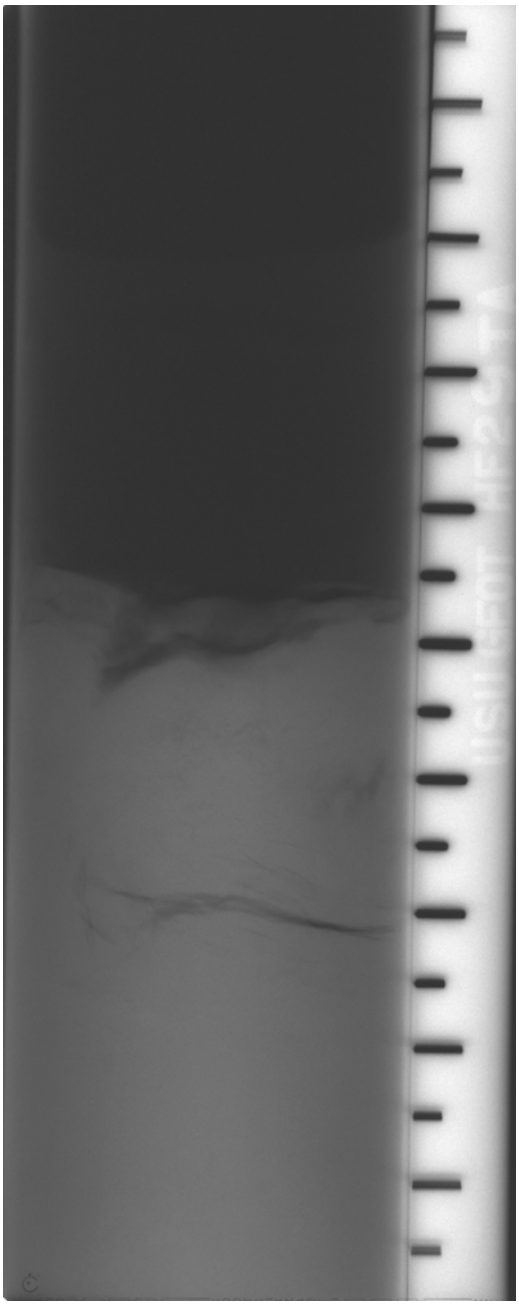

Figure C.55 Top x-ray from the free-piston, hollow stem auger sample at 29.5-31.5 feet designated HF2 9TA.

Figure C.56 Middle x-ray from the free-piston, hollow stem auger sample at 29.5-31.5 feet designated HF2 9MA.

Figure C.57 Bottom x-ray from the free-piston, hollow stem auger sample at 29.5-31.5 feet designated HF2 9BA.

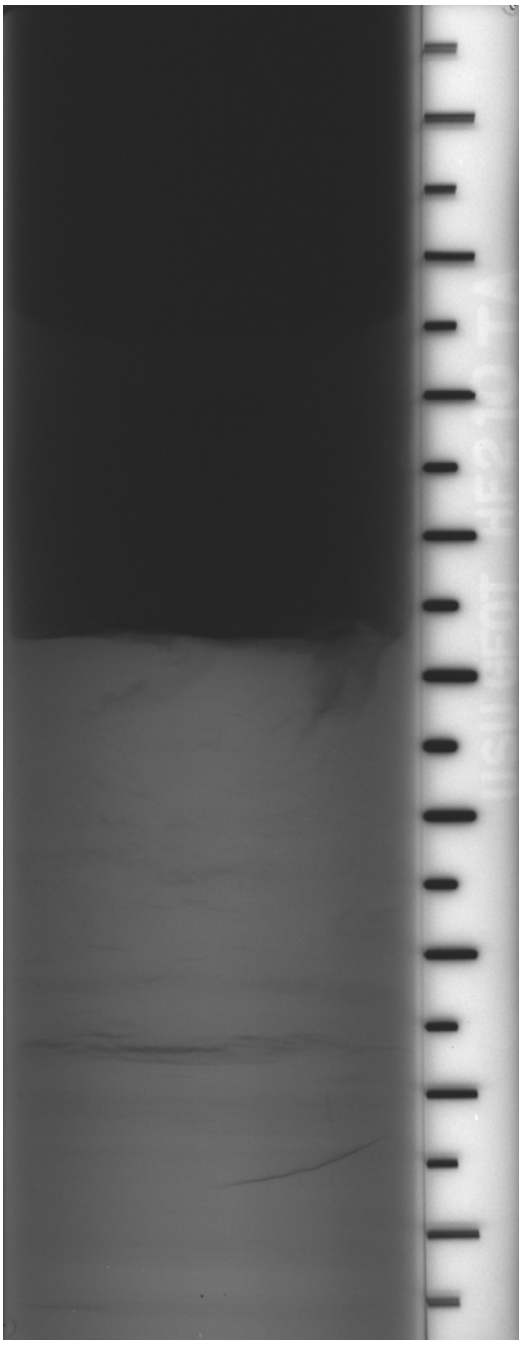

Figure C.58 Top x-ray from the free-piston, hollow stem auger sample at 32-34 feet designated HF2 10TA.

Figure C.59 Middle x-ray from the free-piston, hollow stem auger sample at 32-34 feet designated HF2 10MA.

Figure C.60 Bottom x-ray from the free-piston, hollow stem auger sample at 32-34 feet designated HF2 10B2A.

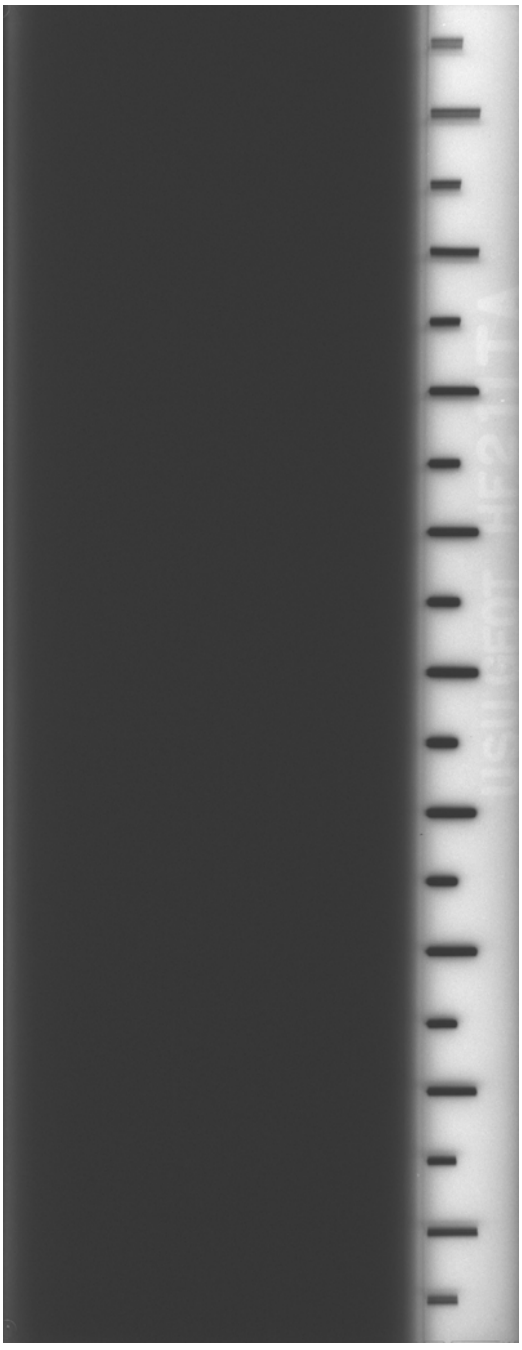

Figure C.61 Top x-ray from the free-piston, hollow stem auger sample at 34.5-36.5 feet designated HF2 11TA.

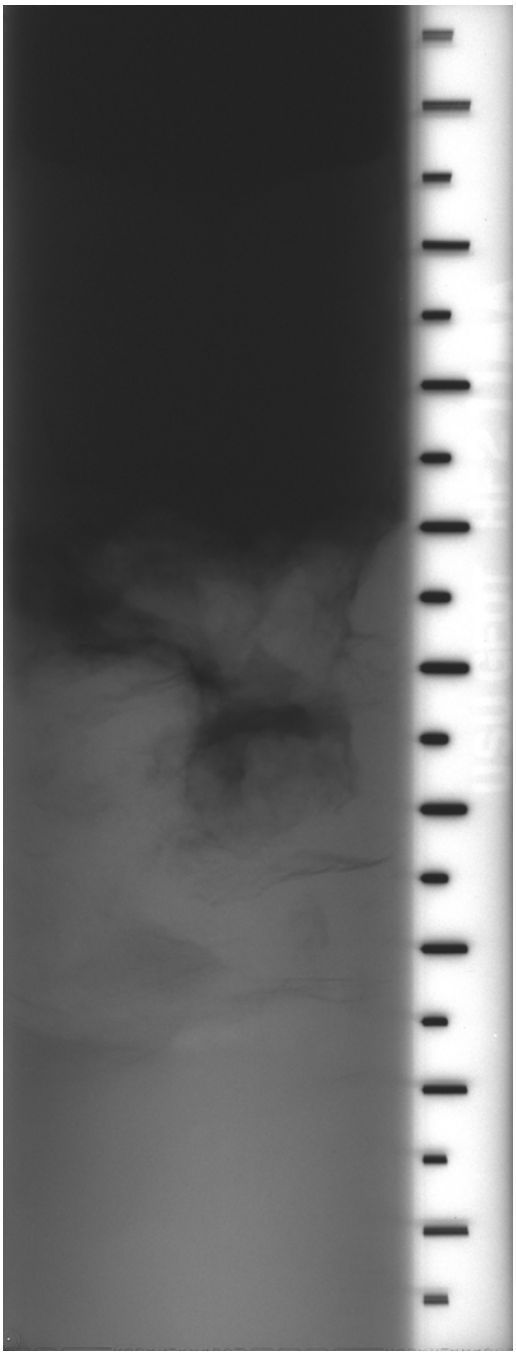

Figure C.62 Middle x-ray from the free-piston, hollow stem auger sample at 34.5-36.5 feet designated HF2 11MA.

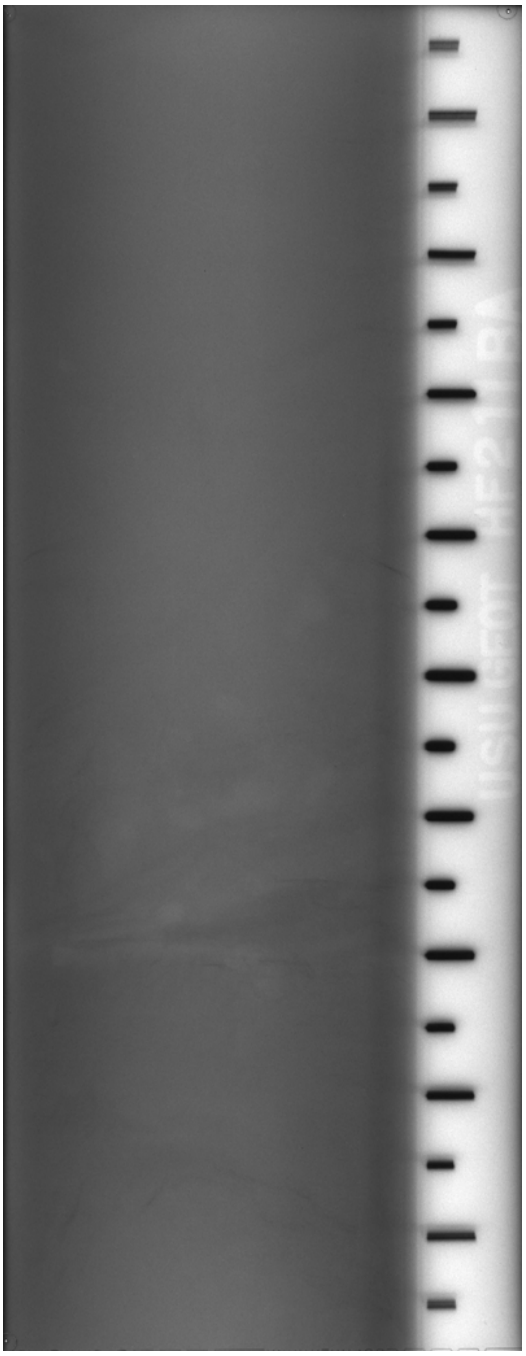

Figure C.63 Bottom x-ray from the free-piston, hollow stem auger sample at 34.5-36.5 feet designated HF2 11BA.

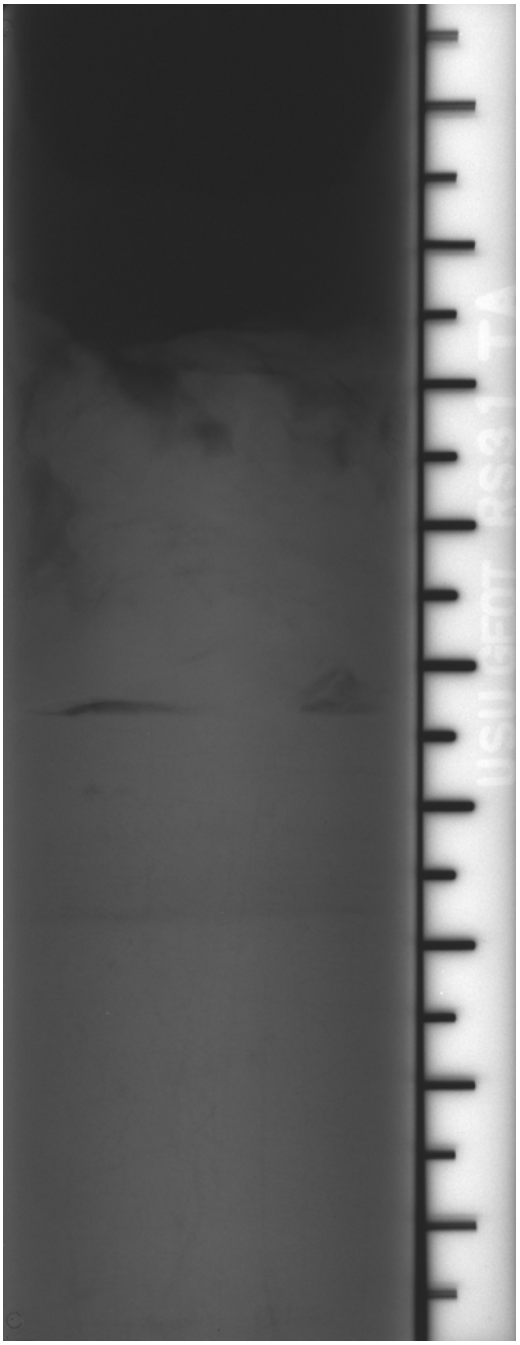

Figure C.64 Top x-ray from the shelby tube, rotary wash sample at 9.5-11.5 feet designated RS3 1TA.

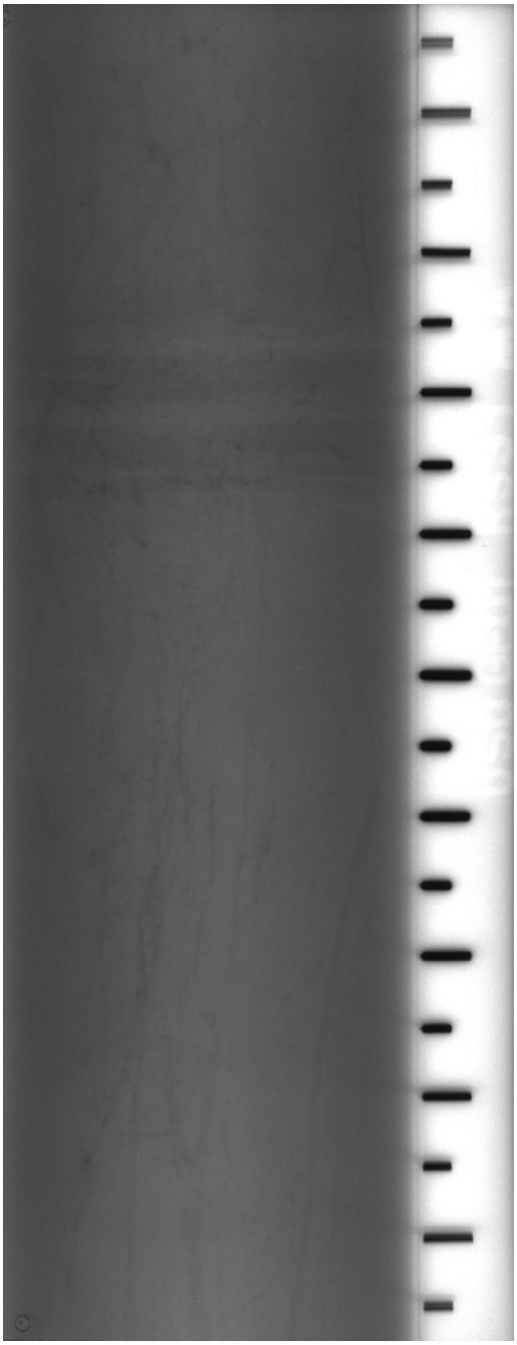

Figure C.65 Middle x-ray from the shelby tube, rotary wash sample at 9.5-11.5 feet designated RS3 1MA.

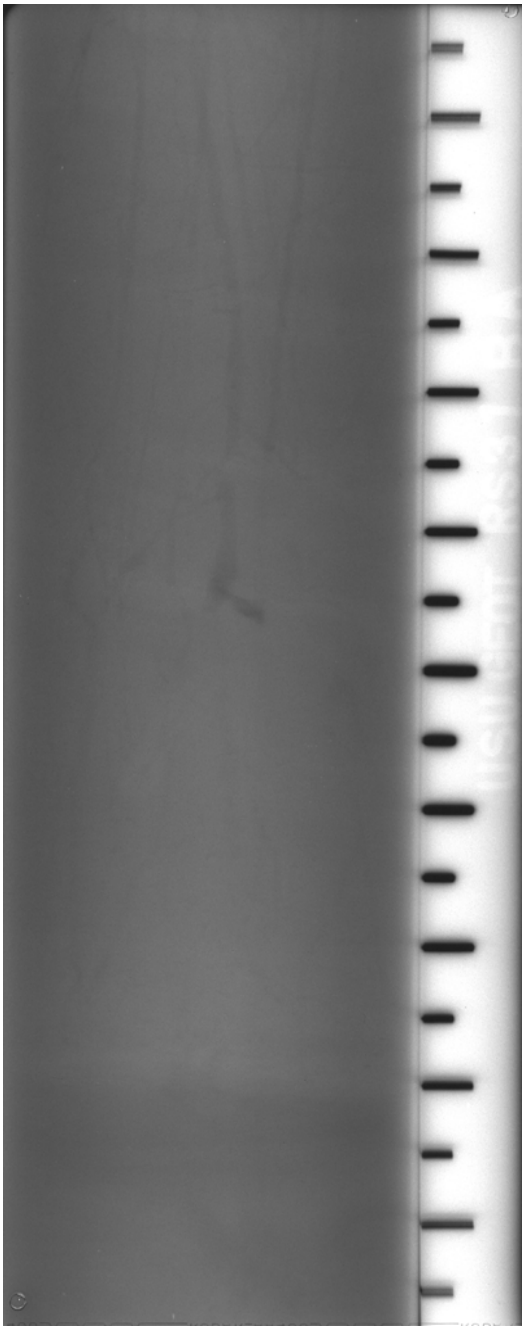

Figure C.66 Bottom x-ray from the shelby tube, rotary wash sample at 9.5-11.5 feet designated RS3 1BA.

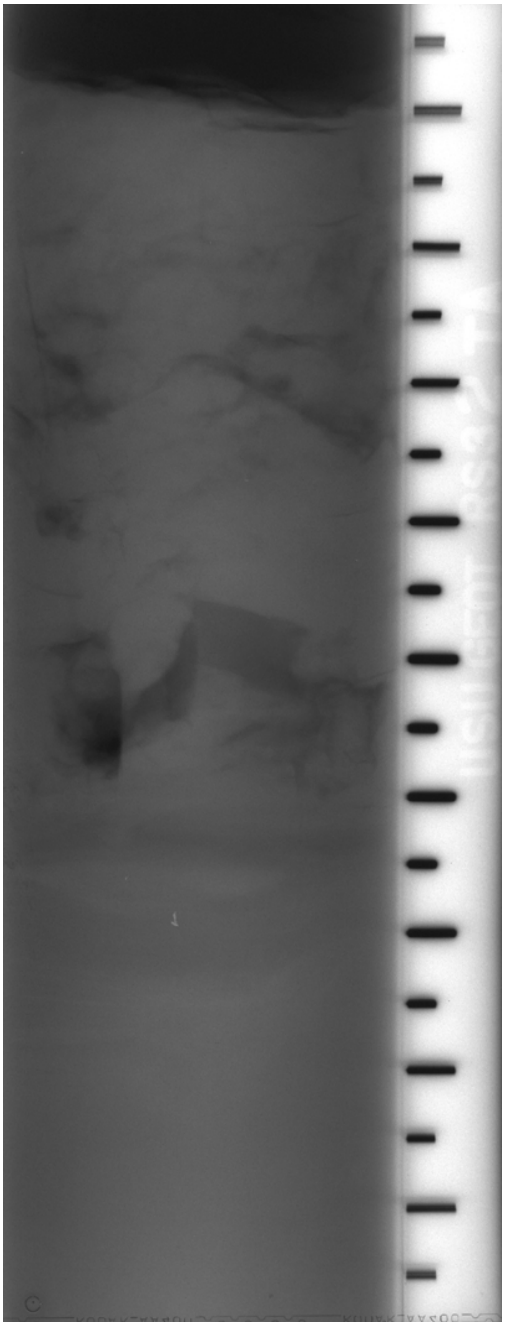

Figure C.67 Top x-ray from the shelby tube, rotary wash sample at 12-14 feet designated RS3 2TA.

Figure C.68 Middle x-ray from the shelby tube, rotary wash sample at 12-14 feet designated RS3 2MA.

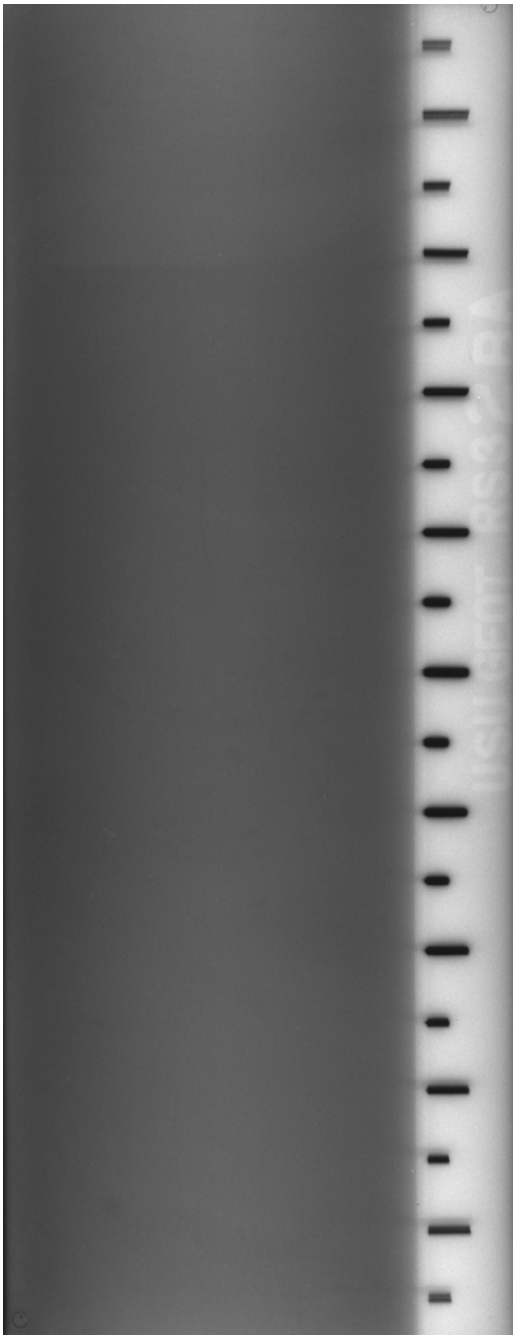

Figure C.69 Bottom x-ray from the shelby tube, rotary wash sample at 12-14 feet designated RS3 2BA.

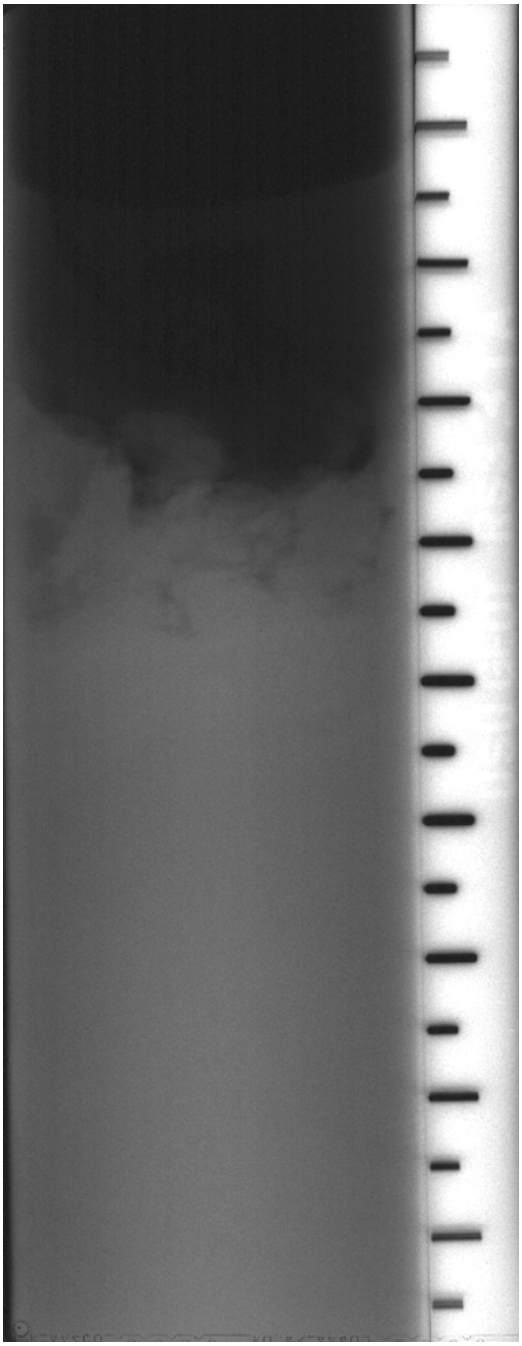

Figure C.70 Top x-ray from the shelby tube, rotary wash sample at 14.5-16.5 feet designated RS3 3TA.

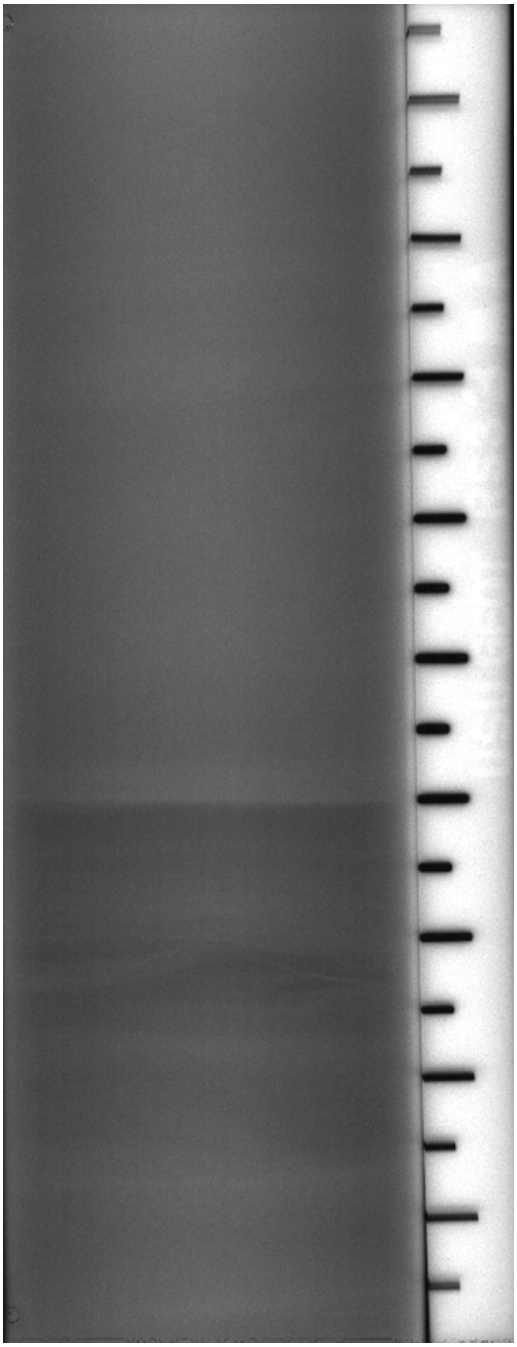

Figure C.71 Middle x-ray from the shelby tube, rotary wash sample at 14.5-16.5 feet designated RS3 3MA.

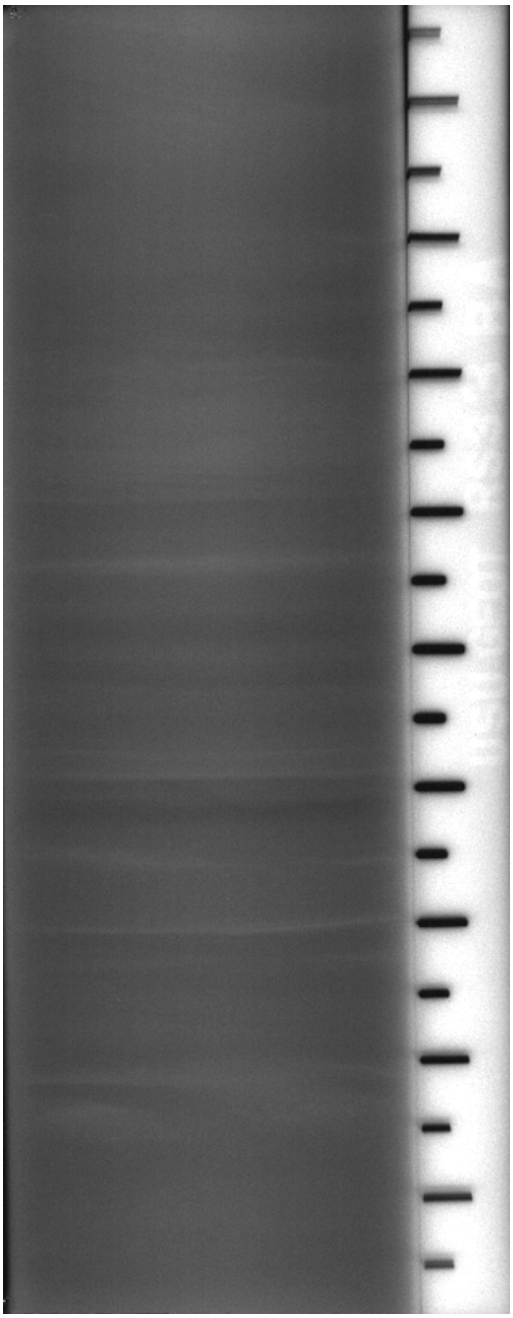

Figure C.72 Bottom x-ray from the shelby tube, rotary wash sample at 14.5-16.5 feet designated RS3 3BA.

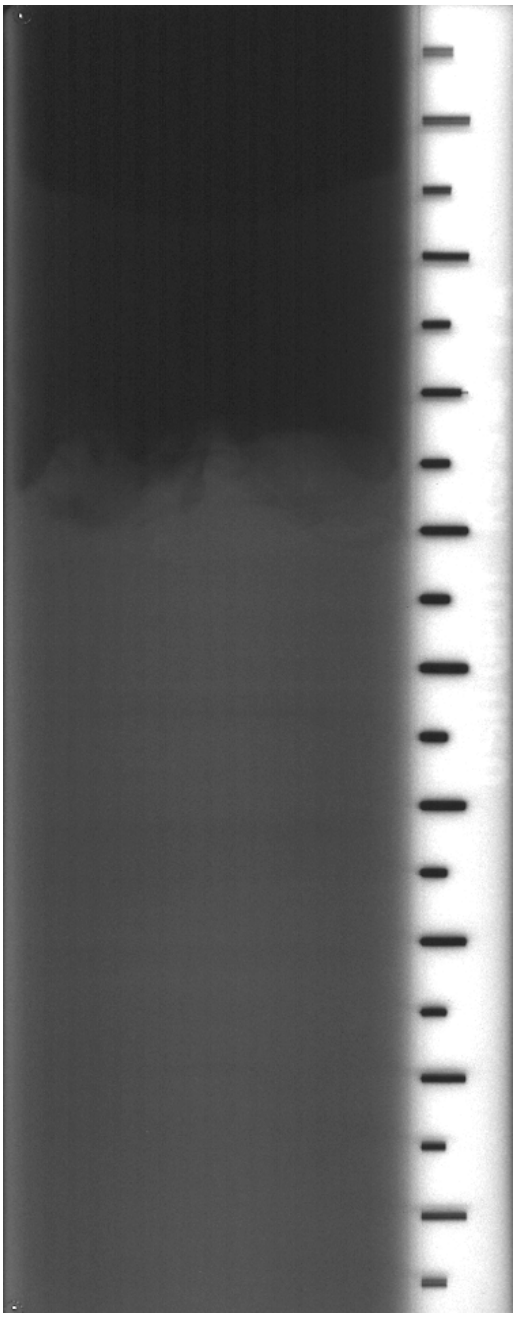

Figure C.73 Top x-ray from the shelby tube, rotary wash sample at 17-19 feet designated RS3 4TA.

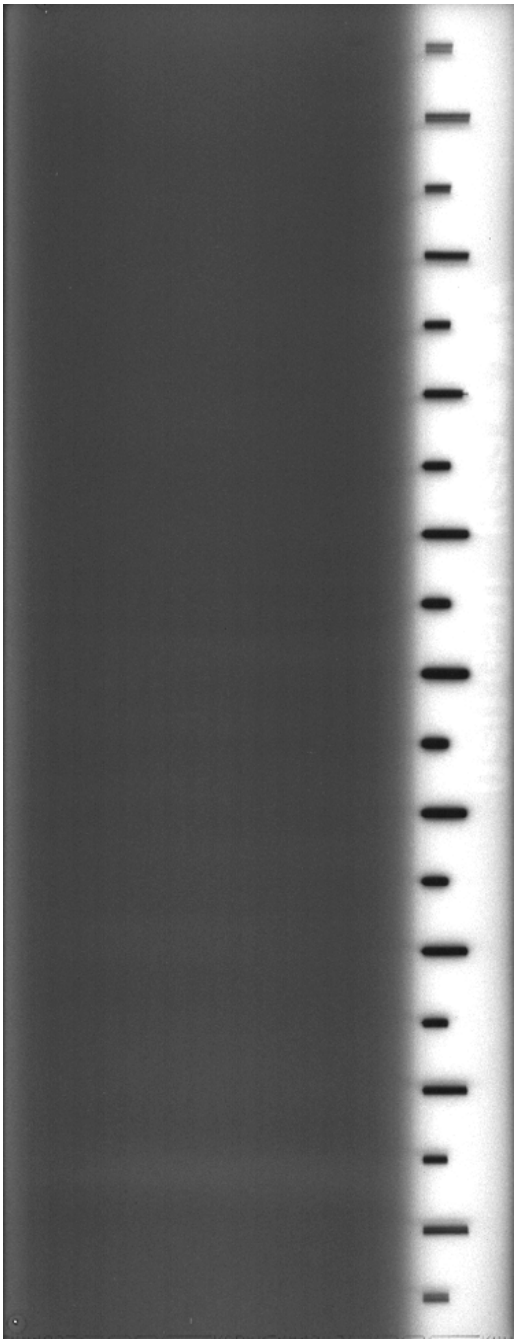

Figure C.74 Middle x-ray from the shelby tube, rotary wash sample at 17-19 feet designated RS3 4MA.

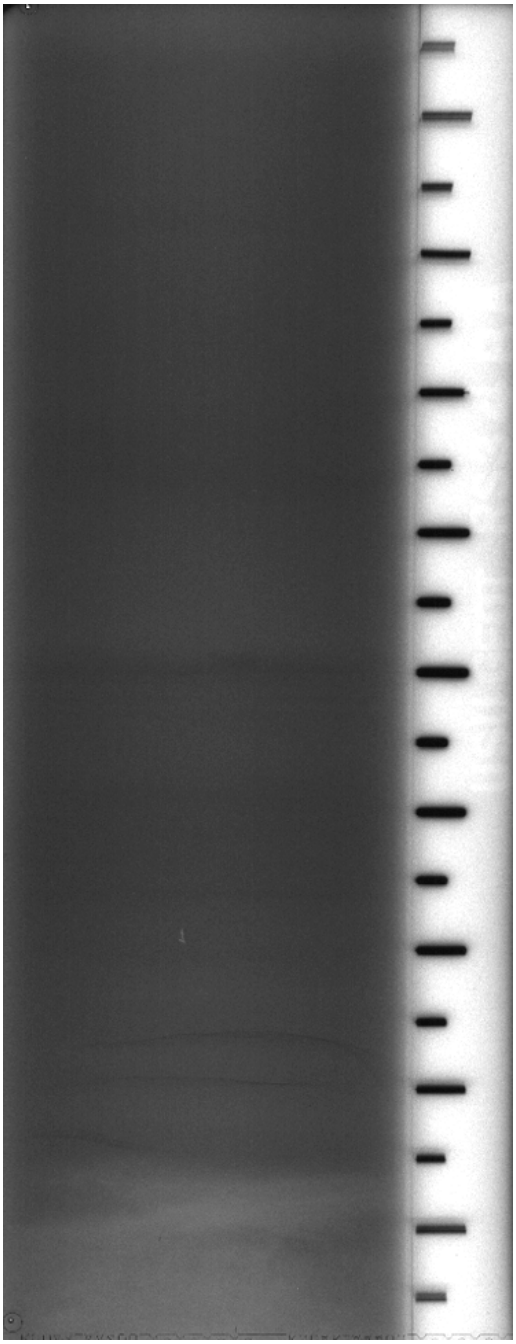

Figure C.75 Bottom x-ray from the shelby tube, rotary wash sample at 17-19 feet designated RS3 4BA.

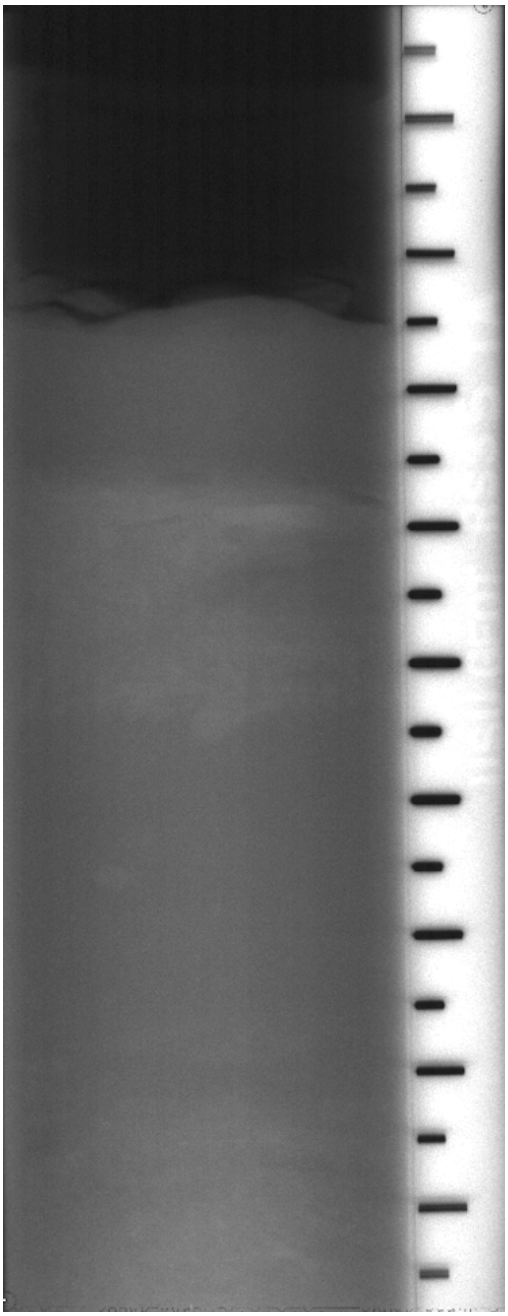

Figure C.76 Top x-ray from the shelby tube, rotary wash sample at 19.5-21.5 feet designated RS3 5TA.

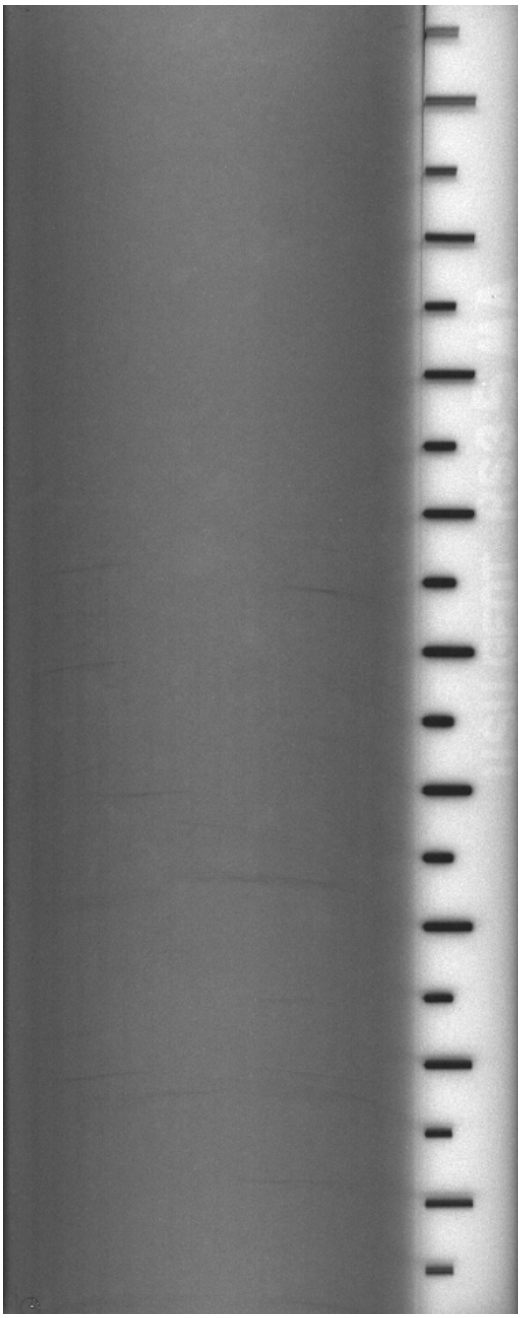

Figure C.77 Middle x-ray from the shelby tube, rotary wash sample at 19.5-21.5 feet designated RS3 5MA.

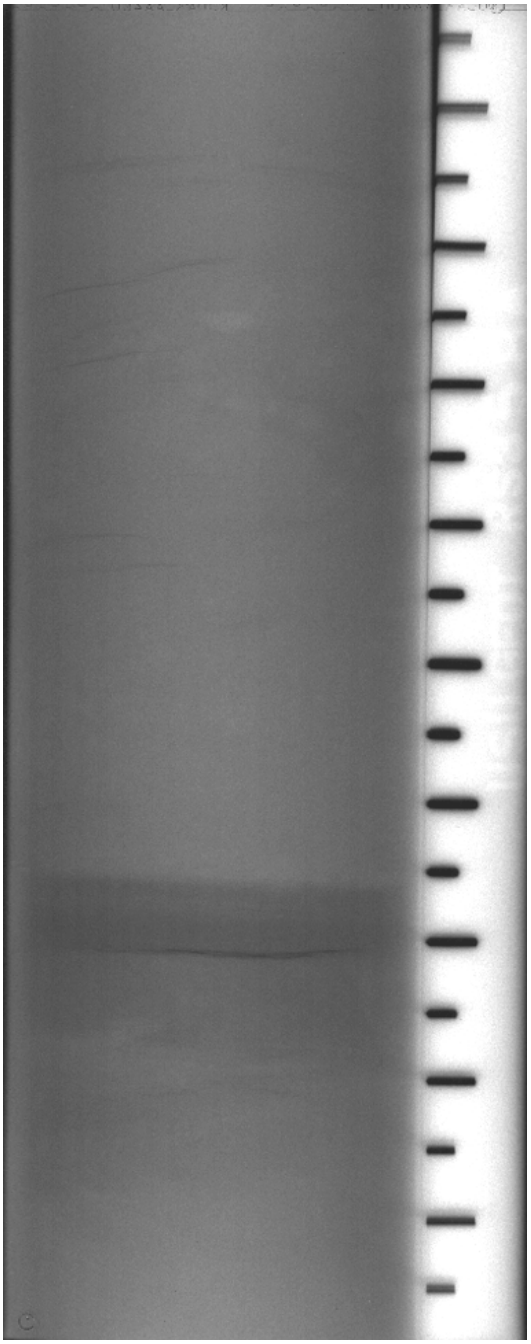

Figure C.78 Bottom x-ray from the shelby tube, rotary wash sample at 19.5-21.5 feet designated RS3 5BA.

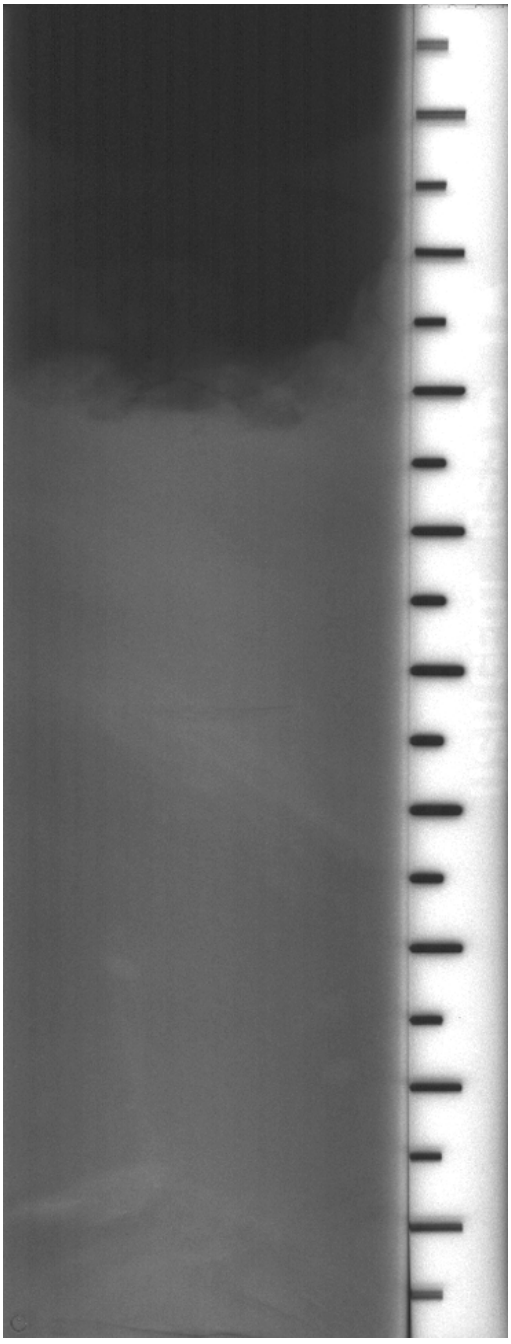

Figure C.79 Top x-ray from the shelby tube, rotary wash sample at 22-24 feet designated RS3 6TA.

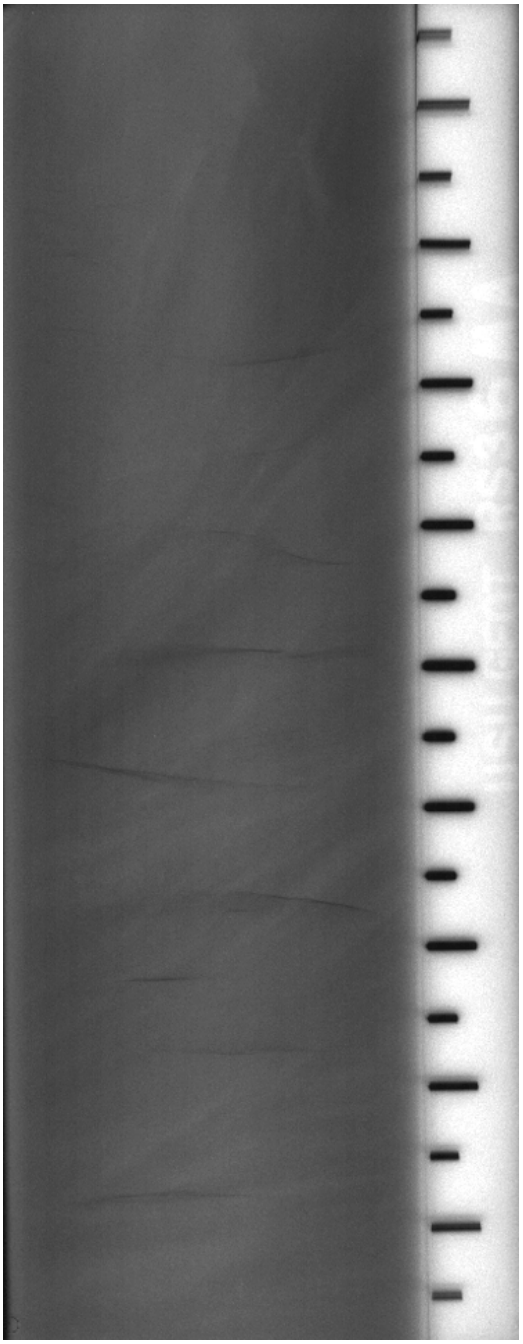

Figure C.80 Middle x-ray from the shelby tube, rotary wash sample at 22-24 feet designated RS3 6MA.

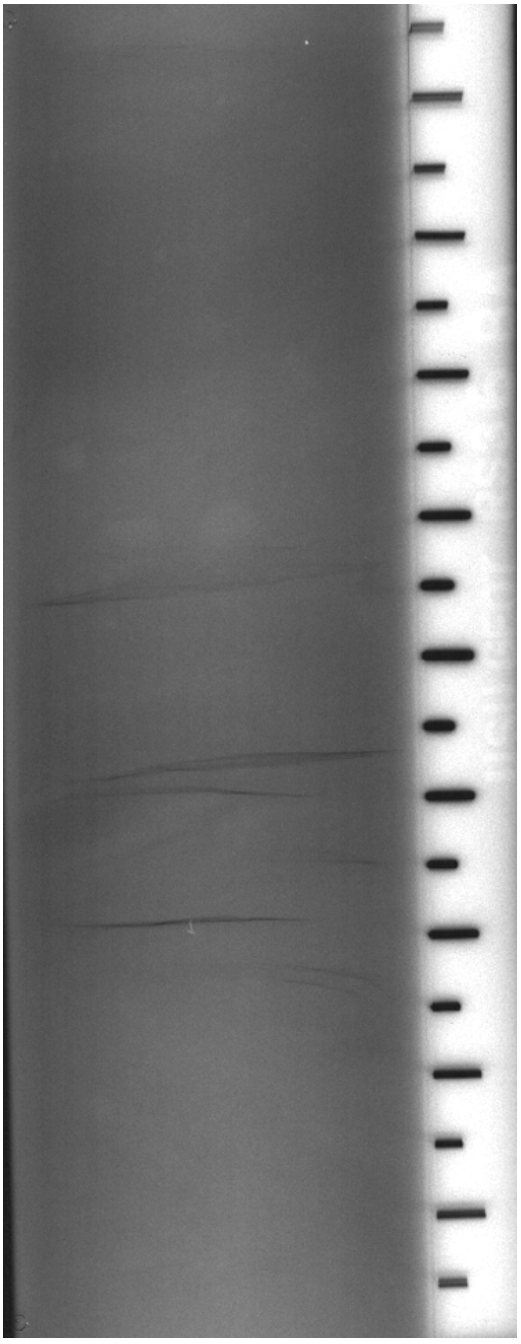

Figure C.81 Bottom x-ray from the shelby tube, rotary wash sample at 22-24 feet designated RS3 6BA.

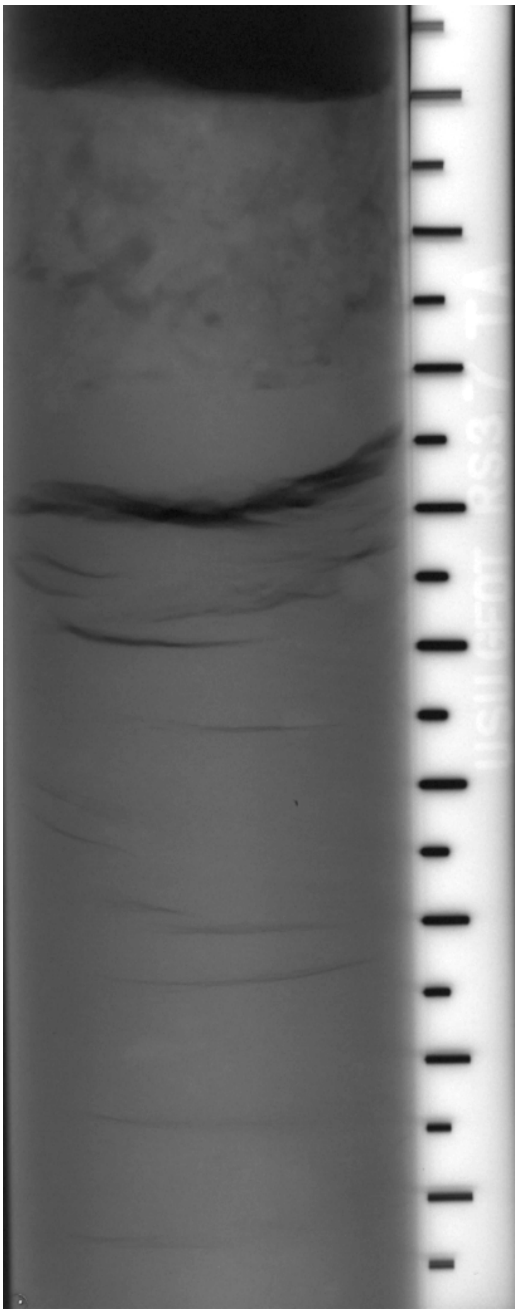

Figure C.82 Top x-ray from the shelby tube, rotary wash sample at 24.5-26.5 feet designated RS3 7TA.

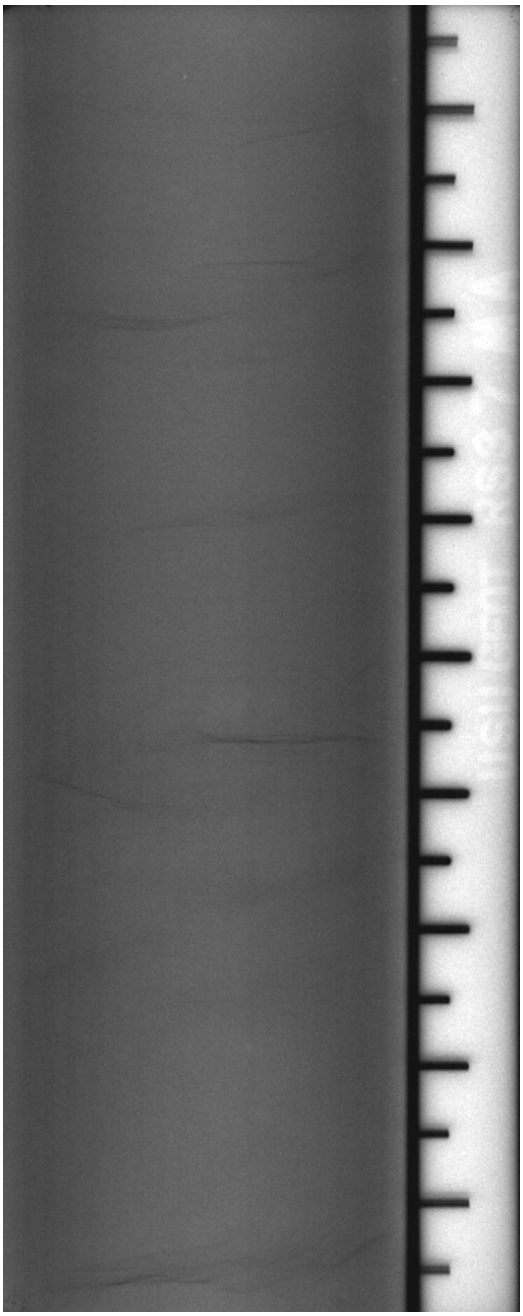

Figure C.83 Middle x-ray from the shelby tube, rotary wash sample at 24.5-26.5 feet designated RS3 7MA.

Figure C.84 Bottom x-ray from the shelby tube, rotary wash sample at 24.5-26.5 feet designated RS3 7BA.

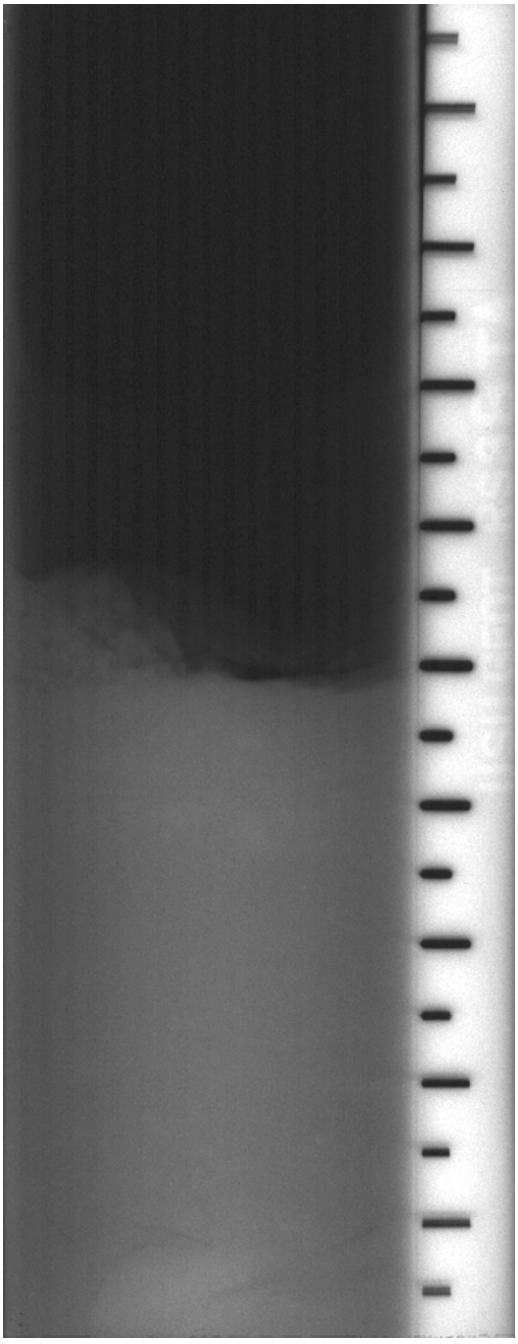

Figure C.85 Top x-ray from the shelby tube, rotary wash sample at 27-29 feet designated RS3 8TA.

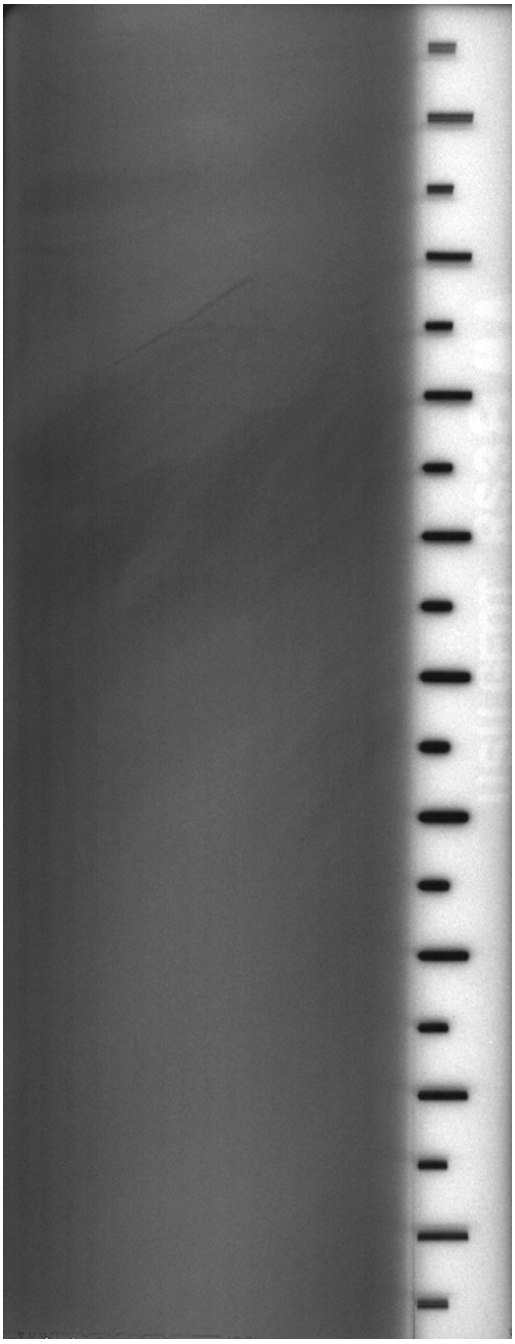

Figure C.86 Middle x-ray from the shelby tube, rotary wash sample at 27-29 feet designated RS3 8MA.

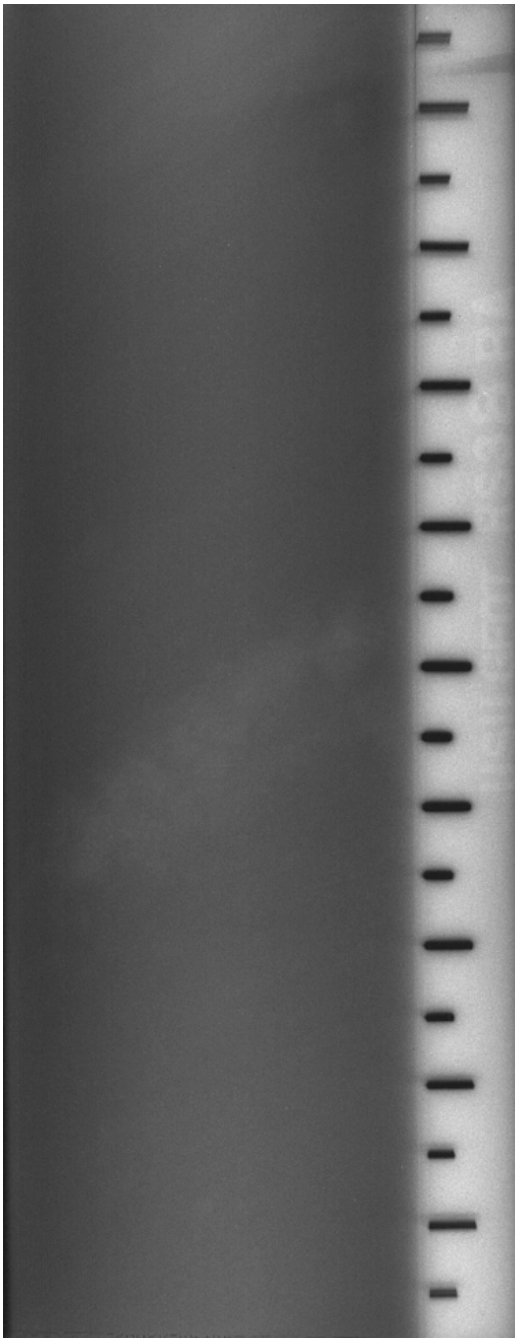

Figure C.87 Bottom x-ray from the shelby tube, rotary wash sample at 27-29 feet designated RS3 8BA.

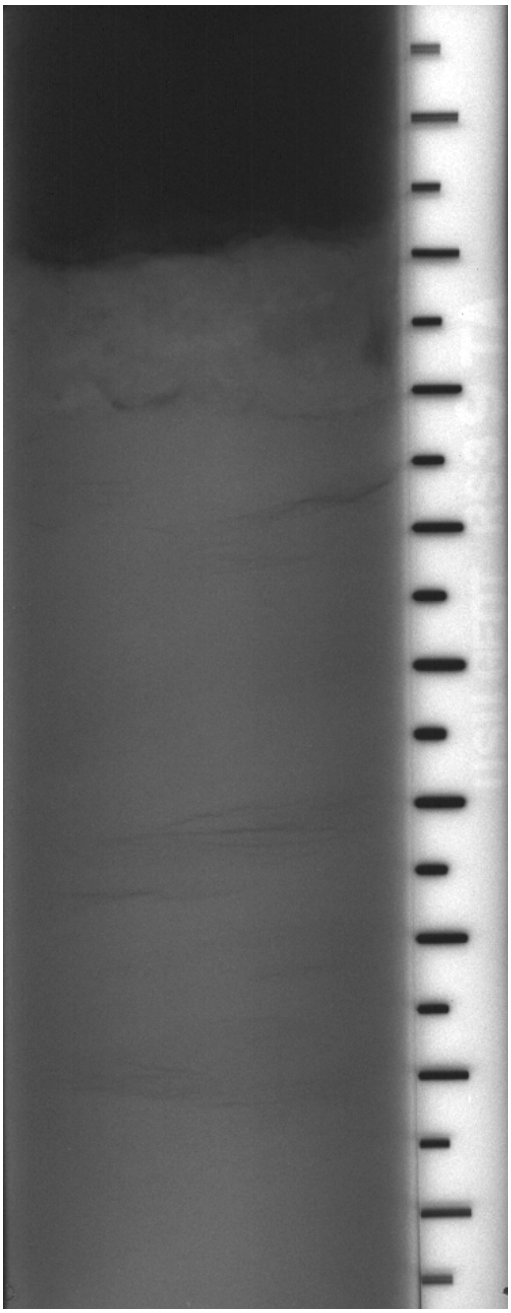

Figure C.88 Top x-ray from the shelby tube, rotary wash sample at 29.5-31.5 feet designated RS3 9TA.

Figure C.89 Middle x-ray from the shelby tube, rotary wash sample at 29.5-31.5 feet designated RS3 9MA.

Figure C.90 Bottom x-ray from the shelby tube, rotary wash sample at 29.5-31.5 feet designated RS3 9BA.

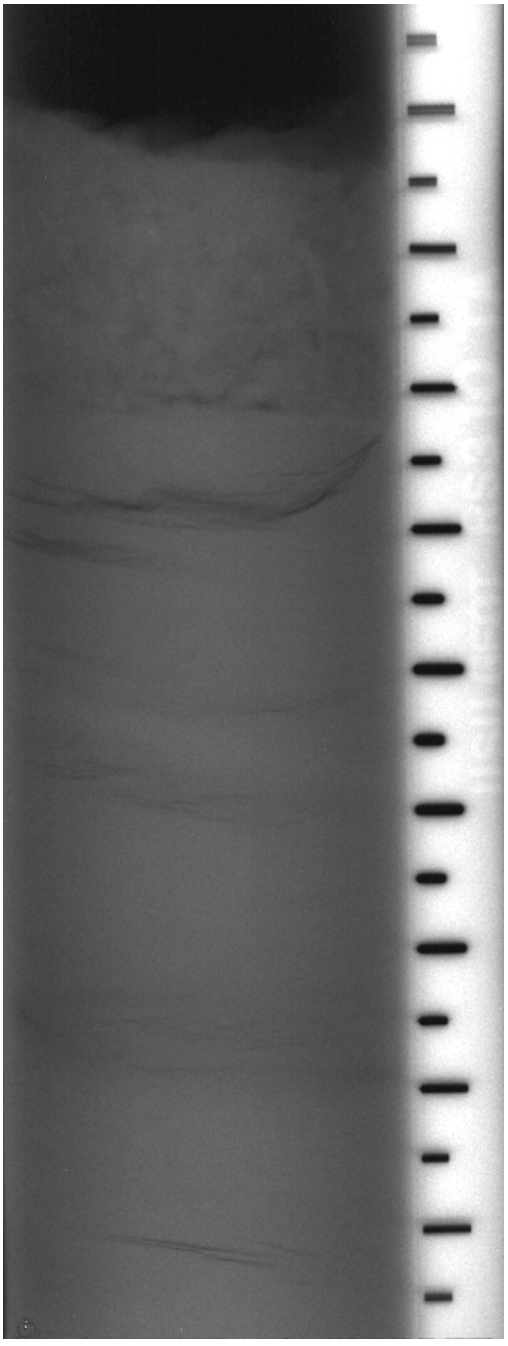

Figure C.91 Top x-ray from the shelby tube, rotary wash sample at 32-34 feet designated RS3 10TA.

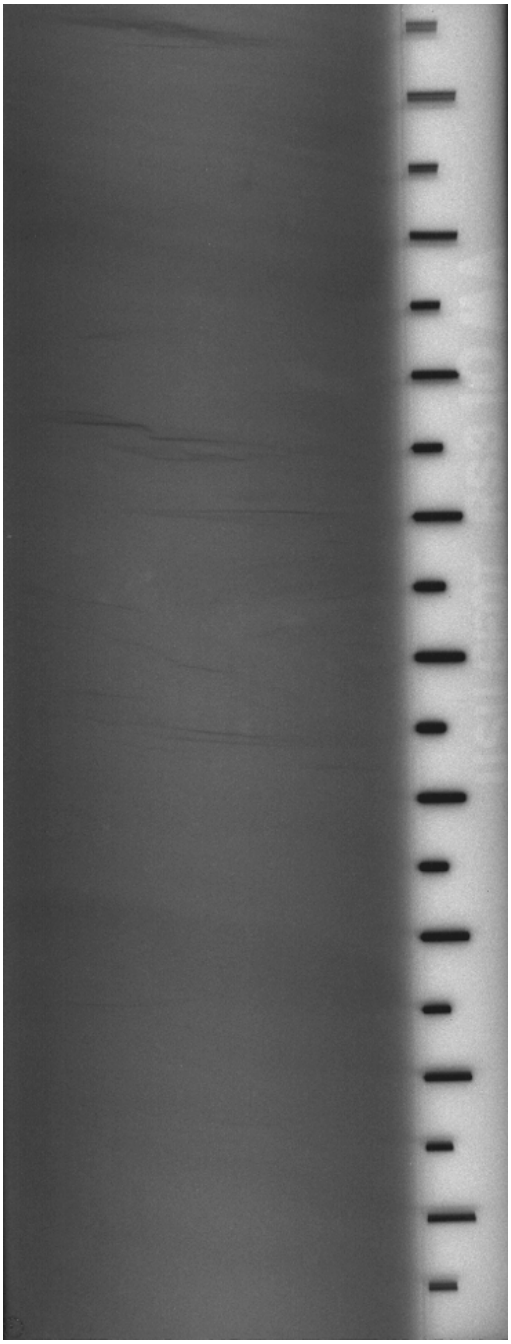

Figure C.92 Middle x-ray from the shelby tube, rotary wash sample at 32-34 feet designated RS3 10MA.

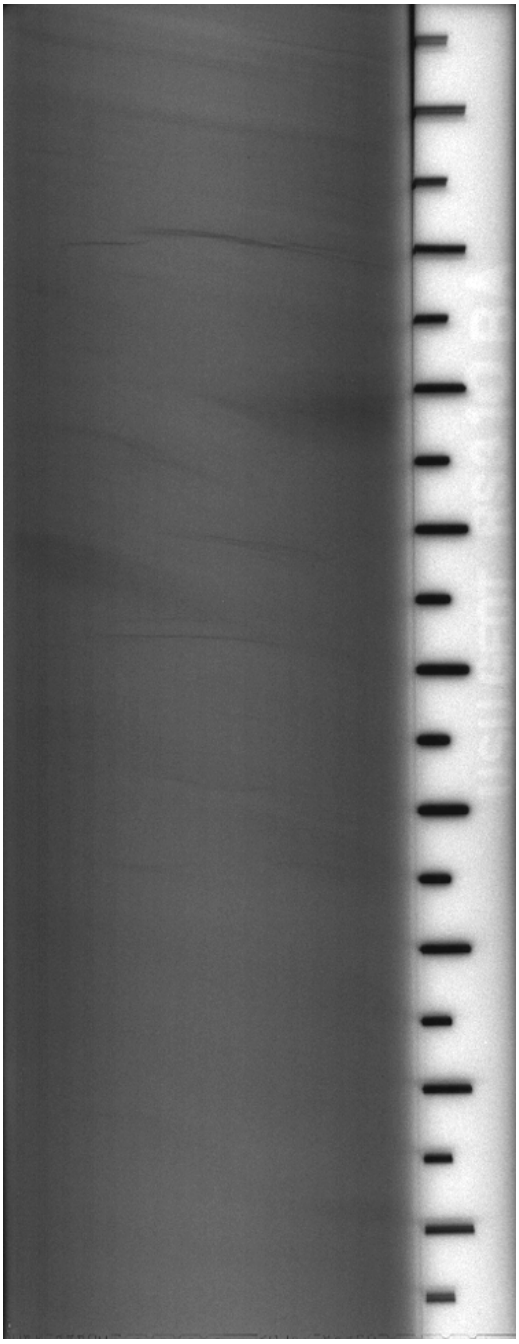

Figure C.93 Bottom x-ray from the shelby tube, rotary wash sample at 32-34 feet designated RS3 10BA.

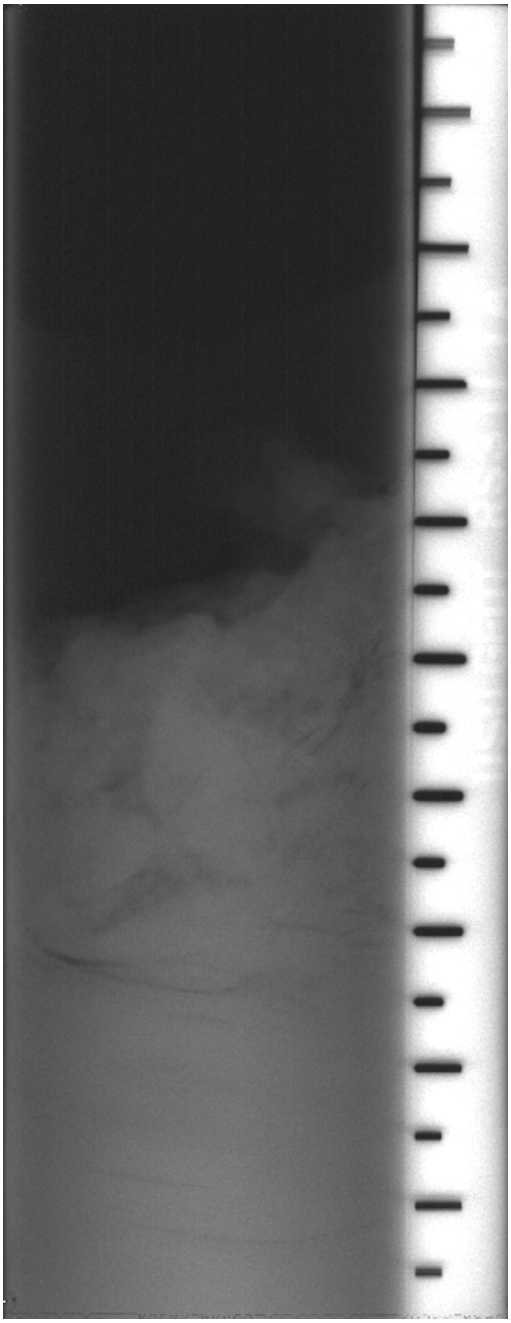

Figure C.94 Top x-ray from the shelby tube, rotary wash sample at 34.5-36.5 feet designated RS3 11TA.

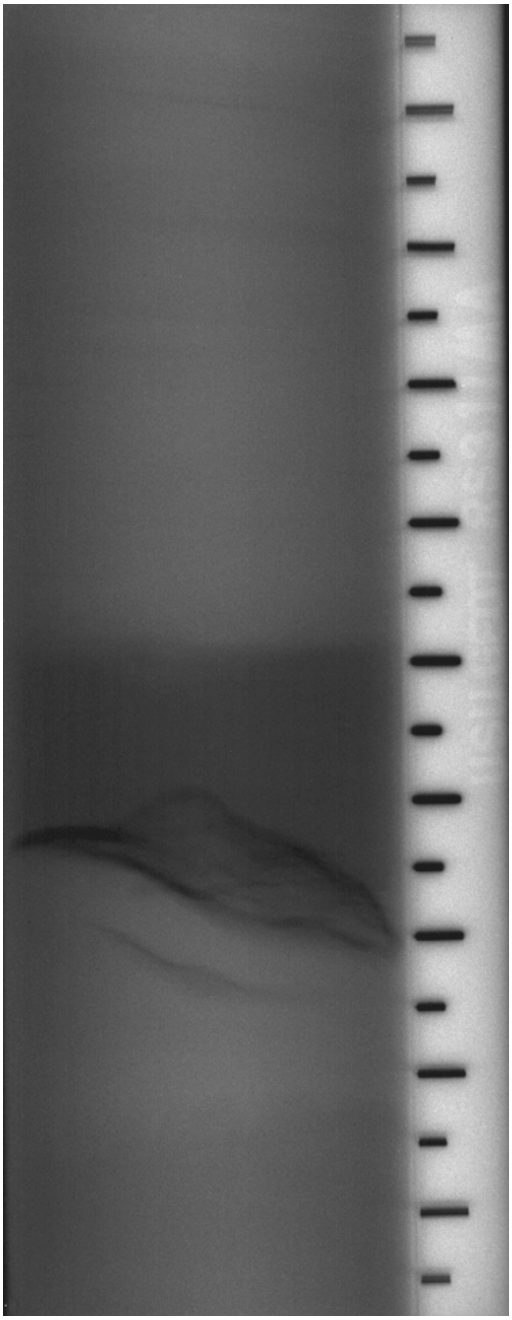

Figure C.95 Middle x-ray from the shelby tube, rotary wash sample at 34.5-36.5 feet designated RS3 11MA.

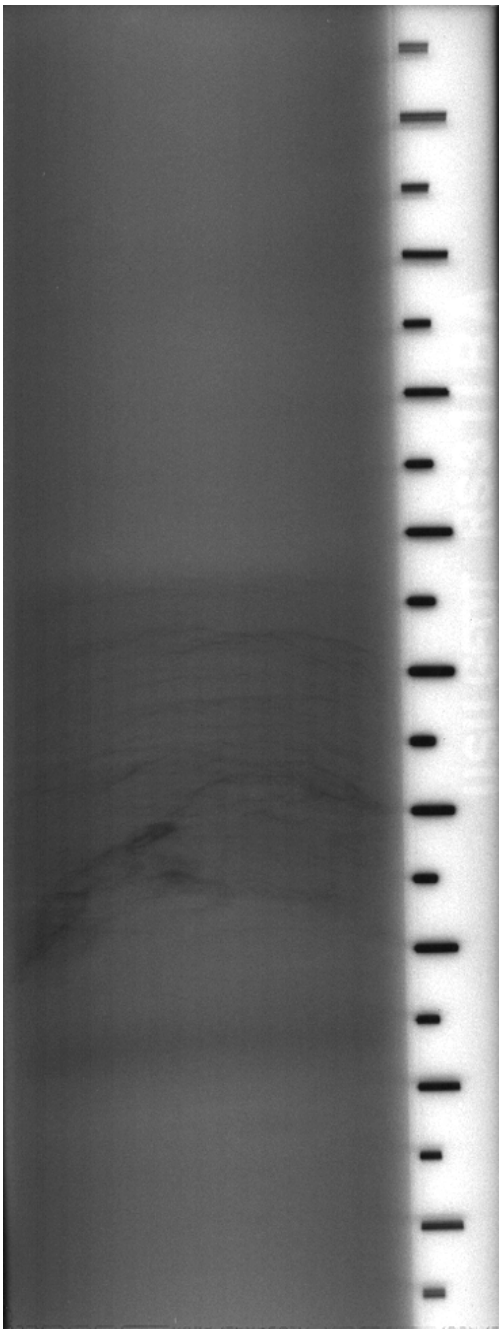

Figure C.96 Bottom x-ray from the shelby tube, rotary wash sample at 34.5-36.5 feet designated RS3 11BA.

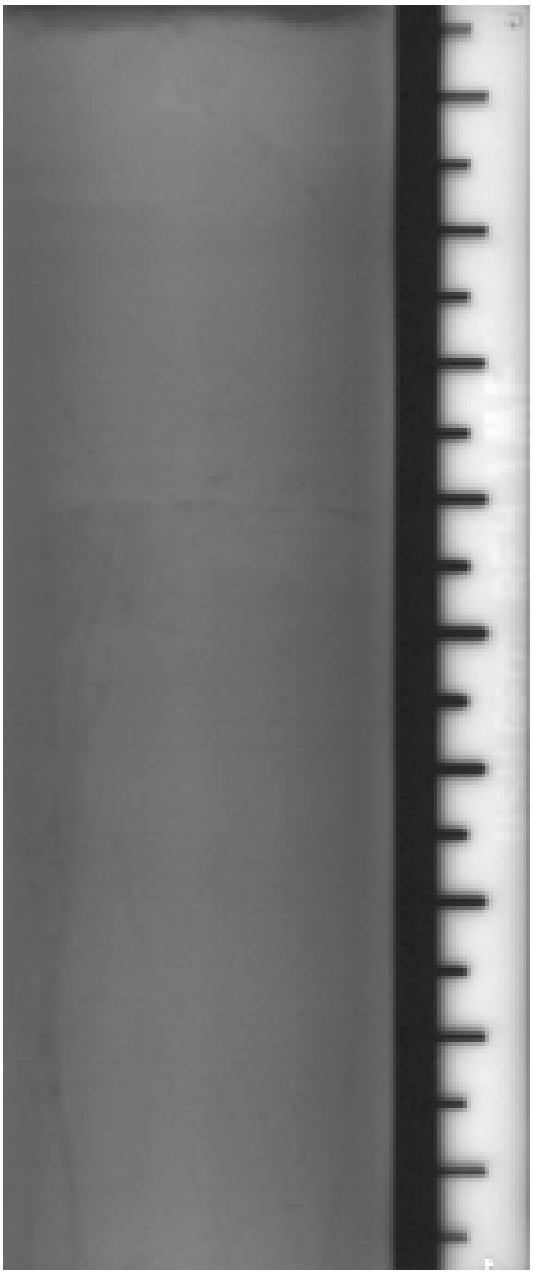

Figure C.97 Middle x-ray from the free-piston, rotary wash sample at 9.5-11.5 feet designated RF4 1MF.

Figure C.98 Bottom x-ray from the free-piston, rotary wash sample at 9.5-11.5 feet designated RF4 1BB.

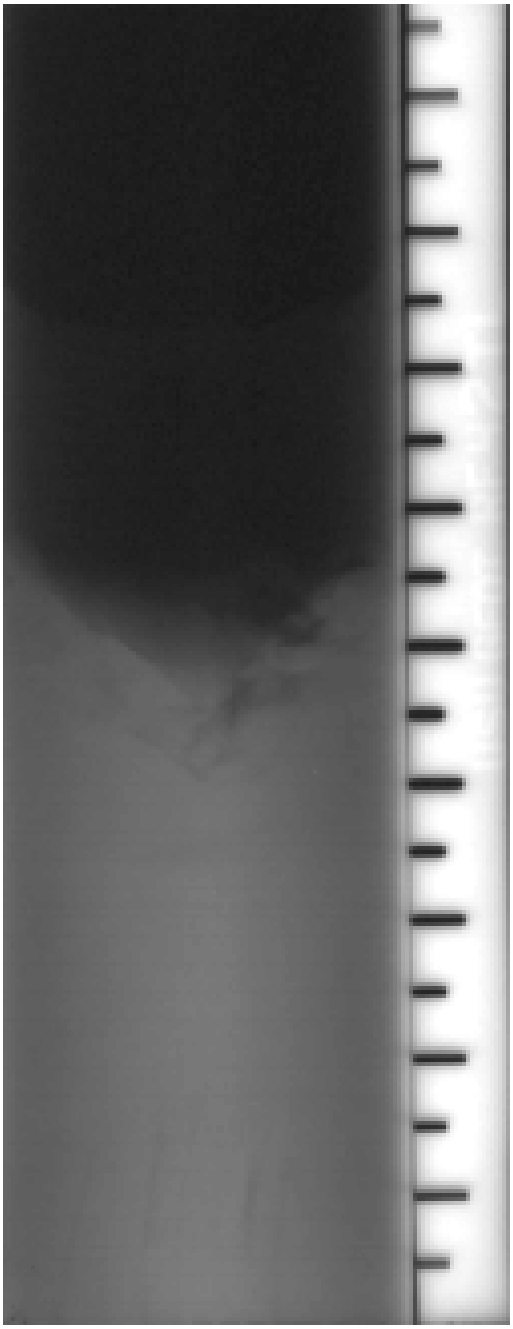

Figure C.99 Top x-ray from the free-piston, rotary wash sample at 12-14 feet designated RF4 2TL.

Figure C.100 Middle x-ray from the free-piston, rotary wash sample at 12-14 feet designated RF4 2MI.

Figure C.101 Bottom x-ray from the free-piston, rotary wash sample at 12-14 feet designated RF4 2BC.

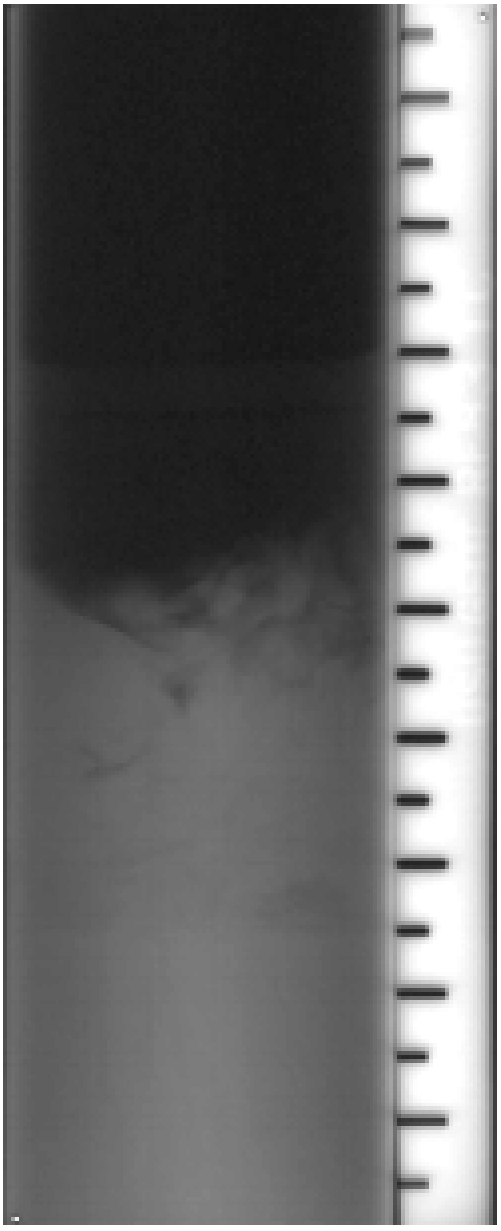

Figure C.102 Top x-ray from the free-piston, rotary wash sample at 14.5-16.5 feet designated RF4 3TC.

Figure C.103 Middle x-ray from the free-piston, rotary wash sample at 14.5-16.5 feet designated RF4 3MC.

Figure C.104 Bottom x-ray from the free-piston, rotary wash sample at 14.5-16.5 feet designated RF4 3BF.

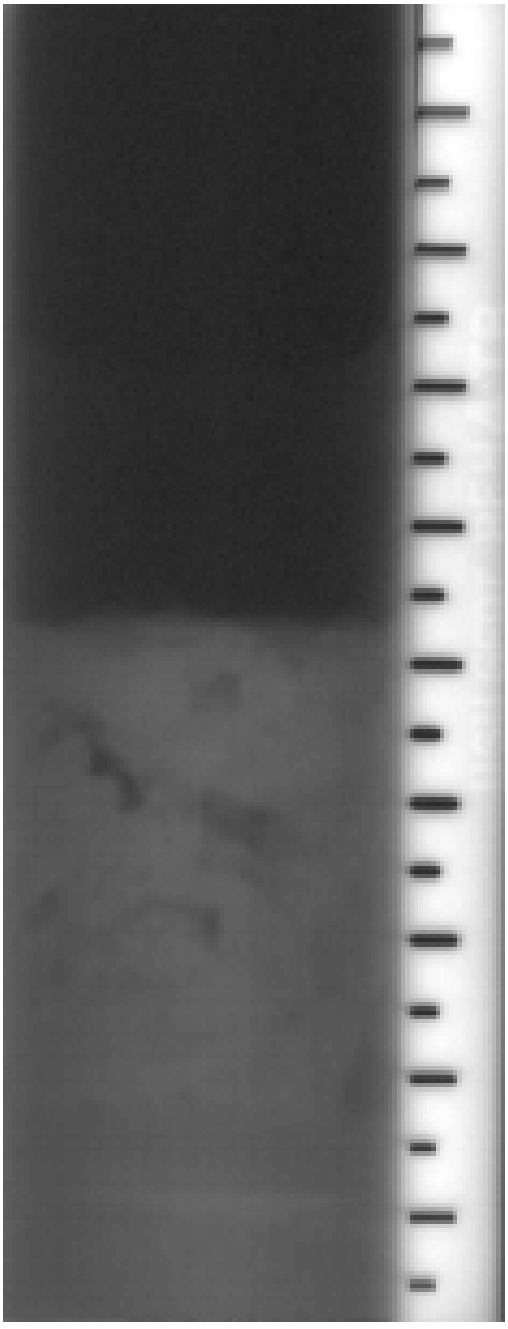

Figure C.105 Top x-ray from the fixed-piston, rotary wash sample at 17-19 feet designated RF4 4TB.

Figure C.106 Middle x-ray from the fixed-piston, rotary wash sample at 17-19 feet designated RF4 4MB.

Figure C.107 Bottom x-ray from the fixed-piston, rotary wash sample at 17-19 feet designated RF4 4BB.

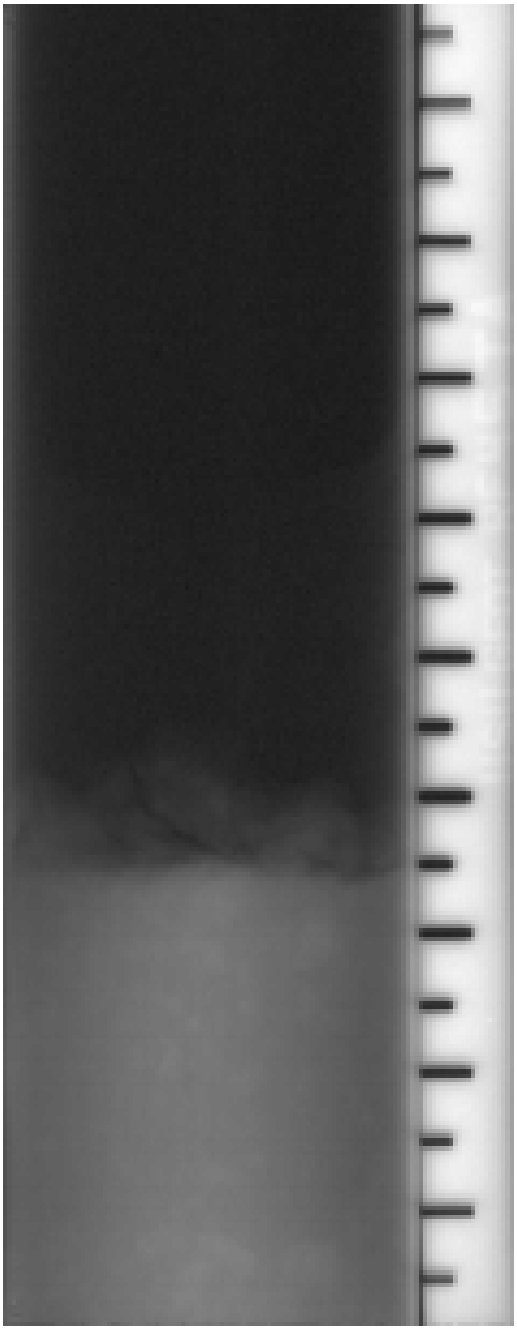

Figure C.108 Top x-ray from the fixed-piston, rotary wash sample at 19.5-21.5 feet designated RF4 5TA.

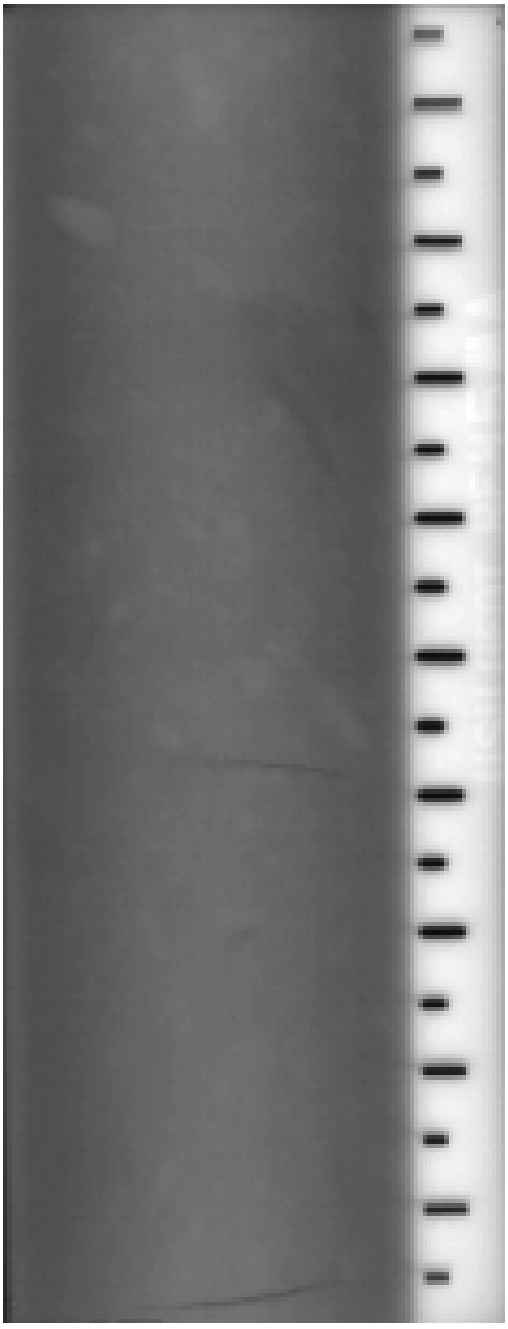

Figure C.109 Middle x-ray from the fixed-piston, rotary wash sample at 19.5-21.5 feet designated RF4 5MA.

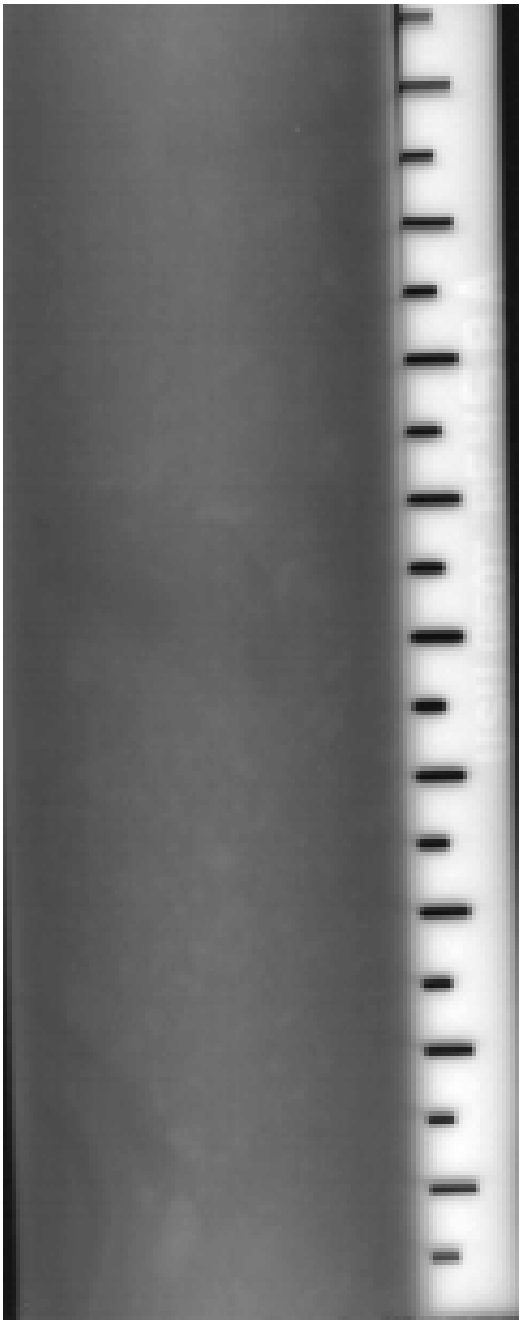

Figure C.110 Bottom x-ray from the fixed-piston, rotary wash sample at 19.5-21.5 feet designated RF4 5BA.

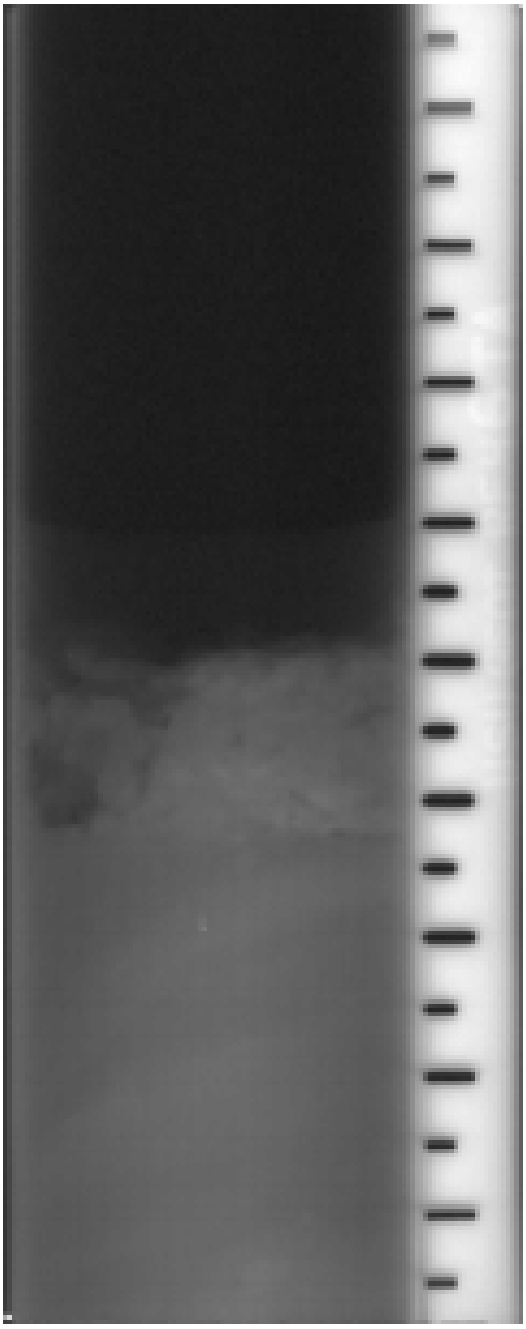

Figure C.111 Top x-ray from the fixed-piston, rotary wash sample at 22-24 feet designated RF4 6TA.

Figure C.112 Middle x-ray from the fixed-piston, rotary wash sample at 22-24 feet designated RF4 6MA.

Figure C.113 Bottom x-ray from the fixed-piston, rotary wash sample at 22-24 feet designated RF4 6BA.

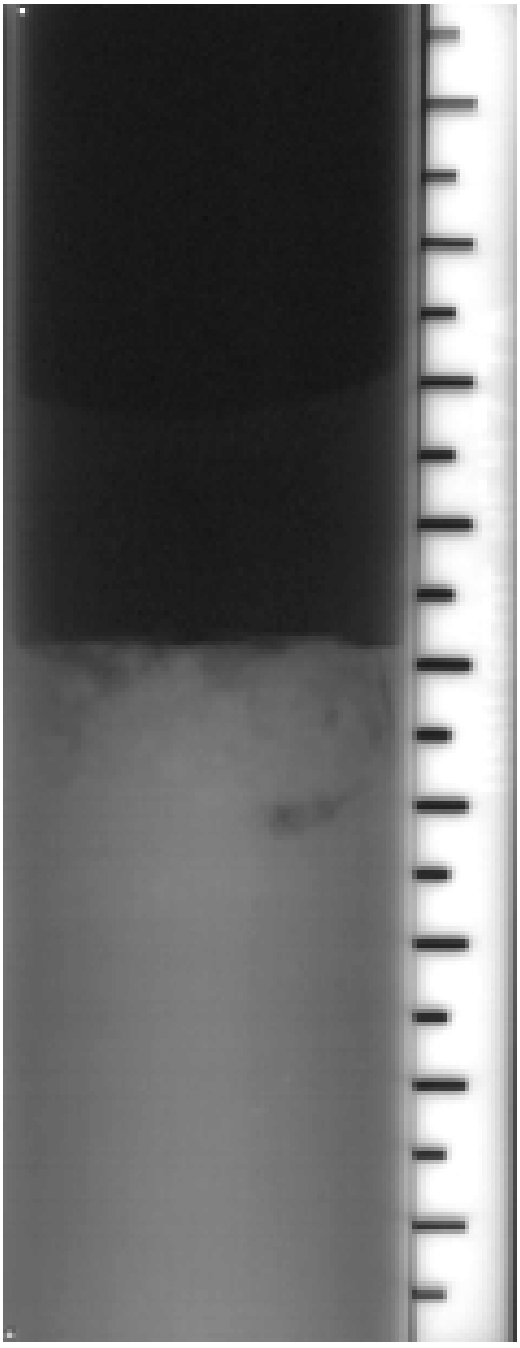

Figure C.114 Top x-ray from the fixed-piston, rotary wash sample at 24.5-26.5 feet designated RF4 7TA.

Figure C.115 Middle x-ray from the fixed-piston, rotary wash sample at 24.5-26.5 feet designated RF4 7MA.

Figure C.116 Bottom x-ray from the fixed-piston, rotary wash sample at 24.5-26.5 feet designated RF4 7BA.

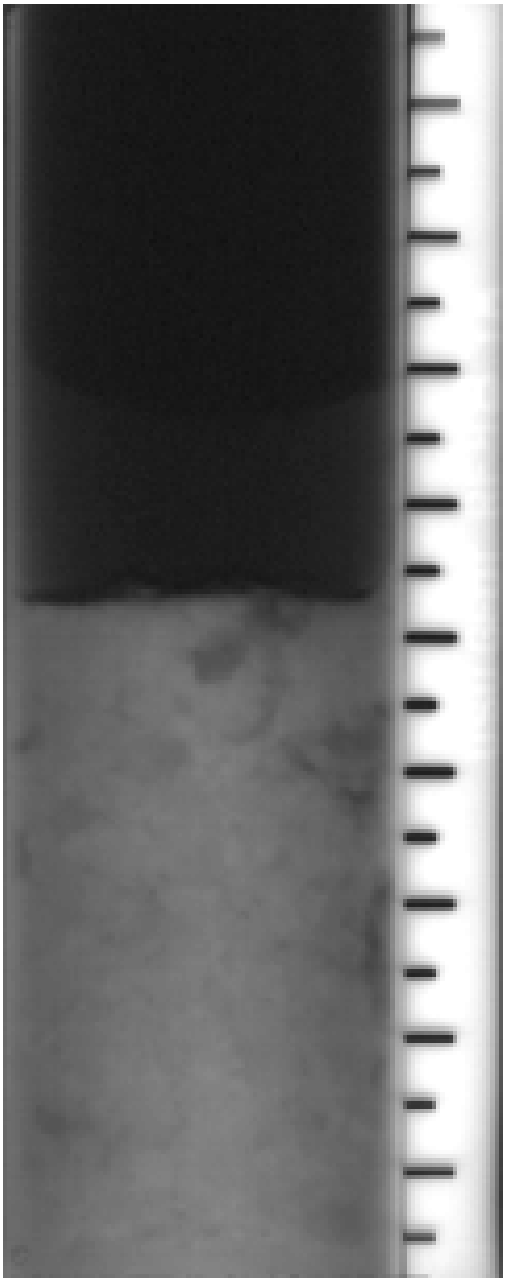

Figure C.117 Top x-ray from the fixed-piston, rotary wash sample at 27-29 feet designated RF4 8TA.

Figure C.118 Middle x-ray from the fixed-piston, rotary wash sample at 27-29 feet designated RF4 8MA.

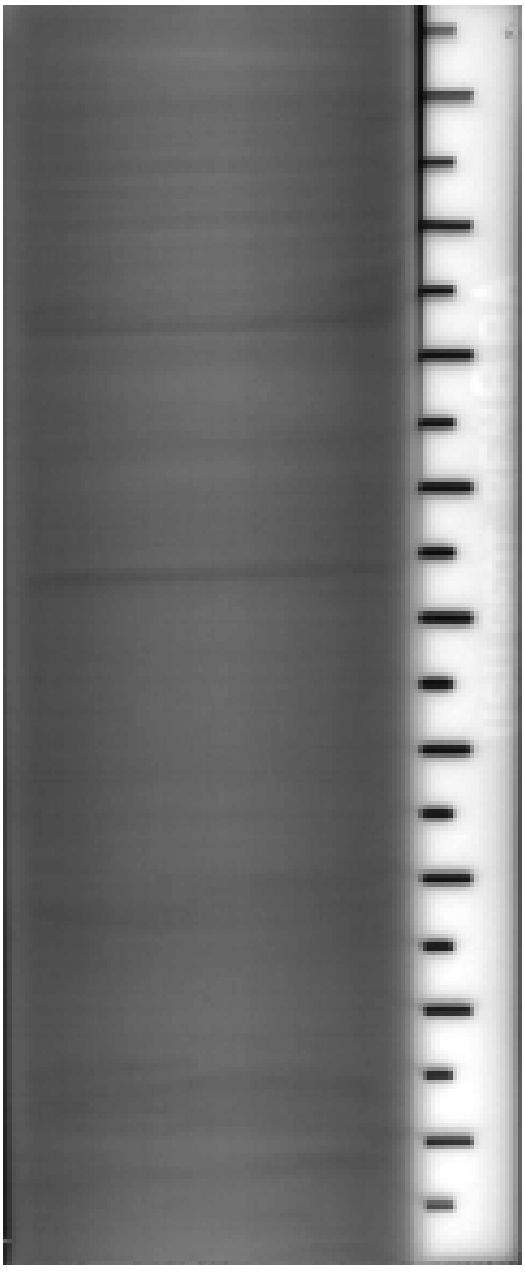

Figure C.119 Bottom x-ray from the fixed-piston, rotary wash sample at 27-29 feet designated RF4 8BA.

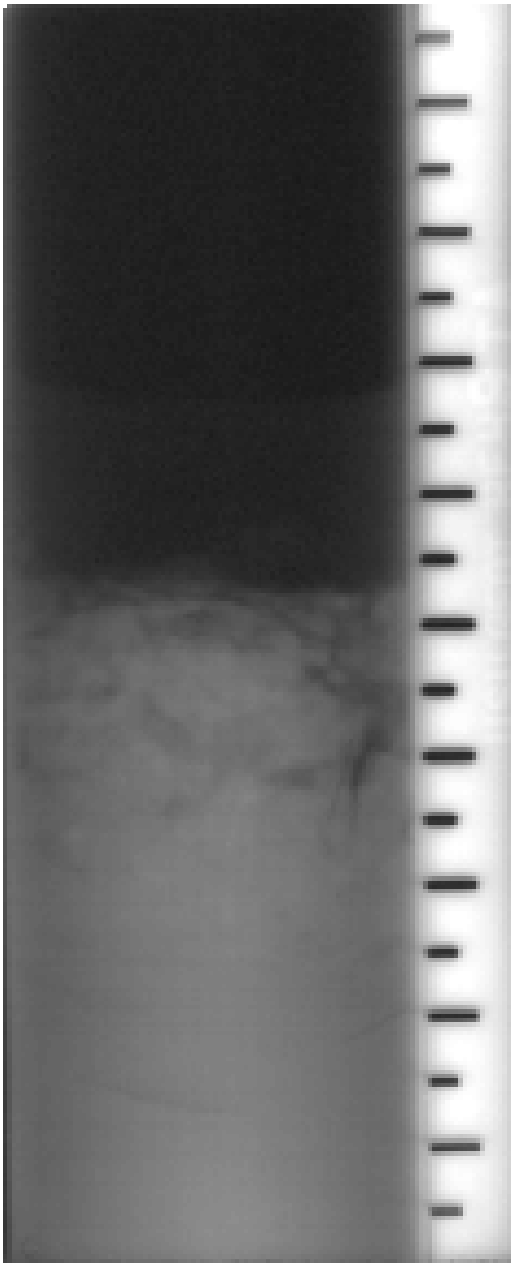

Figure C.120 Top x-ray from the fixed-piston, rotary wash sample at 29.5-31.5 feet designated RF4 9TA.

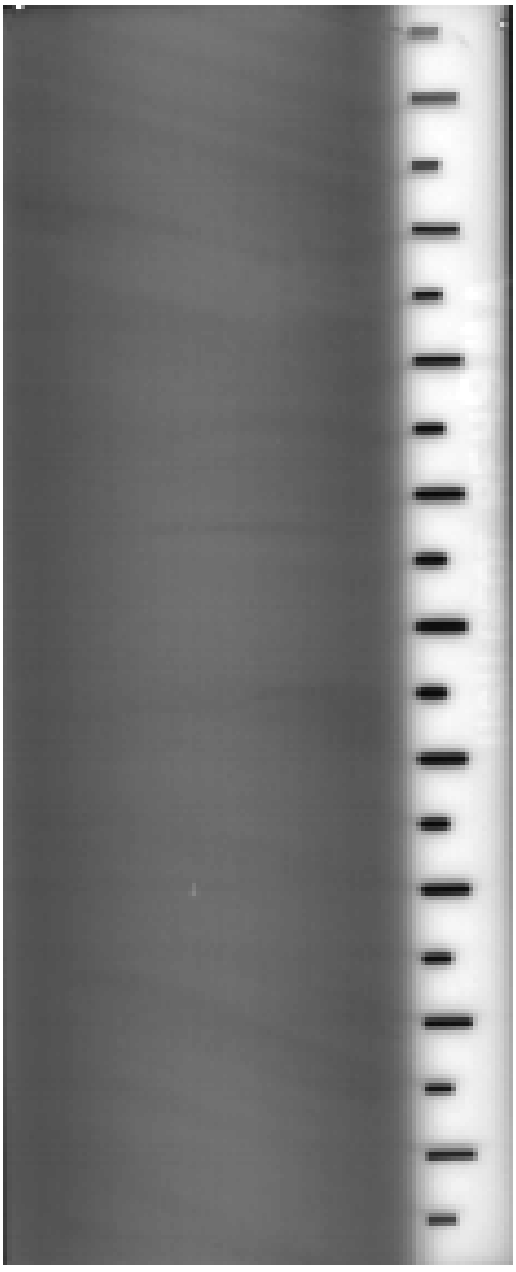

Figure C.121 Middle x-ray from the fixed-piston, rotary wash sample at 29.5-31.5 feet designated RF4 9MA.

Figure C.122 Bottom x-ray from the fixed-piston, rotary wash sample at 29.5-31.5 feet designated RF4 9BA.

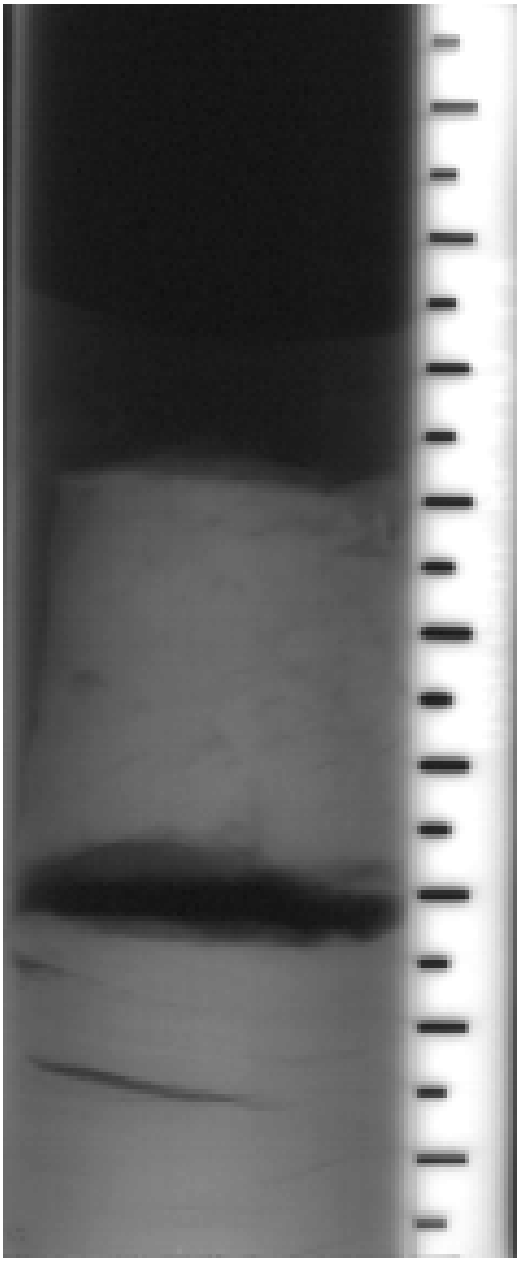

Figure C.123 Top x-ray from the fixed-piston, rotary wash sample at 32-34 feet designated RF4 10TA.

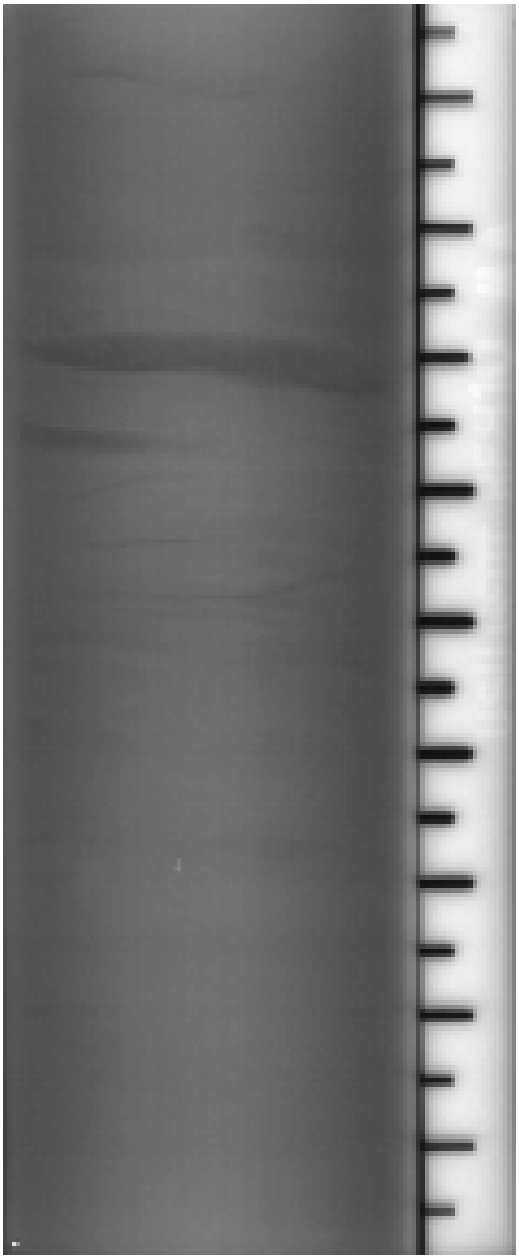

Figure C.124 Middle x-ray from the fixed-piston, rotary wash sample at 32-34 feet designated RF4 10MA.

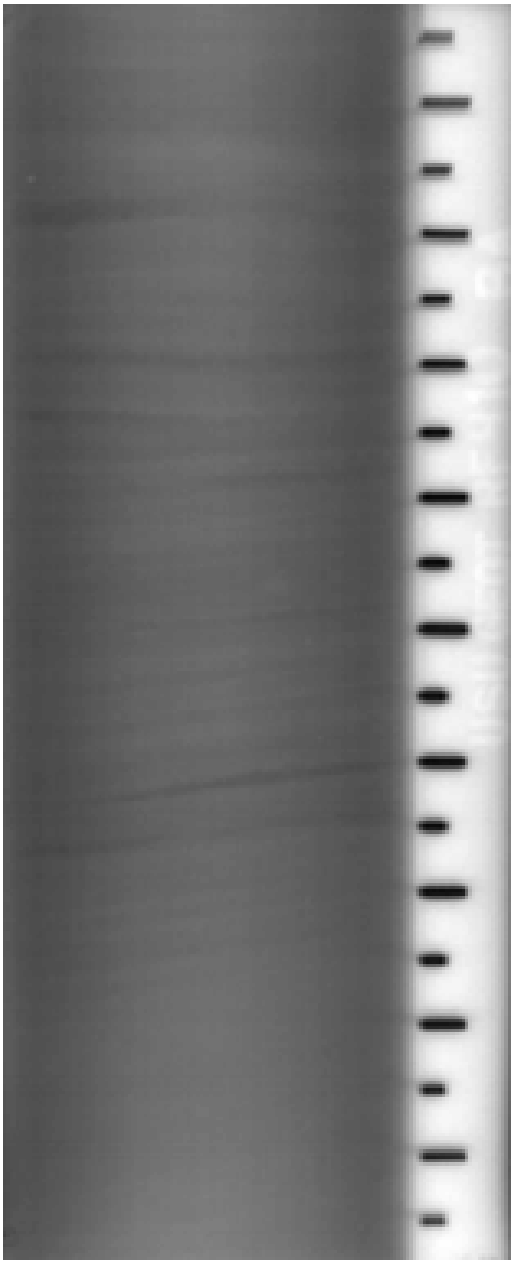

Figure C.125 Bottom x-ray from the fixed-piston, rotary wash sample at 32-34 feet designated RF4 10BA.

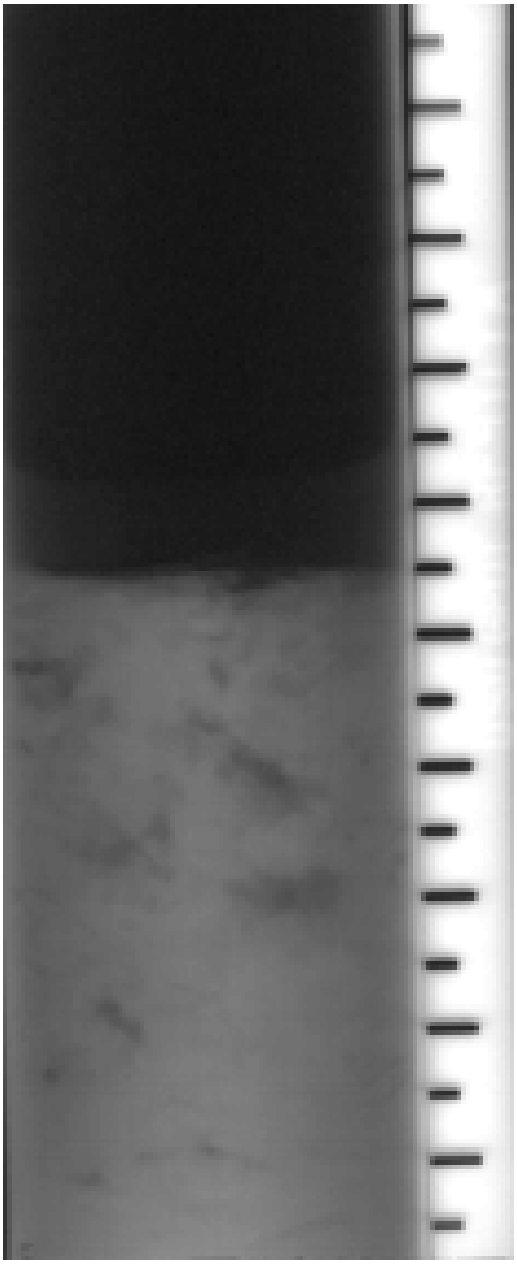

Figure C.126 Top x-ray from the fixed-piston, rotary wash sample at 34.5-36.5 feet designated RF4 11TA.

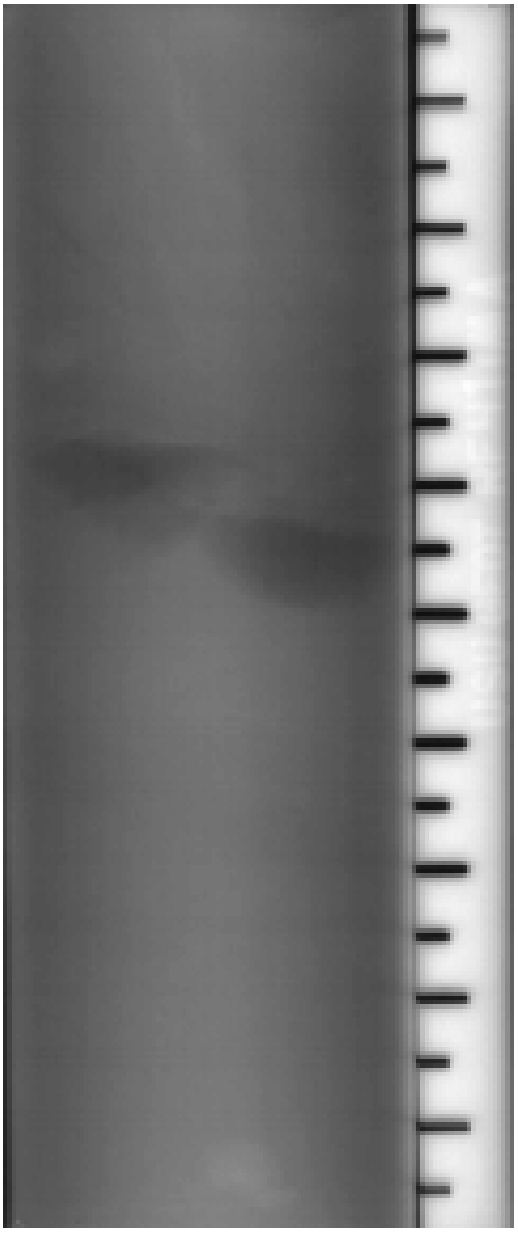

Figure C.127 Middle x-ray from the fixed-piston, rotary wash sample at 34.5-36.5 feet designated RF4 11MA.

Figure C.128 Bottom x-ray from the fixed-piston, rotary wash sample at 34.5-36.5 feet designated RF4 11BA.

# Appendix D

## X-Ray Fracture Data Tables

Table D.1 X-Ray fracture data from boring HS-1

| DEPTH (FT) | FRACTURE SIZE | NUMBER OF FRACTURES | LOCATION | NOTES |
|---|---|---|---|---|
| 9.5-11.5 | Large (>1.5”) | 0 | | |
| | Medium (0.5-1.5”) | 0 | | |
| | Small (<0.5”) | 0 | | |
| 12-14 | Large | 0 | | |
| | Medium | 0 | | |
| | Small | 0 | | |
| 14.5-16.5 | Large | 0 | | |
| | Medium | 0 | | |
| | Small | 0 | | |
| 17-19 | Large | 0 | | |
| | Medium | 0 | | |
| | Small | 0 | | |
| 19.5-21.5 | Large | 1 | Middle | |
| | Medium | 3 | Bottom 5” | |
| | Small | 5+ | Bottom 10” | |
| 22-24 | Large | 2 | At bottom and 1’ up | Some edge turning |
| | Medium | 1 | Right below slough | |
| | Small | 2 | Right below slough | |
| 24.5-26.5 | Large | 2 | 5” from bottom | Some fractures at angles |
| | Medium | 4 | Middle | |
| | Small | 4 | At middle on edges | |
| 27-29 | Large | 5 | Top, middle, bottom | |
| | Medium | 2 | Near top | |
| | Small | 2 | Right under slough | |
| 29.5-31.5 | Large | 3 | Bottom 8” | Faint |
| | Medium | 1 | Near bottom | |
| | Small | 0 | | |
| 32-34 | Large | 1 | Right under slough | Faint |
| | Medium | 5+ | Right under slough | |
| | Small | 4 | Near middle | |
| 34.5-36.5 | Large | 0 | | Edge turned |
| | Medium | 0 | | |
| | Small | 3 | At bottom | |

Table D.2 X-Ray fracture data from boring HF-2

| DEPTH (FT) | FRACTURE SIZE | NUMBER OF FRACTURES | LOCATION | NOTES |
|---|---|---|---|---|
| 9.5-11.5 | Large (>1.5”) | 0 | | |
| | Medium (0.5-1.5”) | 0 | | |
| | Small (<0.5”) | 0 | | |
| 12-14 | Large | 0 | | |
| | Medium | 0 | | |
| | Small | 0 | | |
| 14.5-16.5 | Large | 0 | | |
| | Medium | 0 | | |
| | Small | 0 | | |
| 17-19 | Large | 0 | | |
| | Medium | 0 | | |
| | Small | 0 | | |
| 19.5-21.5 | Large | 0 | | No sample |
| | Medium | 0 | | |
| | Small | 0 | | |
| 22-24 | Large | 0 | | |
| | Medium | 0 | | |
| | Small | 0 | | |
| 24.5-26.5 | Large | 0 | | |
| | Medium | 0 | | |
| | Small | 0 | | |
| 27-29 | Large | 0 | | |
| | Medium | 0 | | |
| | Small | 0 | | |
| 29.5-31.5 | Large | 0 | | Faint |
| | Medium | 2 | Middle | |
| | Small | 0 | | |
| 32-34 | Large | 2 | Under slough, middle | Faint |
| | Medium | 0 | | |
| | Small | 1 | Right under slough | |
| 34.5-36.5 | Large | 0 | | |
| | Medium | 0 | | |
| | Small | 2 | 6” from bottom | |

Table D.3 X-Ray fracture data from boring RS-3

| DEPTH (FT) | FRACTURE SIZE | NUMBER OF FRACTURES | LOCATION | NOTES |
|---|---|---|---|---|
| 9.5-11.5 | Large (>1.5”) | 0 | | |
| | Medium (0.5-1.5”) | 0 | | |
| | Small (<0.5”) | 0 | | |
| 12-14 | Large | 0 | | |
| | Medium | 0 | | |
| | Small | 0 | | |
| 14.5-16.5 | Large | 0 | | |
| | Medium | 0 | | |
| | Small | 0 | | |
| 17-19 | Large | 2 | Bottom 3” | |
| | Medium | 1 | Bottom 3” | |
| | Small | 0 | | |
| 19.5-21.5 | Large | 2 | At sand/clay interface | Mostly near edges. Some edge turning |
| | Medium | 8 | Middle and bottom | |
| | Small | 5+ | Middle and bottom | |
| 22-24 | Large | 10+ | Throughout | Many tiny fractures along edges |
| | Medium | 5+ | Throughout | |
| | Small | 5+ | Throughout | |
| 24.5-26.5 | Large | 10 | Throughout | |
| | Medium | 15+ | Throughout | |
| | Small | 1 | Throughout | |
| 27-29 | Large | 0 | | |
| | Medium | 2 | 4” from top | |
| | Small | 2 | 4” from top | |
| 29.5-31.5 | Large | 10+ | Middle | Fracturing is bunched up, heavy |
| | Medium | 10+ | Middle | |
| | Small | 10+ | Middle | |
| 32-34 | Large | 12 | Throughout | |
| | Medium | 7 | Throughout | |
| | Small | 5 | Throughout | |
| 34.5-36.5 | Large | 4 | Top and middle | One fracture is very thick and large |
| | Medium | 2 | Top | |
| | Small | 0 | | |

Table D.4 X-Ray fracture data from boring RF-4

| DEPTH (FT) | FRACTURE SIZE | NUMBER OF FRACTURES | LOCATION | NOTES |
|---|---|---|---|---|
| 9.5-11.5 | Large (>1.5”) | 0 | | |
| | Medium (0.5-1.5”) | 0 | | |
| | Small (<0.5”) | 0 | | |
| 12-14 | Large | 0 | | |
| | Medium | 0 | | |
| | Small | 0 | | |
| 14.5-16.5 | Large | 0 | | |
| | Medium | 0 | | |
| | Small | 0 | | |
| 17-19 | Large | 0 | | |
| | Medium | 0 | | |
| | Small | 0 | | |
| 19.5-21.5 | Large | 2 | Middle 6” | Lots of gravel |
| | Medium | 0 | | |
| | Small | 0 | | |
| 22-24 | Large | 2 | 4” and 7” from top | One curves downward from edge 3” |
| | Medium | 0 | | |
| | Small | 0 | | |
| 24.5-26.5 | Large | 0 | | |
| | Medium | 0 | | |
| | Small | 0 | | |
| 27-29 | Large | 0 | | Faint |
| | Medium | 0 | | |
| | Small | 1 | Middle at edge | |
| 29.5-31.5 | Large | 0 | | |
| | Medium | 2 | 2” under slough | |
| | Small | 0 | | |
| 32-34 | Large | 1 | Right under slough | |
| | Medium | 3 | Middle | |
| | Small | 4 | 3” under slough | |
| 34.5-36.5 | Large | 0 | | |
| | Medium | 0 | | |
| | Small | 0 | | |

# Appendix E

## CRS Test Curves

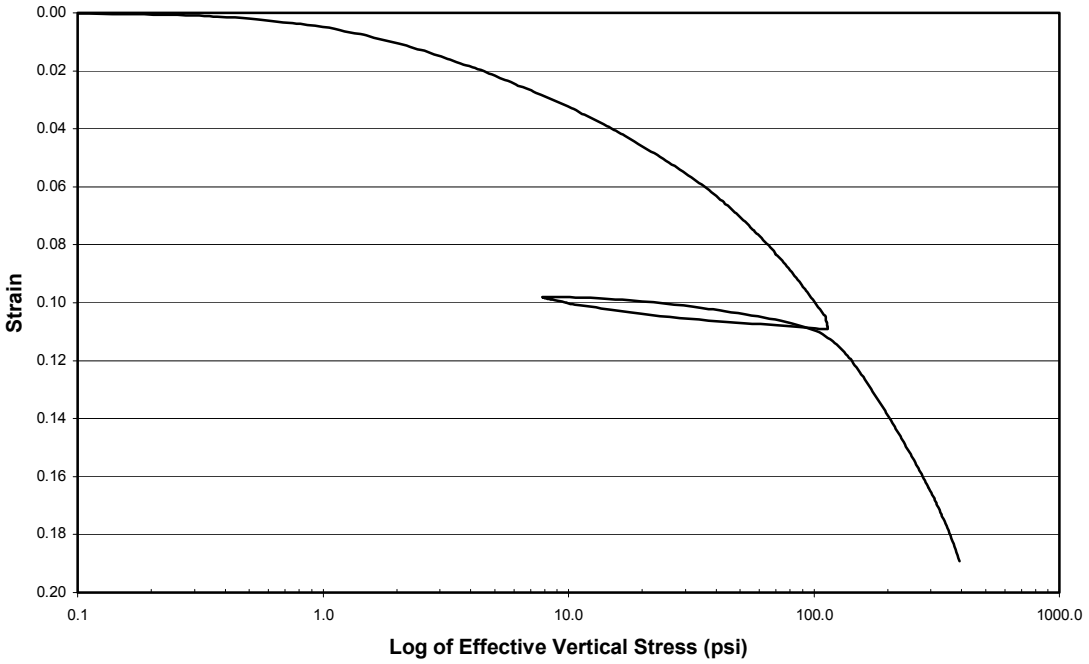


Figure E.1 Curve of strain vs. the log of effective vertical stress for a shelby tube, hollow stem auger sample at 9.5-11.5 feet.

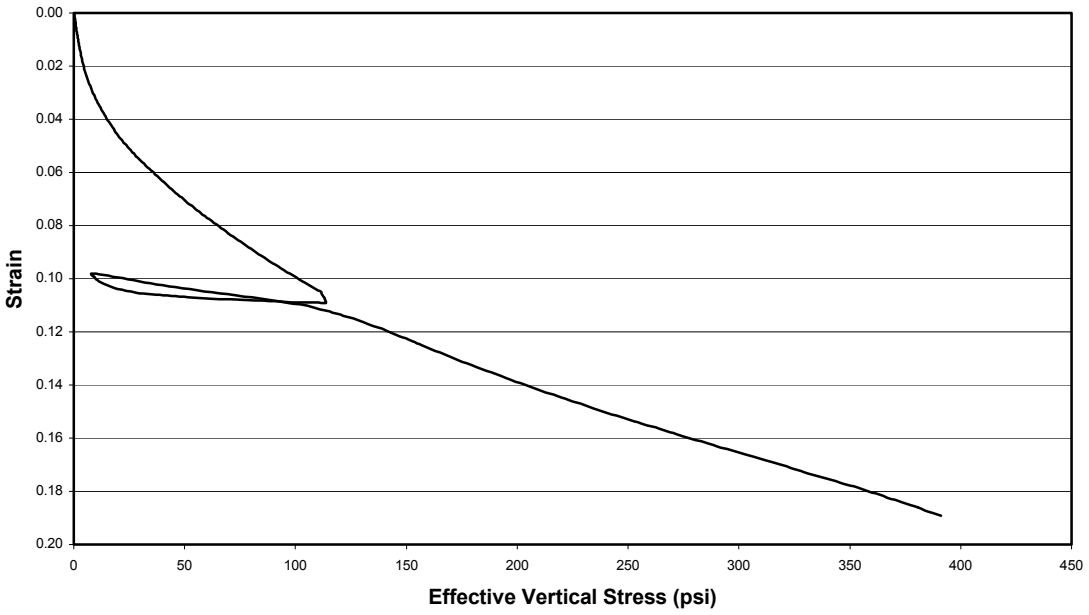


Figure E.2 Linear curve of strain vs. effective vertical stress for a shelby tube, hollow stem auger sample at 9.5-11.5 feet.

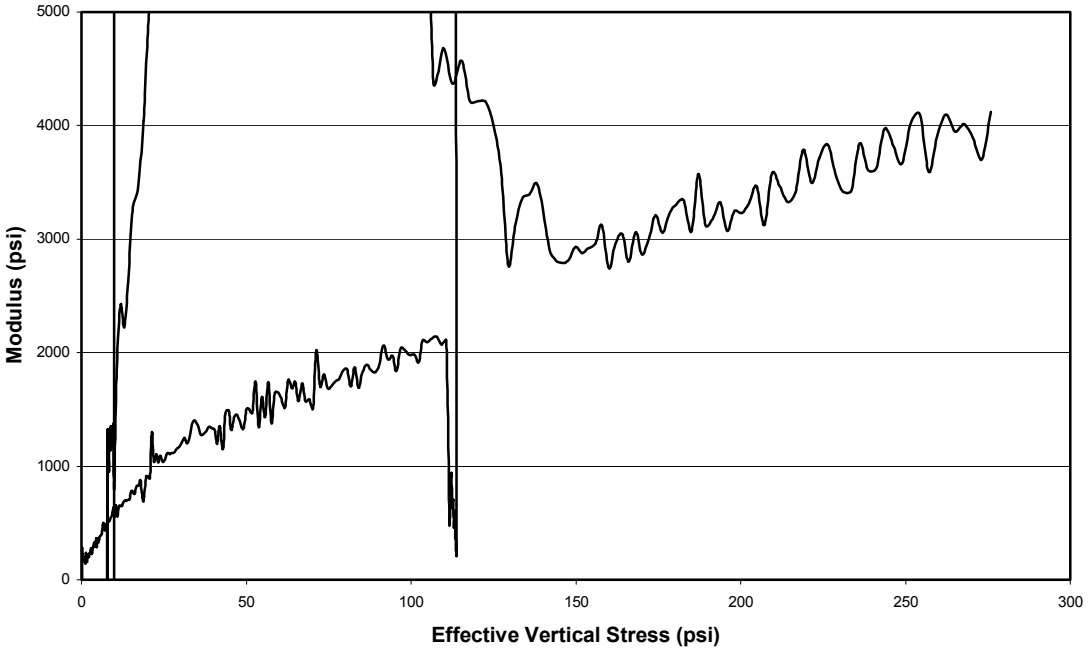


Figure E.3 Curve of modulus vs. effective vertical stress for a shelby tube, hollow stem auger sample at 9.5-11.5 feet.

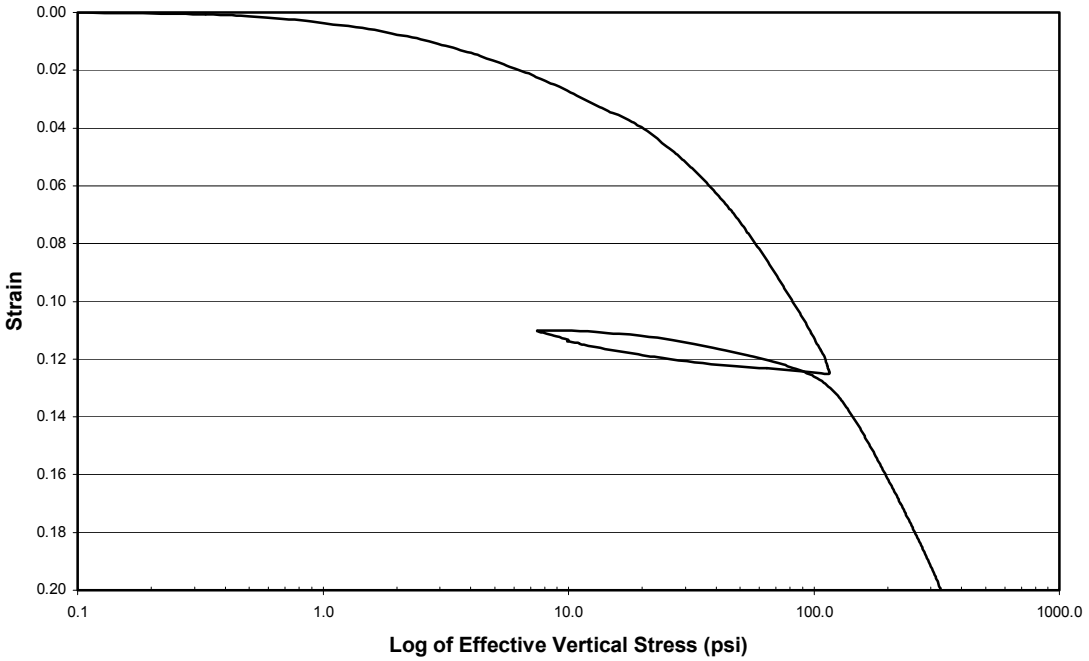


Figure E.4 Curve of strain vs. the log of effective vertical stress for a shelby tube, hollow stem auger sample at 12-14 feet.

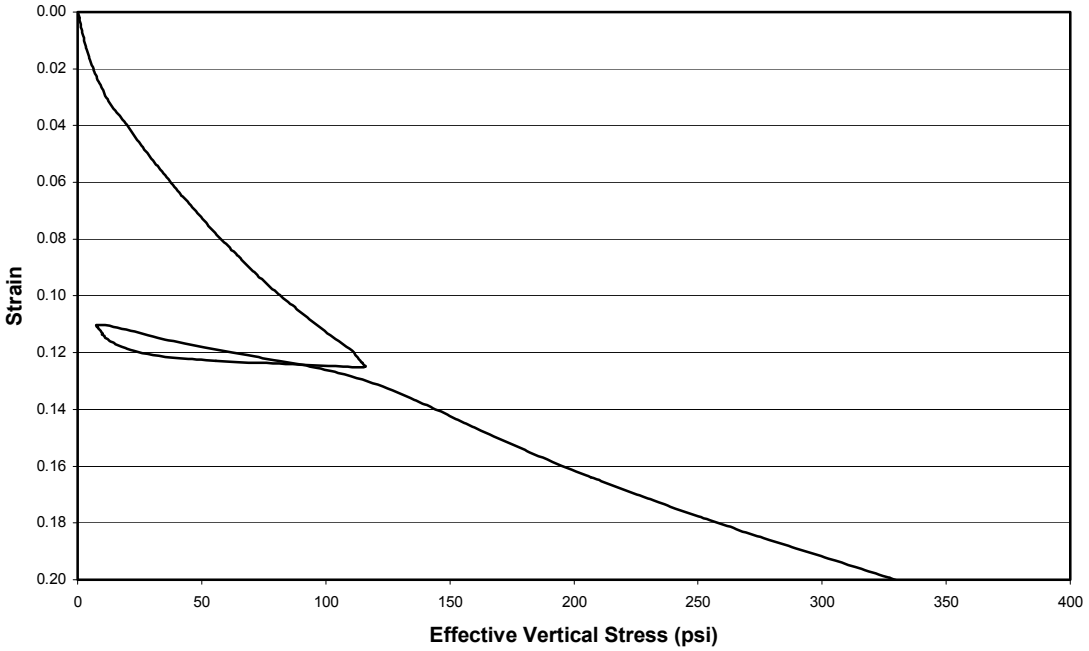


Figure E.5 Linear curve of strain vs. effective vertical stress for a shelby tube, hollow stem auger sample at 12-14 feet.

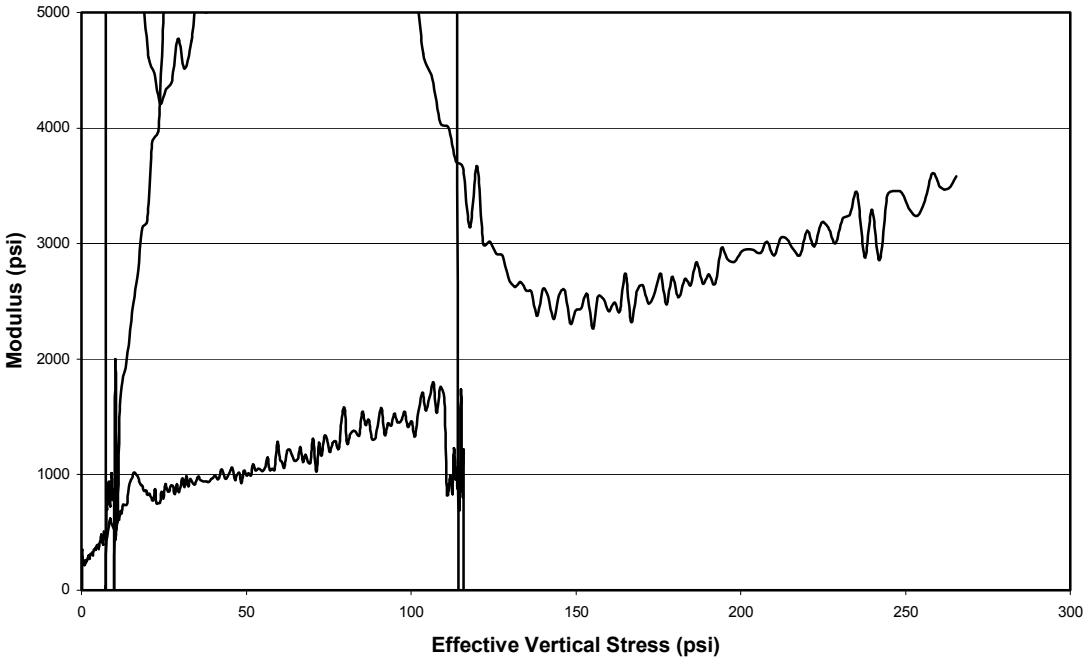


Figure E.6 Curve of modulus vs. effective vertical stress for a shelby tube, hollow stem auger sample at 12-14 feet.

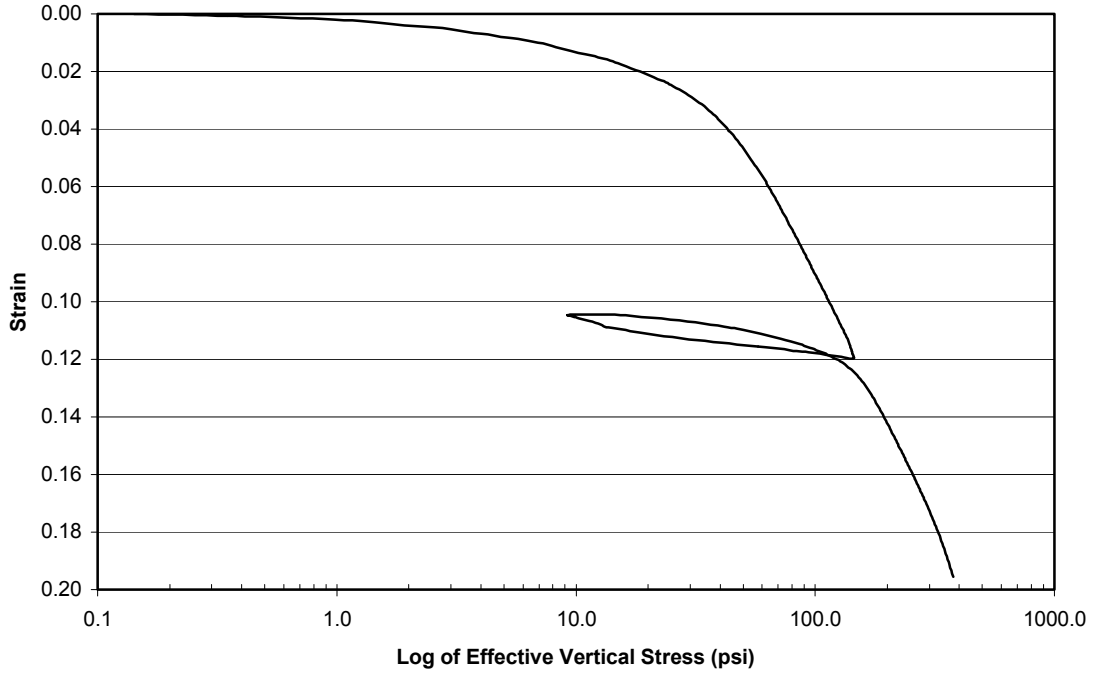


Figure E.7 Curve of strain vs. the log of effective vertical stress for a shelby tube, hollow stem auger sample at 14.5-16.5 feet.

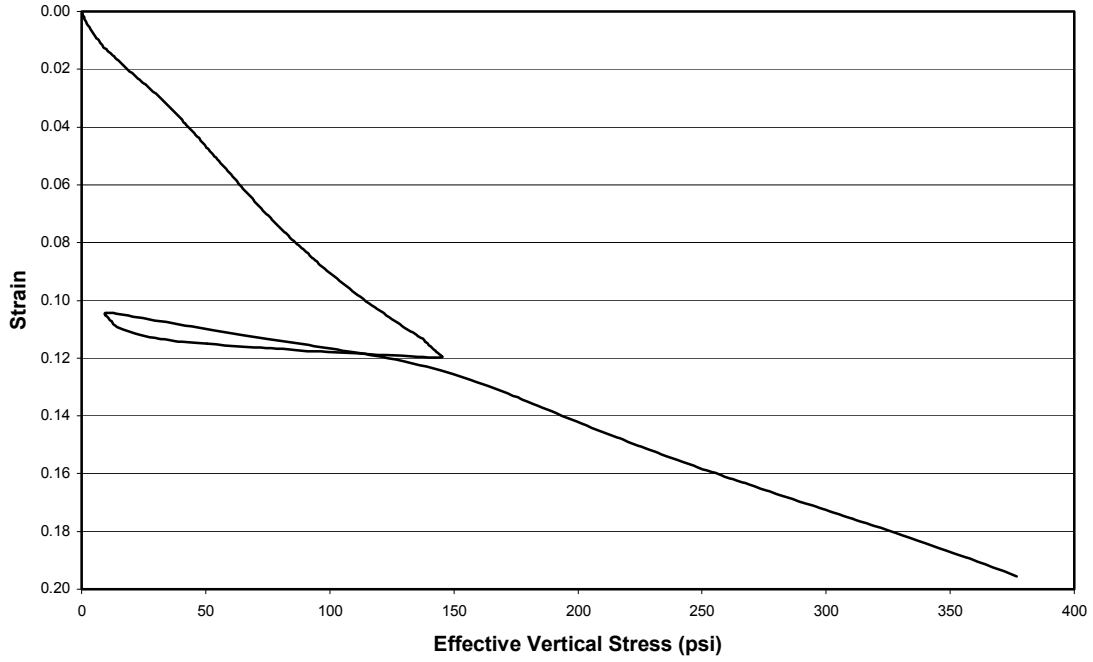


Figure E.8 Linear curve of strain vs. effective vertical stress for a shelby tube, hollow stem auger sample at 14.5-16.5 feet.

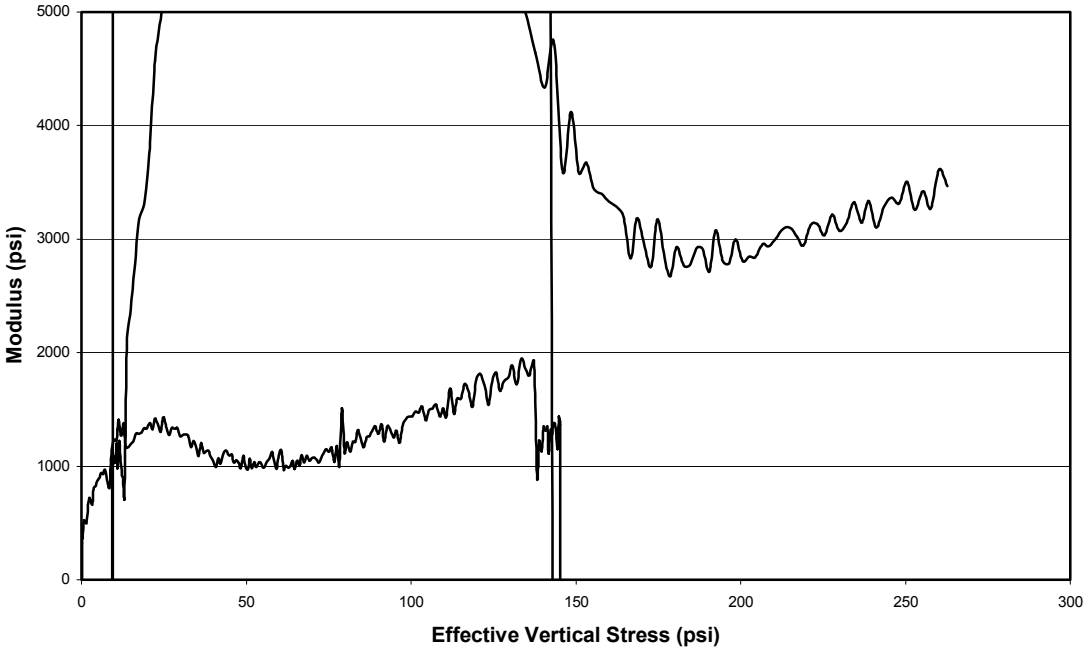


Figure E.9 Curve of modulus vs. effective vertical stress for a shelby tube, hollow stem auger sample at 14.5-16.5 feet.

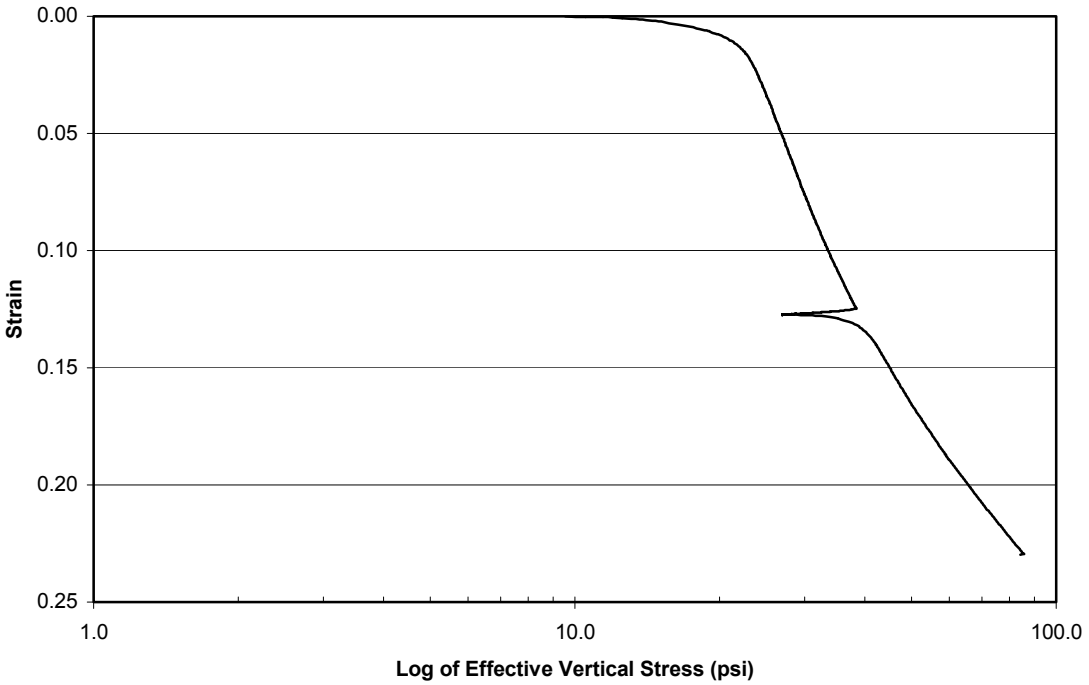


Figure E.10 Curve of strain vs. the log of effective vertical stress for a shelby tube, hollow stem auger sample at 17-19 feet.

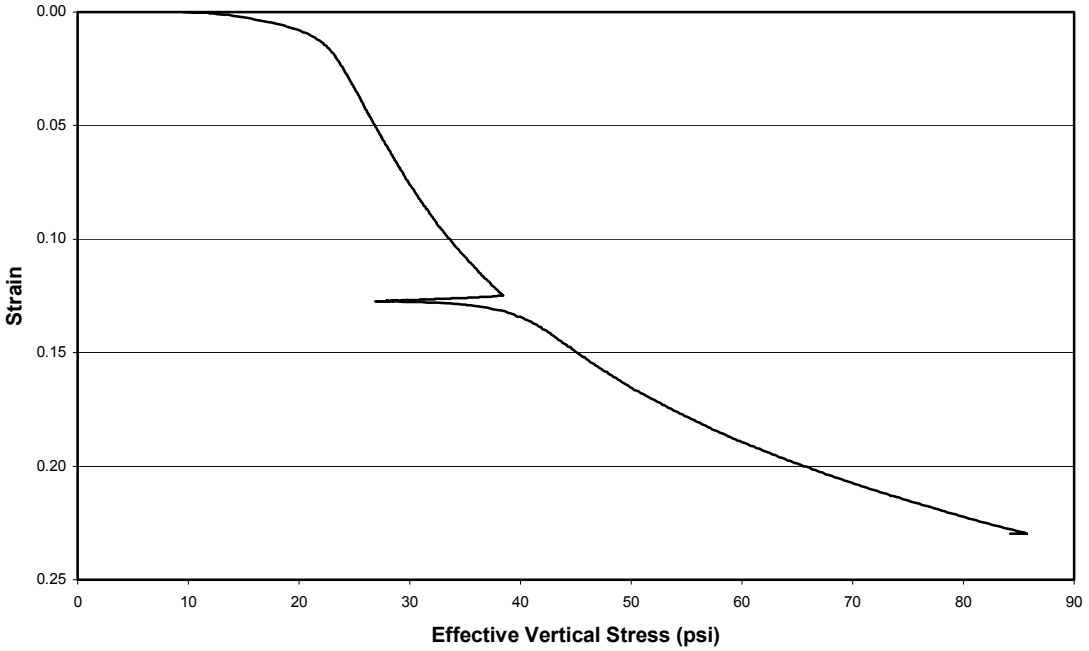


Figure E.11 Linear curve of strain vs. effective vertical stress for a shelby tube, hollow stem auger sample at 17-19 feet.

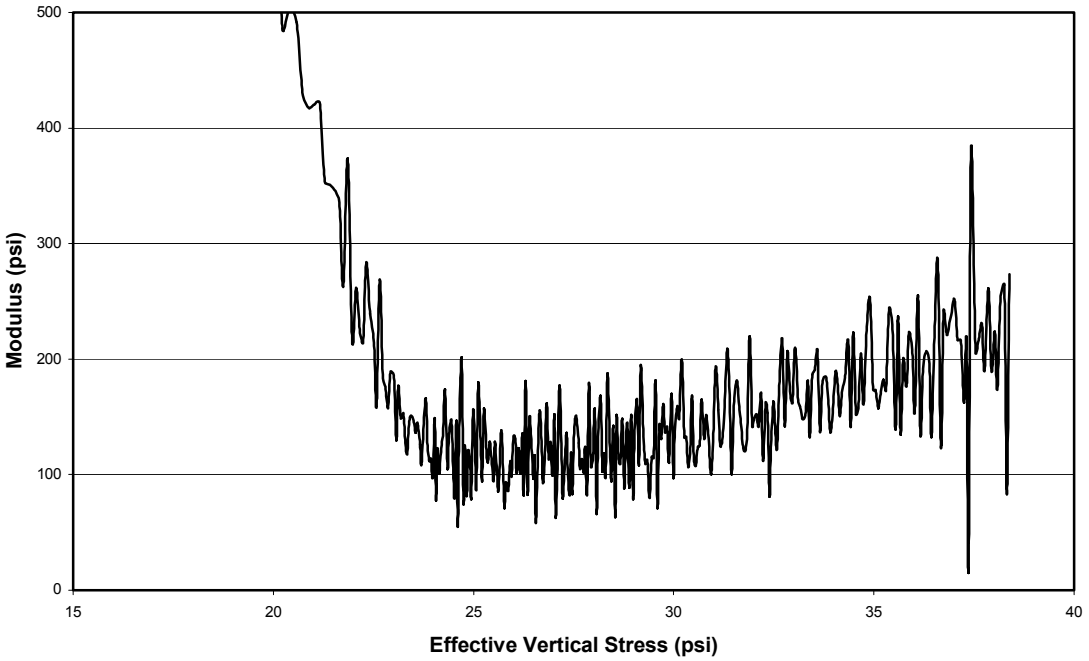


Figure E.12 Curve of modulus vs. effective vertical stress for a shelby tube, hollow stem auger sample at 17-19 feet.

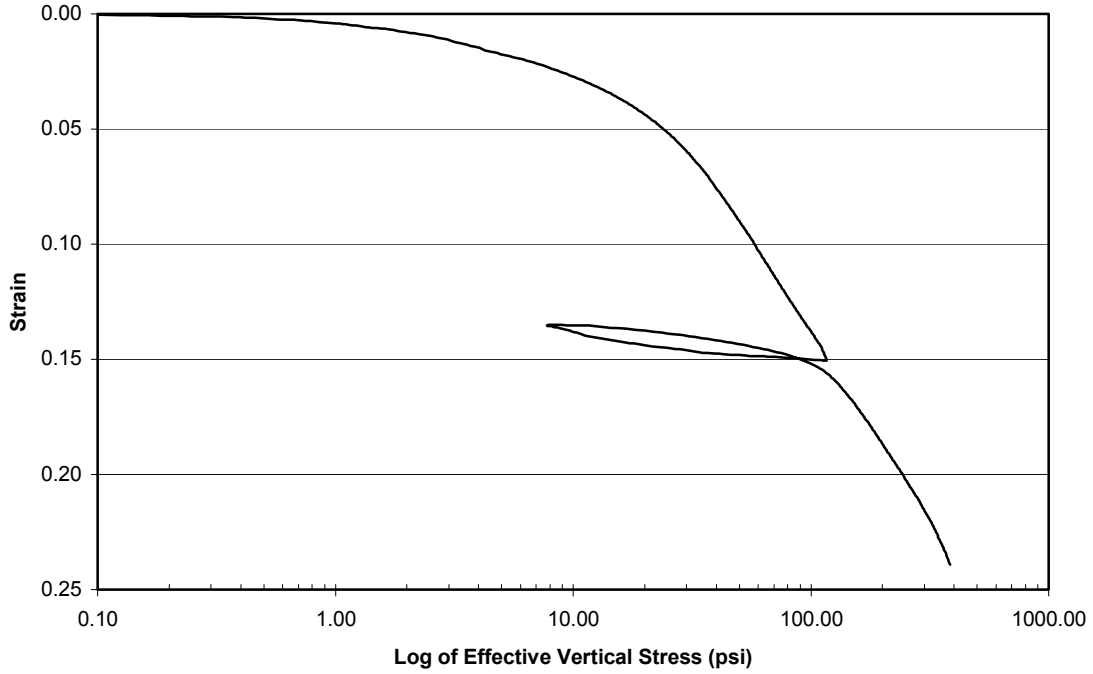


Figure E.13 Curve of strain vs. the log of effective vertical stress for a shelby tube, hollow stem auger sample at 22-24 feet.

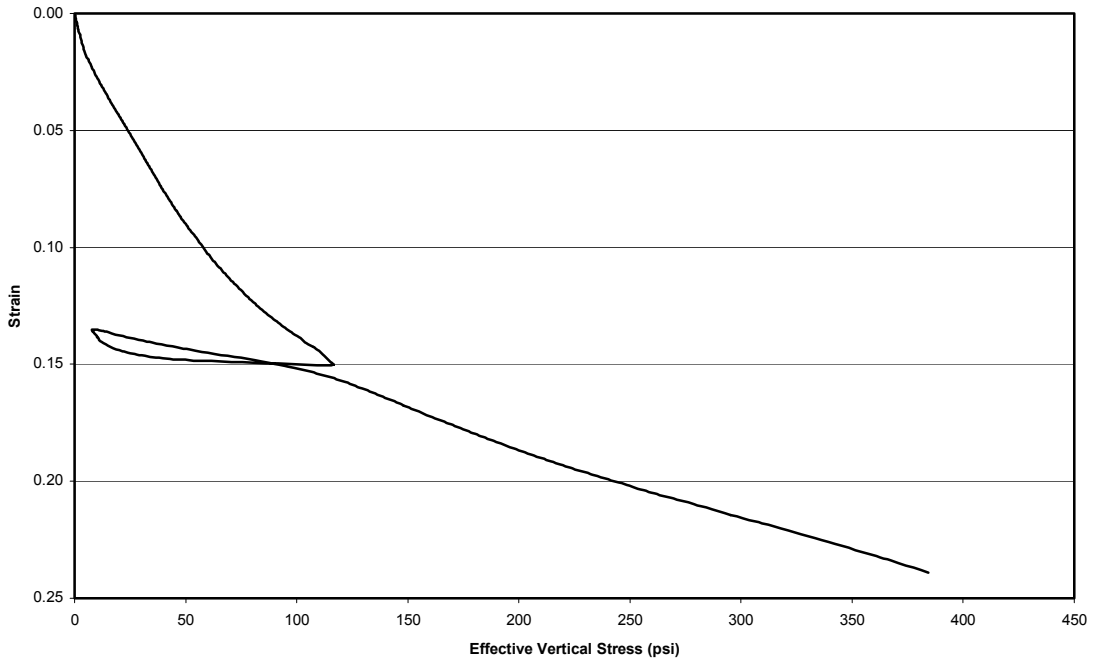


Figure E.14 Linear curve of strain vs. effective vertical stress for a shelby tube, hollow stem auger sample at 22-24 feet.

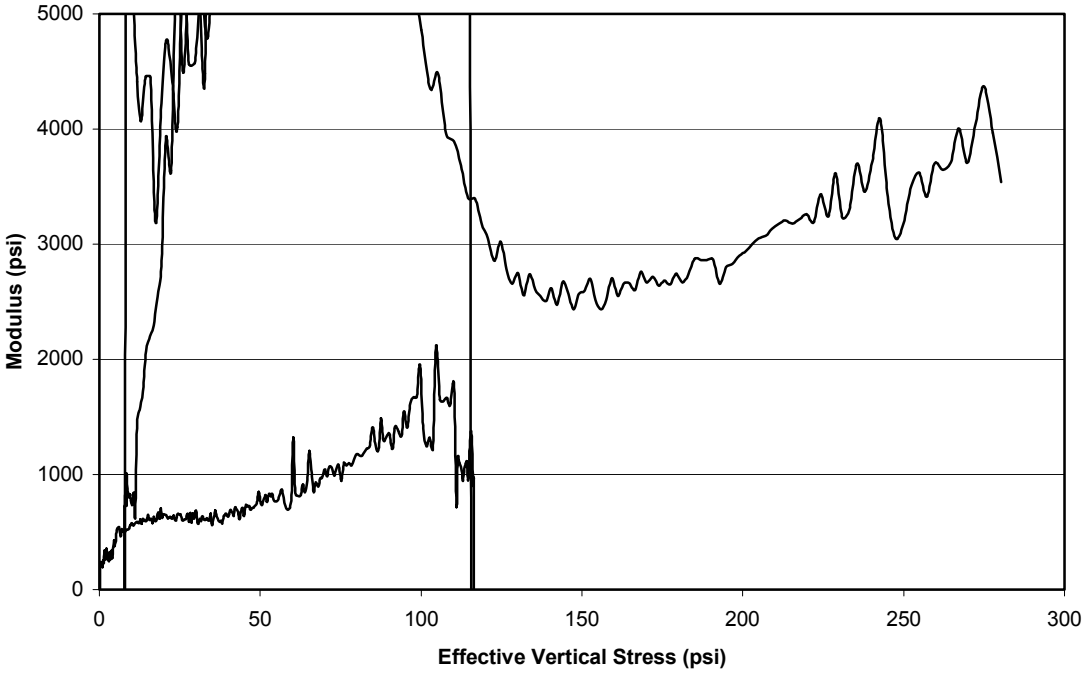


Figure E.15 Curve of modulus vs. effective vertical stress for a shelby tube, hollow stem auger sample at 22-24 feet.

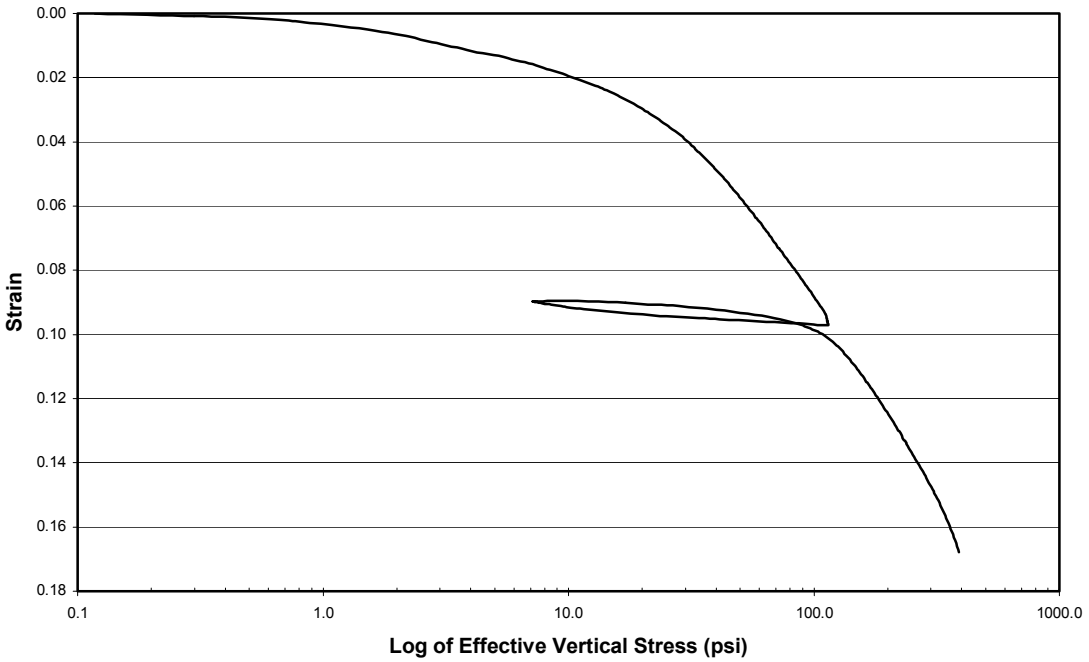


Figure E.16 Curve of strain vs. the log of effective vertical stress for a shelby tube, hollow stem auger sample at 24.5-26.5 feet.

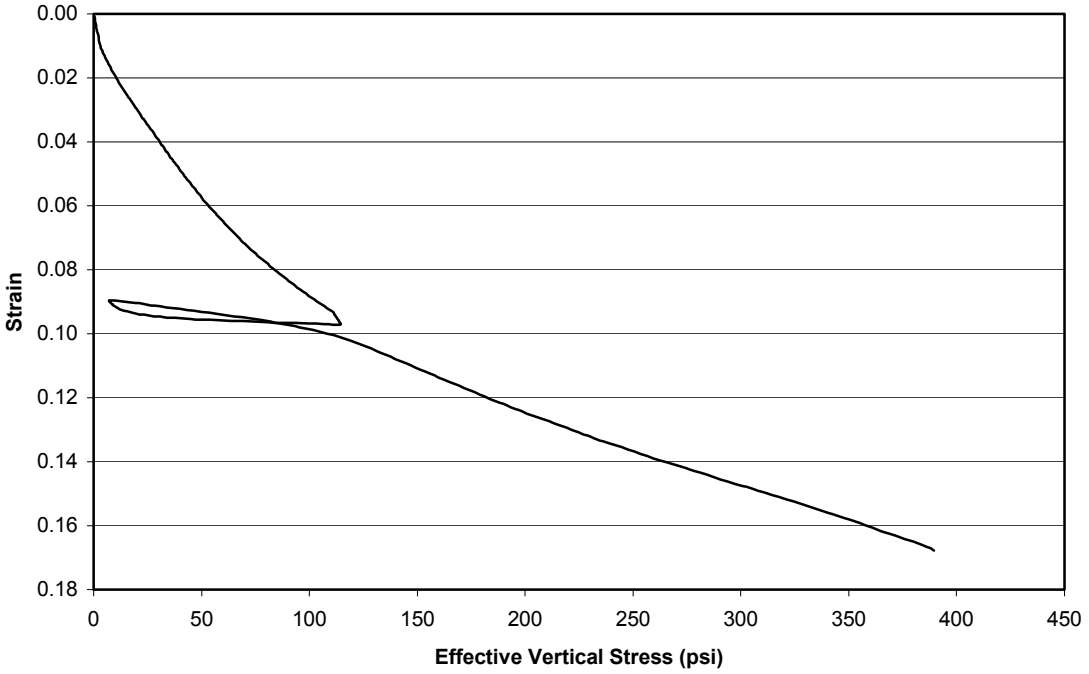


Figure E.17 Linear curve of strain vs. effective vertical stress for a shelby tube, hollow stem auger sample at 24.5-26.5 feet.

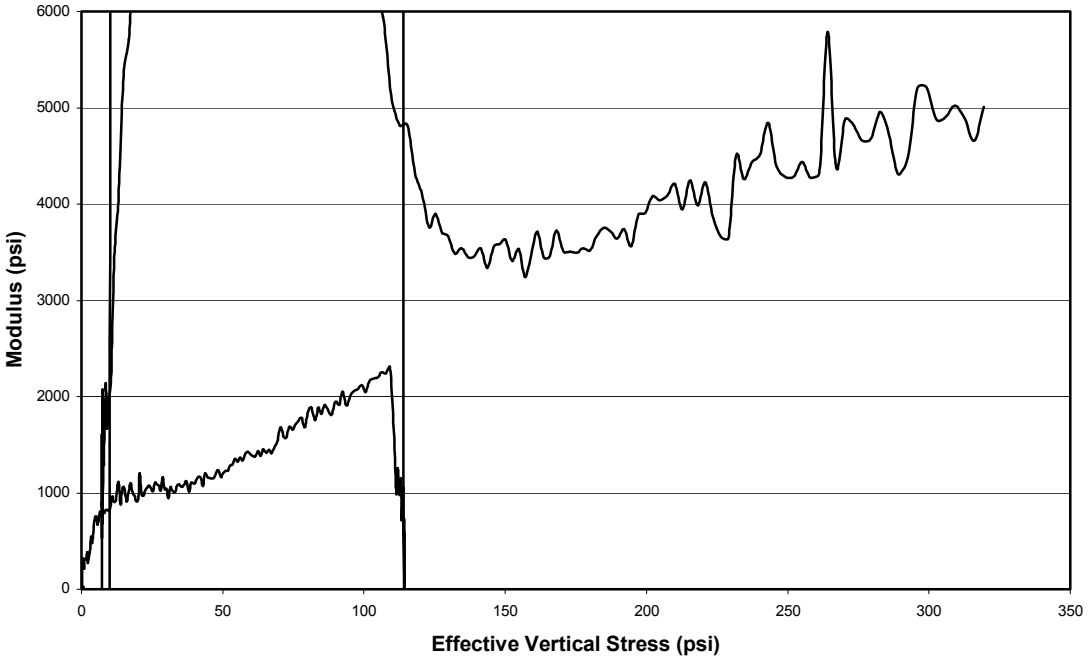


Figure E.18 Curve of modulus vs. effective vertical stress for a shelby tube, hollow stem auger sample at 24.5-26.5 feet.

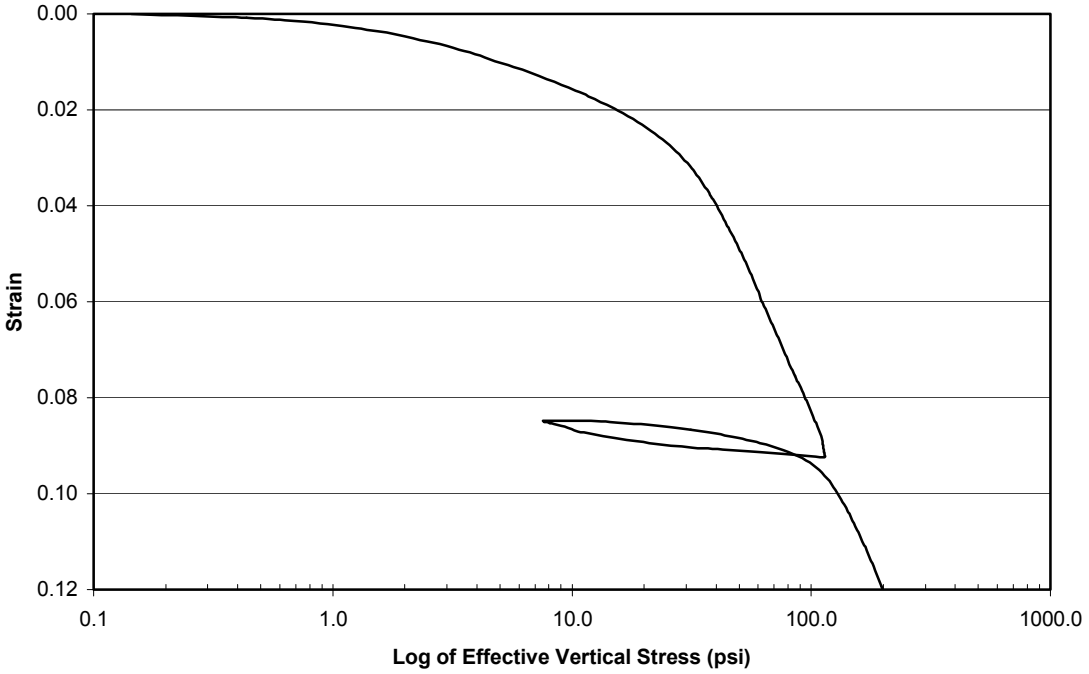


Figure E.19 Curve of strain vs. the log of effective vertical stress for a shelby tube, hollow stem auger sample at 27-29 feet.

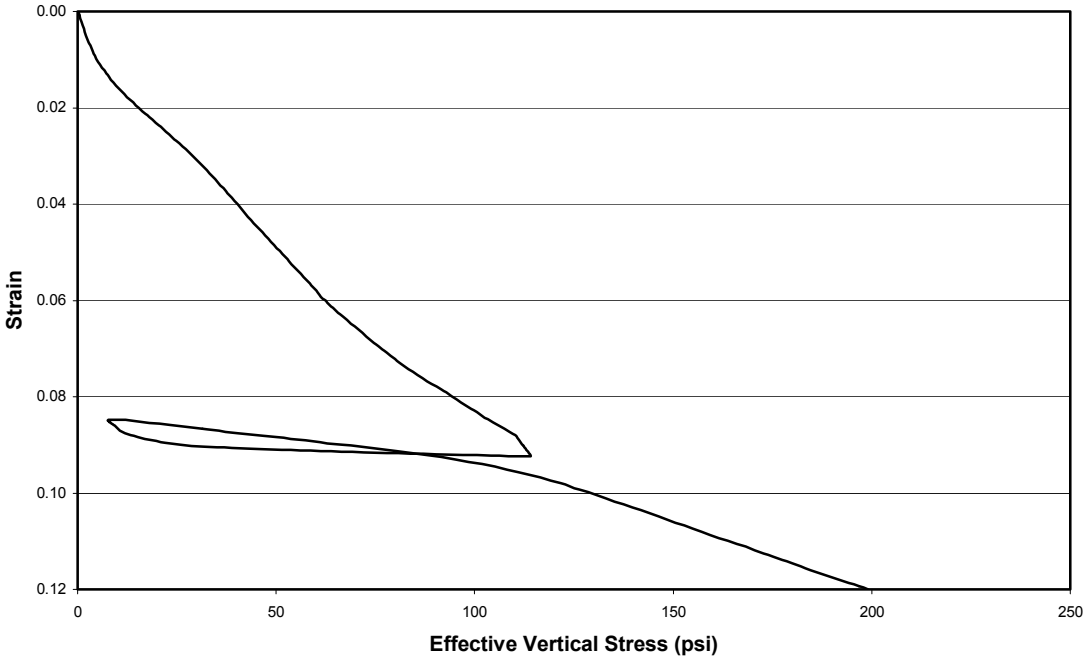


Figure E.20 Linear curve of strain vs. effective vertical stress for a shelby tube, hollow stem auger sample at 27-29 feet.

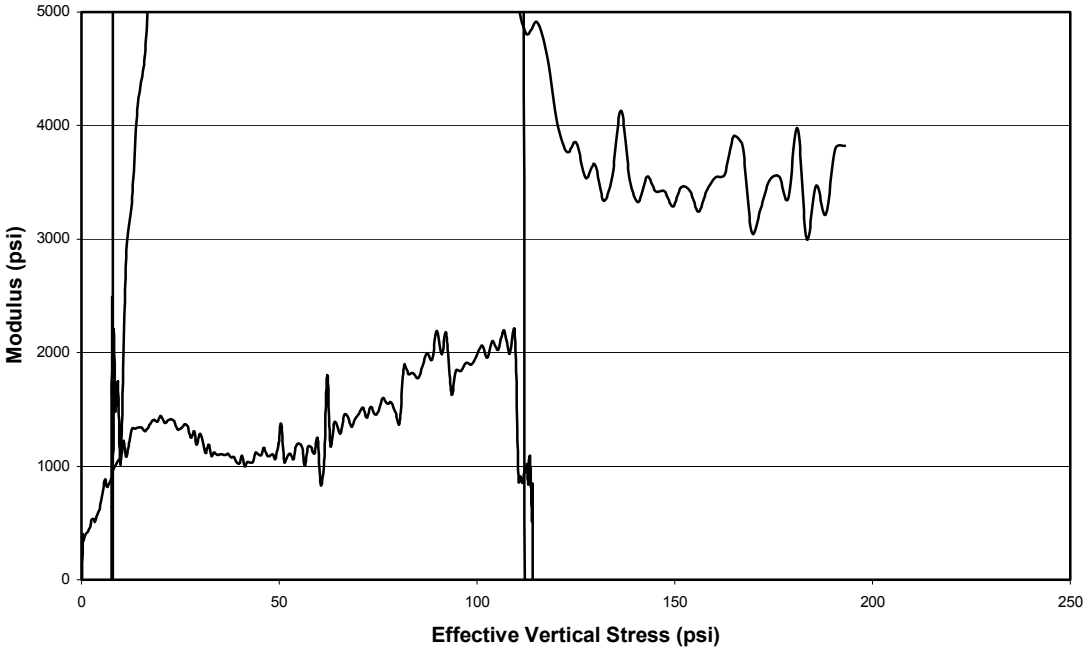


Figure E.21 Curve of modulus vs. effective vertical stress for a shelby tube, hollow stem auger sample at 27-29 feet.

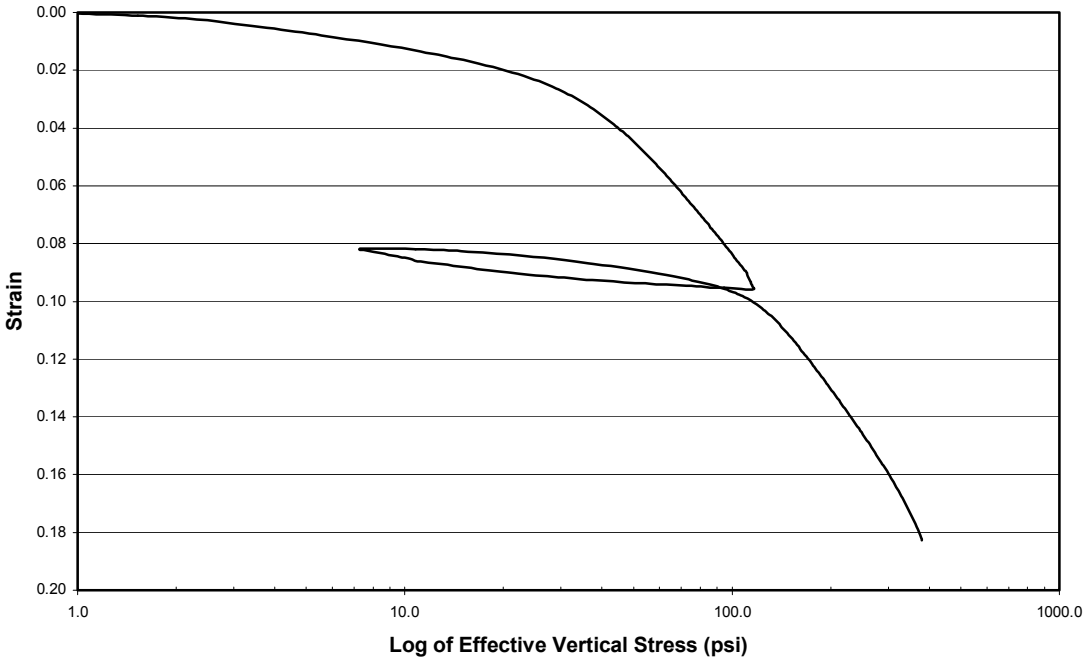


Figure E.22 Curve of strain vs. the log of effective vertical stress for a fixed-piston, hollow stem auger sample at 9.5-11.5 feet.

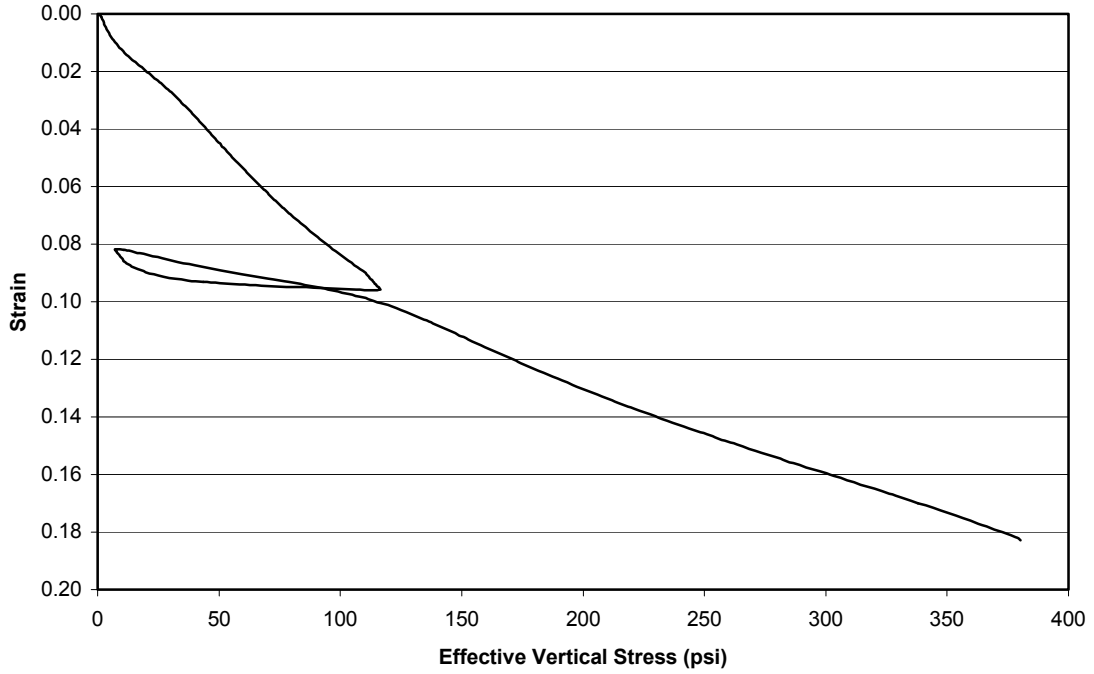


Figure E.23 Linear curve of strain vs. effective vertical stress for a fixed-piston, hollow stem auger sample at 9.5-11.5 feet.

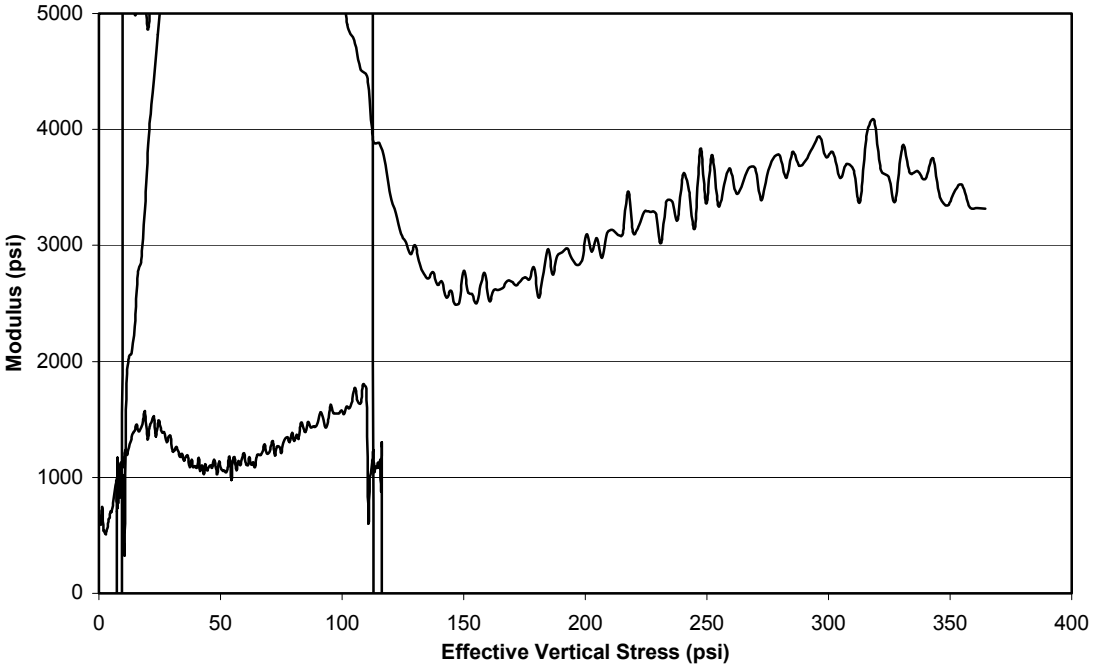


Figure E.24 Curve of modulus vs. effective vertical stress for a fixed-piston, hollow stem auger sample at 9.5-11.5 feet.

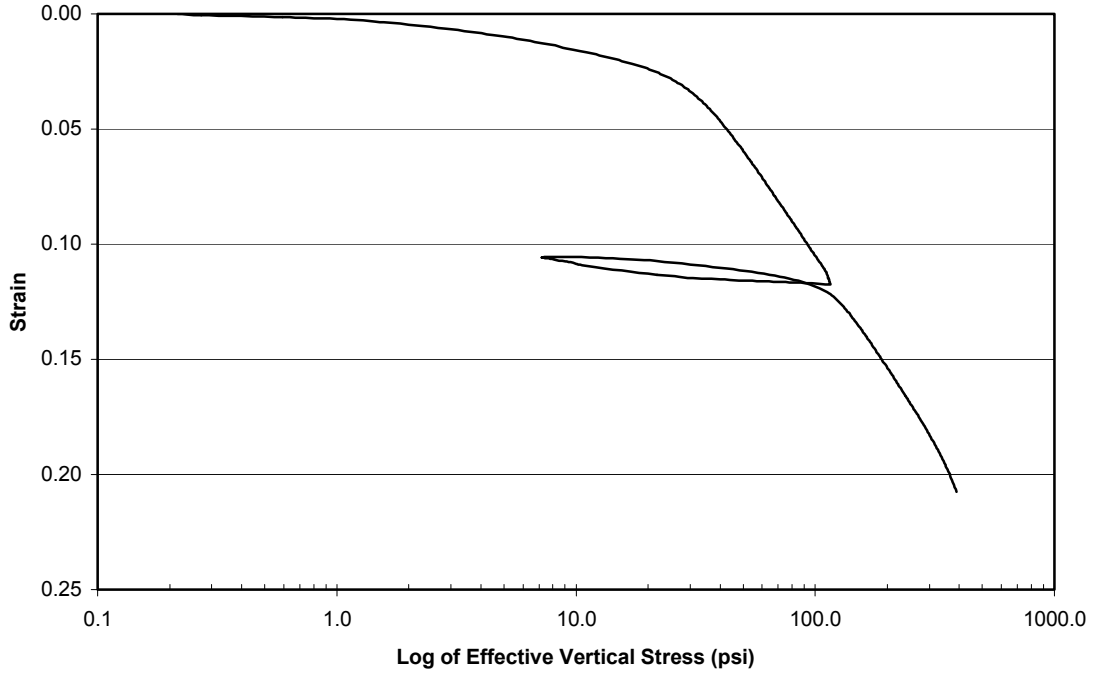


Figure E.25 Curve of strain vs. the log of effective vertical stress for a fixed-piston, hollow stem auger sample at 12-14 feet.

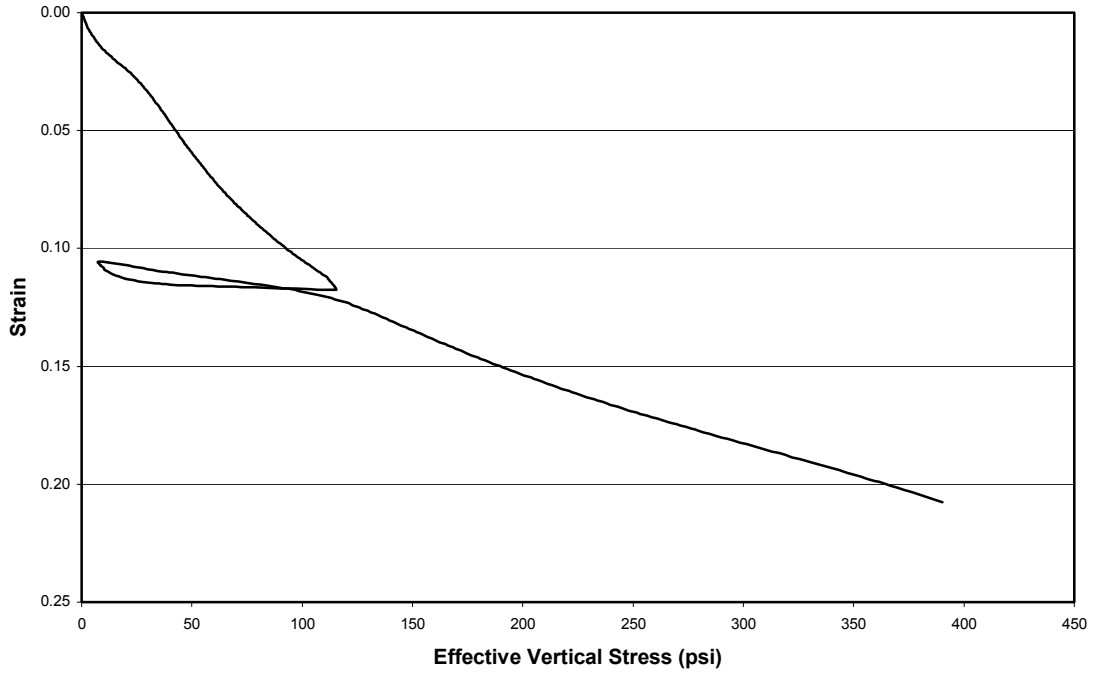


Figure E.26 Linear curve of strain vs. effective vertical stress for a fixed-piston, hollow stem auger sample at 12-14 feet.

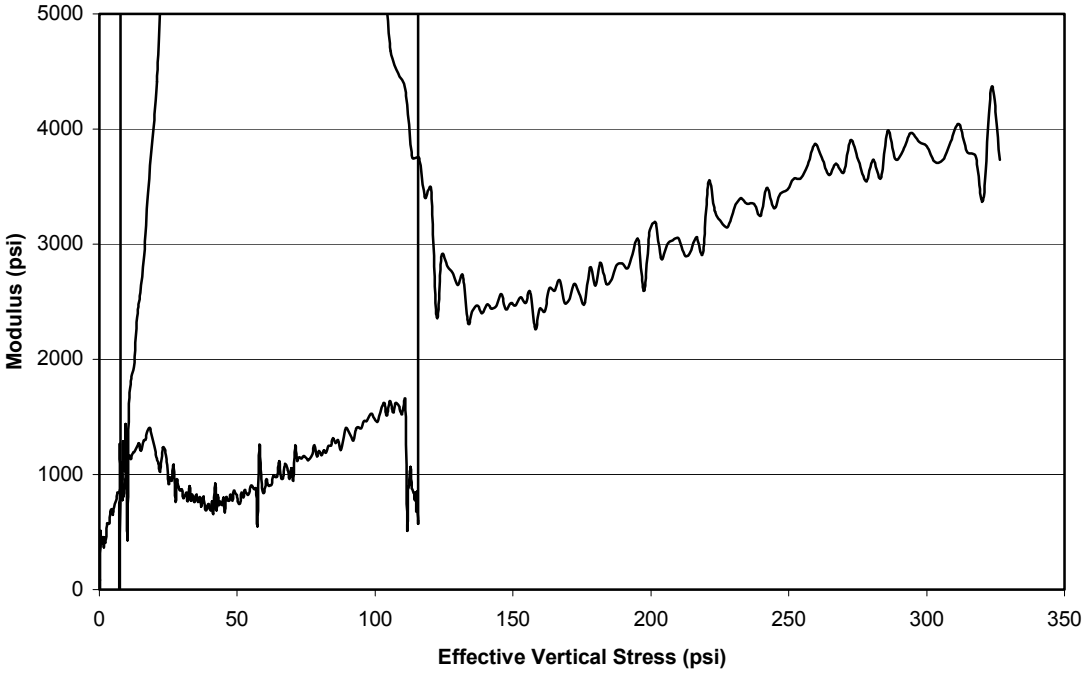


Figure E.27 Curve of modulus vs. effective vertical stress for a fixed-piston, hollow stem auger sample at 12-14 feet.

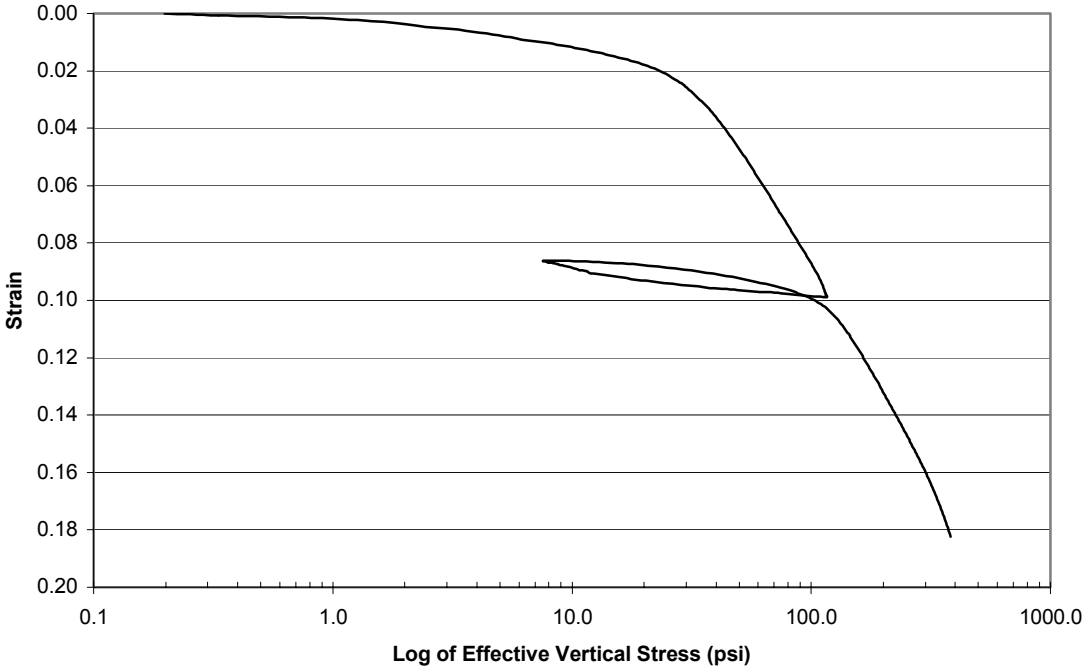


Figure E.28 Curve of strain vs. the log of effective vertical stress for a fixed-piston, hollow stem auger sample at 14.5-16.5 feet.

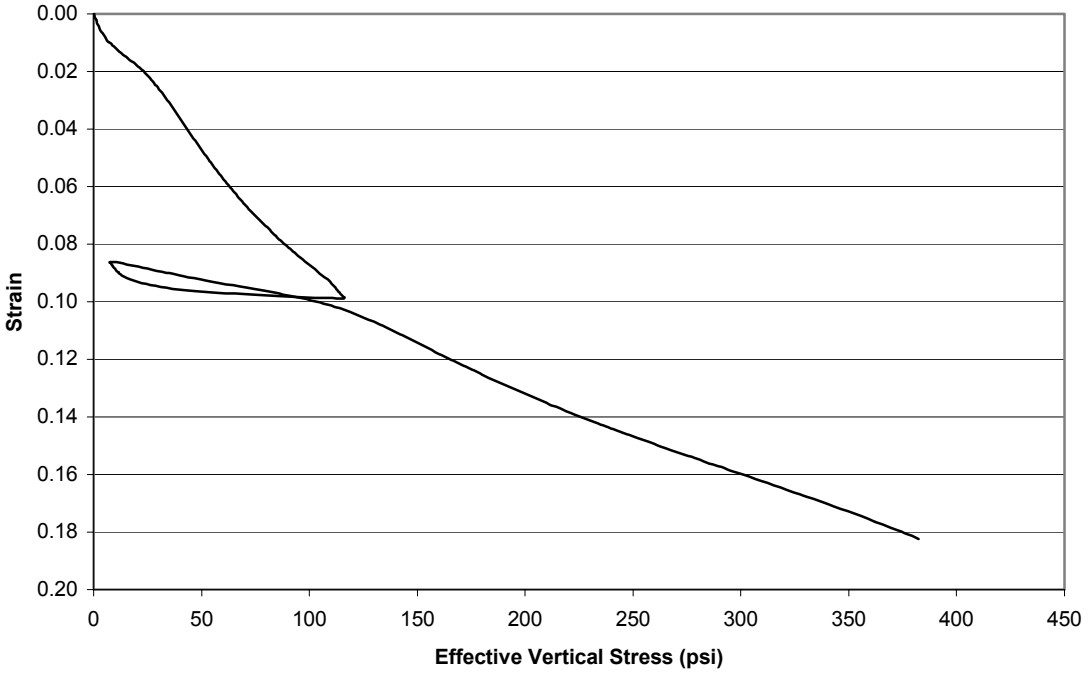


Figure E.29 Linear curve of strain vs. effective vertical stress for a fixed-piston, hollow stem auger sample at 14.5-16.5 feet.

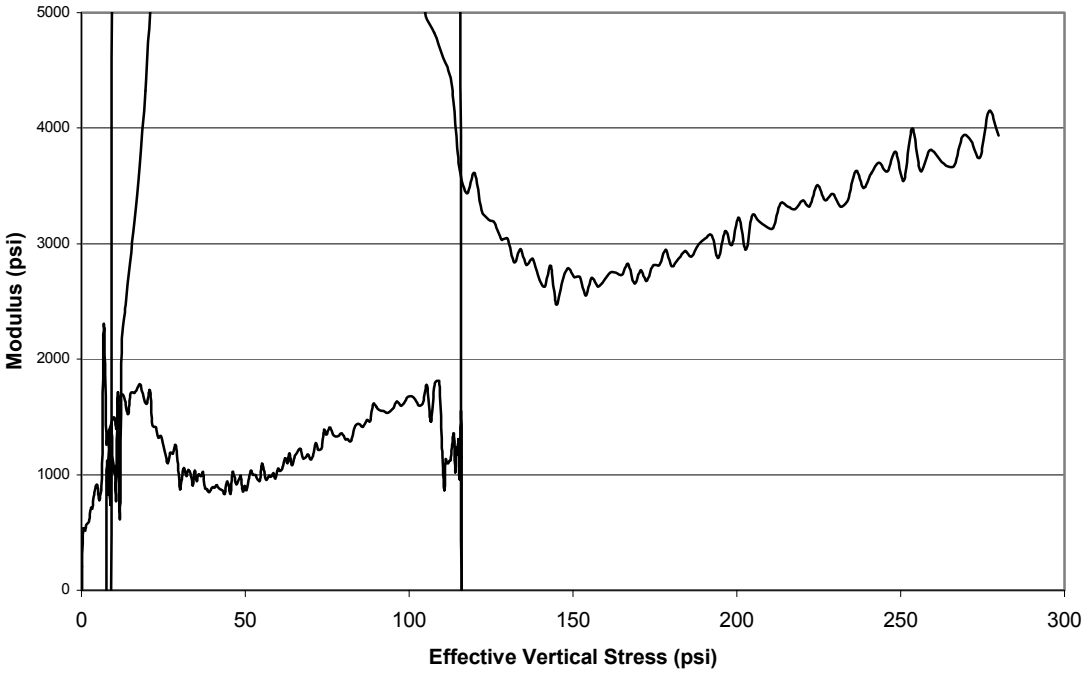


Figure E.30 Curve of modulus vs. effective vertical stress for a fixed-piston, hollow stem auger sample at 14.5-16.5 feet.

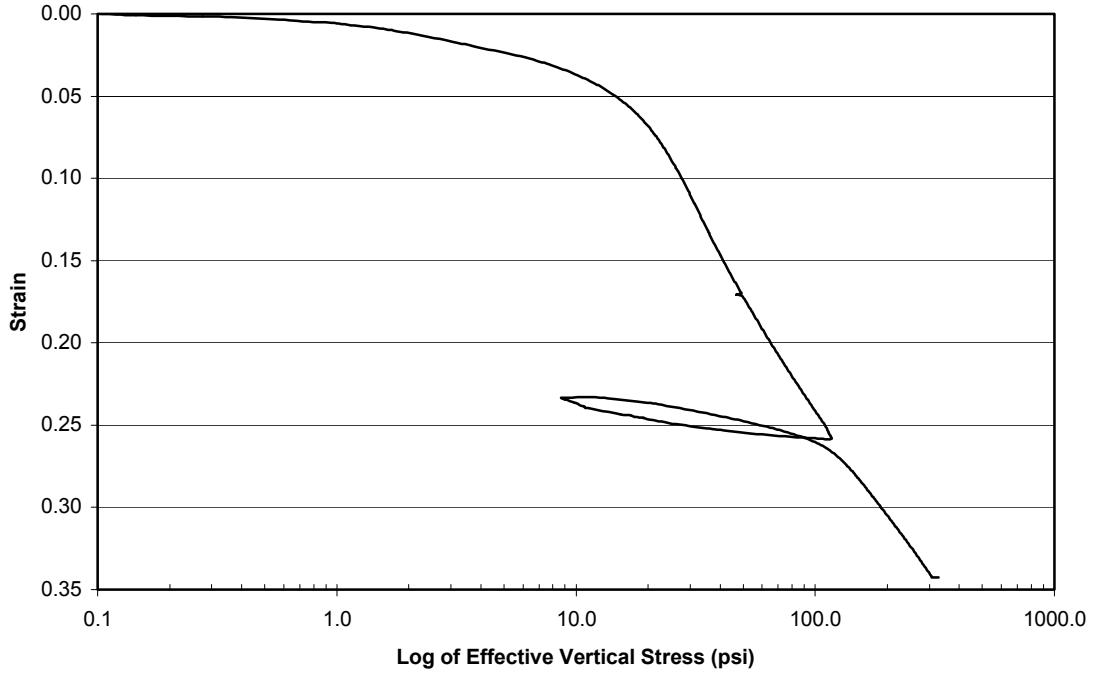


Figure E.31 Curve of strain vs. the log of effective vertical stress for a free-piston, hollow stem auger sample at 17-19 feet.

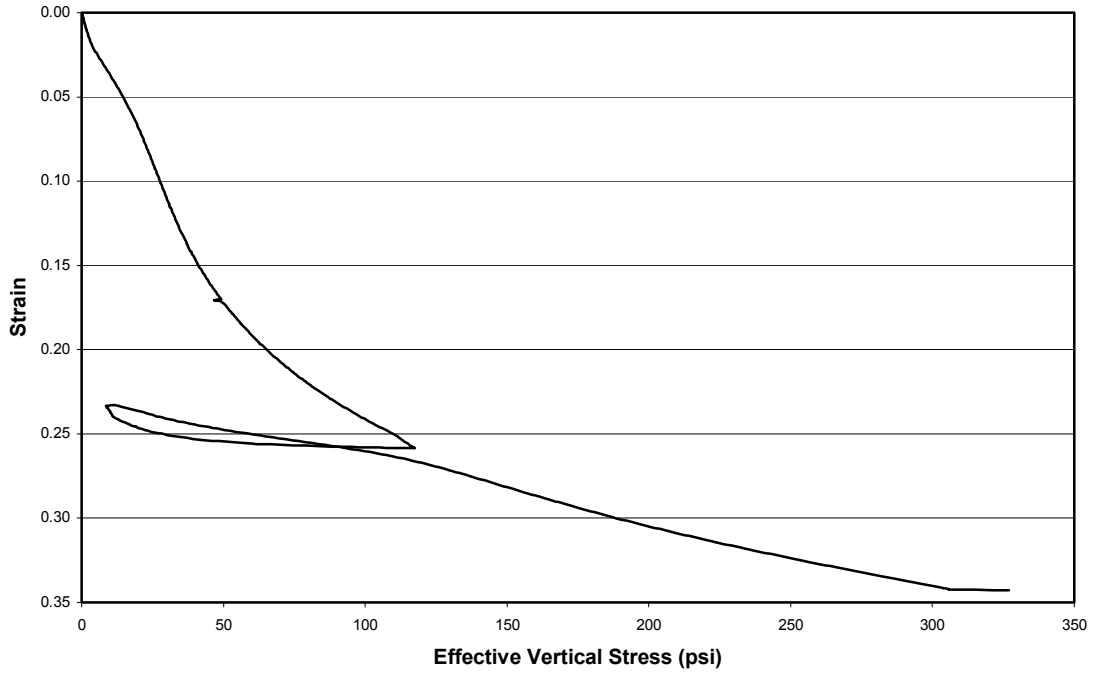


Figure E.32 Linear curve of strain vs. effective vertical stress for a free-piston, hollow stem auger sample at 17-19 feet.

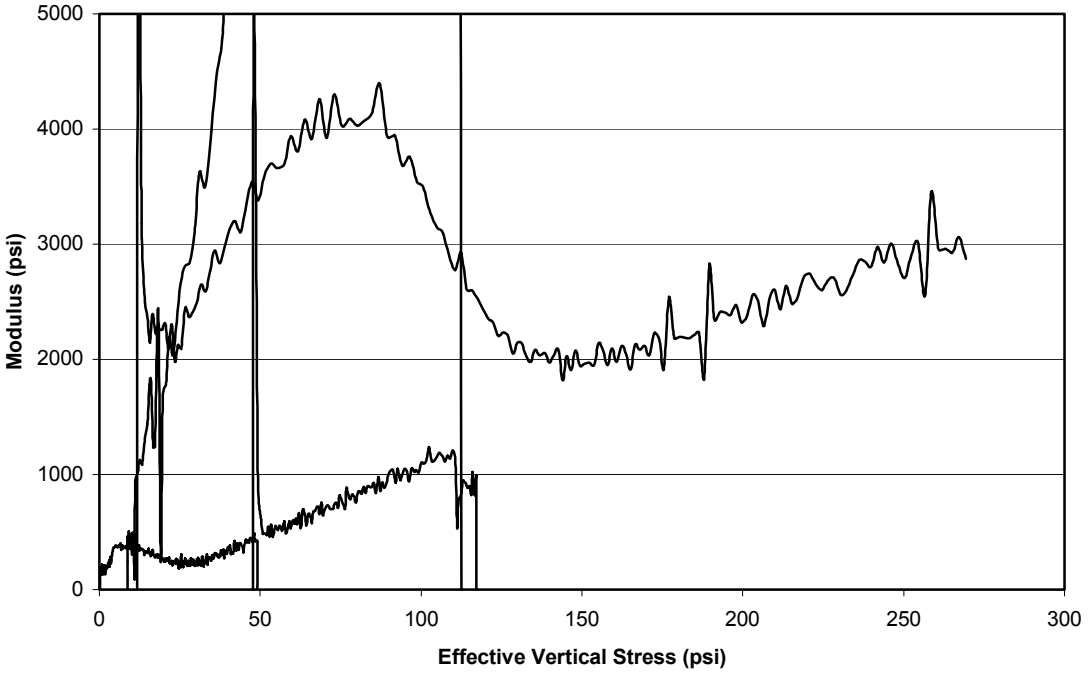


Figure E.33 Curve of modulus vs. effective vertical stress for a free-piston, hollow stem auger sample at 17-19 feet.

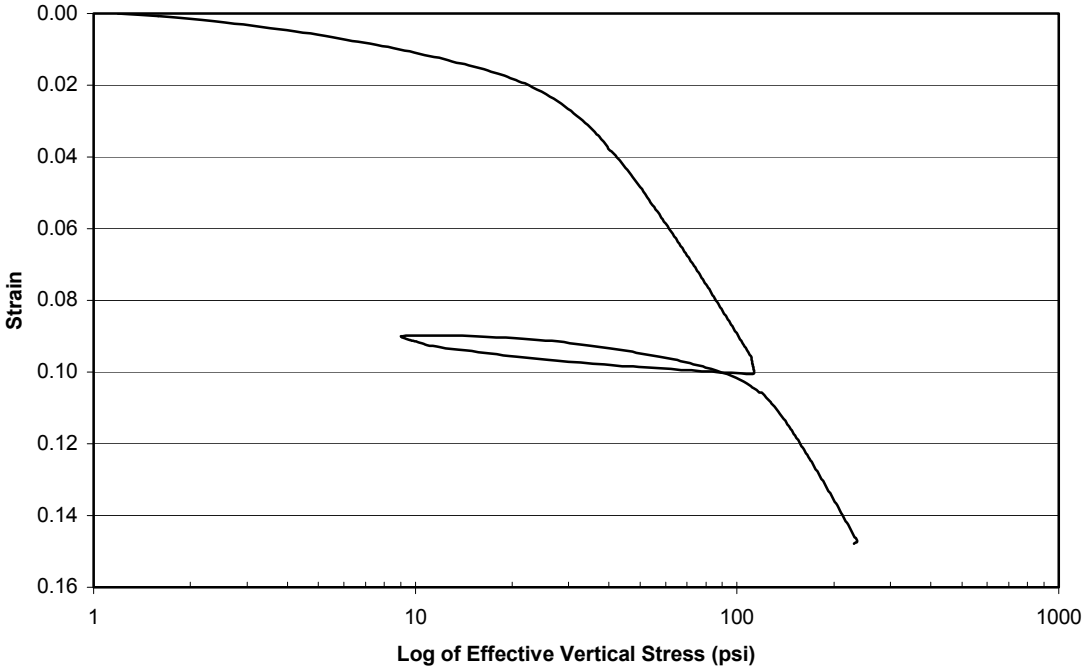


Figure E.34 Curve of strain vs. the log of effective vertical stress for a shelby tube, rotary wash sample at 12-14 feet.

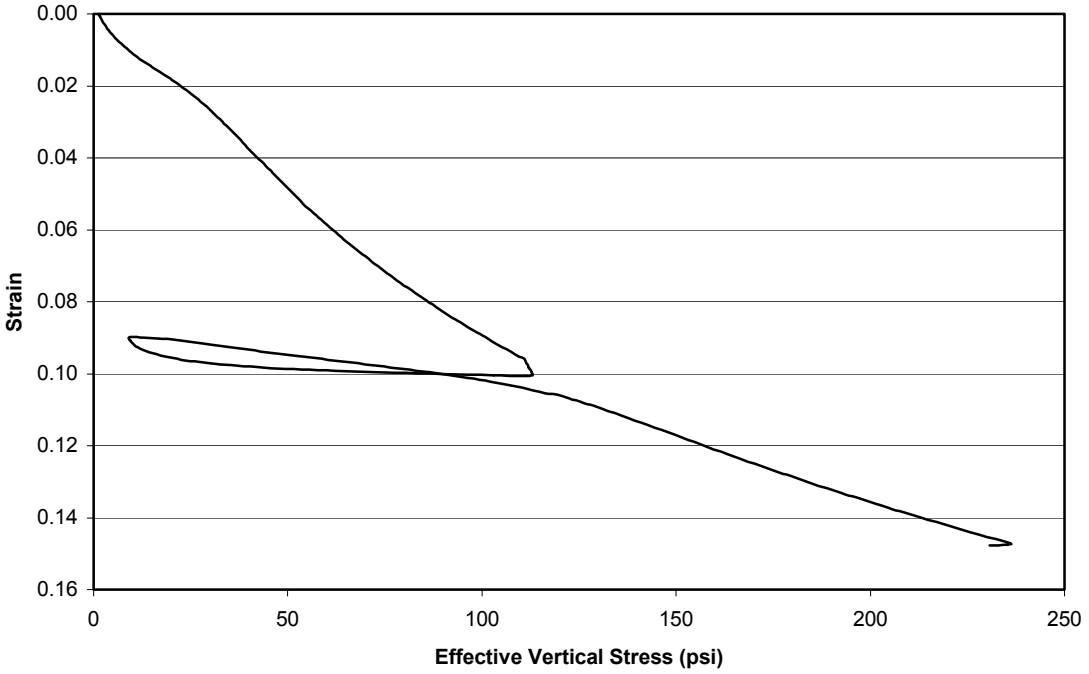


Figure E.35 Linear curve of strain vs. effective vertical stress for a shelby tube, rotary wash sample at 12-14 feet.

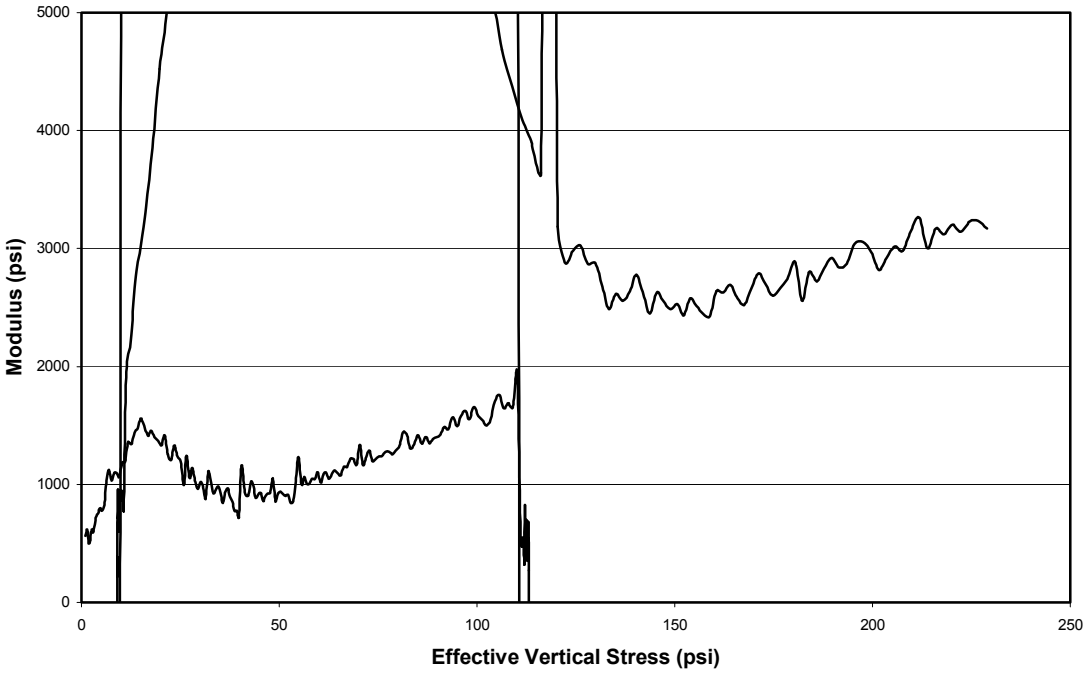


Figure E.36 Curve of modulus vs. effective vertical stress for a shelby tube, rotary wash sample at 12-14 feet.

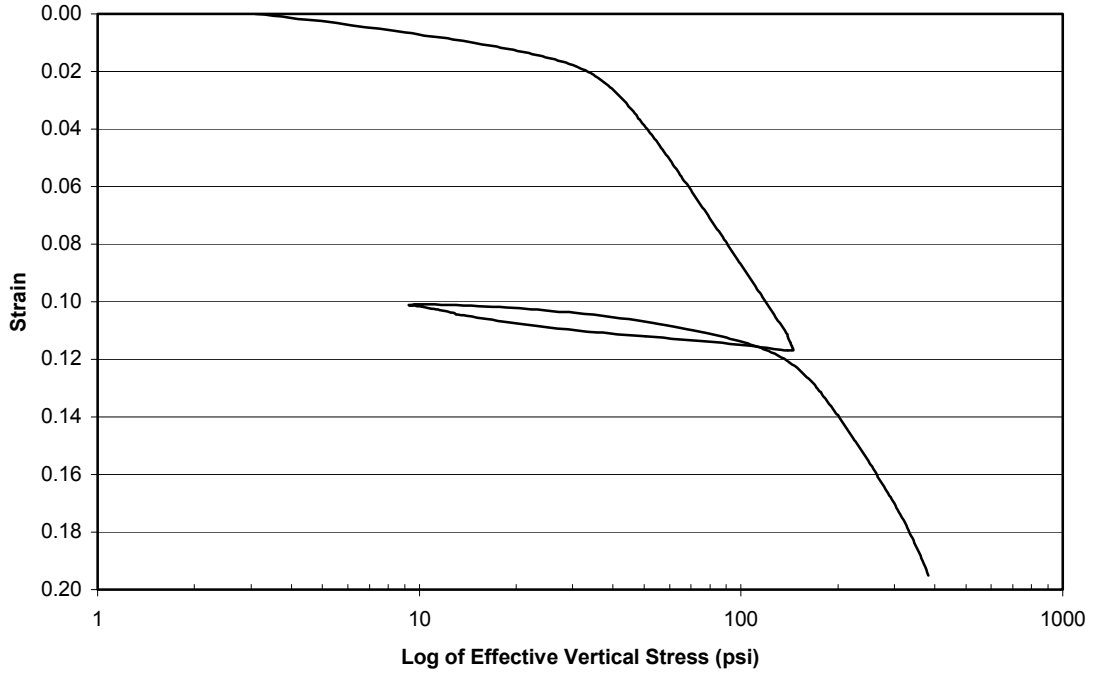


Figure E.37 Curve of strain vs. the log of effective vertical stress for a shelby tube, rotary wash sample at 14.5-16.5 feet.

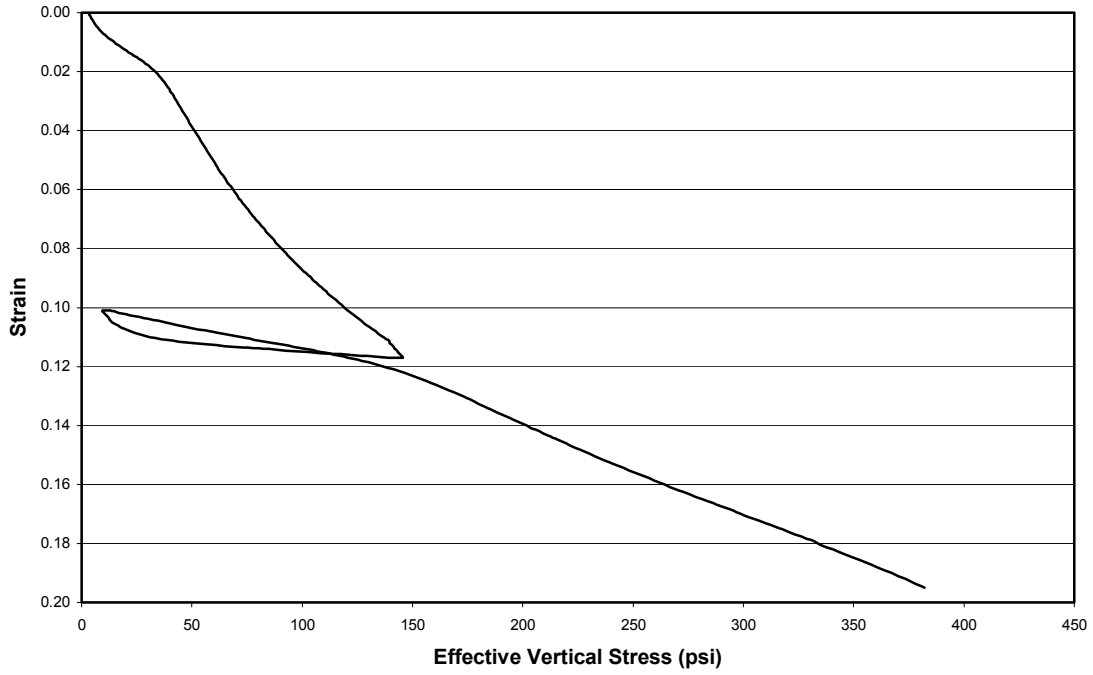


Figure E.38 Linear curve of strain vs. effective stress for a shelby tube, rotary wash sample at 14.5-16.5 feet.

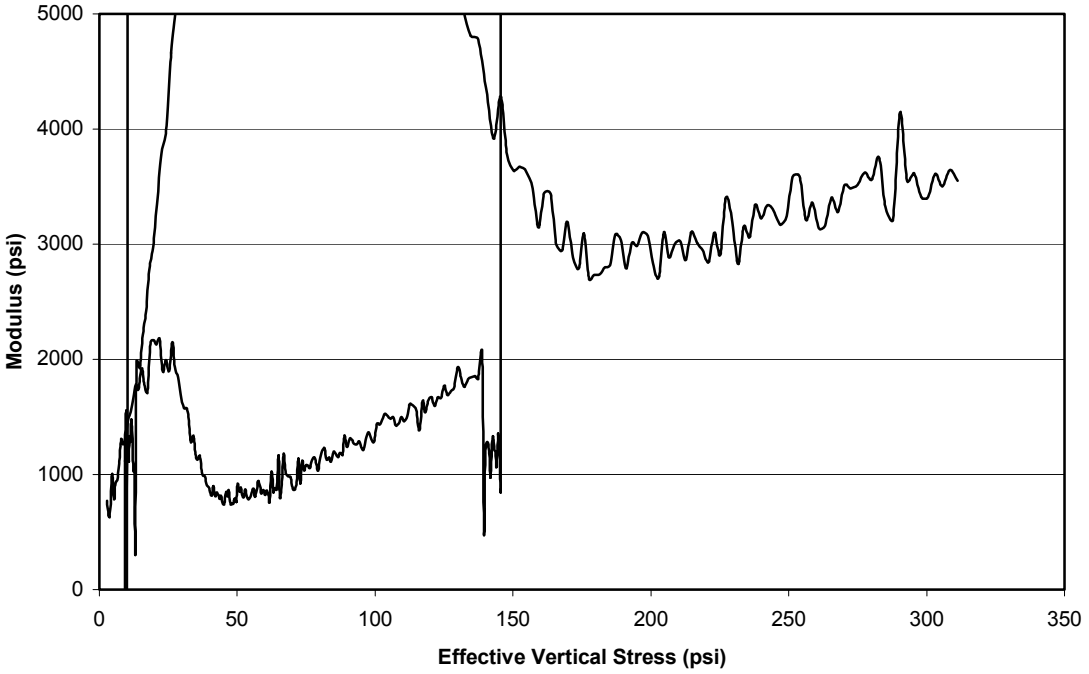


Figure E.39 Curve of modulus vs. effective vertical stress for a shelby tube, rotary wash sample at 14.5-16.5 feet.

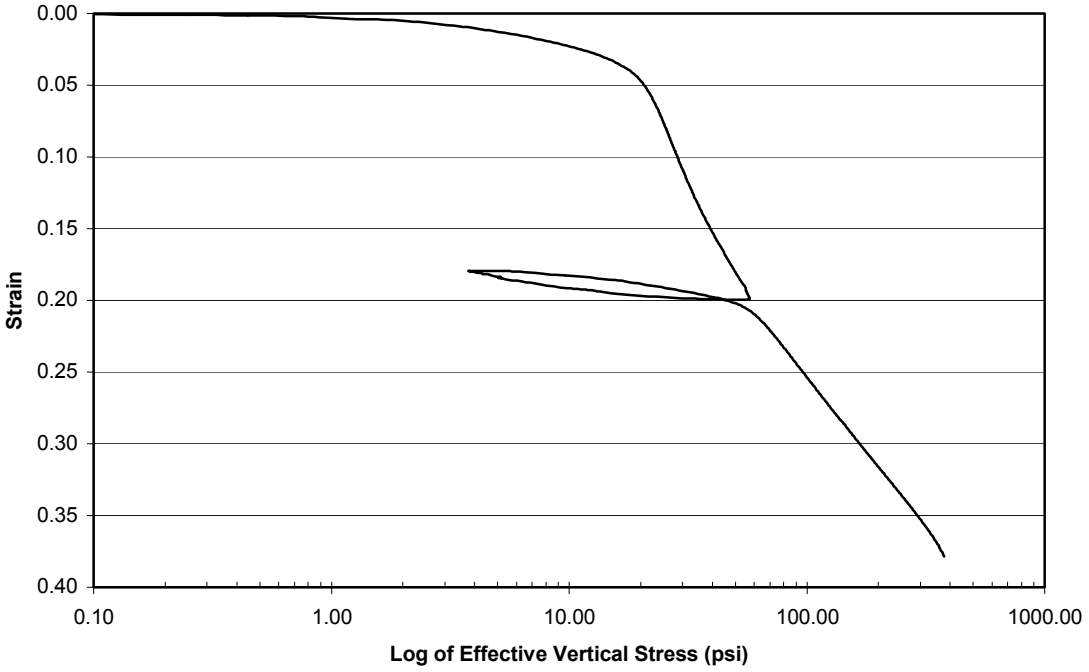


Figure E.40 Curve of strain vs. the log of effective vertical stress for a shelby tube, rotary wash sample at 17-19 feet.

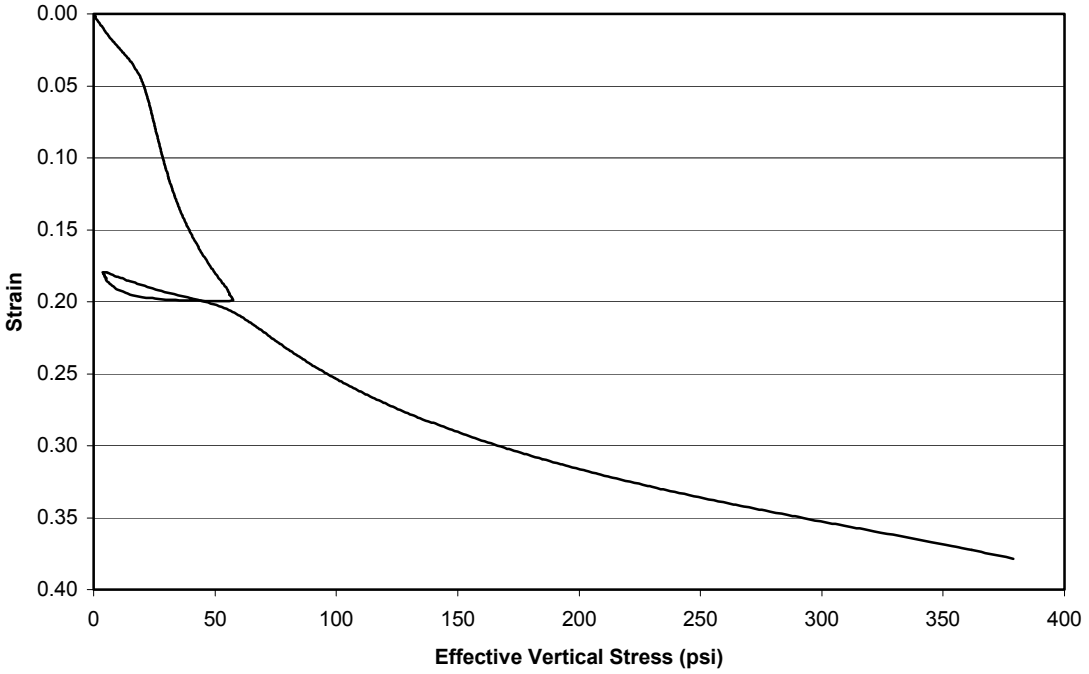


Figure E.41 Linear curve of strain vs. effective vertical stress for a shelby tube, rotary wash sample at 17-19 feet.

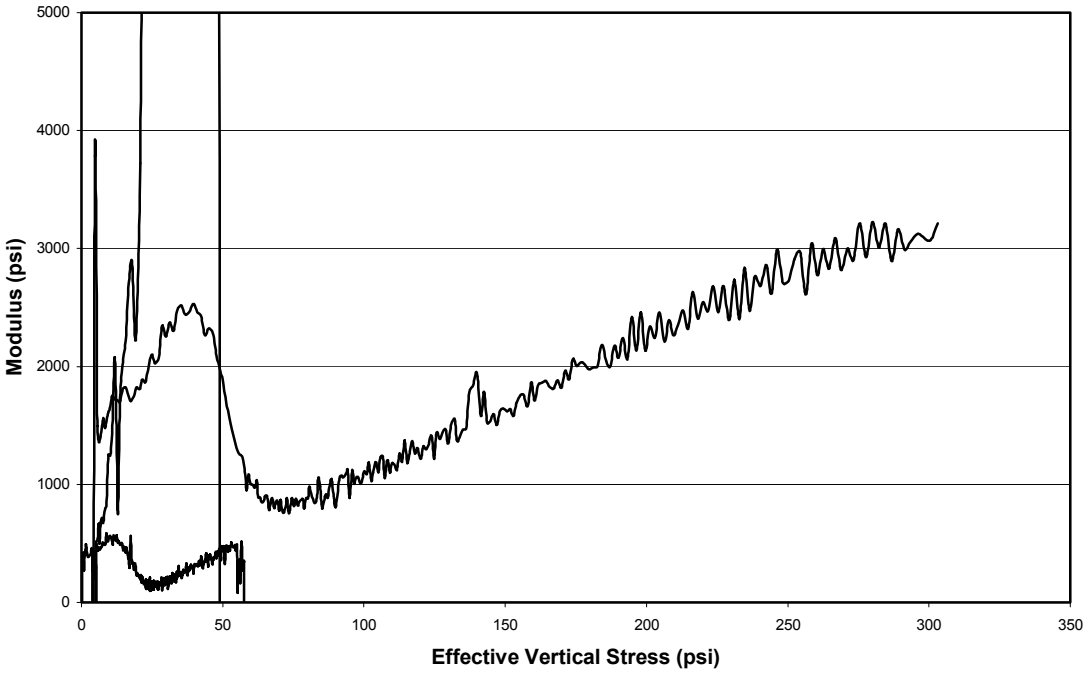


Figure E.42 Curve of modulus vs. effective vertical stress for a shelby tube, rotary wash sample at 17-19 feet.

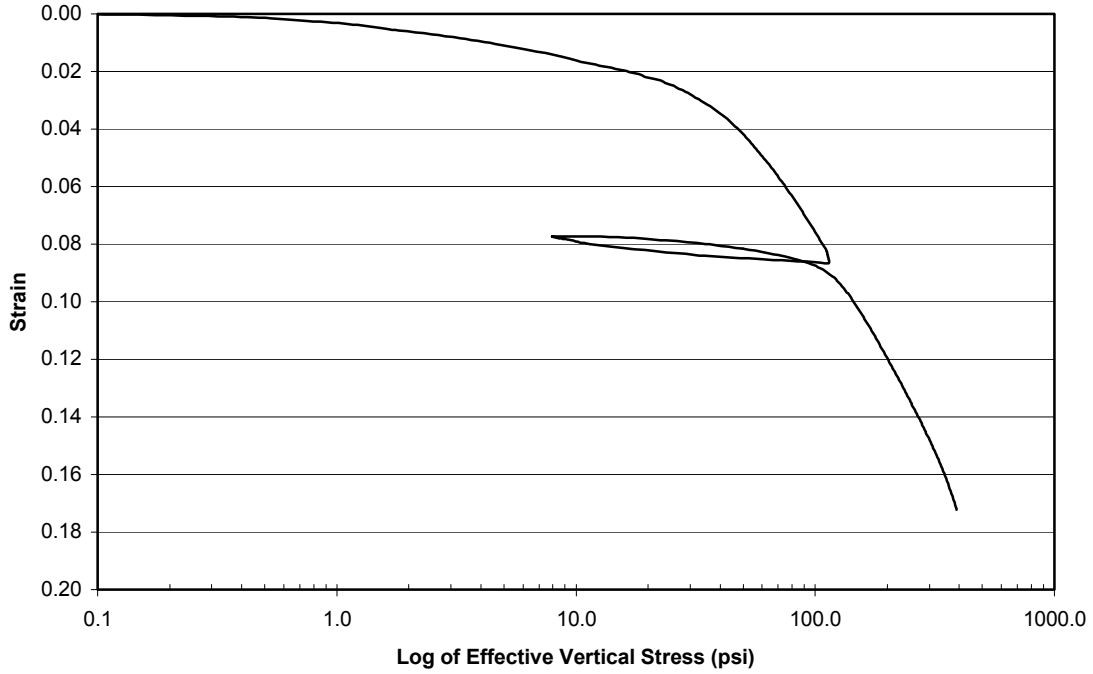


Figure E.43 Curve of strain vs. the log of effective vertical stress for a fixed-piston, rotary wash sample at 12-14 feet.

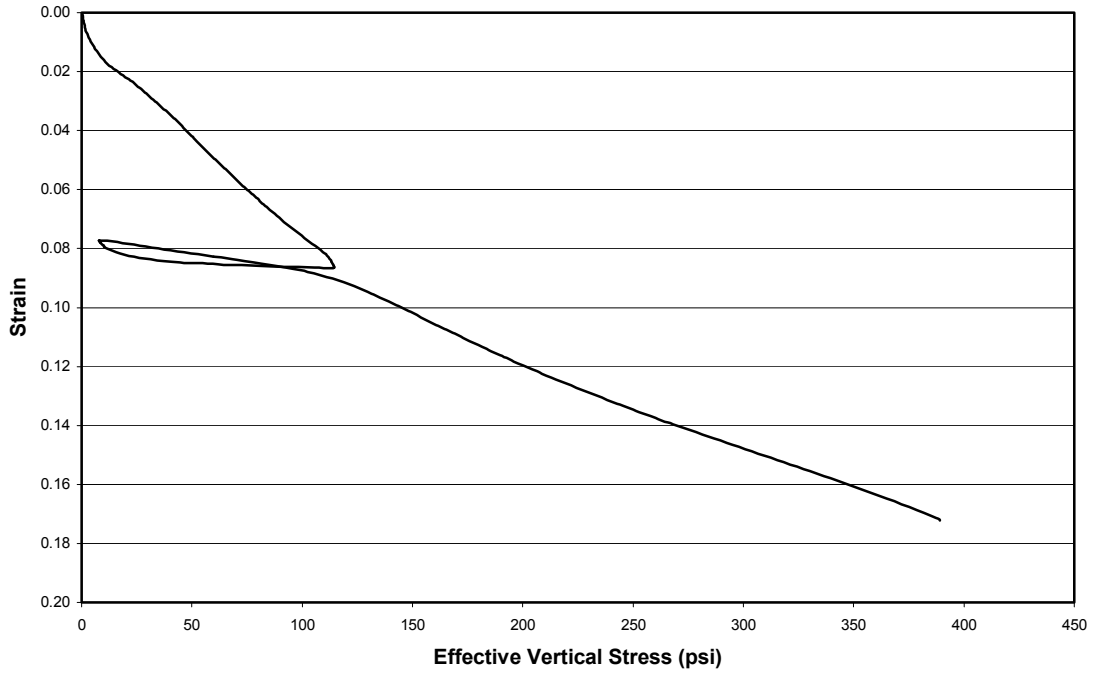


Figure E.44 Linear curve of strain vs. effective vertical stress for a fixed-piston, rotary wash sample at 12-14 feet.

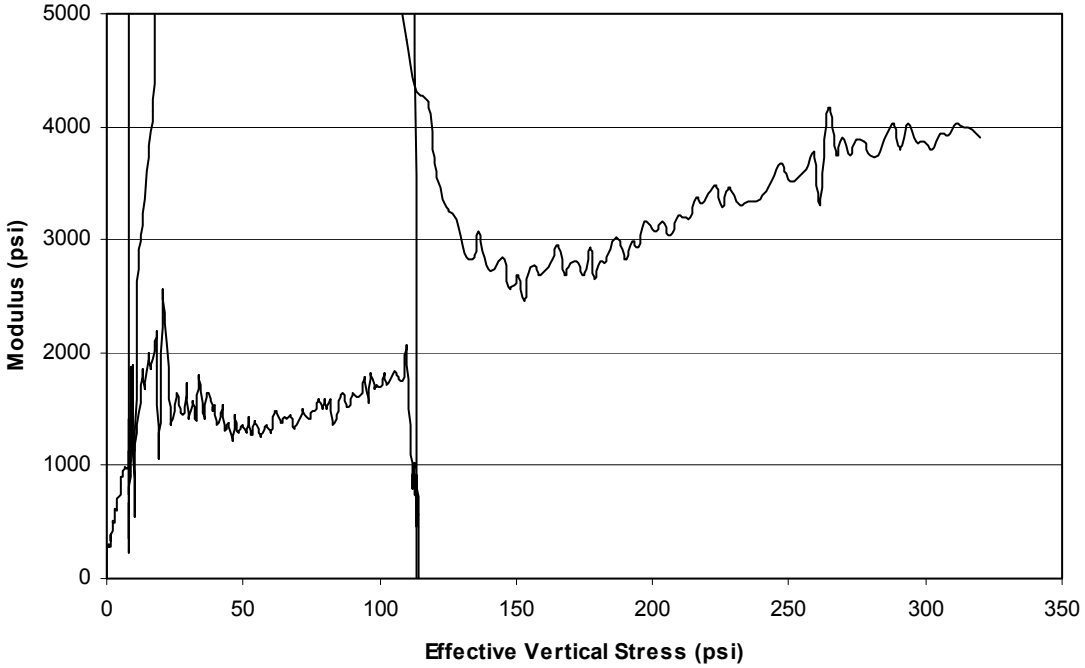


Figure E.45 Curve of modulus vs. effective vertical stress for a fixed-piston, rotary wash sample at 12-14 feet.

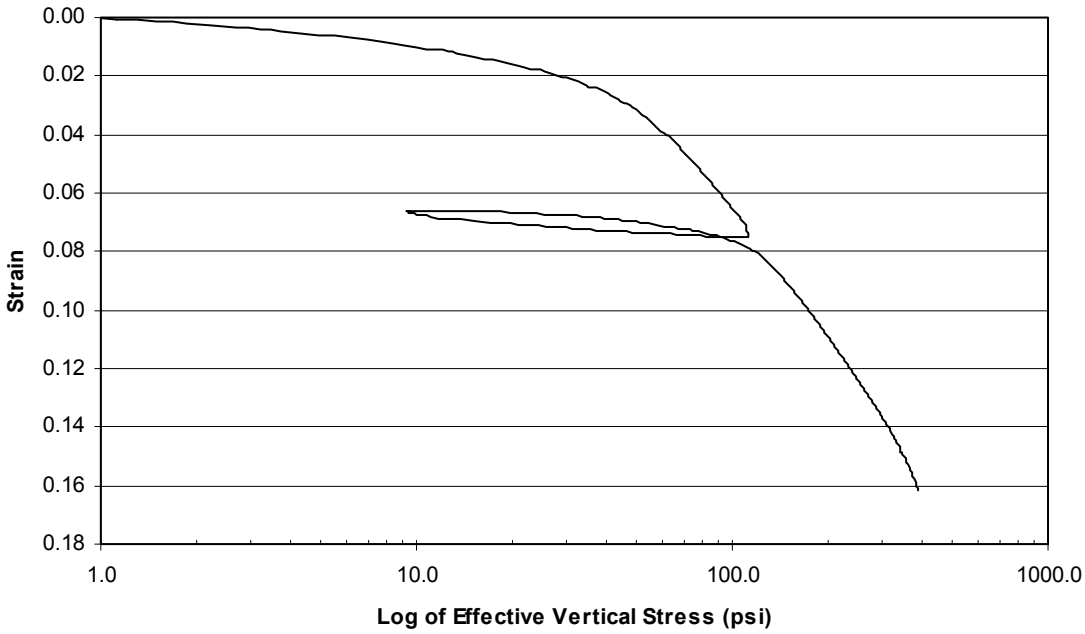


Figure E.46 Curve of strain vs. the log of effective vertical stress for a fixed-piston, rotary wash sample at 14.5-16.5 feet.

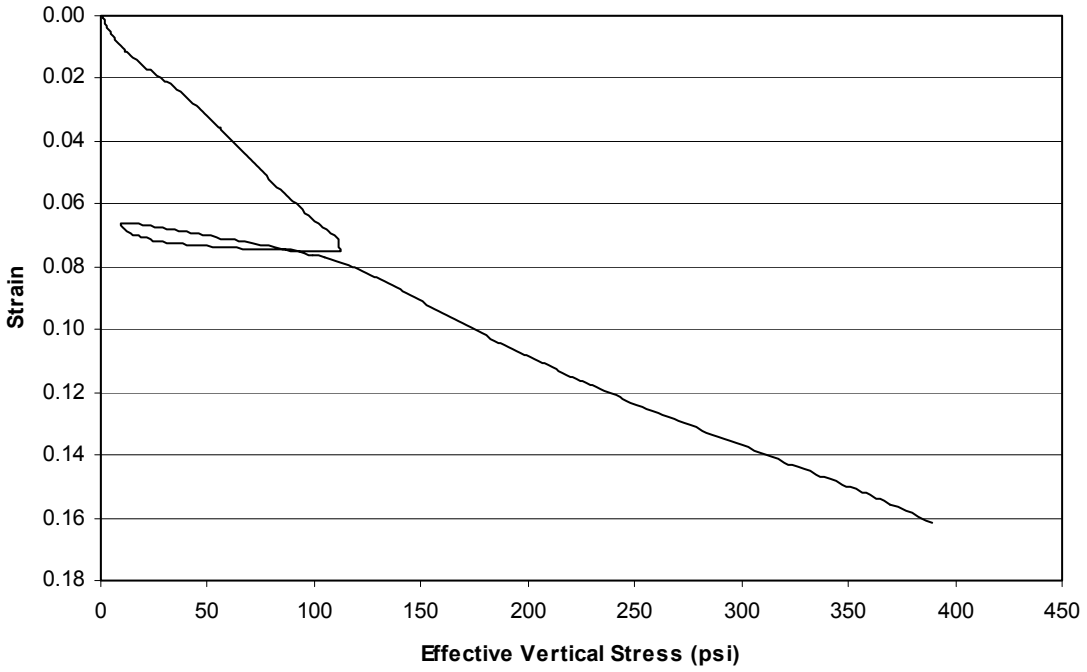


Figure E.47 Linear curve of strain vs. effective vertical stress for a fixed-piston, rotary wash sample at 14.5-16.5 feet.

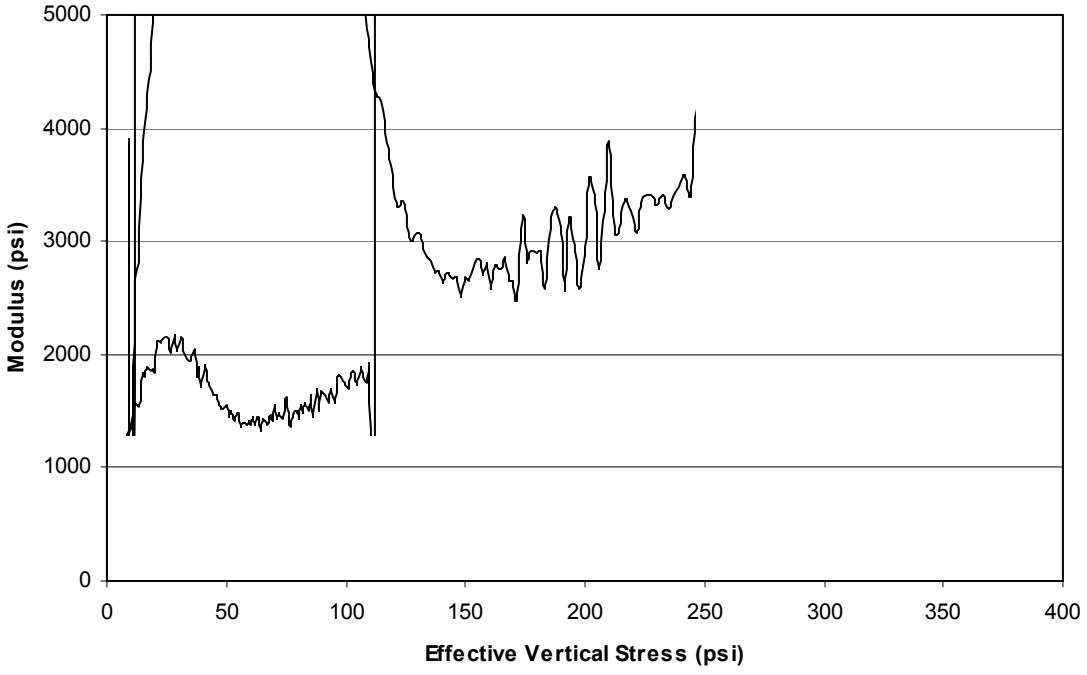


Figure E.48 Curve of modulus vs. effective vertical stress for a fixed-piston, rotary wash sample at 14.5-16.5 feet.

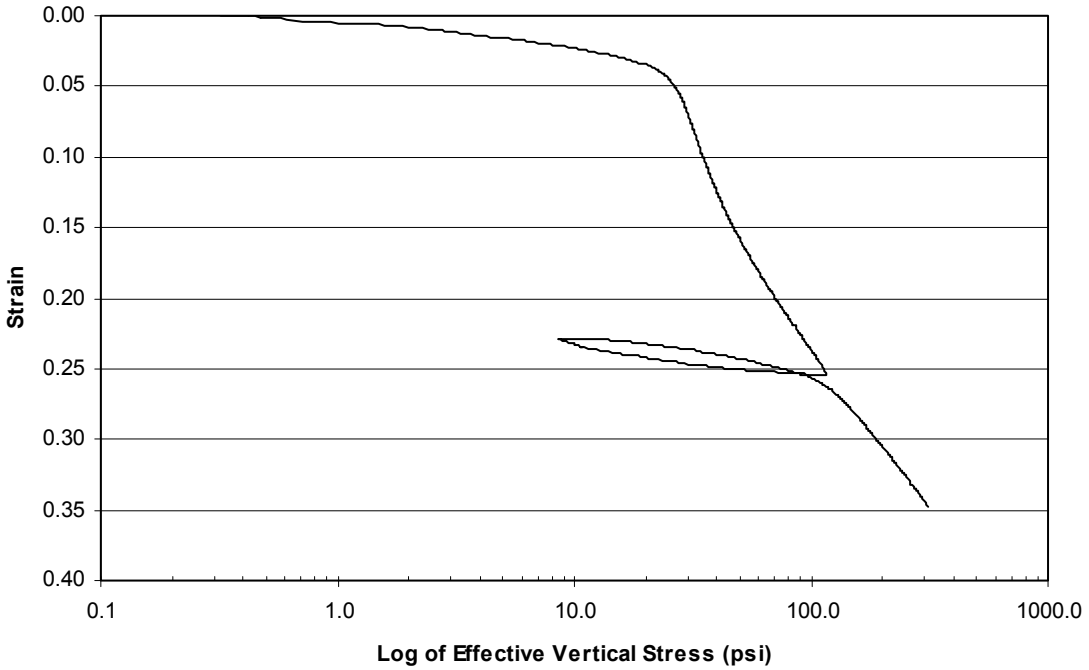


Figure E.49 Curve of strain vs. the log of effective vertical stress for a fixed-piston, rotary wash sample at 17-19 feet.

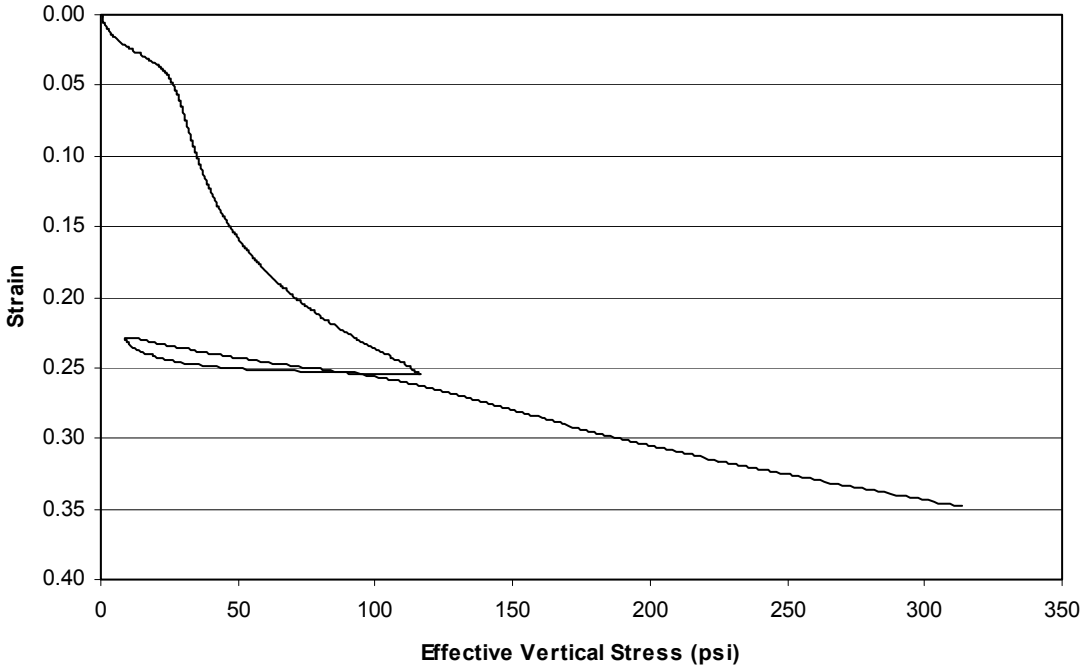


Figure E.50 Linear curve of strain vs. effective vertical stress for a fixed-piston, rotary wash sample at 17-19 feet.

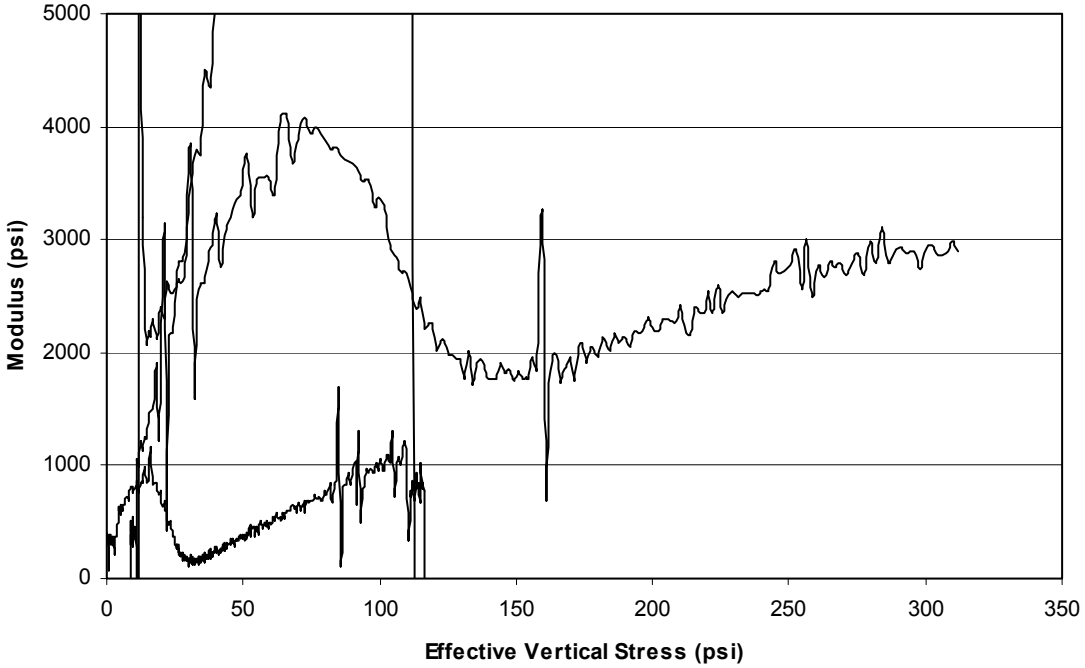


Figure E.51 Curve of modulus vs. effective vertical stress for a fixed-piston, rotary wash sample at 17-19 feet.

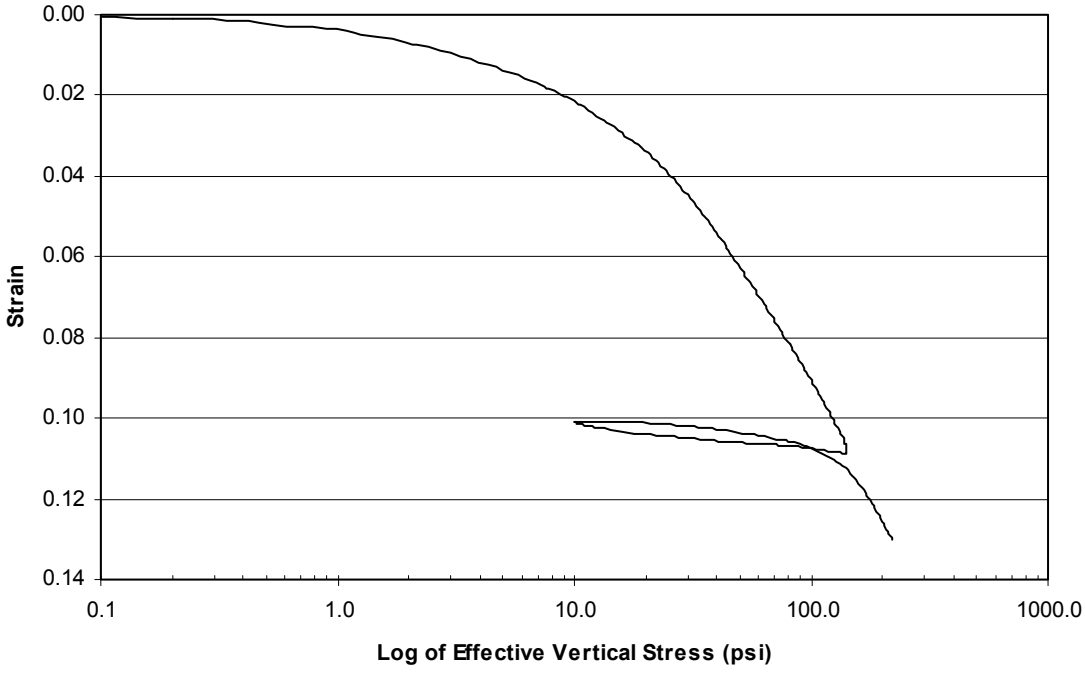


Figure E.52 Curve of strain vs. the log of effective vertical stress for a fixed-piston, rotary wash sample at 22-24 feet.

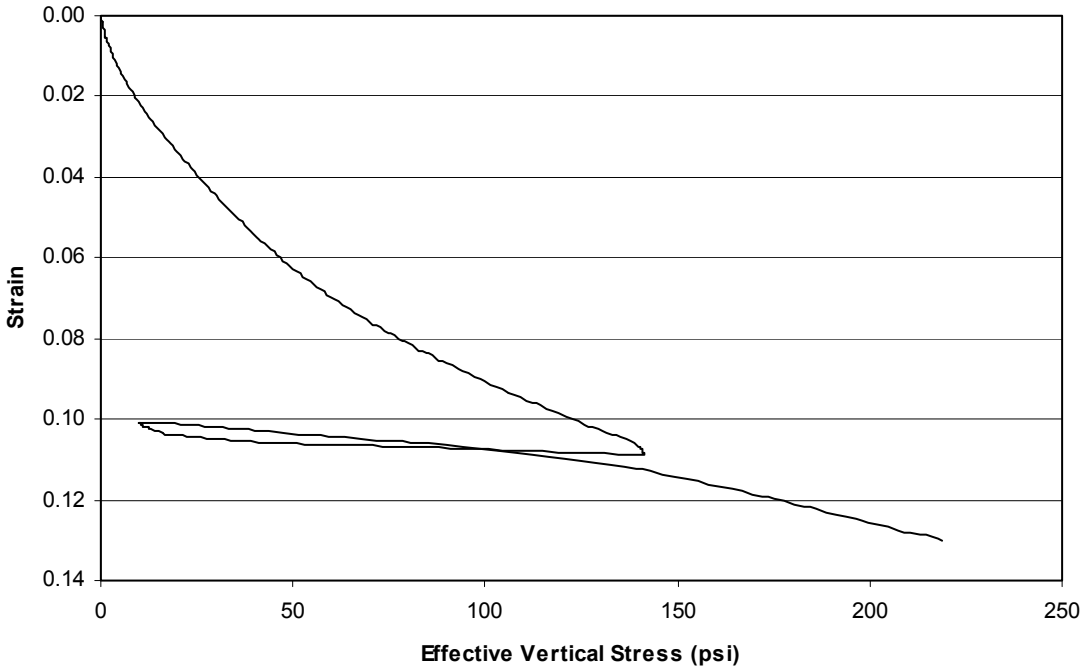


Figure E.53 Linear curve of strain vs. effective vertical stress for a fixed-piston, rotary wash sample at 22-24 feet.

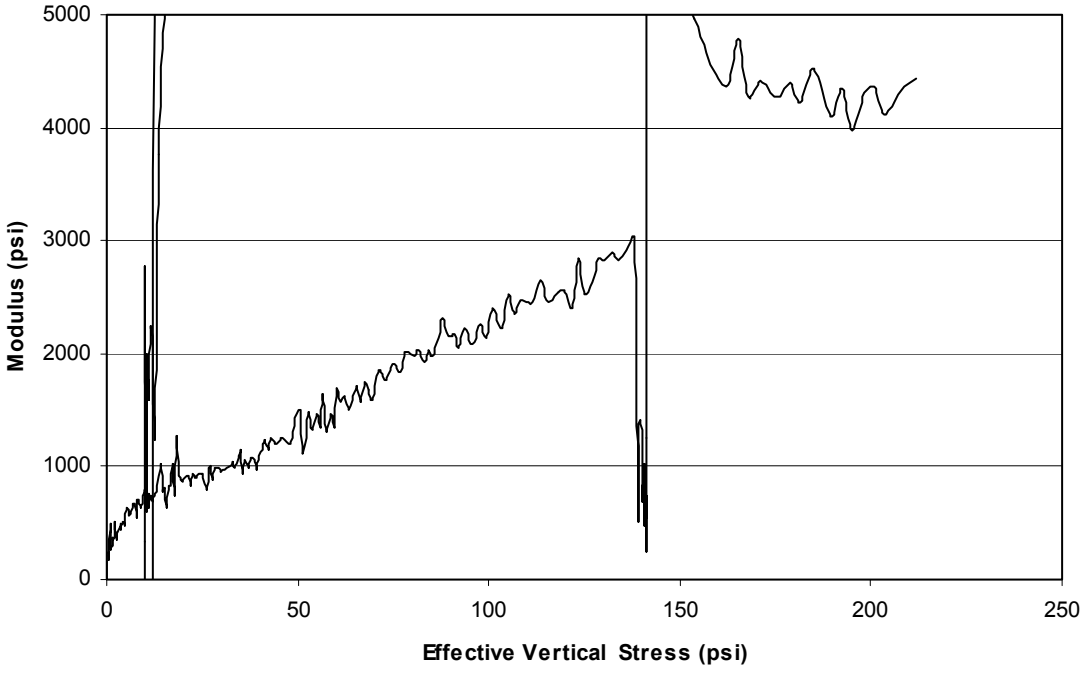


Figure E.54 Curve of modulus vs. effective vertical stress for a fixed-piston, rotary wash sample at 22-24 feet.

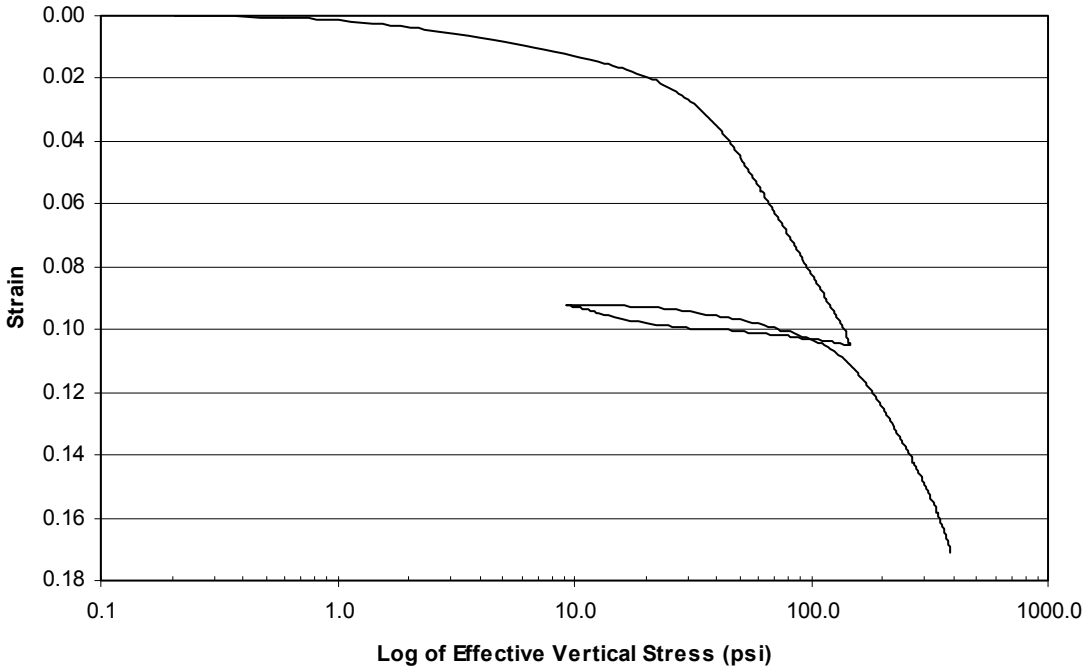


Figure E.55 Curve of strain vs. the log of effective vertical stress for a fixed-piston, rotary wash sample at 24.5-26.5 feet.

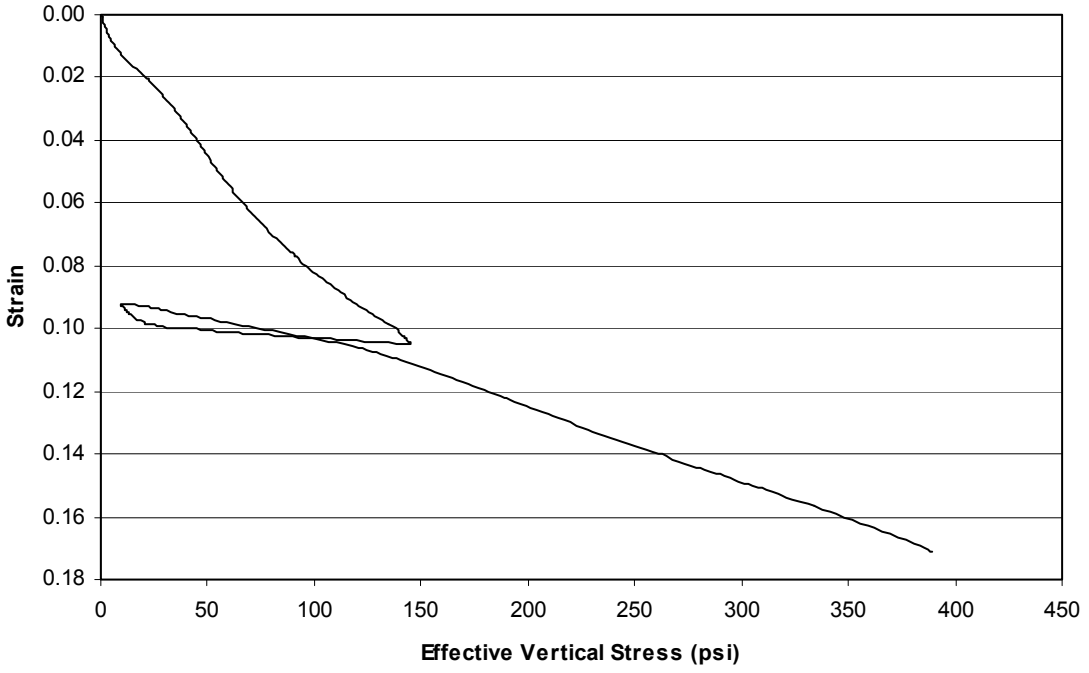


Figure E.56 Linear curve of strain vs. effective vertical stress for a fixed-piston, rotary wash sample at 24.5-26.5 feet.

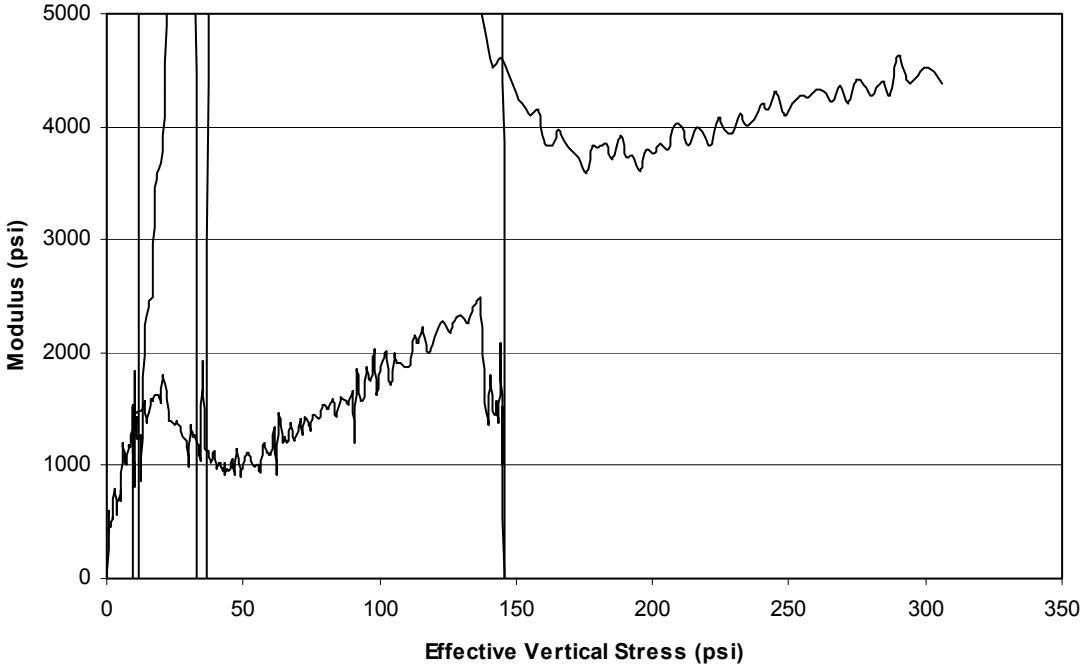


Figure E.57 Curve of modulus vs. effective vertical stress for a fixed-piston, rotary wash sample at 24.5-26.5 feet.

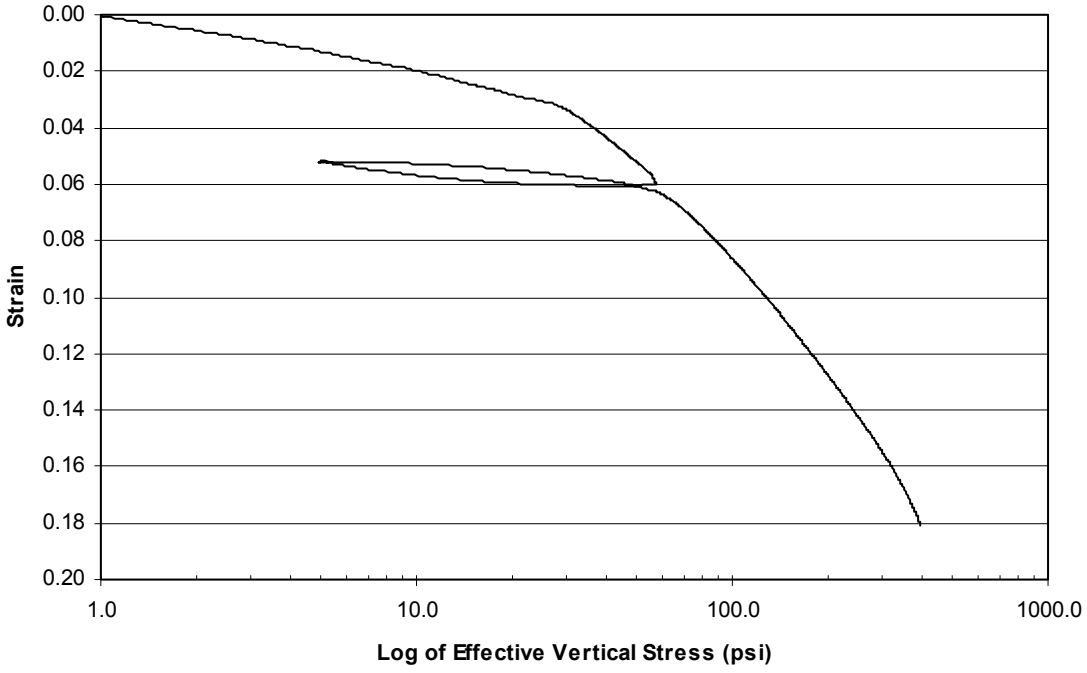


Figure E.58 Curve of strain vs. the log of effective vertical stress for a sample from boring I2 at 10-12 feet.

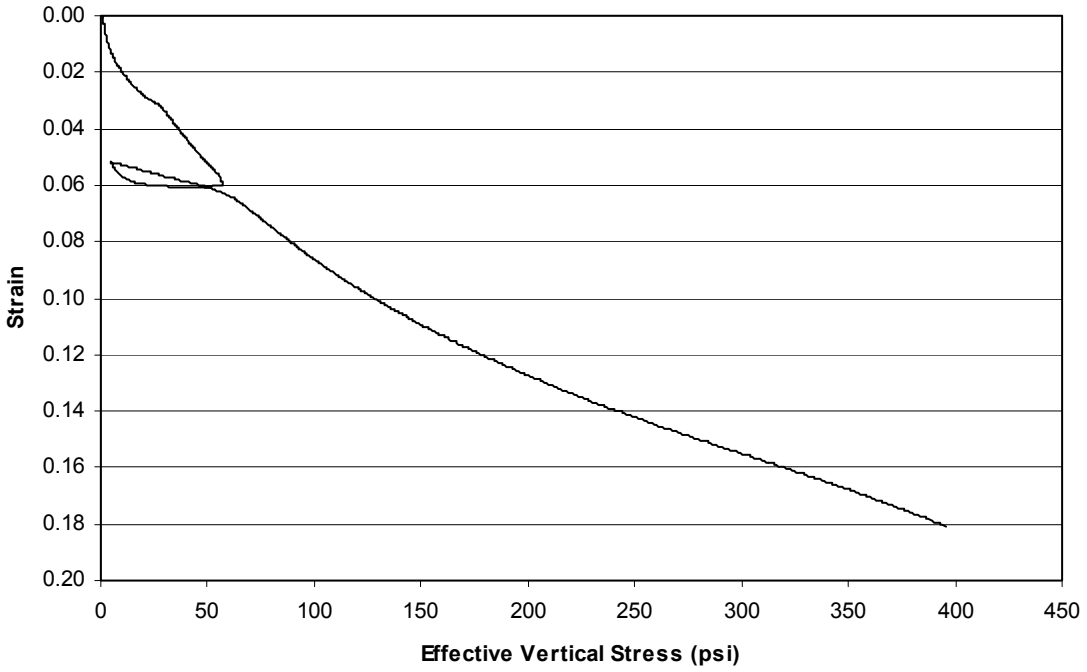


Figure E.59 Linear curve of strain vs. effective vertical stress for a sample from boring I2 at 10-12 feet.

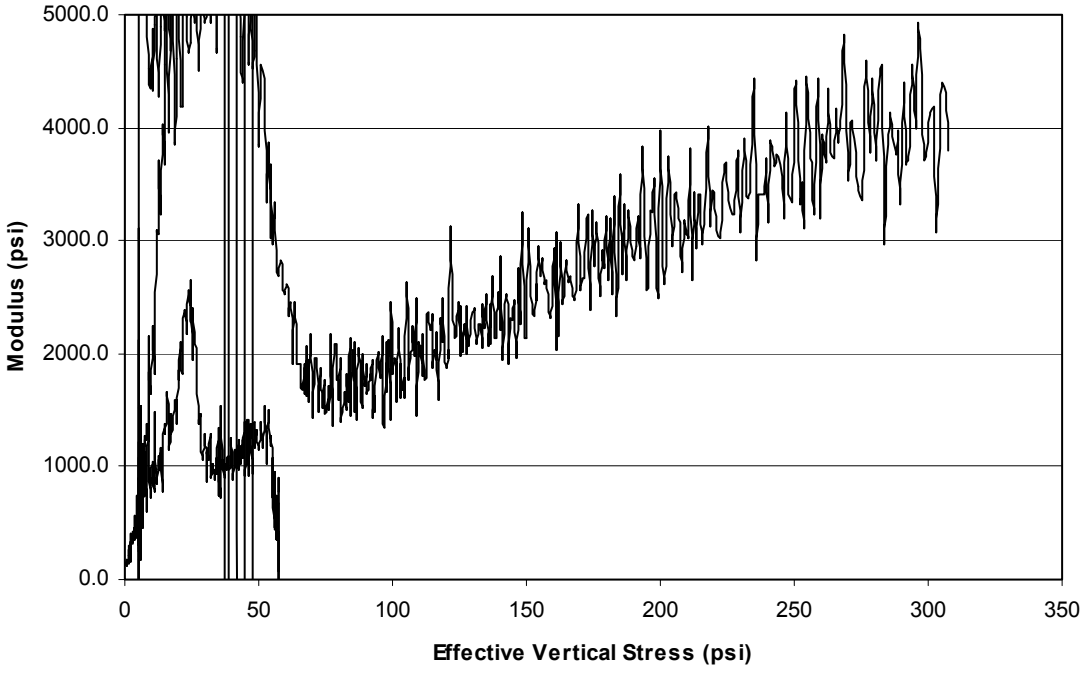


Figure E.60 Curve of modulus vs. effective vertical stress for a sample from boring I2 at 10-12 feet.

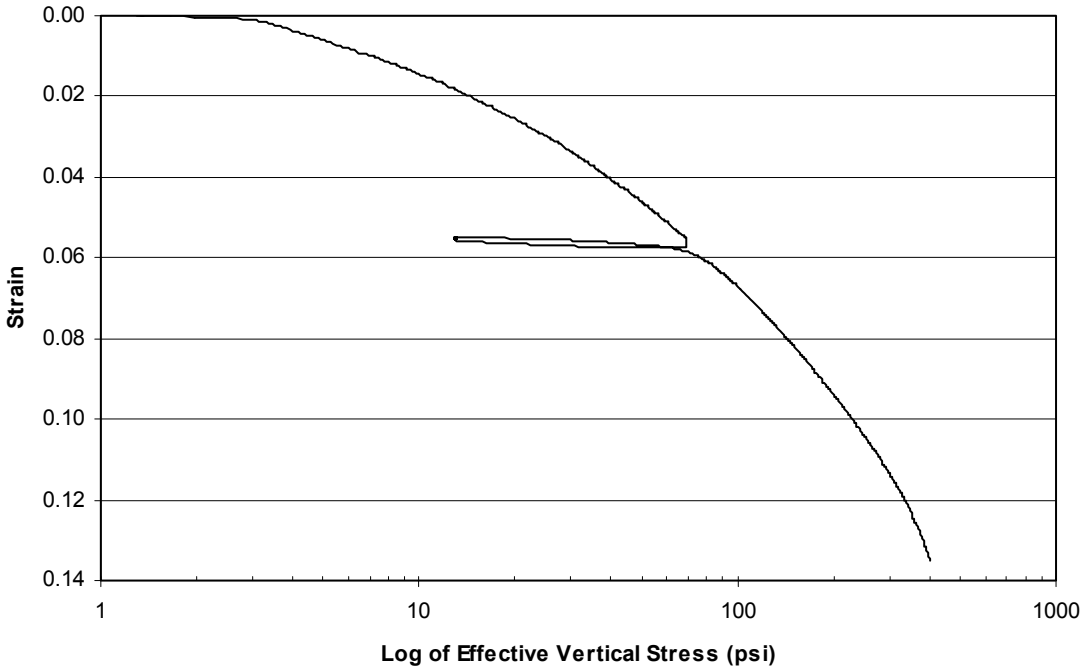


Figure E.61 Curve of strain vs. the log of effective vertical stress for a sample from boring I2 at 25-27 feet.

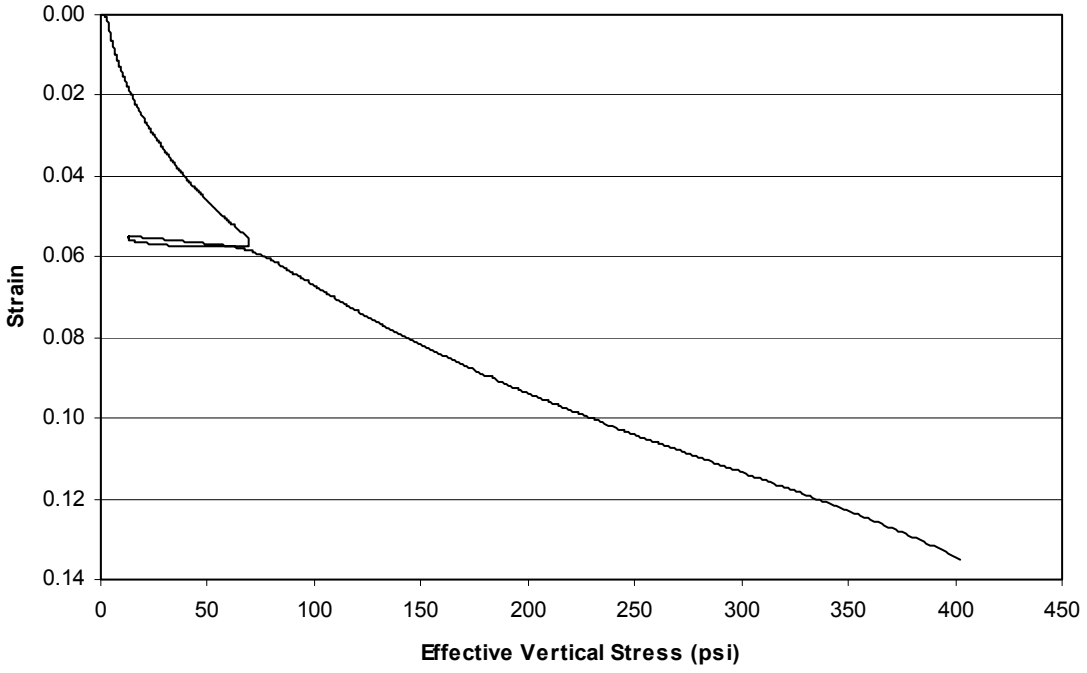


Figure E.62 Linear curve of strain vs. effective vertical stress for a sample from boring I2 at 25-27 feet.

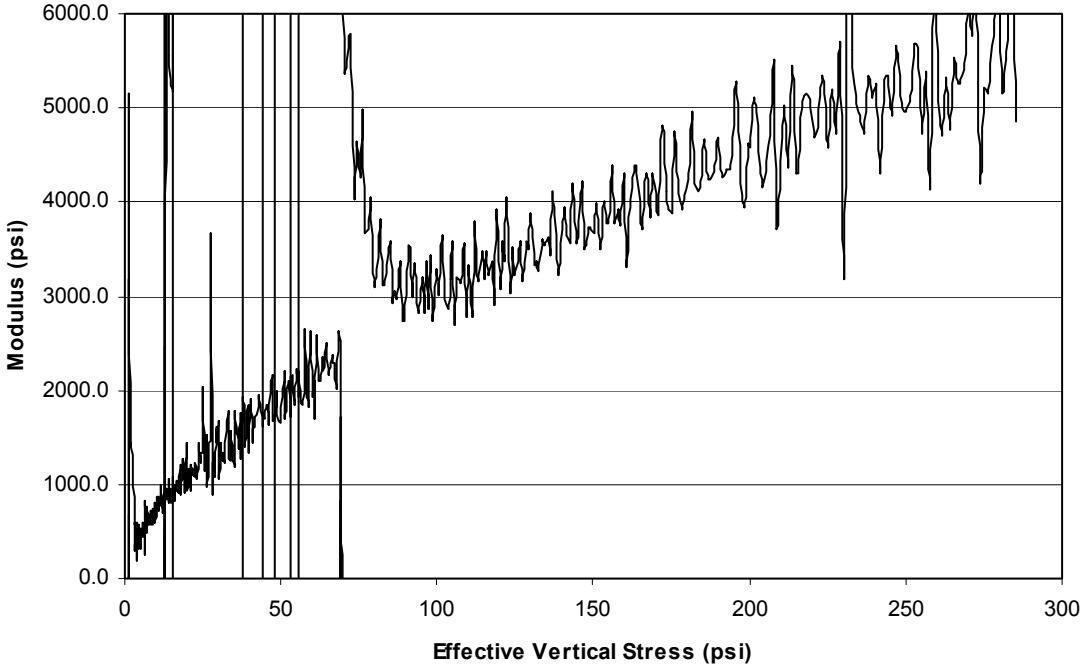


Figure E.63 Curve of modulus vs. effective vertical stress for a sample from boring I2 at 25-27 feet.

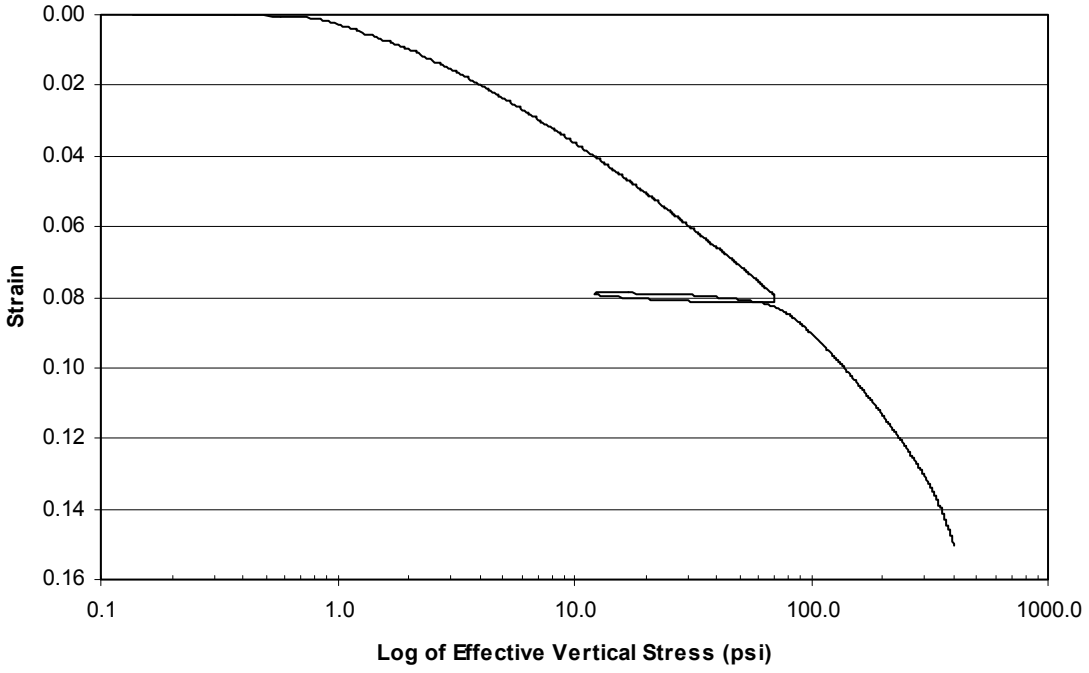


Figure E.64 Curve of strain vs. the log of effective vertical stress for a sample from boring I2 at 55-57 feet.

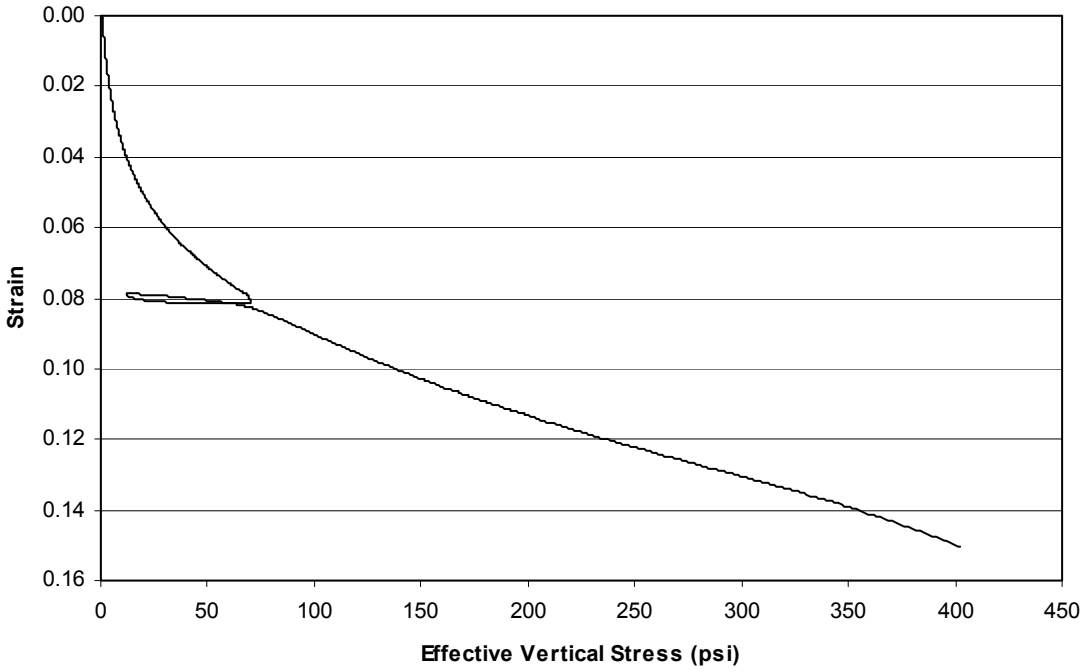


Figure E.65 Linear curve of strain vs. effective vertical stress for a sample from boring I2 at 55-57 feet.

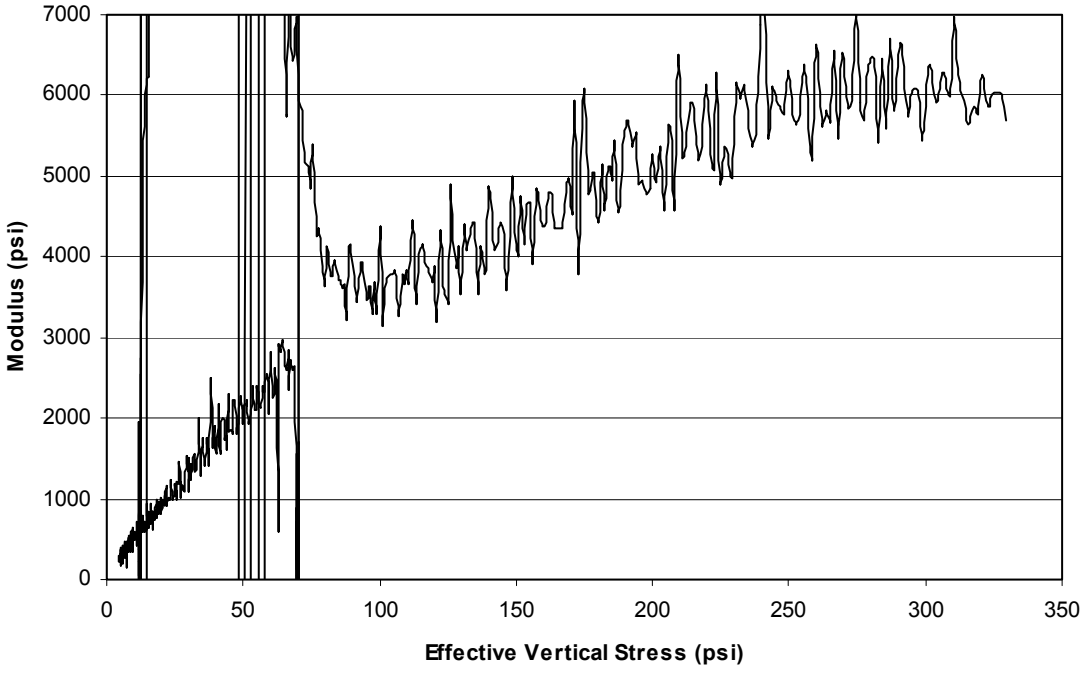


Figure E.66 Curve of modulus vs. effective vertical stress for a sample from boring I2 at 55-57 feet.

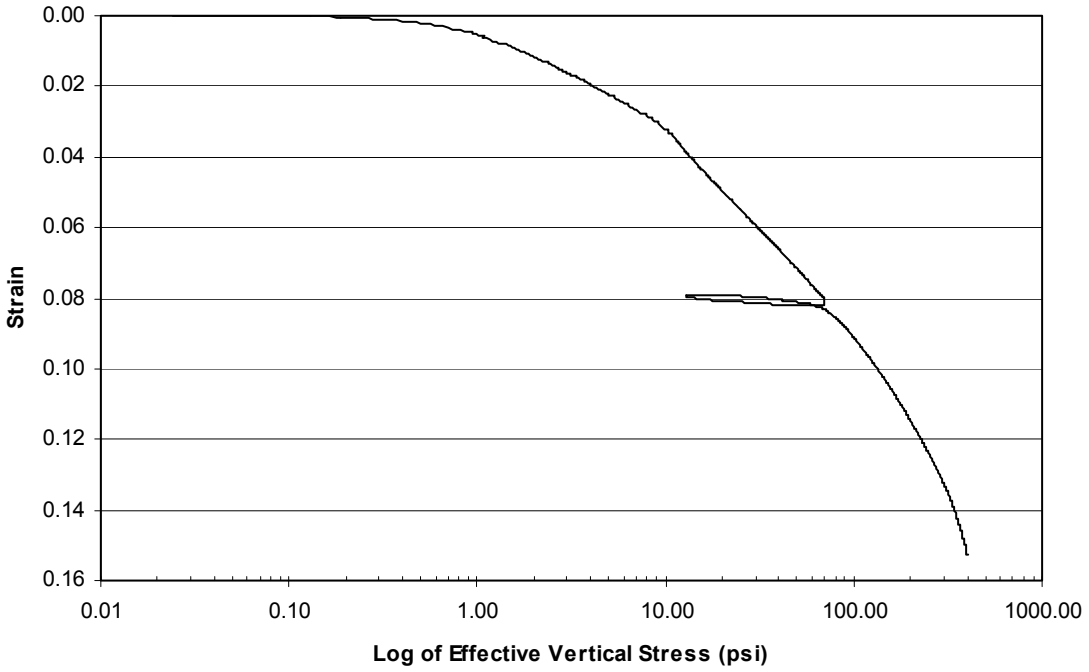


Figure E.67 Curve of strain vs. the log of effective vertical stress for a sample from boring I2 at 65-67 feet.

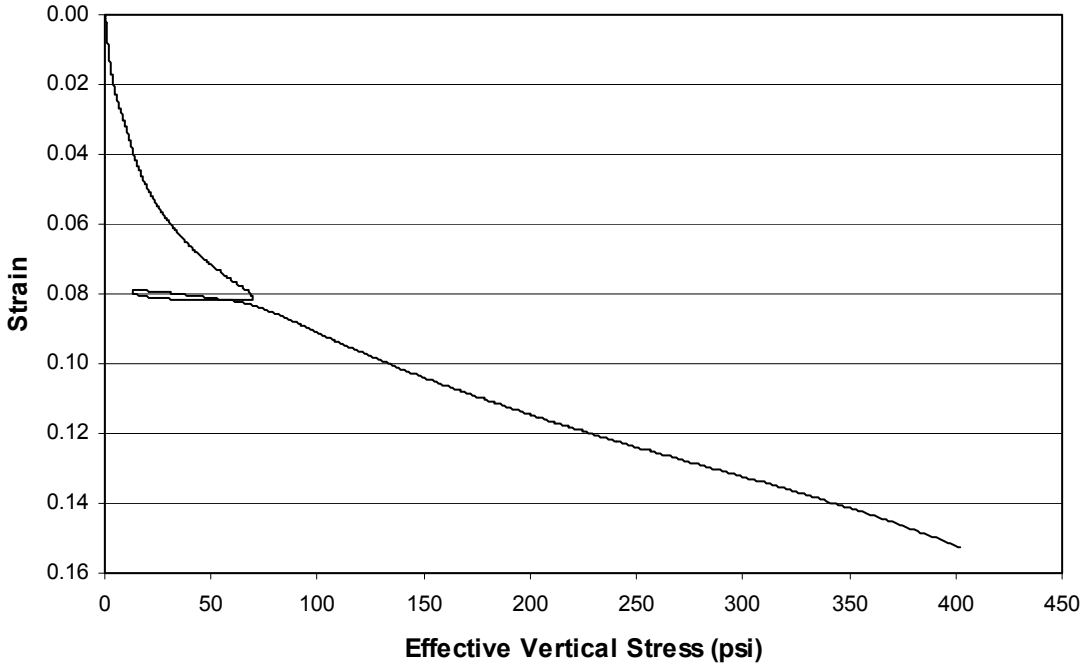


Figure E.68 Linear curve of strain vs. effective vertical stress for a sample from boring I2 at 65-67 feet.

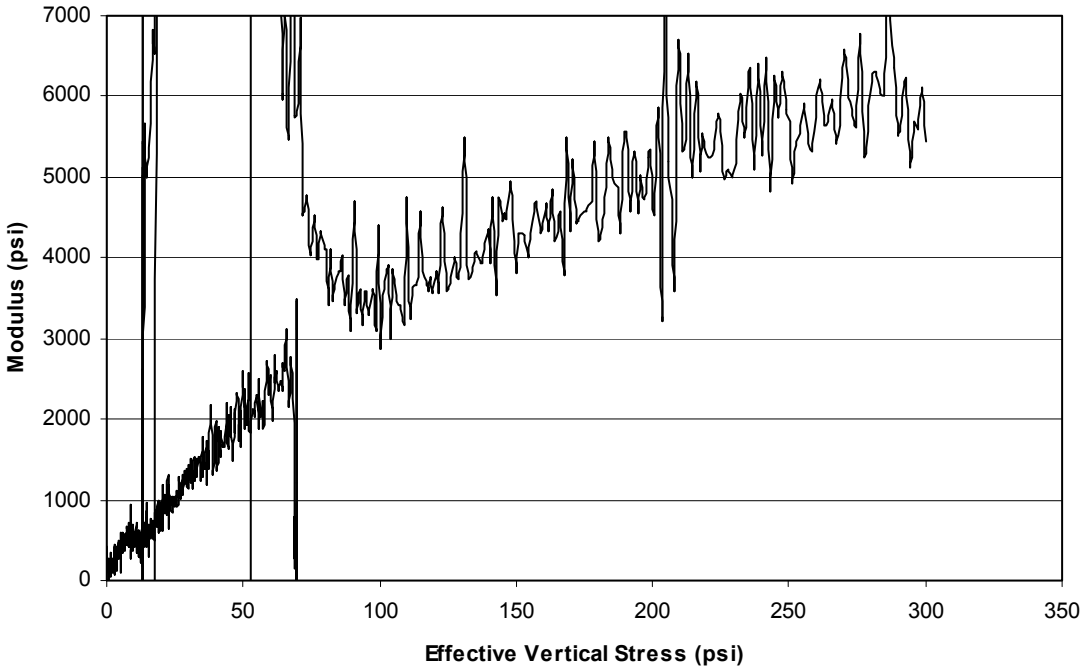


Figure E.69 Curve of modulus vs. effective vertical stress for a sample from boring I2 at 65-67 feet.

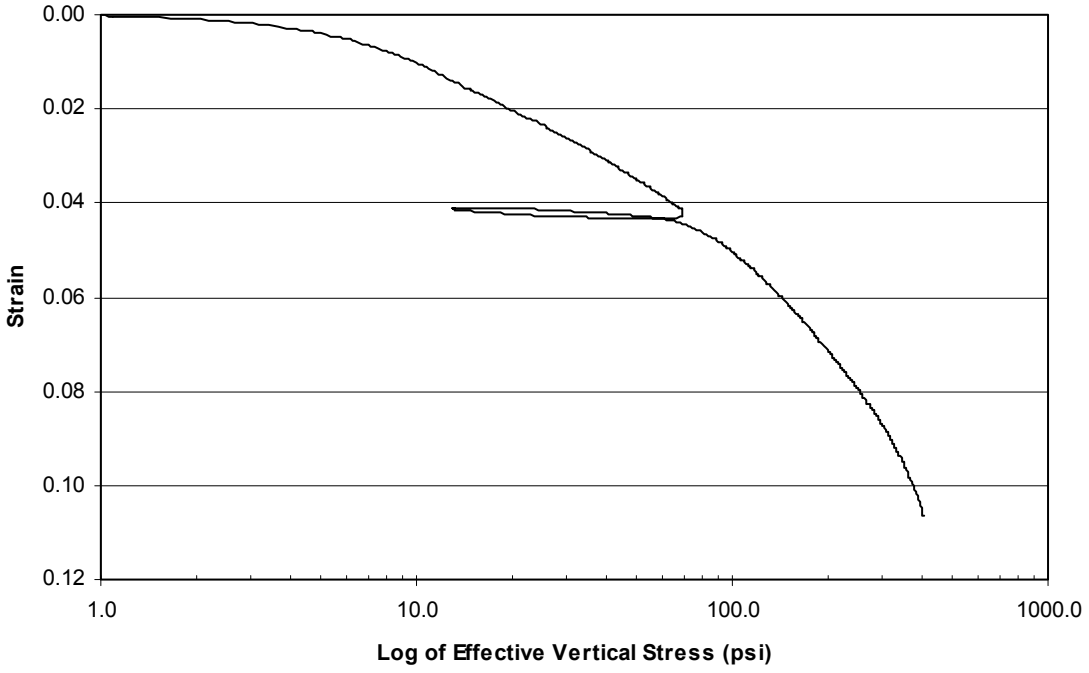


Figure E.70 Curve of strain vs. the log of effective vertical stress for a sample from boring I2 at 75-77 feet.

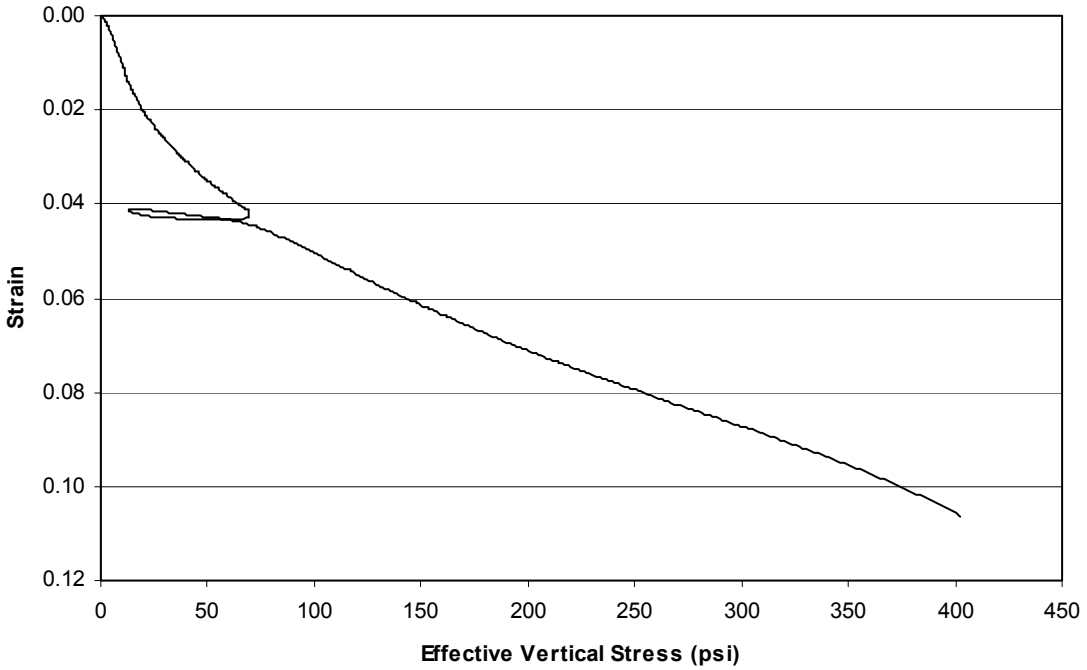


Figure E.71 Linear curve of strain vs. effective vertical stress for a sample from boring I2 at 75-77 feet.

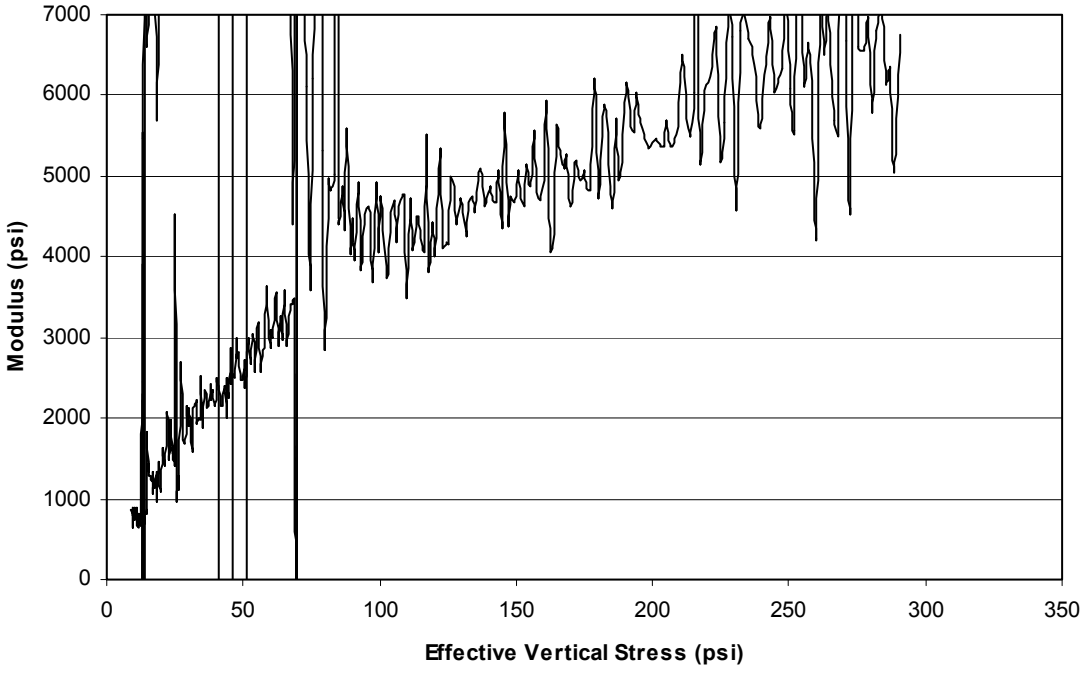


Figure E.72 Curve of modulus vs. effective vertical stress for a sample from boring I2 at 75-77 feet.

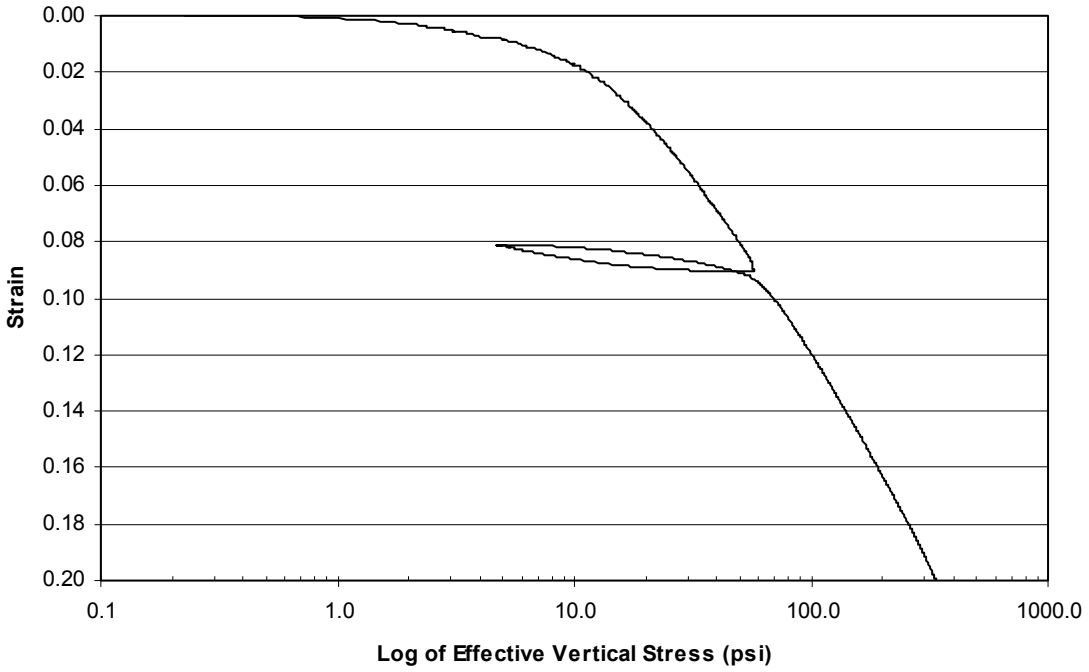


Figure E.73 Curve of strain vs. the log of effective vertical stress for a sample from boring S2 at 10-12 feet.

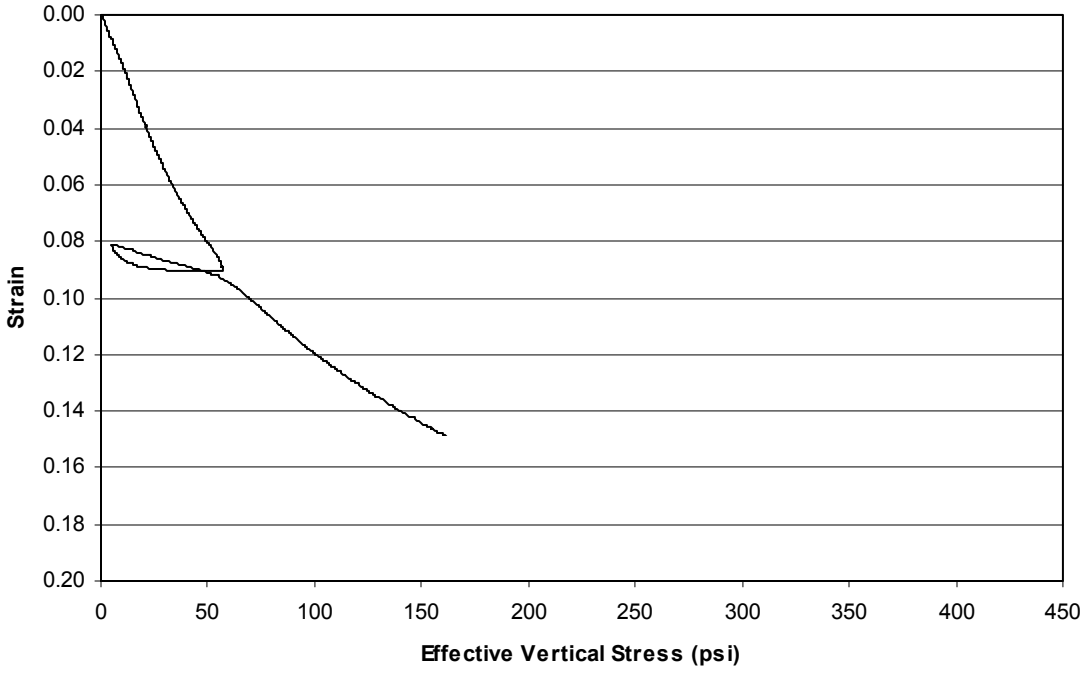


Figure E.74 Linear curve of strain vs. effective vertical stress for a sample from boring S2 at 10-12 feet.

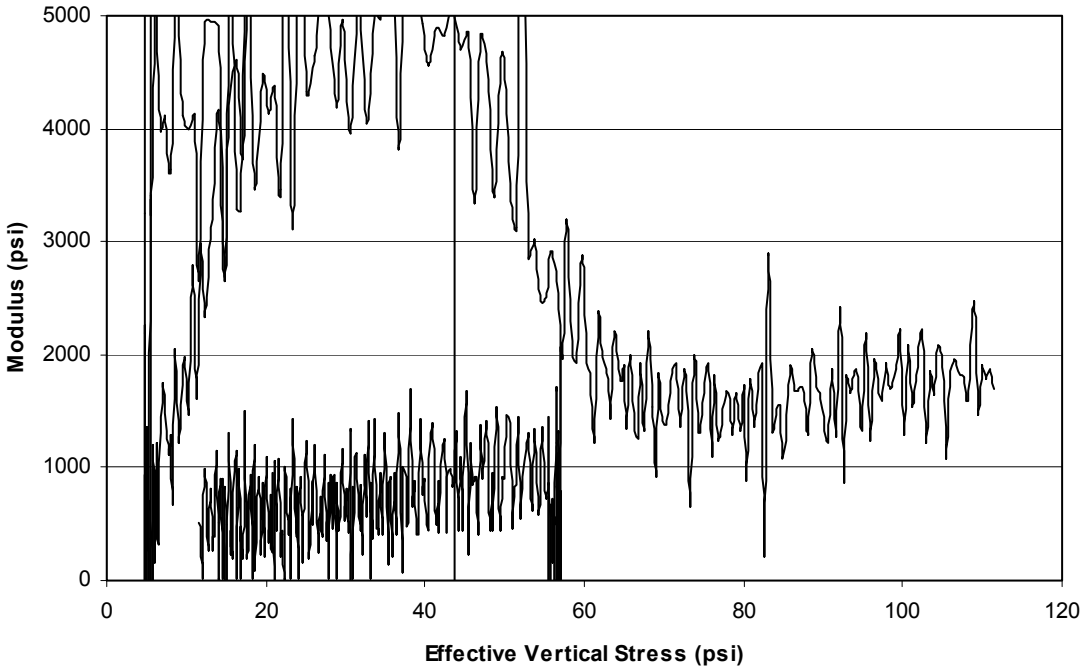


Figure E.75 Curve of modulus vs. effective vertical stress for a sample from boring S2 at 10-12 feet.

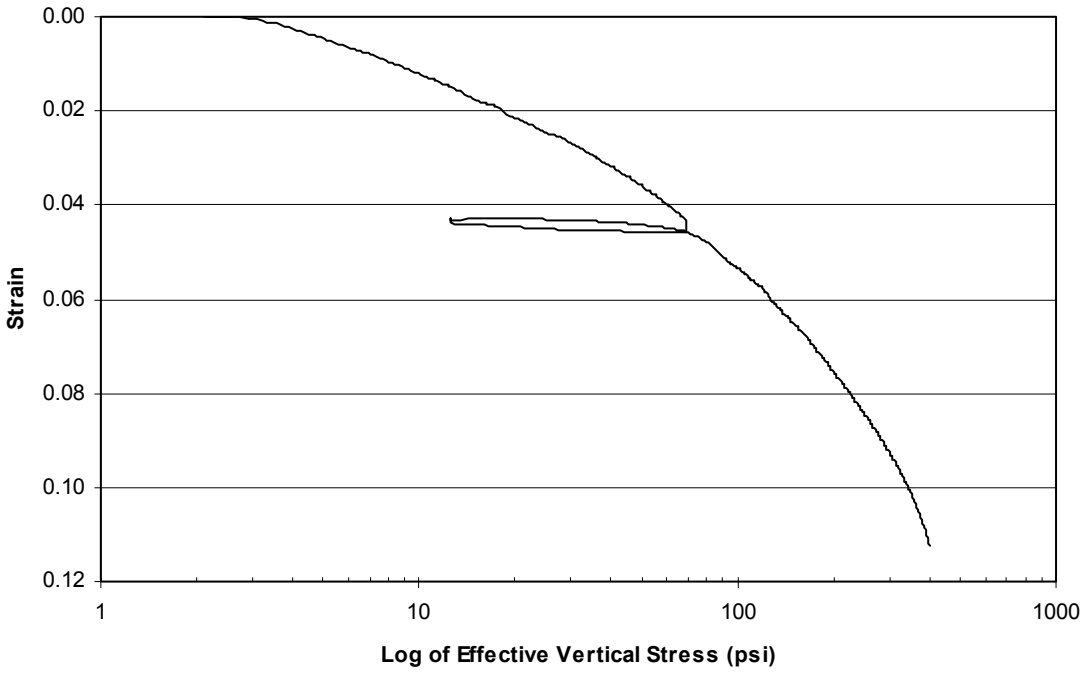


Figure E.76 Curve of strain vs. the log of effective vertical stress for a sample from boring S2 at 55-57 feet.

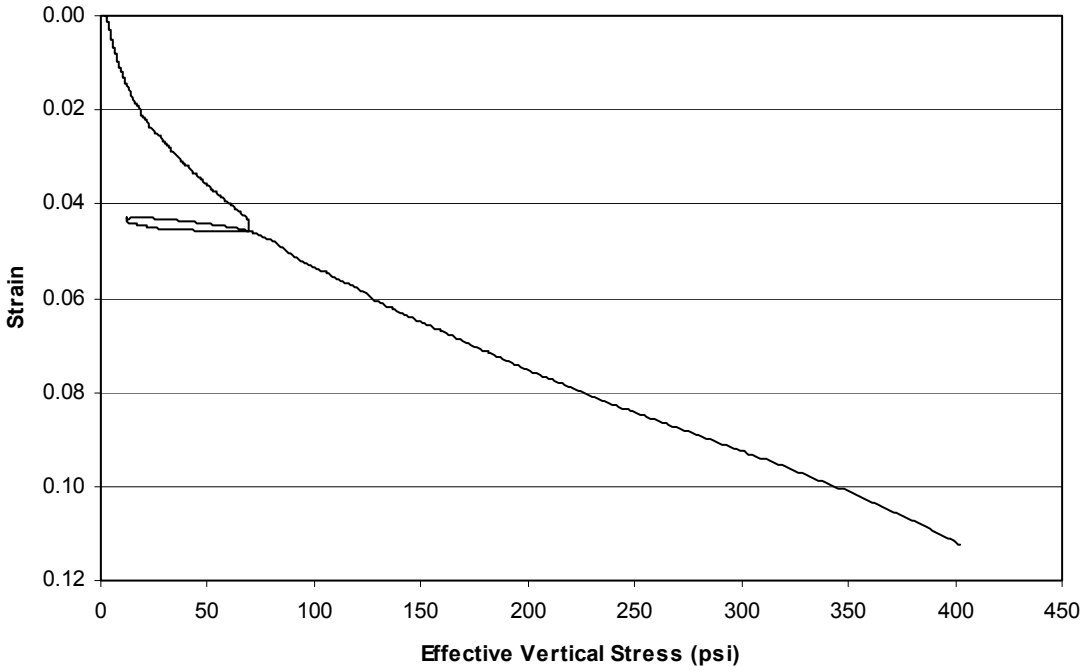


Figure E.77 Linear curve of strain vs. effective vertical stress for a sample from boring S2 at 55-57 feet.

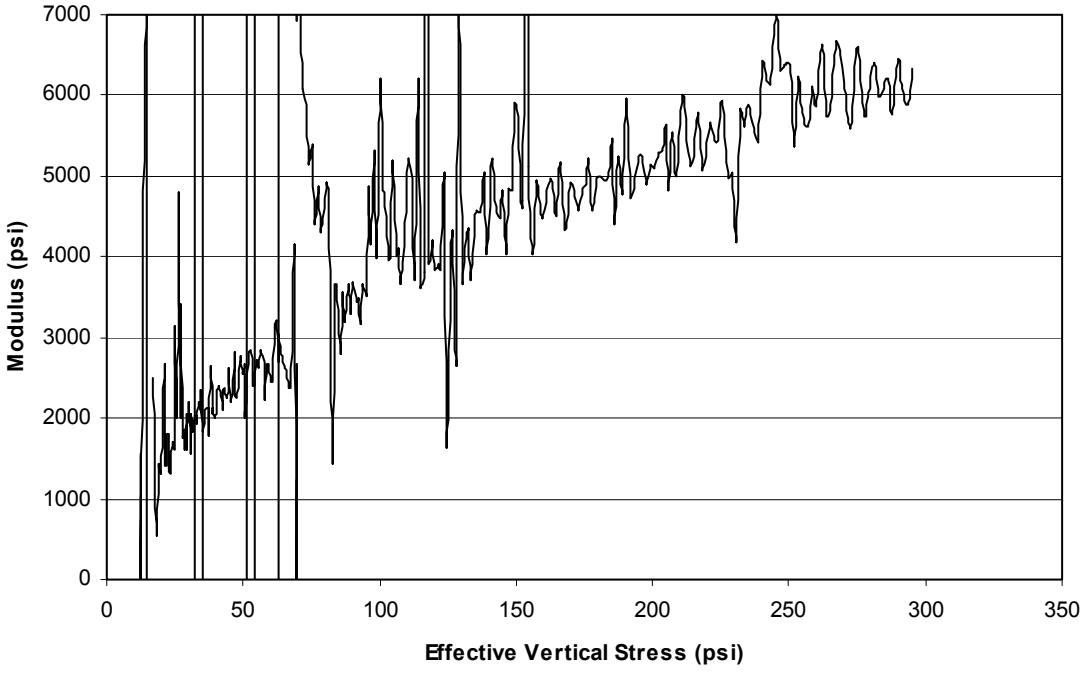


Figure E.78 Curve of modulus vs. effective vertical stress for a sample from boring S2 at 55-57 feet.

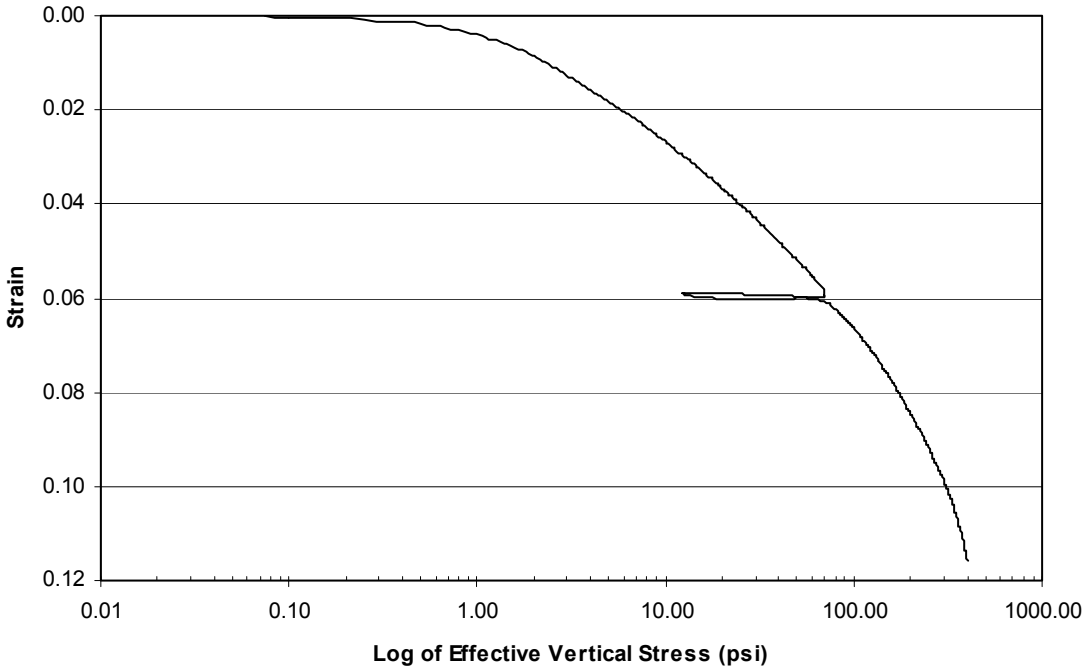


Figure E.79 Curve of strain vs. the log of effective vertical stress for a sample from boring S2 at 65-67 feet.

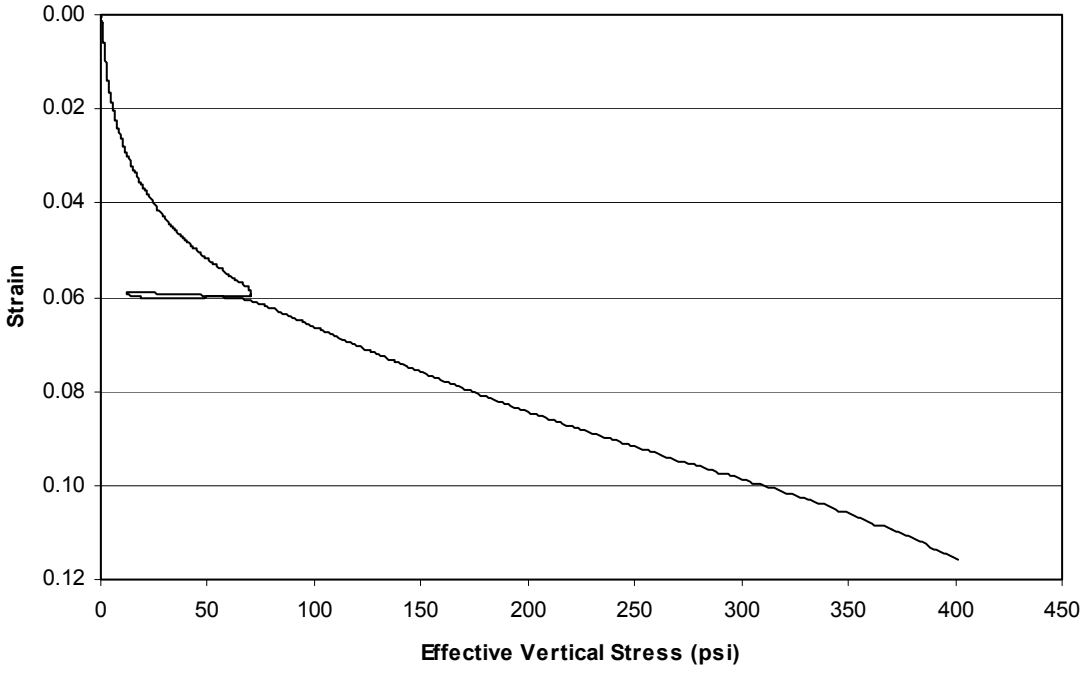


Figure E.80 Linear curve of strain vs. effective vertical stress for a sample from boring S2 at 65-67 feet.

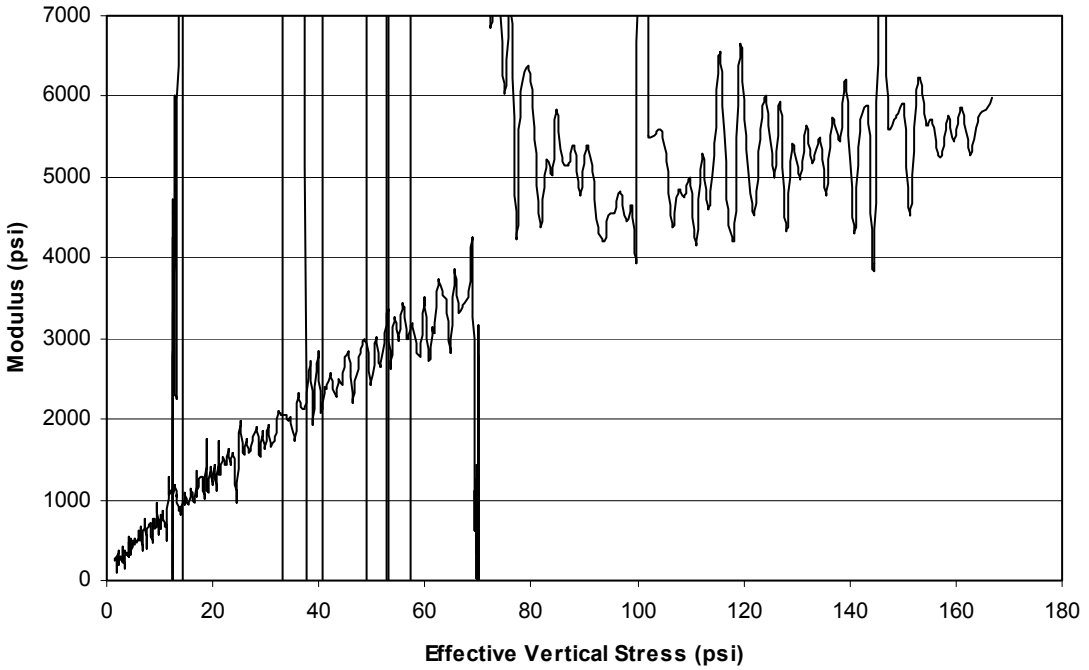


Figure E.81 Curve of modulus vs. effective vertical stress for a sample from boring S2 at 65-67 feet.

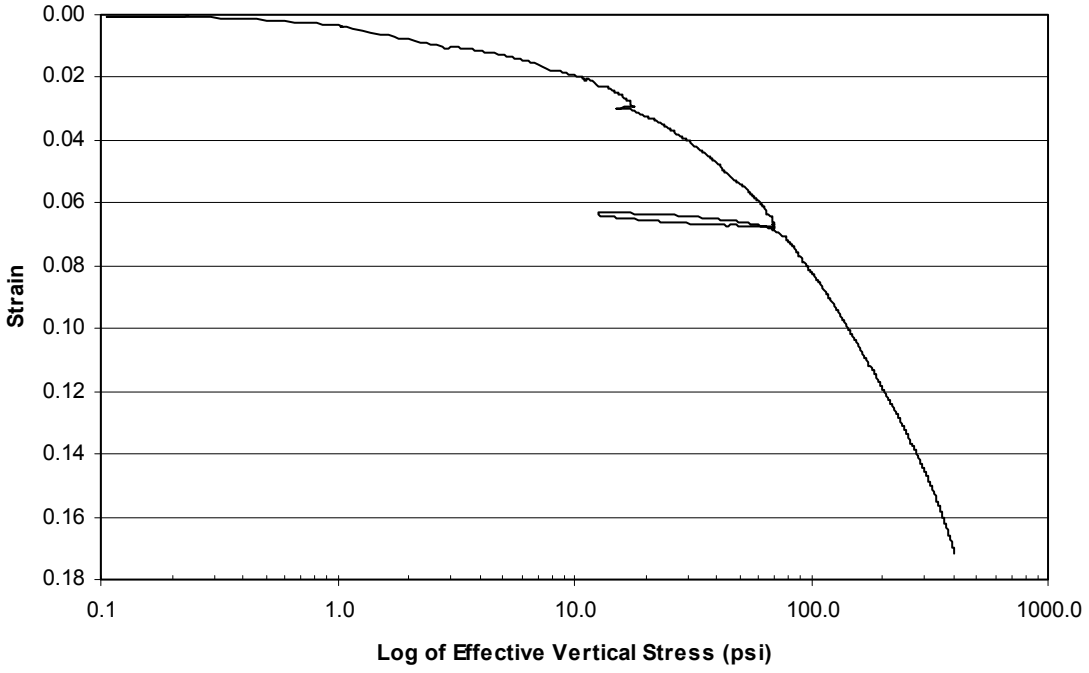


Figure E.82 Curve of strain vs. the log of effective vertical stress for a sample from boring S2 at 75-77 feet.

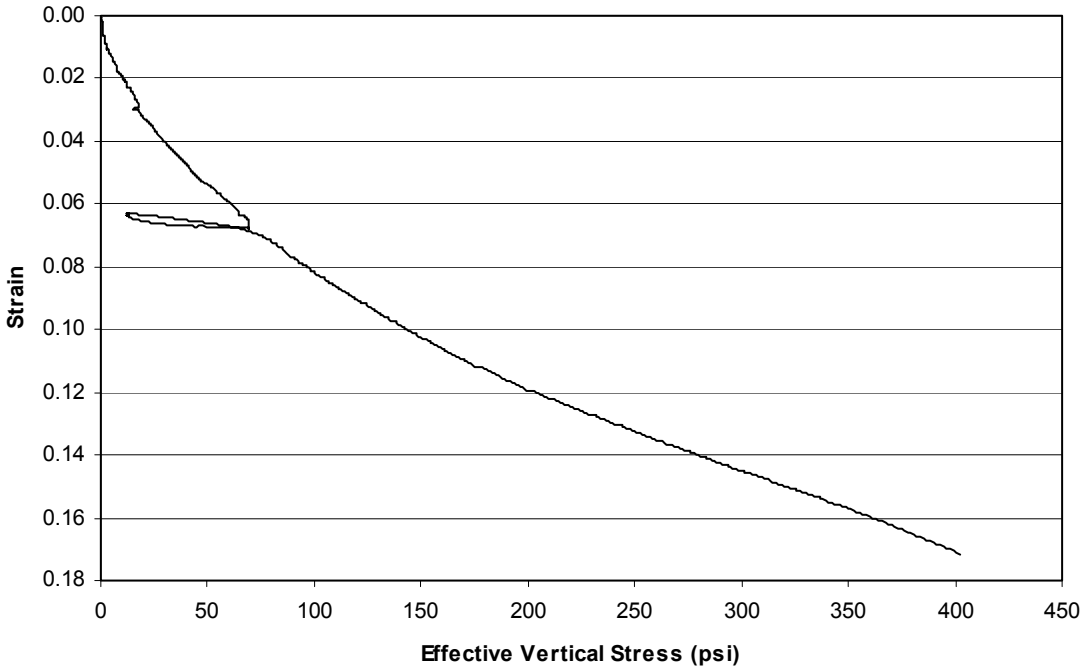


Figure E.83 Linear curve of strain vs. effective vertical stress for a sample from boring S2 at 75-77 feet.

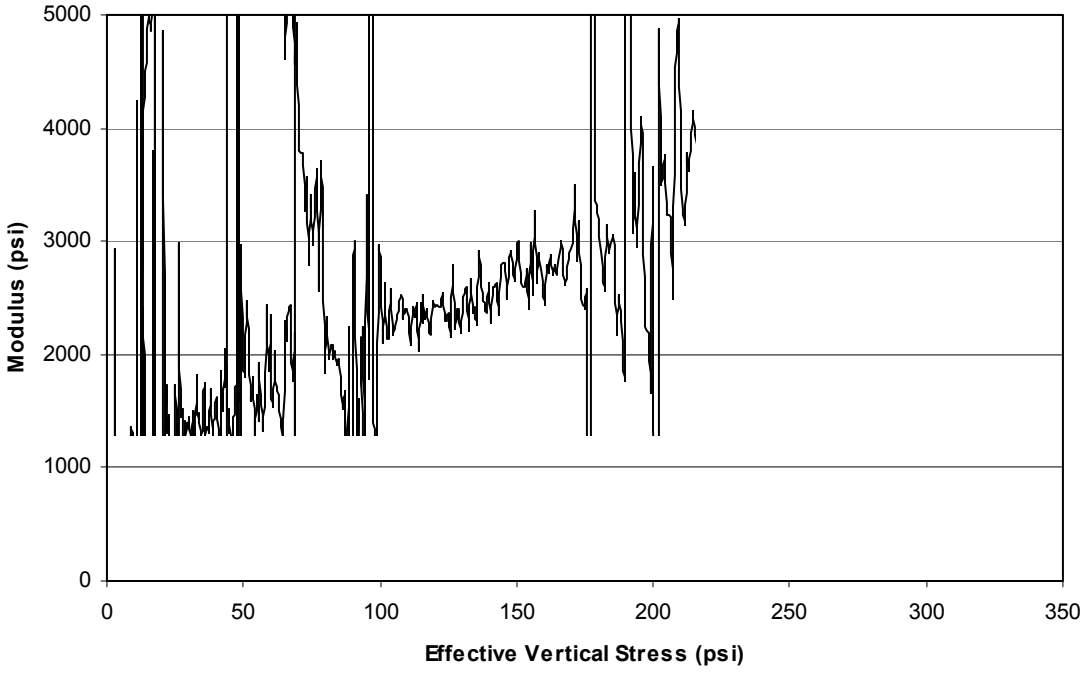


Figure E.84 Curve of modulus vs. effective vertical stress for a sample from boring S2 at 75-77 feet.